JAAVSO

Volume 45
Number 2
2017

The Journal of the American Association of Variable Star Observers

Multi-color Photometry of the Hot R Coronae Borealis Star, MV Sagittarii

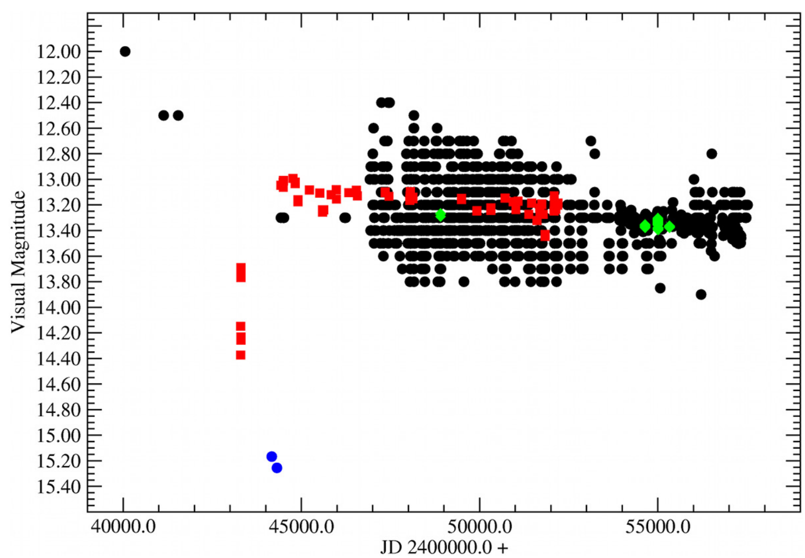

Visual AAVSO database magnitudes plus V photoelectric and CCD magnitudes for MV Sgr. Black color coding indicates AAVSO data, red photoelectric data, green CCD data, and blue two photoelectric possible MV Sgr data points.

Also in this issue...

THE AMERICAN ASSOCIATION OF VARIABLE STAR OBSERVERS • FOUNDED 1911 •

Complete table of contents inside...

The American Association of Variable Star Observers
49 Bay State Road, Cambridge, MA 02138, USA

The Journal of the American Association of Variable Star Observers

Editor
John R. Percy
Dunlap Institute of Astronomy and Astrophysics and University of Toronto
Toronto, Ontario, Canada

Associate Editor
Elizabeth O. Waagen

Production Editor
Michael Saladyga

Editorial Board

Geoffrey C. Clayton
Louisiana State University
Baton Rouge, Louisiana

Zhibin Dai
Yunnan Observatories
Kunming City, Yunnan, China

Kosmas Gazeas
University of Athens
Athens, Greece

Edward F. Guinan
Villanova University
Villanova, Pennsylvania

John B. Hearnshaw
University of Canterbury
Christchurch, New Zealand

Laszlo L. Kiss
Konkoly Observatory
Budapest, Hungary

Katrien Kolenberg
Universities of Antwerp and of Leuven, Belgium
and Harvard-Smithsonian Center for Astrophysics
Cambridge, Massachusetts

Kristine Larsen
Department of Geological Sciences, Central Connecticut State University,
New Britain, Connecticut

Vanessa McBride
IAU Office of Astronomy for Development; South African Astronomical Observatory; and University of Cape Town, South Africa

Ulisse Munari
INAF/Astronomical Observatory of Padua
Asiago, Italy

Nikolaus Vogt
Universidad de Valparaiso
Valparaiso, Chile

David B. Williams
Whitestown, Indiana

The Council of the American Association of Variable Star Observers 2016–2017

Director	Stella Kafka
President	Kristine Larsen
Past President	Jennifer L. Sokoloski
1st Vice President	Roger S. Kolman
2nd Vice President	Kevin B. Marvel
Secretary	Gary Walker
Treasurer	Robert Stephens

Councilors

Richard Berry	Katrien Kolenberg
Tom Calderwood	Richard S. Post
Joyce A. Guzik	Gregory R. Sivakoff
Michael Joner	William Stein

ISSN 0271-9053 (print)
ISSN 2380-3606 (online)

JAAVSO

The Journal of
The American Association
of Variable Star Observers

Volume 45
Number 2
2017

AAVSO
49 Bay State Road
Cambridge, MA 02138
USA

ISSN 0271-9053 (print)
ISSN 2380-3606 (online)

Publication Schedule

The Journal of the American Association of Variable Star Observers is published twice a year, June 15 (Number 1 of the volume) and December 15 (Number 2 of the volume). The submission window for inclusion in the next issue of JAAVSO closes six weeks before the publication date. A manuscript will be added to the table of contents for an issue when it has been fully accepted for publication upon successful completion of the referee process; these articles will be available online prior to the publication date. An author may not specify in which issue of JAAVSO a manuscript is to be published; accepted manuscripts will be published in the next available issue, except under extraordinary circumstances.

Page Charges

Page charges are waived for Members of the AAVSO. Publication of unsolicited manuscripts in JAAVSO requires a page charge of US $100/page for the final printed manuscript. Page charge waivers may be provided under certain circumstances.

Publication in *JAAVSO*

With the exception of abstracts of papers presented at AAVSO meetings, papers submitted to JAAVSO are peer-reviewed by individuals knowledgable about the topic being discussed. We cannot guarantee that all submissions to JAAVSO will be published, but we encourage authors of all experience levels and in all fields related to variable star astronomy and the AAVSO to submit manuscripts. We especially encourage students and other mentees of researchers affiliated with the AAVSO to submit results of their completed research.

Subscriptions

Institutions and Libraries may subscribe to JAAVSO as part of the Complete Publications Package or as an individual subscription. Individuals may purchase printed copies of recent JAAVSO issues via Createspace. Paper copies of JAAVSO issues prior to volume 36 are available in limited quantities directly from AAVSO Headquarters; please contact the AAVSO for available issues.

Instructions for Submissions

The *Journal of the AAVSO* welcomes papers from all persons concerned with the study of variable stars and topics specifically related to variability. All manuscripts should be written in a style designed to provide clear expositions of the topic. Contributors are encouraged to submit digitized text in MS WORD, LATEX+POSTSCRIPT, or plain-text format. Manuscripts may be mailed electronically to journal@aavso.org or submitted by postal mail to JAAVSO, 49 Bay State Road, Cambridge, MA 02138, USA.

Manuscripts must be submitted according to the following guidelines, or they will be returned to the author for correction:

Manuscripts must be:
1) original, unpublished material;
2) written in English;
3) accompanied by an abstract of no more than 100 words.
4) not more than 2,500–3,000 words in length (10–12 pages double-spaced).

Figures for publication must:
1) be camera-ready or in a high-contrast, high-resolution, standard digitized image format;
2) have all coordinates labeled with division marks on all four sides;
3) be accompanied by a caption that clearly explains all symbols and significance, so that the reader can understand the figure without reference to the text.

Maximum published figure space is 4.5" by 7". When submitting original figures, be sure to allow for reduction in size by making all symbols, letters, and division marks sufficiently large.

Photographs and halftone images will be considered for publication if they directly illustrate the text.

Tables should be:
1) provided separate from the main body of the text;
2) numbered sequentially and referred to by Arabic number in the text, e.g., Table 1.

References:
1) References should relate directly to the text.
2) References should be keyed into the text with the author's last name and the year of publication, e.g., (Smith 1974; Jones 1974) or Smith (1974) and Jones (1974).
3) In the case of three or more joint authors, the text reference should be written as follows: (Smith et al. 1976).
4) All references must be listed at the end of the text in alphabetical order by the author's last name and the year of publication, according to the following format: Brown, J., and Green, E. B. 1974, *Astrophys. J.*, **200**, 765.
   Thomas, K. 1982, *Phys. Rep.*, **33**, 96.
5) Abbreviations used in references should be based on recent issues of JAAVSO or the listing provided at the beginning of *Astronomy and Astrophysics Abstracts* (Springer-Verlag).

Miscellaneous:
1) Equations should be written on a separate line and given a sequential Arabic number in parentheses near the right-hand margin. Equations should be referred to in the text as, e.g., equation (1).
2) Magnitude will be assumed to be visual unless otherwise specified.
3) Manuscripts may be submitted to referees for review without obligation of publication.

Online Access

Articles published in JAAVSO, and information for authors and referees may be found online at: https://www.aavso.org/apps/jaavso/

© 2017 The American Association of Variable Star Observers. All rights reserved.

The Journal of the American Association of Variable Star Observers
Volume 45, Number 2, 2017

Table of Contents continued on following pages

Abstracts of Papers Presented at the Joint Meeting of the Society for Astronomical Sciences and the American Association of Variable Star Observers (AAVSO 106th Spring Meeting), Held in Ontario, California, June 16–17, 2017

Table of Contents continued on next page

Errata

Editorial

JAAVSO: Past, Present, and Future

John R. Percy
Editor-in-Chief, *Journal of the AAVSO*

Department of Astronomy and Astrophysics, and Dunlap Institute for Astronomy and Astrophysics, University of Toronto, 50 St. George Street, Toronto, ON M5S 3H4, Canada; john.percy@utoronto.ca

Received November 24, 2017

JAAVSO was created in 1972 as a place "where professional and non-professional astronomers can publish papers on research of interest to the observer"—a statement which defined the intended authorship and readership. The first volumes also contained various reports, and abstracts of papers presented at AAVSO meetings. Only the latter are still published in *JAAVSO*; the reports are now published elsewhere on the AAVSO website.

JAAVSO grew steadily, in size and quality, under the long-time editorship of Dr. Charles Whitney (1929–2017). Special issues were produced, in connection with AAVSO's European Meetings, its Centennial, and its IYA *Citizen Sky* project. Review articles appeared, and still do.

JAAVSO's core mission is to publish papers on variable star astronomy and related topics. It exists within an ecosphere of other journals which also publish such papers. In an earlier Editorial (vol. 44, no. 2), I discussed the "wild west" aspects of journal publishing today. Most professional (technical) papers are published in the non-profit *Astronomical Journal*, *Astronomy and Astrophysics*, *Astrophysical Journal*, or *Monthly Notices of the Royal Astronomical Society*. Additionally, there are a few for-profit astronomical journals, and also journals based in a few countries such as Australia, China, Japan, Russia, etc. which cater to astronomers from those countries. One of the specialties of the non-profit *Publications of the Astronomical Society of the Pacific* is stars. In addition, there are journals or newsletters published by variable star observing groups in many parts of the world, many of them in languages other than English.

There is also the *International Bulletin on Variable Stars*, originally a project of the International Astronomical Union (IAU), now published on-line, open-access by the Konkoly Observatory in Hungary. Its papers are short, and many but not all of them come from Europe. The vast majority of authors are professionals, who are writing for other professionals.

The editor of *JAAVSO* (currently me) is supported by HQ staff, especially Michael Saladyga and Elizabeth Waagen, and advised by an international Editorial Board. We report to the AAVSO Director, and Council.

AAVSO Director Stella Kafka has a special interest and several years' experience in non-profit scientific publishing, and she has stimulated discussion of many aspects of *JAAVSO*, including how it might evolve. Here are some possibilities for thought and feedback.

More International Content: When *JAAVSO* began, it was very much North American. More recently, its international content has increased. We have more international representation on the Editorial Board. I choose referees from around the world, as appropriate (though I do try to choose ones who have some knowledge of our authorship and readership). The fraction of papers with at least one non-North American author was 10% two decades ago, 37% one decade ago, and 48% last year. These international authors tend to be much like the North American ones: professional variable-star astronomers with long-term access to small telescopes, skilled amateurs, supervisors of research students, etc. They come primarily from Europe, Australia, and New Zealand; very few are from Asia, Africa, or Latin America. The AAVSO's European conferences and our Directors' travels have certainly raised our international profile.

More internationalism would enable us to have an even higher profile, internationally, and perhaps be part of indexes such as the (for-profit) Web of Science: http://clarivate.com/products/web-of-science/ (we are already indexed on the Astrophysics Data Service: ADS). That could possibly get us more international professional authors, though the fact that we charge page charges to non-members, and very few non-American professional astronomers choose to become AAVSO members, and *JAAVSO* is only available (for the first year) to members and subscribers makes this less attractive to them.

As with other aspects of the AAVSO's work, the name "American" may create the impression that we are a North American journal. Perhaps it's time to re-brand as "*JAAVSO: The International Journal on Variable Stars*"!

More Education Content: Observation and/or analysis of variable stars is an excellent way for students to develop and integrate their skills in science, math, and computing. That was the idea behind AAVSO's *Hands-On Astrophysics* project. The AAVSO website has many public resources to support student research. *JAAVSO* already publishes many papers which are based on student projects, almost all of them at the post-secondary level. Most of my own papers are, and I have recently reflected on my four decades of experience with these: http://arxiv.org/abs/1710.04492.

There has also been some interest, on the part of at least one group of astronomers, in finding a place to publish authentic research by "seminars" of secondary or post-secondary students. That is challenging: we require the content of *JAAVSO* papers to be both correct and significant, and not all education projects meet the second criterion. We do encourage papers which *describe* educational projects, involving variable stars (including the sun), which are both effective and novel.

Papers on Outreach: We encourage outreach, for reasons that I described in my last Editorial (vol. 45, no. 1). If you use variable stars successfully in outreach, we would like to hear about it. For general papers on outreach, the IAU publishes a free on-line *Communicating Astronomy with the Public* (*CAP*) *Journal* with papers on all aspects of the subject.

Papers on History and Biography: The history and biography of variable star astronomy is rich and interesting, and we should continue to encourage papers in these areas, as we did, for instance, in our Centennial issue.

Papers Related to International Astronomy Development: Two decades ago, AAVSO Director Janet Mattei and I promoted the idea that variable star observation and analysis could be one way that professional and amateur astronomers and students in developing countries could undertake and publish research in astronomy. Since several members of the *JAAVSO* Editorial Board are active in astronomical development, especially through the IAU, we hope that they will continue to promote this idea.

Fast-Turnaround Papers in JAAVSO: This suggestion was recently made, and discussed by the Editorial Board. At present, I am not sure what kinds of papers would be included. Alert notices can be posted elsewhere on the AAVSO website. Professionals can publish "hot" results in journals such as *Astrophysical Journal*, or on the preprint server *astro-ph*. In principle, many *JAAVSO* papers can be formatted for publication online in a few hours, once they have been refereed and accepted for publication, and approved by AAVSO staff.

An interesting new development is *Research Notes of the American Astronomical Society*, published by the Institute of Physics, searchable on ADS, fully citable, free to publish and read, archived for perpetuity, available online within 72 hours of acceptance, and moderated prior to publication to ensure legitimacy. Response is good, so far.

Other Niches? Are there other niches that *JAAVSO* could expand into? One might be *short* reviews or updates on topics which are directly relevant to our primary audience—the observers. These might be on new techniques for observation or analysis, or on new developments in variable star astronomy. I welcome suggestions of suitable topics.

Incremental Building on the Status Quo: We could continue to do the best possible job of attracting and publishing papers by advanced amateurs, astronomy students, and professionals whose work is relevant to AAVSO observers/members—whether those papers come from North America or elsewhere. I suspect that there are still authors around the world who would benefit from the advantages that *JAAVSO* provides. Two-thirds of our observers are from outside the USA! This returns us to our original goal: "papers on research of interest to the observer." Whether or not we strive for more internationalism, we must not lose track of our core mission—to serve an authorship and readership which includes both professionals and amateurs.

There is one slight anomaly in *JAAVSO*, at present: the majority of recent papers deal with a relatively small number of topics: eclipsing binaries, for instance. I would like to see more papers on other fields in which AAVSO observers are active, such as cataclysmic variables, young stellar objects, and the sun, as well as on techniques of observation and analysis, and on education, history, and biography. I, the Editorial Board, and the section leaders should be more active in soliciting these.

It is for the Director and Council to decide on the purpose and funding of *JAAVSO*, but input from members and other readers is always welcome. That's one of the main goals of this Editorial: to ask for your feedback! Please send it to: aavso@aavso.org, with "JAAVSO Feedback" in the subject line.

Acknowledgements

I am grateful to Drs. John Hearnshaw, Stella Kafka, Kristine Larsen, Ulisse Munari, and Michael Saladyga for their comments on a draft of this Editorial.

A Photometric Study of the Eclipsing Binary QT Ursae Majoris

Edward J. Michaels
Stephen F. Austin State University, Department of Physics, Engineering and Astronomy, P.O. Box 13044, Nacogdoches, TX 75962; emichaels@sfasu.edu

Received June 6, 2017; revised July 25, 2017; accepted July 25, 2017

Abstract Presented are the first multiband light curves of the eclipsing binary QT Ursae Majoris. The light curves were analyzed using the Wilson-Devinney program to find the best-fit stellar model. Asymmetries in the light curves required spots to be included in the model. The solution results give a Roche Lobe fill-out of 13%, which is consistent with a W-type contact binary. New linear and quadratic ephemerides were computed using 31 times of minima, including 8 new ones from this study.

1. Introduction

The variability of QT UMa (GSC 03429-0424) was discovered in the Northern Sky Variability Survey database (NSVS; Wozniak *et al.* 2004) (Otero *et al.* 2004). This star was classified as an EW eclipsing binary with a magnitude range of 11.0–11.8. An automated variable star classification method also found the star to be a W UMa type binary (Hoffman *et al.* 2009). The orbital period, 0.473522 d, was determined from the NSVS data (Otero *et al.* 2004). The light curve was reported to show a slight O'Connell effect. From Tycho 2 data this star's effective temperature was found to be 6065 K with a color excess of E(B–V) = 0.006 (Ammons *et al.* 2006). The LAMOST spectroscopic survey gives an effective temperature of 5493 K (Luo *et al.* 2015) (Sichervskij 2017). A parallax measurement from the first data release of the Gaia mission gives a distance of 247 ± 15 pc (Gaia Data Release 1; Gaia Collaboration *et al.*, 2016) (Astraatmadja and Bailer-Jones 2016).

In this paper, a photometric study of QT UMa is presented in organized sections. Section 2 presents the first set of multi-wavelength photometric observations for this star, new ephemerides are presented in section 3, a light curve analysis is given in section 4, and conclusions in section 5.

Table 1. Stars used in this study.

Star	*R.A. (2000)* *h m s*	*Dec. (2000)* *° ′ ″*	*g′*	*r′*	*i′*
QT UMa	09 36 29.2	+48 52 46			
[1]GSC 3429-1671 (C1)	09 35 49.4	+48 55 33	11.405 ± 0.063	10.773 ± 0.055	10.535 ± 0.038
[1]GSC 3429-0263 (C2)	09 37 15.4	+48 48 43	11.428 ± 0.090	11.057 ± 0.053	10.973 ± 0.040
[1]GSC 3429-1192 (C3)	09 36 51.3	+48 43 42	12.447 ± 0.060	11.677 ± 0.044	11.418 ± 0.030
[1]GSC 3429-1426 (C4)	09 35 48.2	+48 48 25	12.476 ± 0.052	11.945 ± 0.055	11.788 ± 0.040
[2]GSC 3429-0822 (K)	09 36 54.8	+48 45 05	12.530 ± 0.062	11.830 ± 0.048	11.592 ± 0.036
Observed check star (K) magnitudes			12.533 ± 0.036	11.832 ± 0.027	11.596 ± 0.022
Standard deviation of check star magnitudes			± 0.008	± 0.009	± 0.009

APASS [1]comparison stars (C1–C4) and [2]check star (K) magnitudes and errors.

2. Observations

Photometric observations were acquired using the 0.31-m Ritchey-Chrétien robotic telescope at the Waffelow Creek Observatory (http://obs.ejmj.net/index.php). A SBIG-STXL camera equipped with a cooled KAF-6303E CCD (–30° C) was used for imaging on five nights in 2016, February 25, 26, 27, and March 1 and 3. A total of 2,957 images were obtained in three passbands: 966 in Sloan g', 995 in Sloan r', and 966 in Sloan i'. This data set was used in the light curve analysis in section 4 of this paper. Additional images were acquired in February 2015 and February 2017. These observations provided additional times of minima. Bias, dark, and flat frames were obtained before each night's observing run. Calibration and ensemble differential aperture photometry of the light images was performed using MIRA software (Mirametrics 2015). Table 1 contains the comparison and check stars used in this study, with a finder chart shown in Figure 1. The standard magnitudes of these stars were taken from the AAVSO Photometric All-

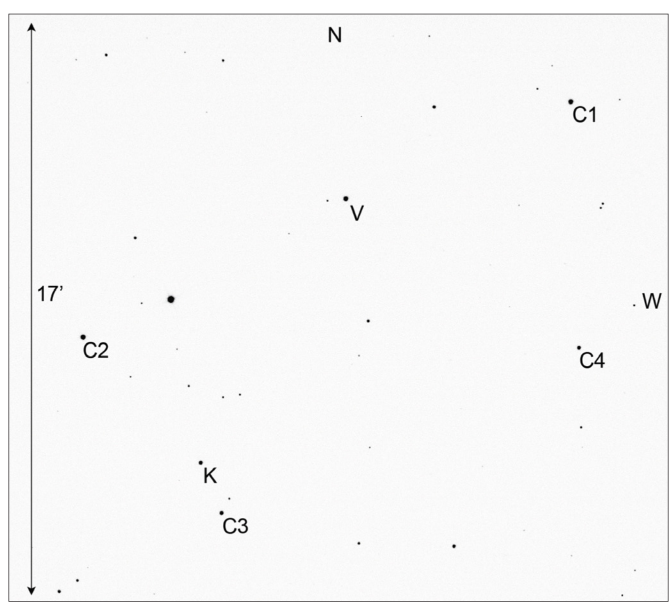

Figure 1. Finder chart for QT UMa (V), comparison (C1–C4), and check (K) stars.

Sky Survey (APASS) database (Henden *et al.* 2015). The instrumental magnitudes of QT UMa were converted to standard magnitudes using these comparison stars. The Heliocentric Julian Date (T) of each observation was converted to orbital phase using an epoch of $T_o = 2457446.7202$ and an orbital period of P = 0.4735397 d. Figure 2 shows the folded light curves in standard magnitudes. All light curves in this paper are plotted from phase –0.6 to 0.6 with negative orbital phase defined as φ – 1. The bottom panel of Figure 2 shows the Sloan r' check star magnitudes for all nights. Plots of the check star magnitudes were inspected each night but no significant variability was found. The 2016 observations in this study can be accessed from the AAVSO International Database (Kafka 2016).

3. Ephemerides

The Heliocentric Julian Date (HJD) of eight new times of minimum light were determined from the observations. These values are listed in Table 2 along with all minima times available in the literature. Figure 3 shows the O–C residuals calculated from the linear ephemeris of Otero et. al (2004) given by

$$\text{HJD Min I} = 2451563.948 + 0.473522E . \quad (1)$$

From the residuals of Equation 1 a new linear ephemeris was computed by least-squares solution and is given by

$$\text{HJD Min I} = 2457446.7202(5) + 0.4735397(2)E . \quad (2)$$

The best-fit linear line from Equation 2 is the dotted line in Figure 3. Using the residuals from Equation 2, a second least-squares solution gives the following quadratic ephemeris:

$$\text{HJD Min I} = 2457446.7169(5) + 0.4735417(5)E + 3.0(6) \times 10^{-9} E^2. \quad (3)$$

Figure 4 shows the general trend of the O–C residuals from the new quadratic ephemeris which has a positive curve.

4. Analysis

4.1. Temperature, spectral type

The effective temperature of the larger secondary star was determined from the observed (g'–r') color at primary eclipse. The primary eclipse is nearly total, therefore most of the system light at orbital phase φ = 0 is from the secondary star. To determine the secondary star's color, the phase and magnitude of the g' and r' observations were binned with a phase width of 0.01. The phases and magnitudes in each bin interval were averaged. Figure 5 shows the resulting binned r' magnitude light curve with the bottom panel showing the (g'–r') color index. The observed color at primary eclipse is (g'–r') = 0.592 ± 0.012. The equation,

$$(B\text{–}V) = \frac{(g'\text{–}r') + 0.23}{1.09}, \quad (4)$$

was used to transform the observed (g'–r') color to (B–V) = 0.754 ± 0.015 (Jester *et al.* 2005). The color excess, E(B–V)

Table 2. Times of minima and O–C residuals from Equation 2.

Epoch HJD 2400000+	*Error*	*Cycle*	*O–C Linear*	*References*
55932.8144	0.00020	0.0	0.00054	Nelson 2013
55944.8923	0.00040	25.5	0.00318	Diethelm 2012
56002.6601	0.00100	147.5	–0.00087	Hübscher 2013
56029.6547	0.00020	204.5	0.00197	Diethelm 2012
56311.8814	0.00020	800.5	–0.00098	Diethelm 2013
56706.5770	0.00460	1634.0	–0.00070	Hübscher and Lehmann 2015
56709.4202	0.00040	1640.0	0.00126	Hübscher and Lehmann 2015
56711.3104	0.00110	1644.0	–0.00270	Hübscher and Lehmann 2015
56728.5957	0.00010	1680.5	–0.00160	Hübscher 2016
57029.7681	0.00020	2316.5	–0.00043	Samolyk 2016b
57030.0043	0.00120	2317.0	–0.00100	Samolyk 2016b
57035.4491	0.00070	2328.5	–0.00191	Hübscher 2016
57035.6872	0.00020	2329.0	–0.00058	Hübscher 2016
57067.8880	0.00004	2397.0	–0.00050	Present paper
57072.8604	0.00004	2407.5	–0.00024	Present paper
57090.3807	0.00070	2444.5	–0.00091	Hübscher 2016
57121.3985	0.00100	2510.0	0.00004	Hübscher 2017
57132.5256	0.00010	2533.5	–0.00104	Hübscher 2017
57386.1063	—	3069.0	–0.00084	Nagai 2016
57386.3447	—	3069.5	0.00079	Nagai 2016
57415.7038	0.00010	3131.5	0.00043	Samolyk 2016a
57423.2811	—	3147.5	0.00109	Juryšek 2017
57444.8263	0.00010	3193.0	0.00027	Present paper
57445.7734	0.00009	3195.0	0.00024	Present paper
57446.7205	0.00012	3197.0	0.00026	Present paper
57465.4249	0.00250	3236.5	–0.00014	Hübscher 2017
57449.7989	0.00012	3203.5	0.00066	Present paper
57451.6929	0.00012	3207.5	0.00053	Present paper
57474.4227	—	3255.5	0.00041	Juryšek 2017
57498.5735	0.00400	3306.5	0.00069	Samolyk 2016b
57807.7963	0.00004	3959.5	0.00208	Present paper

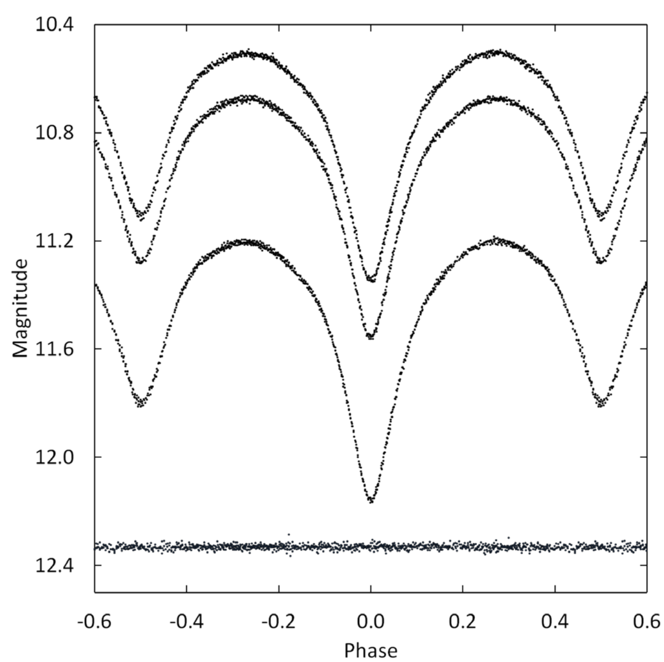

Figure 2. Folded light curves for each observed passband. The differential magnitudes of the variable were converted to standard magnitudes using the calibrated magnitudes of the comparison stars. From top to bottom the light curve passbands are Sloan i', Sloan r', Sloan g'. The bottom curve shows the Sloan r' magnitudes of the check star (offset +0.7 magnitudes). The standard deviations of the check star magnitudes (all nights) are shown in Table 1. Error bars are not shown for clarity.

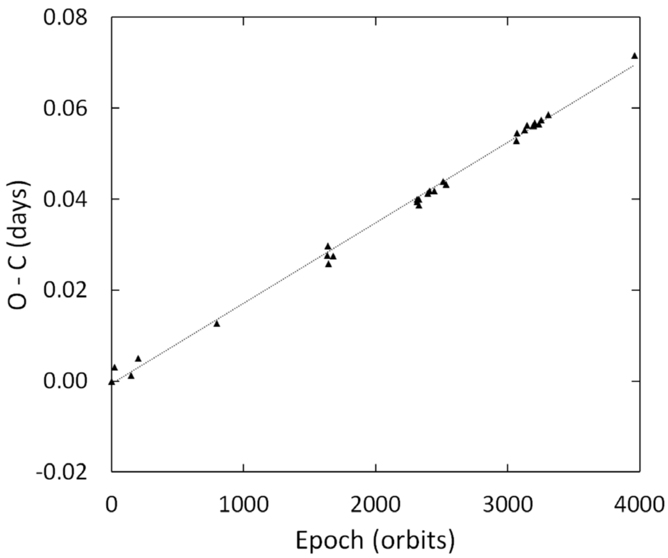

Figure 3. The O–C residuals from Equation 1 with the dotted line the linear ephemeris fit of Equation 2.

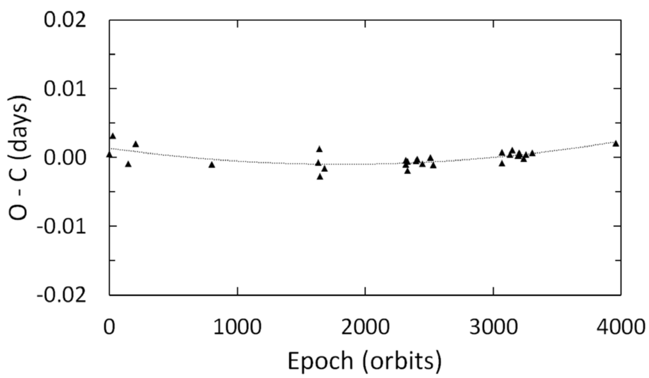

Figure 4. The O–C residuals from Equation 2 with the dotted line the quadratic ephemeris fit of Equation 3.

= 0.021 ± 0.052, was determined from Schlafly's (2014) map of interstellar reddening. This gives the secondary star's color as (B–V) = 0.733 ± 0.054 and an effective temperature of T_{eff} = 5497 ± 171K (Pecaut and Mamajek 2013). This value agrees well with the effective temperature determined from LAMOST spectral survey data, T_{eff} = 5493 ± 241K (Sichervskij 2017). Assuming the secondary is a main-sequence star, the corrected color index gives a spectral type of G8 (Table 5 of Pecaut and Mamajek 2013).

4.2. Synthetic light curve modeling

For light curve modeling, the Sloan g', r', and i' observations acquired in 2016 were binned in both phase and magnitude. A bin phase width of 0.005 was used which resulted in five observations per bin on average. The binned magnitudes were converted to relative flux for modeling. A preliminary fit to each individual light curve was made using BINARY MAKER 3.0 (BM3; Bradstreet and Steelman 2002). Standard convective parameters and tabulated limb darkening coefficients determined by the effective temperatures were utilized in the models. Once a reasonable fit was made for each light curve, the resulting stellar parameters were averaged. These parameters were used as the

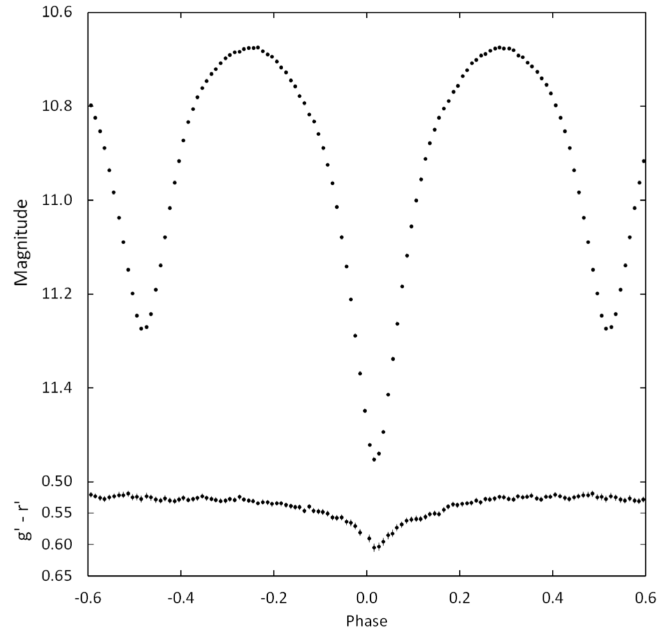

Figure 5. Light curve of all r'-band observations in standard magnitudes (top panel). The observations were binned with a phase width of 0.01. The errors for each binned point are about the size of the plotted points. The g'–r' colors were calculated by subtracting the binned Sloan g' magnitudes from the linearly interpolated binned Sloan r' magnitudes.

initial values for computation of a simultaneous three-color light curve solution using the Wilson-Devinney program (WD; Wilson and Devinney 1971; van Hamme and Wilson 1998). Mode 3, the contact configuration, was set in this program. A common convective envelope was assumed. The weight assigned to each input data point was equal to the number of observations that formed that point. The Method of Multiple Subsets (MMS) was utilized to minimize strong correlations, and the Kurucz stellar atmosphere model was applied (Wilson and Biermann 1976). For fixed inputs, the effective temperature of the secondary star was set to T_2 = 5497 K (see section 4.1) and standard convective values for gravity darkening and albedo, $g_1 = g_2 = 0.32$ (Lucy 1968) and $A_1 = A_2 = 0.5$ (Ruciński 1969), respectively. Logarithmic limb darkening coefficients were calculated by the program from tabulated values using the method of van Hamme (1993). The adjustable parameters include the inclination (i), mass ratio ($q = M_2/M_1$), potential (Ω), temperature of the primary star (T_1), the normalized flux for each wavelength (L), and third light (ℓ). To determine the system's approximate mass ratio (q), a series of WD solutions were made using fixed values that ranged from 0.4 to 2.8 with a step size of 0.10. Figure 6 shows the result of this q-search, which gave a minimum residual value for a mass ratio of 1.7. This value was used as the starting point for the final solution iterations where the mass ratio was a free parameter. The final WD solution parameters are listed in column 2 of Table 3. No third light was seen in the solution. Only negligible or negative values resulted when included as an adjustable parameter. The filling-factor in Table 3 was computed using

$$f = \frac{\Omega_{inner} - \Omega}{\Omega_{inner} - \Omega_{outer}}, \qquad (5)$$

where Ω_{inner} and Ω_{outer} are the inner and outer critical equipotential

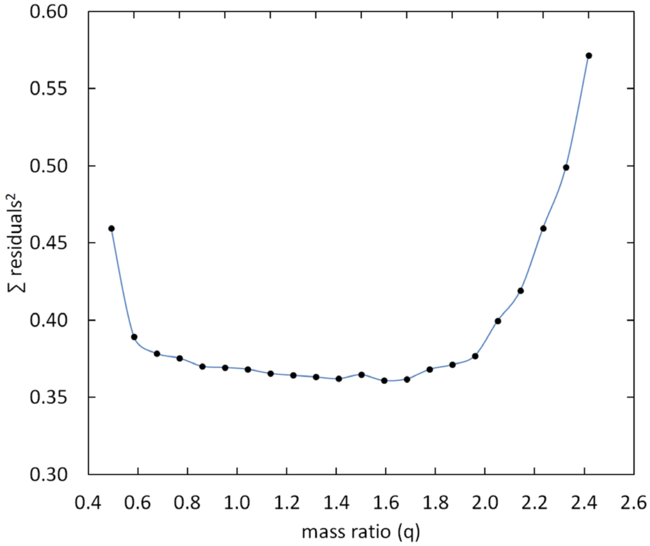

Figure 6. Results of the q-search showing the relation between the sum of the residuals squared and the mass ratio q.

Table 3. Results derived from light curve modeling.

Parameter	*Solution 1 (no spots)*	*Solution 2 (2 spots)*
phase shift	0.0005 ± 0.0002	0.0005 ± 0.0001
i (°)	82.0 ±0.2	81.9 ±0.2
T_1 (K)	6117 ±12	6053 ±20
T_2 (K)	* 5497	* 5497
$\Omega_1 = \Omega_2$	4.76 ± 0.05	4.75 ± 0.01
q(M2/M1)	1.72 ± 0.04	1.71 ± 0.01
filling factor	13%	13%
$L_1 / (L_1 + L_2)$ (g')	0.526 ±0.002	0.523 ±0.003
$L_1 / (L_1 + L_2)$ (r')	0.488 ±0.002	0.485 ±0.002
$L_1 / (L_1 + L_2)$ (i')	0.471 ±0.002	0.470 ±0.002
r_1 side	0.3225 ±0.0012	0.3309 ±0.0006
r_2 side	0.5233 ±0.0104	0.4391 ±0.0024
$\sum res^2$	0.318	0.060
Spot Parameters	—	*Star 1—cool spot*
colatitude (°)	—	112 ± 17
longitude (°)	—	359 ± 1
spot radius (°)	—	34 ± 7
Temp.-factor	—	0.95 ± 0.04
Spot Parameters		*Star 2—hot spot*
colatitude (°)	—	78 ± 6
longitude (°)	—	0.2 ± 0.2
spot radius (°)	—	34 ± 5
Temp.-factor	—	1.10 ± 0.02

** Assumed.*

The subscripts 1 and 2 refer to the star being eclipsed at primary and secondary minimum, respectively.

Note: The errors in the stellar parameters result from the least squares fit to the model. The actual uncertainties of the parameters are considerably larger (T1 and T2 have uncertainties of about ± 170 K).

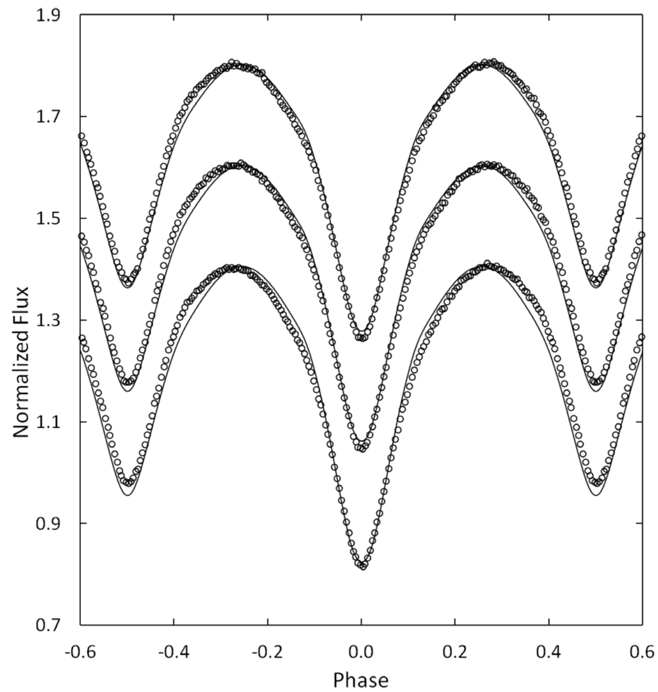

Figure 7. The WD model fit without spots (solid curve) to the observed normalized flux curves for each passband. From top to bottom the passbands are Sloan i', Sloan r', and Sloan g'. Each curve is offset by 0.2 for this combined plot. The best-fit parameters are given in column 2 of Table 3. Error bars are omitted from the points for clarity.

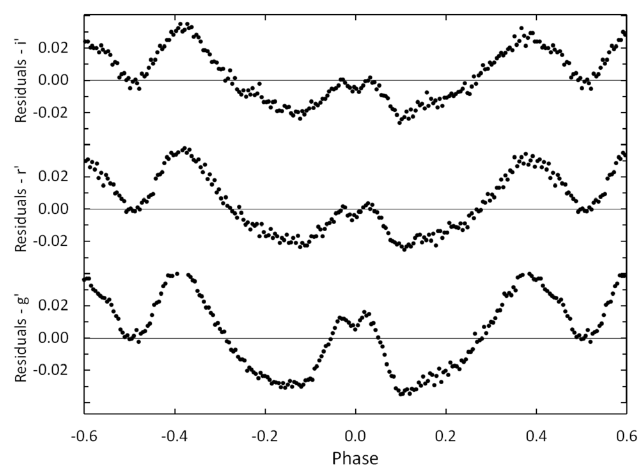

Figure 8. The residuals for the best-fit WD model without spots. Error bars are omitted from the points for clarity.

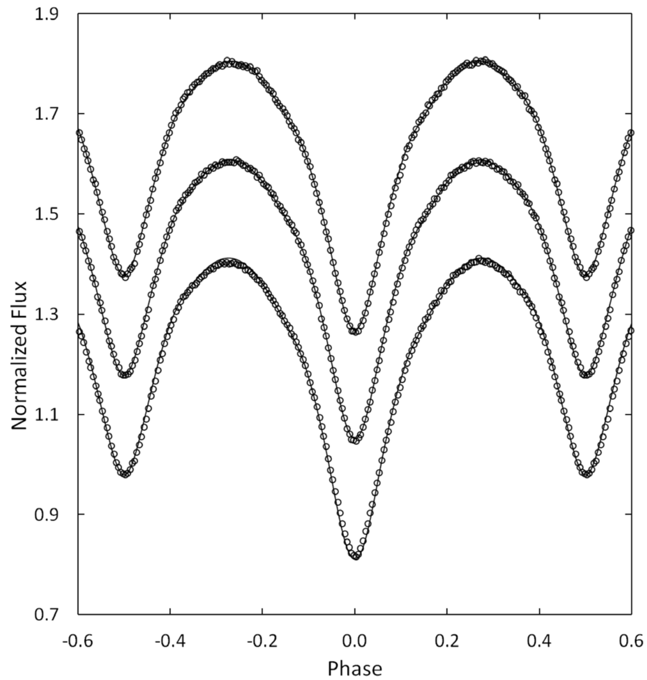

Figure 9. The WD model fit with spots (solid curve) to the observed normalized flux curves for each passband. From top to bottom the passbands are Sloan i', Sloan r', and Sloan g'. Each curve is offset by 0.2 for this combined plot. The best-fit parameters are given in column 3 of Table 3. Error bars are omitted from the points for clarity.

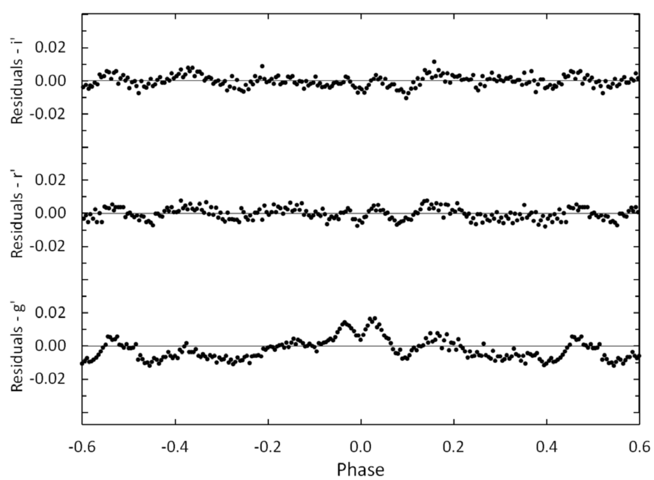

Figure 10. The residuals for the spotted WD model in each passband. Error bars are omitted from the points for clarity.

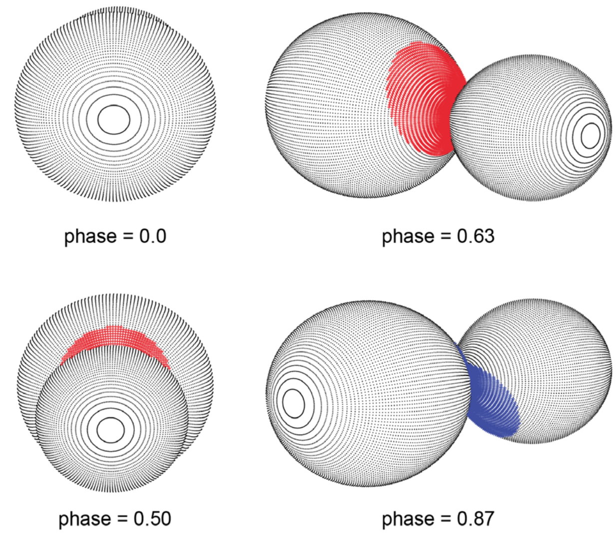

Figure 11. Roche Lobe surfaces of the best-fit WD spot model with orbital phase shown below each diagram.

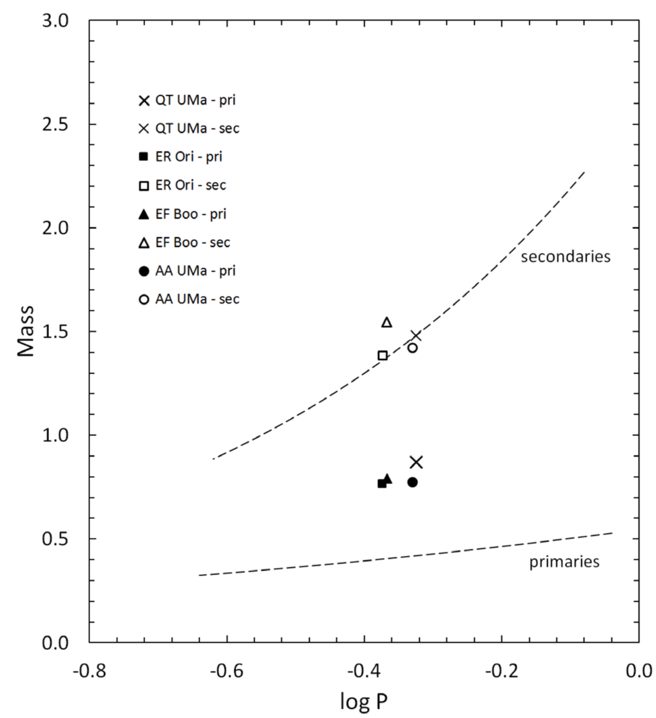

Figure 12. Comparison of the primary and secondary masses of four contact binaries. The dashed lines are the primary and secondary star period-mass relations for contact binaries (Gazeas and Stępień 2008). The masses are in solar units.

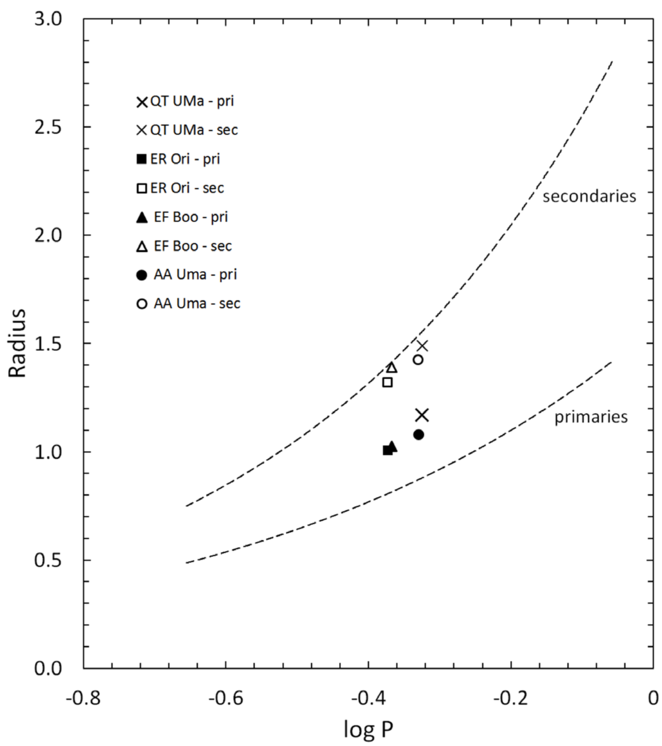

Figure 13. Comparison of the primary and secondary radii of four contact binaries. The dashed lines are the primary and secondary star period-radius relations for contact binaries (Gazeas and Stępień 2008). The radii are in solar units.

surfaces that pass through the Lagrangian points L_1 and L_2 and Ω is the equipotential surface which describes the stellar surface (Lucy and Wilson 1979). The normalized light curves for each passband, overlaid by the synthetic solution curves, are shown in Figure 7 with the residuals shown in Figure 8.

4.3. Spot model

Considerable asymmetries are apparent in the light curves. These are usually attributed to cool spots or hot spots such as faculae on the stars. Best seen in the residuals of Figure 8, there are two broad regions where the observations deviate from the synthetic light curves. First, there is excess light centered on secondary eclipse ($\varphi = 0.5$) with a phase width of approximately 0.2. This indicates a possible over luminous region on the cooler secondary star located near the line of centers between the two stars. The second region is under luminous and is centered on primary eclipse with a phase width of 0.8. This would indicate a possible cool spot located on the hotter primary star, also near the line of centers. Using BM3, two spots were modeled in these two locations. The resulting best-fit spot parameters of latitude, longitude, size, and temperature-factor were then incorporated into a new WD model. Initially the stellar parameters in the WD solution iterations were held fixed, with only the lights and spot parameters adjusted. Once this solution converged, the spot parameters were then held fixed and the stellar parameters adjusted until the solution converged again. This process was repeated until the model converged to a final solution. The new spotted solution parameters are listed in column 3 of Table 3. The normalized light curves overlaid by the synthetic solution curves are shown in Figure 9 and the residuals in Figure 10. The residuals are 5.3 times smaller compared to the spotless solution

Table 4. Estimated absolute parameters for QT UMa.

Parameter	*Symbol*	*Value*
Stellar masses	M_1 ($M_\odot$)	0.87 ± 0.07
	M_2 ($M_\odot$)	1.48 ± 0.11
Semi-major axis	a ($R_\odot$)	3.40 ± 0.01
Mean stellar radii	R_1 ($R_\odot$)	1.17 ± 0.01
	R_2 ($R_\odot$)	1.49 ± 0.02
Stellar luminosity	L_1 ($L_\odot$)	1.66 ± 0.11
	L_2 ($L_\odot$)	1.82 ± 0.17
Bolometric magnitude	$M_{bol,1}$	4.21 ± 0.12
	$M_{bol,2}$	4.10 ± 0.19
Surface gravity	log g_1 (cgs)	4.24 ± 0.03
	log g_2 (cgs)	4.26 ± 0.04
Mean density	$\bar{\rho}_1$ (g cm^{-3})	0.76 ± 0.04
	$\bar{\rho}_2$ (g cm^{-3})	0.63 ± 0.07

The calculated values in this table are provisional. Radial velocity observations are necessary for direct determination of M_1, M_2, and a.

with a much improved fit between the synthetic and observed light curves. The Roche lobe surfaces from this solution are displayed in Figure 11.

5. Discussion and conclusions

Radial velocity measurements are not available for this star, but the absolute mass of the more massive secondary star (M2) can be estimated from the orbital period. The period-mass relation for contact binaries,

$$M_2 = (0.755 \pm 0.059) \log P + (0.416 \pm 0.024), \qquad (6)$$

gives a provisional mass for the secondary star of $M_2 = 1.48 \pm 0.11 M_\odot$ (Gazeas and Stępień 2008). The remaining absolute parameter values can now be determined. Combining the secondary star's mass with the mass ratio from the spotted solution gives the primary star's mass as $M_1 = 0.87 \pm 0.07 M_\odot$. Kepler's Third Law gives a distance of $3.398 \pm 0.007 R_\odot$ between the mass centers of the two stars. The WD light curve program (LC) computed the stellar radii, surface gravities, and bolometric magnitudes. The mean stellar densities were determined from the following equations,

$$\bar{\rho}_1 = \frac{0.0189}{r_1^3\,(1+q)\,P^2} \quad \text{and} \quad \bar{\rho}_2 = \frac{0.0189q}{r_2^3\,(1+q)\,P^2}, \qquad (7)$$

where the stellar radius is normalized to the semi-major axis and P is in days (Mochnacki 1981). Table 4 contains all the calculated stellar parameter values. To assess the reasonableness of the masses, radii and the mass ratio found in this study, it is useful to compare QT UMa to a number of similar contact binaries. Figure 12 shows the period-mass relation and Figure 13 the period-radius relation for contact binaries (dashed lines) (Gazeas and Stępień 2008). The primary and secondary stars of QT UMa are indicated with an "X" in both figures. The primary star is more massive than predicted by the period-mass relation and slightly larger than predicted by the period-radius relation. Also included in Figures 12 and 13 are the masses and radii of three contact binaries (ER Ori, EF Boo, and AA UMa) that are very similar to QT UMa in terms of orbital period, primary and secondary masses, mass ratio,

Table 5. Comparison of QT UMa with similar W-type contact binaries.

Star	*Period (d)*	M_1	M_2	*q*	R_1	R_2	M_V	*References*
QT UMa	0.4735	0.872	1.490	1.707	1.172	1.320	3.86	—
ER Ori	0.4234	0.765	1.385	1.812	1.007	1.392	3.69	1, 2, 3
EF Boo	0.4295	0.792	1.547	1.953	1.026	1.424	3.46	1, 2, 3
AA UMa	0.4680	0.773	1.419	1.835	1.079	1.653	3.87	1, 2, 3

The masses and radii are in solar units ($M_\odot$ and $R_\odot$). References: 1. Gazeas and Stępień 2008; 2. Ammons et al. 2006; 3. Gaia Collaboration et al. 1, 2016.

radii, and absolute magnitudes. Listed in Table 5 are the well-determined geometrical and physical properties of these three stars. The absolute magnitudes in the table were calculated using Gaia parallaxes for distance with the observed visual apparent magnitudes corrected for extinction. The radius and mass of QT UMa are in good agreement with the properties of these three stars. The current evolutionary state of all four stars and their evolutionary histories may be very similar.

The O–C residuals in Figure 4 indicates the orbital period of QT UMa is increasing. The quadratic least-squares solution gives a period change rate of $dP/dt = 1.10(0.22) \times 10^{-6}\,d\,yr^{-1}$ (about 9.5 seconds per century), which is quite rapid compared to other binaries of this type. This result should be considered preliminary, given that the available times of minima only span five years. If this is a secular period change, then it likely results from conservative mass exchange from the lower mass primary star to the more massive secondary. In this case the rate of mass exchange would be $1.6\,(0.4) \times 10^{-6}\,M_\odot\,yr^{-1}$. The observed period change could also result from light time effects as the binary orbits a third body. The O–C curve in Figure 4 may only be a portion of a sinusoidal ephemeris. Additional precision times of minima over several years would be invaluable in confirming the existence of the period change and in determining its cause. The study confirms QT UMa is a W-type eclipsing binary with the larger cooler secondary star eclipsing the smaller hotter star at primary minimum. As is typical for this class of stars, the primary star is over luminous compared to a single main-sequence star of the same mass. The WD solution gives a fill-out of 13%, which is consistent with a contact binary. The primary and secondary stars have spectral types of F9 and G8, respectively. The temperature difference of 556 K between the stars may indicate poor thermal contact. A future spectroscopic study of this system would provide the radial velocity measurements necessary for direct determination of the stellar masses.

6. Acknowledgements

This research was made possible through the use of the AAVSO Photometric All-Sky Survey (APASS), funded by the Robert Martin Ayers Sciences Fund. This research has made use of the SIMBAD database and the VizieR catalogue access tool, operated at CDS, Strasbourg, France.

References

Ammons, S. M., Robinson, S. E., Strader, J., Laughlin, G., Fischer, D., and Wolf, A. 2006, *Astrophys. J.*, **638**, 1004.

Astraatmadja, T. L., and Bailer-Jones, C. A. L. 2016, *Astrophys. J.*, **833**, 119.

Bradstreet, D. H., and Steelman, D. P. 2002, *Bull. Amer. Astron. Soc.*, **34**, 1224.

Diethelm, R. 2012, *Inf. Bull. Var. Stars*, No. 6029, 1.

Diethelm, R. 2013, *Inf. Bull. Var. Stars*, No. 6063, 1.

Gaia Collaboration, *et al.* 2016, *Astron. Astrophys.*, **595**, A2.

Gazeas, K., and Stępień, K. 2008, *Mon. Not. Roy. Astron. Soc.*, **390**, 1577.

Henden, A. A., *et al.* 2015, AAVSO Photometric All-Sky Survey, data release 9, (https//:www.aavso.org/apass).

Hoffman, D. I., Harrison, T. E., and McNamara, B. J. 2009, *Astron. J.*, **138**, 466.

Hübscher, J. 2013, *Inf. Bull. Var. Stars*, No. 6084, 1.

Hübscher, J. 2016, *Inf. Bull. Var. Stars*, No. 6157, 1.

Hübscher, J. 2017, *Inf. Bull. Var. Stars*, No. 6196, 1.

Hübscher, J., and Lehmann, P. B. 2015, *Inf. Bull. Var. Stars*, No. 6149, 1.

Jester, S. *et al.* 2005, *Astron. J.*, **130**, 873.

Juryšek, J. *et al.* 2017, *Open Eur. J. Var. Stars*, **179**, 135.

Kafka, S. 2016, variable star observations from the AAVSO International Database, (https://www.aavso.org/aavso-international-database).

Lucy, L. B. 1968, *Astrophys. J.*, **151**, 1123.

Lucy, L. B., and Wilson, R. E. 1979, *Astrophys. J.*, **231**, 502.

Luo, A-Li, *et al.* 2015, *Res. Astron. Astrophys.*, **15**, i.d. 1095.

Mirametrics. 2015, Image Processing, Visualization, Data Analysis, (http://www.mirametrics.com).

Mochnacki, S. W. 1981, *Astrophys. J.*, **245**, 650.

Nagai, K. 2016, *Bull. Var. Star Obs. League Japan*, No. 61, 7.

Nelson, R. H. 2013, *Inf. Bull. Var. Stars*, No. 6050, 1.

Otero, S. A., Wils, P., and Dubovsky, P. A. 2004, *Inf. Bull. Var. Stars*, No. 5570, 1.

Pecaut, M. J., and Mamajek, E. E. 2013, *Astrophys. J., Suppl. Ser.*, **208**, 9 (http://www.pas.rochester.edu/~emamajek/EEM_dwarf_UBVIJHK_colors_Teff.txt).

Ruciński, S. M. 1969, *Acta Astron.*, **19**, 245.

Samolyk, G. 2016a, *J. Amer. Assoc. Var. Star Obs.*, **44**, 69.

Samolyk, G. 2016b, *J. Amer. Assoc. Var. Star Obs.*, **44**, 164.

Schlafly, E. F., *et al.* 2014, *Astrophys. J.*, **789**, 15 (http://faun.rc.fas.harvard.edu/eschlafly/2dmap/querymap.php).

Sichervskij, S. G. 2017, *Astrophys. Bull.*, **72**, 51.

van Hamme, W. 1993, *Astron. J.*, **106**, 2096.

van Hamme, W., and Wilson, R. E. 1998, *Bull. Amer. Astron. Soc.*, **30**, 1402.

Wilson, R. E., and Biermann, P. 1976, *Astron. Astrophys.*, **48**, 349.

Wilson, R. E., and Devinney, E. J. 1971, *Astrophys. J.*, **166**, 605.

Wozniak, P. R., *et al.* 2004, *Astron. J.*, **127**, 2436.

Observations and Analysis of the Extreme Mass Ratio, High Fill-out Solar Type Binary, V1695 Aquilae

Ronald G. Samec
Christopher R. Gray
Natural Sciences Department, Emmanuel College,181 Springs Street, Franklin Springs, GA 30639; ronaldsamec@gmail.com

Daniel Caton
Dark Sky Observatory, Department of Physics and Astronomy, Appalachian State University, 525 Rivers Street, Boone, NC 28608

Danny R. Faulkner
Johnson Observatory, 1414 Bur Oak Court, Hebron, KY 41048

Robert Hill
Department of Chemistry and Physics, Bob Jones University, 1700 Wade Hampton Boulevard, Greenville, SC 29614

Walter Van Hamme
Department of Physics, Florida International University,11200 SW 8th Street, CP 204, Miami, FL 33199

Received June 28, 2017; revised August 8, 2017; accepted August 14, 2017

Abstract CCD BVR_cI_c light curves of V1695 Aquilae were taken during the Fall 2016 season at the Cerro Tololo InterAmerican Observatory with the 0.6-meter reflector of the SARA South observatory in remote mode. It is an eclipsing binary with a period of 0.41283 d. The light curves yield a total eclipse (duration: 59 minutes) but have an amplitude of only ~0.4 mag. The spectral type is ~G8V (~5500 K). Four times of minimum light were calculated, all primary eclipses, from our present observations. We calculated linear and quadratic ephemerides from all available times of minimum light. A 17-year period study reveals a quadratic orbital period decrease at a high level of confidence. The orbital period is changing at a rapid rate of of $dp/dt = -1.73 \times 10^{-6}$ d/yr. The solution is that of an Extreme Mass Ratio Binary. The mass ratio is found to be near 0.16. Its Roche Lobe fill-out is a hefty 83%. The small component has the slightly hotter temperature of ~5650 K, which makes it a W-type W UMa Binary. As expected in binaries of this spectral type, it has cool spot regions.

1. Introduction

In this study of V1695 Aql, our analysis includes its observation, a period study, and light curve analysis of an extreme mass ratio solar type Southern eclipsing binary. We used the Wilson-Devinney Program (WD; Wilson and Devinney 1971) for this calculation. This paper represents the first published BVRcIc light curves and analysis of V1695 Aql. Observers prize total eclipsing contact binaries since they give unambiguous solutions with mass ratios even without difficult-to-obtain precision radial velocity curves. These require large telescopes (we estimate a 3.5 to 4-meter telescope is needed for this variable). Many forget about velocity smearing with such a system which requires a higher signal-to-noise.

Contact binaries are numerous in number and represent a challenge to present-day stellar theory. It is believed that (for those of solar type), that they begin their existence as well detached fast spinning stars in groups that undergo gravitational interactions which leave them as binaries with several-day periods. Since they are highly magnetic in nature, due to their convective envelopes and fast rotation, they undergo magnetic braking as plasma winds leave the stars on stiff rotating dipole fields. This action torques the binary, eventually bringing them into contact and finally leaving a single, fast rotating star.

2. History and observations

V1695 Aql (GSC 5149 2845) was discovered as part of an initiative to classify variable stars using CCD observations by Bernhard *et al.* (2002). The star was typed as a W UMa binary with a V magnitude ≈11.0. Their light curve is shown as Figure 1.

Their ephemeris is:

$$\text{MinI} = \text{HJD } 2452522.440 \pm 0.007 + 0.4128 \pm 0.0001 \text{ d} \times E \quad (1)$$

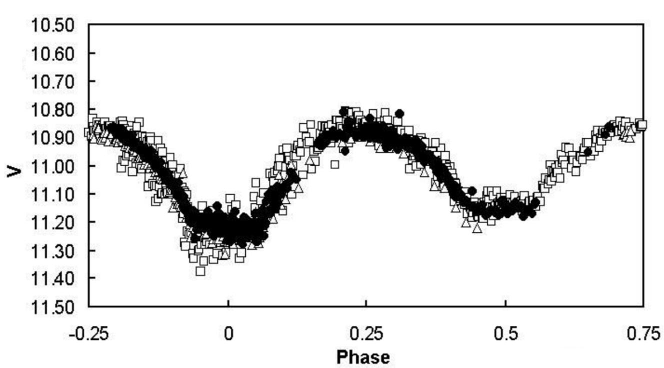

Figure 1. Light curve of V1695 Aql by Bernhard *et al.* 2002.

Kreiner (2004) gives the following:

$$\text{MinI} = \text{HJD } 2456102.460 + 0.4127768 \text{ d} \times E \quad (2)$$

A number of eclipse timings are given by Pejcha (2005), Berhard *et al.* (2002), and Paschke (1994, 2002).

V1695 Aql is likely an x-ray source (1RXSJ193821.2-033245), which is not unusual for active W UMa variables (Szczygiel *et al.* 2008). It is included in the Automated Variable Star classification (ID 14143847) via the NSVS (Hoffman *et al.* 2009) and is listed in the 78th name list (Kazarovets *et al.* 2006). The observations were undertaken by Samec, Gray, Faulkner, Hill, and Van Hamme. Reduction and analyses were done by Samec and Gray.

3. Photometry

Our photometry was taken with the Southeastern Association for Research in Astronomy (SARA South) Telescope at Cerro Tololo InterAmerican Observatory (CTIO) in remote mode. The 24-inch f/11 Boller and Chivens reflector was used on four nights, 14 August and 3–5 September, 2016, with the ARC Camera cooled to –60° C. We used standard BVR_cI_c Johnson-Cousins filters. The precision of a single observation was good, 0.010 in B, V, I_c, and 0.014 in R_c. The observations included 185 in B, 187 in V, 162 in R_c, and 187 in I_c. Exposure times varied from 250–275 seconds in B, 80–90 seconds in V, and 30–50 seconds in R_c and I_c. Nightly images were calibrated with 25 bias frames, at least five flat frames in each filter, and ten 300-second dark frames. Figure 2a and 2b show sample observations of B, V, and B–V color curves on the night of August 14 and September 23, 2016. Our observations are given in Table 1, in delta magnitudes, ΔB, ΔV, ΔR_c, and ΔI_c, in the sense of variable minus comparison star.

4. Finding chart

The finding chart is shown as Figure 3. The coordinates and magnitudes of the variable star, comparison star, and check star are given in Table 2. Our B–V and R_c–I_c Comparison-Variable magnitude curves show that the variable and comparison stars are near spectral matches with Δ(B–V) and Δ (R–I) ≈ 0. The nightly C–K values stayed constant throughout the observing run with a precision of $\approx 1\%$.

5. Period study

Four times of minimum light were calculated from our present observations, all primary eclipses, using the method of Kwee and Van Woerden (1956) performed by Caton:

$$\begin{aligned}\text{HJD} = \;& 2457614.68359 \pm 0.0002 \text{ d}\\ & 2457634.49320 \pm 0.00037 \text{ d}\\ & 2457636.56250 \pm 0.00006 \text{ d}\\ & 2457635.68247 \pm 0.00002 \text{ d}\end{aligned}$$

Additional timings were gathered from other sources using the O–C gateway (http://var2.astro.cz/ocgate/) and the Nelson Database of Times of Minima (Nelson 2016). These included Berhard *et al.* (2002), and Pejcha (2005). We note that our last timing was removed from our analysis due to its large residual. The following linear and quadratic ephemerides were determined from all available times of minimum light:

$$\begin{aligned}\text{JD Hel MinI} = \;& 2452576.3106 \pm 0.0060 \text{ d}\\ & + 0.41282964 \pm 0.00000080 \times E \quad (2)\end{aligned}$$

$$\begin{aligned}\text{JD Hel MinI} = \;& 2452576.3191 \pm 0.0024 \text{ d}\\ & + 0.4128401 \pm 0.0000011 \times E - 9.75 \pm 1.0 \times 10^{-10} \times E^2 \quad (3)\end{aligned}$$

The O–C residuals for both linear and quadratic calculations are given in Table 3. Thus, the 17-year period study reveals that the system is undergoing a smooth quadratic decrease in orbital period. The changing period would be expected for the process of magnetic braking (e.g., Gazeas and Stępień 2008). The value of the rate of change in the orbital period is $dp/dt = -1.73 \times 10^{-6}$ d/yr. Third body interactions and normal stellar evolution may play a role, but a much longer interval of observation is needed to determine if this is the case. A plot of the quadratic term overlying the linear residuals of Equation 3 is shown in Figure 4.

6. Light curve characteristics

The light curves of V1695 Aql phased using Equation 2, delta mag vs. phase, are shown in Figure 5a and 5b. Light curve amplitudes and the differences in magnitudes at various quadratures are given in Table 4. The primary amplitudes of the light curves are about 0.4 magnitude in all filters while the secondary's are ~ 0.3 magnitude. This points to a rather large difference in minima, 0.07–0.08 magnitude, for an over contact binary. These values are usually thought of as indicators of the degree of thermal contact. In this case, it may be an indicator of large spot regions. In general, the asymmetries throughout the light curve point to the presence of spot activity. This is apparent when we compare the early curve (Figure 1) to our present ones. In Figure 6, a plot of the night to night variability in the light curves in B and V is given. This shows that the magnetic activity causes rapid changes in the light curves. The light curves are distinctly over contact. The low amplitudes indicate that the binary has a very small mass ratio so the binary belongs to the family of extreme-mass ratio binaries. To extend this analysis we undertook a Wilson-Devinney program light curve solution. The light curves yielded a very long eclipse duration of 59 minutes for a binary, with a period of 9.9 hours as determined from this solution.

7. Temperature and light curve solution

BINARY MAKER 3.0 (Bradstreet and Steelman 2002) was used to explore the character of our light curves and determine initial parameters of each of the B, V, Rc, Ic light curves. The Wilson-Deviney program requires a fairly good fitting curve to begin the process, however the final solution parameters may have little resemblance to the initial values. For instance, our B-filter light curve gave a mass-ratio of 0.15 using BINARY

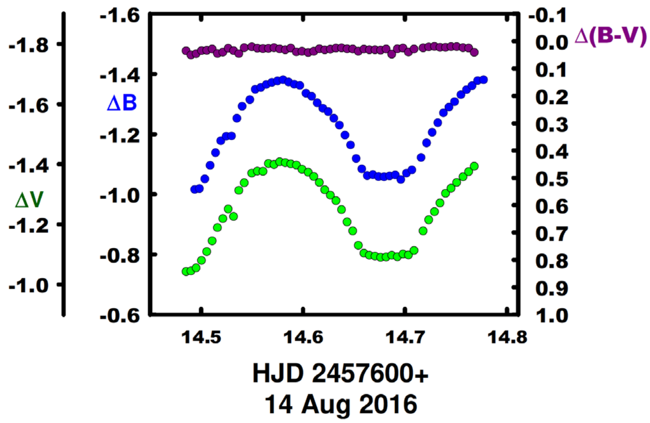

Figure 2a. B, V, and B–V color curves of V1695 Aql on the night of August 14, 2016.

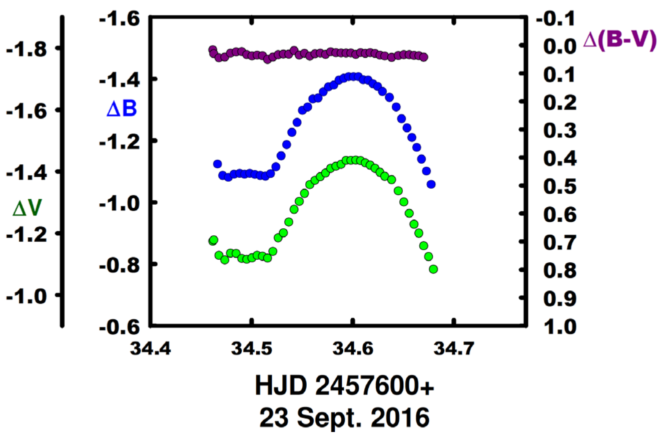

Figure 2b. B, V, and B–V color curves of V1695 Aql on the night of September 23, 2016.

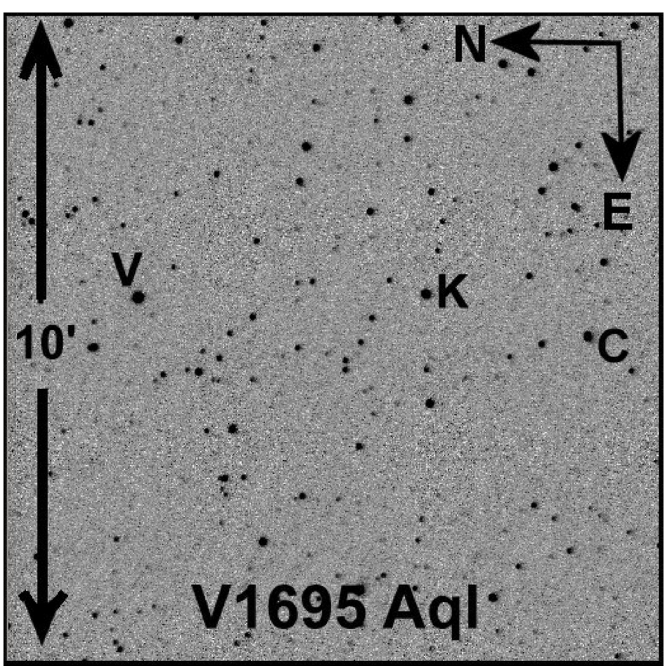

Figure 3. Finding Chart of V1695 Aql including Variable (V), Comparison (C), and Check Stars (K).

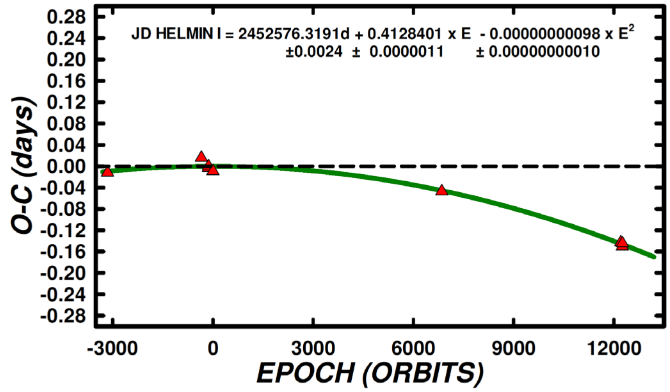

Figure 4. O–C residuals from the quadratic ephemeris of V1695 Aql from Equation 3.

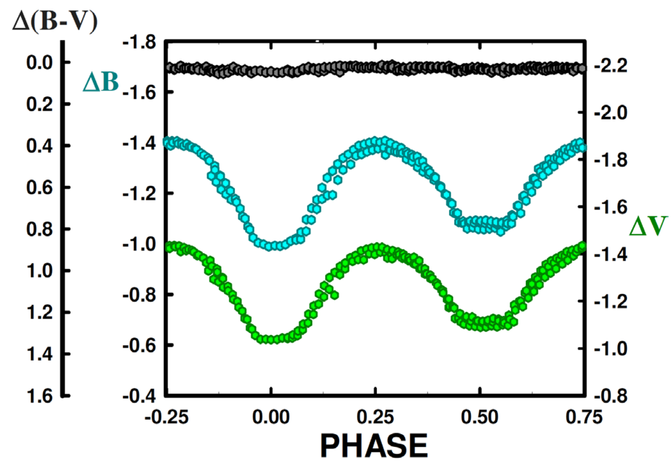

Figure 5a. B, V delta magnitudes of V1695 Aql, phased using Equation 2.

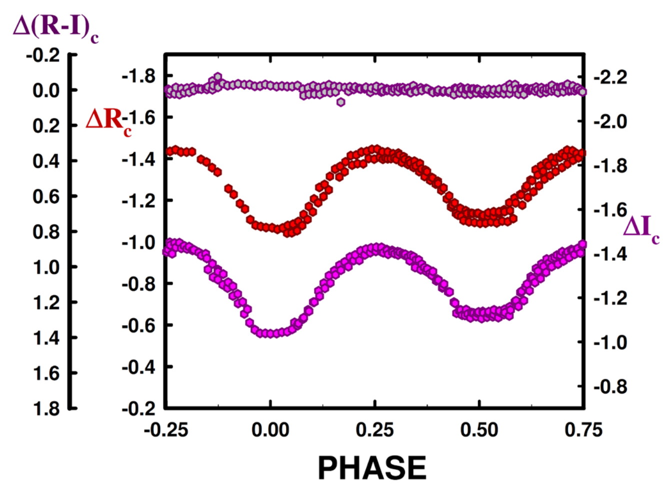

Figure 5b. R_c, I_c delta magnitudes of V1695 Aql, phased using Equation 2.

Table 1. V1695 Aql observations, ΔB, ΔV, ΔR_c, and ΔI_c, variable star minus comparison star.

ΔB	HJD 2457600+	ΔB	HJD 2457600+	ΔB	HJD 2457600+	ΔB	HJD 2457600+	ΔB	HJD 2457600+
–1.042	14.4856	–1.093	14.6709	–1.258	34.538	–1.415	35.604	–1.138	36.549
–1.044	14.4903	–1.089	14.676	–1.297	34.543	–1.418	35.609	–1.137	36.554
–1.054	14.4954	–1.090	14.682	–1.347	34.548	–1.432	35.615	–1.121	36.560
–1.079	14.5006	–1.096	14.687	–1.365	34.553	–1.435	35.620	–1.123	36.565
–1.108	14.5058	–1.091	14.693	–1.381	34.559	–1.445	35.625	–1.123	36.571
–1.144	14.5111	–1.100	14.698	–1.404	34.564	–1.446	35.630	–1.145	36.576
–1.188	14.5163	–1.097	14.704	–1.405	34.569	–1.433	35.635	–1.145	36.582
–1.218	14.5216	–1.112	14.709	–1.424	34.574	–1.433	35.640	–1.151	36.587
–1.250	14.5268	–1.177	14.718	–1.441	34.579	–1.424	35.646	–1.187	36.593
–1.312	14.5373	–1.214	14.724	–1.438	34.585	–1.427	35.651	–1.226	36.598
–1.337	14.5425	–1.241	14.729	–1.256	35.483	–1.410	35.656	–1.269	36.604
–1.369	14.5500	–1.270	14.735	–1.228	35.488	–1.391	35.661	–1.294	36.609
–1.376	14.5554	–1.302	14.740	–1.184	35.494	–1.388	35.667	–1.322	36.614
–1.375	14.5609	–1.319	14.746	–1.158	35.499	–1.377	35.672	–1.339	36.620
–1.401	14.5663	–1.338	14.751	–1.107	35.505	–1.345	35.678	–1.367	36.625
–1.398	14.5718	–1.357	14.757	–1.080	35.510	–1.310	35.684	–1.382	36.631
–1.407	14.5773	–1.374	14.763	–1.074	35.515	–1.292	35.690	–1.406	36.636
–1.404	14.5828	–1.392	14.768	–1.069	35.520	–1.397	36.461	–1.413	36.642
–1.400	14.5882	–1.404	14.774	–1.068	35.526	–1.399	36.466	–1.416	36.647
–1.396	14.5937	–1.168	34.465	–1.060	35.531	–1.404	36.473	–1.425	36.653
–1.382	14.5992	–1.137	34.469	–1.067	35.537	–1.418	36.478	–1.427	36.658
–1.372	14.6052	–1.123	34.475	–1.079	35.542	–1.397	36.483	–1.435	36.664
–1.358	14.6107	–1.137	34.480	–1.085	35.547	–1.379	36.489	–1.443	36.669
–1.338	14.6162	–1.137	34.486	–1.098	35.552	–1.365	36.494	–1.432	36.675
–1.314	14.6216	–1.138	34.491	–1.132	35.557	–1.351	36.500	–1.432	36.680
–1.296	14.6271	–1.127	34.496	–1.170	35.563	–1.338	36.505	–1.433	36.686
–1.278	14.6326	–1.140	34.501	–1.207	35.568	–1.308	36.510	–1.397	36.694
–1.248	14.6381	–1.145	34.507	–1.262	35.573	–1.281	36.516	–1.384	36.700
–1.207	14.6435	–1.136	34.512	–1.276	35.578	–1.259	36.521	–1.357	36.705
–1.177	14.6490	–1.154	34.517	–1.315	35.583	–1.221	36.527	–1.335	36.711
–1.129	14.6545	–1.188	34.522	–1.350	35.588	–1.187	36.532		
–1.103	14.6600	–1.211	34.527	–1.363	35.594	–1.161	36.538		
–1.096	14.6654	–1.228	34.533	–1.385	35.599	–1.150	36.543		

ΔV	HJD 2457600+	ΔV	HJD 2457600+	ΔV	HJD 2457600+	ΔV	HJD 2457600+	ΔV	HJD 2457600+
–1.088	14.493	–1.284	14.634	–1.418	14.781	–1.423	34.590	–1.337	35.677
–1.084	14.497	–1.249	14.640	–1.407	14.779	–1.443	34.595	–1.319	36.511
–1.110	14.502	–1.226	14.645	–1.399	14.785	–1.057	35.546	–1.280	36.516
–1.139	14.507	–1.180	14.651	–1.130	34.470	–1.074	35.551	–1.262	36.522
–1.180	14.513	–1.141	14.656	–1.121	34.476	–1.103	35.557	–1.226	36.527
–1.207	14.518	–1.120	14.662	–1.127	34.481	–1.145	35.562	–1.175	36.533
–1.243	14.523	–1.109	14.667	–1.131	34.487	–1.231	35.572	–1.145	36.538
–1.267	14.528	–1.115	14.673	–1.136	34.492	–1.266	35.577	–1.146	36.544
–1.304	14.534	–1.106	14.678	–1.132	34.497	–1.300	35.582	–1.133	36.549
–1.325	14.539	–1.112	14.683	–1.137	34.502	–1.322	35.588	–1.131	36.555
–1.341	14.546	–1.114	14.689	–1.145	34.507	–1.347	35.593	–1.138	36.560
–1.368	14.552	–1.110	14.694	–1.136	34.512	–1.362	35.598	–1.129	36.566
–1.369	14.557	–1.124	14.700	–1.147	34.517	–1.384	35.603	–1.124	36.571
–1.394	14.562	–1.118	14.705	–1.159	34.523	–1.394	35.608	–1.140	36.577
–1.404	14.568	–1.161	14.714	–1.182	34.528	–1.413	35.614	–1.133	36.582
–1.410	14.573	–1.187	14.720	–1.224	34.533	–1.420	35.619	–1.145	36.588
–1.408	14.579	–1.232	14.725	–1.250	34.538	–1.426	35.624	–1.187	36.593
–1.415	14.584	–1.269	14.731	–1.295	34.543	–1.429	35.629	–1.229	36.598
–1.406	14.590	–1.287	14.736	–1.332	34.549	–1.428	35.634	–1.262	36.604
–1.394	14.595	–1.315	14.742	–1.353	34.554	–1.418	35.640	–1.289	36.609
–1.394	14.601	–1.341	14.747	–1.375	34.559	–1.414	35.645	–1.321	36.615
–1.367	14.607	–1.352	14.753	–1.378	34.564	–1.408	35.650	–1.342	36.620
–1.337	14.612	–1.366	14.759	–1.393	34.569	–1.399	35.655	–1.358	36.626
–1.327	14.618	–1.382	14.764	–1.408	34.575	–1.384	35.661	–1.383	36.631
–1.320	14.623	–1.396	14.770	–1.408	34.580	–1.386	35.666	–1.392	36.637
–1.301	14.629	–1.402	14.776	–1.415	34.585	–1.371	35.671	–1.396	36.642

Table continued on following pages

Table 1. V1695 Aql observations, ΔB, ΔV, ΔR_c, and ΔI_c, variable star minus comparison star, cont.

ΔR_c	*HJD 2457600+*	ΔR_c	*HJD 2457600+*	ΔR_c	*HJD 2457600+*	ΔR_c	*HJD 2457600+*	ΔR_c	*HJD 2457600+*
–1.042	14.486	–1.093	14.671	–1.258	34.538	–1.415	35.604	–1.138	36.549
–1.044	14.490	–1.089	14.676	–1.297	34.543	–1.418	35.609	–1.137	36.554
–1.054	14.495	–1.090	14.682	–1.347	34.548	–1.432	35.615	–1.121	36.560
–1.079	14.501	–1.096	14.687	–1.365	34.553	–1.435	35.620	–1.123	36.565
–1.108	14.506	–1.091	14.693	–1.381	34.559	–1.445	35.625	–1.123	36.571
–1.144	14.511	–1.100	14.698	–1.404	34.564	–1.446	35.630	–1.145	36.576
–1.188	14.516	–1.097	14.704	–1.405	34.569	–1.433	35.635	–1.145	36.582
–1.218	14.522	–1.112	14.709	–1.424	34.574	–1.433	35.640	–1.151	36.587
–1.250	14.527	–1.177	14.718	–1.441	34.579	–1.424	35.646	–1.187	36.593
–1.312	14.537	–1.214	14.724	–1.438	34.585	–1.427	35.651	–1.226	36.598
–1.337	14.543	–1.241	14.729	–1.256	35.483	–1.410	35.656	–1.269	36.604
–1.369	14.550	–1.270	14.735	–1.228	35.488	–1.391	35.661	–1.294	36.609
–1.376	14.555	–1.302	14.740	–1.184	35.494	–1.388	35.667	–1.322	36.614
–1.375	14.561	–1.319	14.746	–1.158	35.499	–1.377	35.672	–1.339	36.620
–1.401	14.566	–1.338	14.751	–1.107	35.505	–1.345	35.678	–1.367	36.625
–1.398	14.572	–1.357	14.757	–1.080	35.510	–1.310	35.684	–1.382	36.631
–1.407	14.577	–1.374	14.763	–1.074	35.515	–1.292	35.690	–1.406	36.636
–1.404	14.583	–1.392	14.768	–1.069	35.520	–1.397	36.461	–1.413	36.642
–1.400	14.588	–1.404	14.774	–1.068	35.526	–1.399	36.466	–1.416	36.647
–1.396	14.594	–1.168	34.465	–1.060	35.531	–1.404	36.473	–1.425	36.653
–1.382	14.599	–1.137	34.469	–1.067	35.537	–1.418	36.478	–1.427	36.658
–1.372	14.605	–1.123	34.475	–1.079	35.542	–1.397	36.483	–1.435	36.664
–1.358	14.611	–1.137	34.480	–1.085	35.547	–1.379	36.489	–1.443	36.669
–1.338	14.616	–1.137	34.486	–1.098	35.552	–1.365	36.494	–1.432	36.675
–1.314	14.622	–1.138	34.491	–1.132	35.557	–1.351	36.500	–1.432	36.680
–1.296	14.627	–1.127	34.496	–1.170	35.563	–1.338	36.505	–1.433	36.686
–1.278	14.633	–1.140	34.501	–1.207	35.568	–1.308	36.510	–1.397	36.694
–1.248	14.638	–1.145	34.507	–1.262	35.573	–1.281	36.516	–1.384	36.700
–1.207	14.644	–1.136	34.512	–1.276	35.578	–1.259	36.521	–1.357	36.705
–1.177	14.649	–1.154	34.517	–1.315	35.583	–1.221	36.527	–1.335	36.711
–1.129	14.655	–1.188	34.522	–1.350	35.588	–1.187	36.532		
–1.103	14.660	–1.211	34.527	–1.363	35.594	–1.161	36.538		
–1.096	14.665	–1.228	34.533	–1.385	35.599	–1.150	36.543		

Table continued on next page

MAKER and fill-out of 0.25. We modeled two cool spots and one hot spot to fit the asymmetries. The hot spot vanished as the Wilson program progressed. Tycho and 2MASS photometry indicated that the spectral type fell in the G6 to G9 range so a temperature of 5500 K was chosen for the primary component with the secondary component modeling at a somewhat higher temperature. Next, the mean values from the BINARY MAKER fits a set of starting values for the WD program (Wilson and Devinney 1971; Wilson 1990, 1994, 2001, 2004; Van Hamme and Wilson 1998, 2003). This version includes Kurucz atmospheres, rather than black body, and a detailed reflection treatment along with two-dimentional limb-darkening coefficients. The differential corrections routine was iterated until convergence was achieved for a solution. The solution was computed in Mode 3, the contact binary mode. Convective parameters g = 0.32, A = 0.5 were used. The light curve solution is given in Table 5.

The normalized curves overlain by our light curve solutions are shown as Figure 7a and 7b. A geometrical (Roche-lobe) representation of the system is given in Figure 8 (a, b, c, d) at light curve quadratures so that the reader may see the placement of the spots and the relative size of the stars as compared to the orbit. Table 6 gives the unspotted solution for V1695 Aql. One can compare the WD program's sum of square residual, 0.19 vs. 0.15, for the unspotted vs. the spotted model. The spotted solution presents a better numerical solution. It is noted that the unspotted solution has a somewhat smaller fill-out, 35%.

8. Conclusion

V1695 Aql is a moderate period (P = 0.4128296 day), W UMa eclipsing binary. The 17-year orbital study (more than 15,000 orbits) reveals a quadratically decreasing ephemeris. Given that the temperature for the primary component is ~5500 K, from T_2 we find the secondary (smaller) star is at a hotter ~5650 K. This effect is believed to be due to the actual saturated spot coverage on the primary component. The WD program solution gives a mass ratio of 0.16. Rasio (1995) stated the runaway event that results in a merger happens when the mass ratio is ~ 0.09, so we are 0.07 away from that event if this is the case. The Roche Lobe fill-out is rather large, 83% for this contact binary. This value could lead the system into an instability which could result in coalescence.

Recently, Molnar *et al.* (2017) predicted that the eclipsing binary KIC 9832227 would become a red nova in the year 2022. Table 7 shows a comparison of the parameters for KIC 9832227 with V1695 Aql to show the similarity of the two systems. Molnar (2017) has examined our period study curves and does not see the expected asymmetry (right side of the curve should

Table 1. V1695 Aql observations, ΔB, ΔV, ΔR_c, and ΔI_c, variable star minus comparison star, cont.

ΔI_c	HJD 2457600+	ΔI_c	HJD 2457600+	ΔI_c	HJD 2457600+	ΔI_c	HJD 2457600+	ΔI_c	HJD 2457600+
–1.088	14.493	–1.124	14.700	–1.408	34.580	–1.103	35.557	–1.262	36.522
–1.084	14.497	–1.118	14.705	–1.415	34.585	–1.145	35.562	–1.226	36.527
–1.110	14.502	–1.161	14.714	–1.423	34.590	–1.180	35.567	–1.175	36.533
–1.139	14.507	–1.187	14.720	–1.443	34.595	–1.231	35.572	–1.145	36.538
–1.180	14.513	–1.232	14.725	–1.451	34.599	–1.266	35.577	–1.146	36.544
–1.207	14.518	–1.269	14.731	–1.448	34.604	–1.300	35.582	–1.133	36.549
–1.243	14.523	–1.287	14.736	–1.449	34.609	–1.322	35.588	–1.131	36.555
–1.267	14.528	–1.315	14.742	–1.435	34.614	–1.347	35.593	–1.138	36.560
–1.304	14.534	–1.341	14.747	–1.431	34.618	–1.362	35.598	–1.129	36.566
–1.325	14.539	–1.352	14.753	–1.417	34.623	–1.384	35.603	–1.124	36.571
–1.341	14.546	–1.366	14.759	–1.405	34.628	–1.394	35.608	–1.140	36.577
–1.368	14.552	–1.382	14.764	–1.399	34.635	–1.413	35.614	–1.133	36.582
–1.369	14.557	–1.396	14.770	–1.354	34.641	–1.420	35.619	–1.145	36.588
–1.394	14.562	–1.402	14.776	–1.327	34.647	–1.426	35.624	–1.187	36.593
–1.404	14.568	–1.418	14.781	–1.307	34.652	–1.429	35.629	–1.229	36.598
–1.410	14.573	–1.407	14.779	–1.270	34.657	–1.428	35.634	–1.262	36.604
–1.408	14.579	–1.399	14.785	–1.252	34.662	–1.418	35.640	–1.289	36.609
–1.415	14.584	–1.130	34.470	–1.217	34.667	–1.414	35.645	–1.321	36.615
–1.406	14.590	–1.121	34.476	–1.181	34.671	–1.408	35.650	–1.342	36.620
–1.394	14.595	–1.127	34.481	–1.148	34.676	–1.399	35.655	–1.358	36.626
–1.394	14.601	–1.131	34.487	–1.328	35.463	–1.384	35.661	–1.383	36.631
–1.367	14.607	–1.136	34.492	–1.293	35.468	–1.386	35.666	–1.392	36.637
–1.337	14.612	–1.132	34.497	–1.282	35.473	–1.371	35.671	–1.396	36.642
–1.327	14.618	–1.137	34.502	–1.259	35.477	–1.337	35.677	–1.418	36.648
–1.320	14.623	–1.145	34.507	–1.244	35.482	–1.310	35.682	–1.421	36.653
–1.301	14.629	–1.136	34.512	–1.208	35.487	–1.276	35.689	–1.438	36.659
–1.284	14.634	–1.147	34.517	–1.174	35.493	–1.245	35.694	–1.438	36.664
–1.249	14.640	–1.159	34.523	–1.127	35.499	–1.404	36.462	–1.428	36.670
–1.226	14.645	–1.182	34.528	–1.087	35.504	–1.397	36.467	–1.424	36.675
–1.180	14.651	–1.224	34.533	–1.055	35.509	–1.399	36.473	–1.421	36.681
–1.141	14.656	–1.250	34.538	–1.039	35.514	–1.405	36.478	–1.415	36.686
–1.120	14.662	–1.295	34.543	–1.039	35.519	–1.397	36.484	–1.391	36.695
–1.109	14.667	–1.332	34.549	–1.037	35.525	–1.392	36.489	–1.378	36.700
–1.115	14.673	–1.353	34.554	–1.038	35.531	–1.372	36.494	–1.353	36.706
–1.106	14.678	–1.375	34.559	–1.044	35.536	–1.352	36.500	–1.318	36.711
–1.112	14.683	–1.378	34.564	–1.046	35.541	–1.330	36.505		
–1.114	14.689	–1.393	34.569	–1.057	35.546	–1.319	36.511		
–1.110	14.694	–1.408	34.575	–1.074	35.551	–1.280	36.516		

Table 2. Information on the stars used in this study.

Star	Name	R.A. (2000) h m s	Dec. (2000) ° ′ ″	V	J–K	B–V
V	V1695 Aql GSC 5149-2845 BD–03 4659	19 38 22.3027	–03 32 37.461[1]	10.92[1]	0.40	0.72 ± 0.08[1]
C	GSC 5149-2931	19 38 23.9189	–03 35 56.965[1]	11.04	—	—
K (Check)	3UC174-2249292	19 38 22.5783	–03 28 3.356[3]	12.25	0.30	—

[1] *Høg, E., et al. 2000.*

be steeper than that left as it is in Figure 12 of their paper, Molnar *et al.* 2017). So while the period is decreasing, it is not exponentially decaying at this time. If this phenomenon were present, it would lead to a rapid coalescence.

The extreme mass ratio binary has an inclination of 86°, which yields the rather long-duration total eclipse. The W UMa binary is of W-type (the less massive component is slightly hotter). This is unusual for deep contact binaries. Two cool spots were needed in the WD solution.

This initial study of V1695 Aql lays the groundwork for future work. More eclipse timings are needed to make a definitive study of its orbital evolution. We plan future follow-up observations. Of course, radial velocity curves should be obtained to determine its absolute physical character (masses in kg, radii in km, etc.).

Table 3. V1695 Aql period study.

	Epoch 2400000+	Cycles	Linear Residuals	Quadratic Residuals	Reference
1	51275.0350	–15409.5	–0.0366	–0.0024	Paschke 1994, 2002
2	52433.6990	–12603.0	0.0210	0.0163	Paschke 1994, 2002
3	52522.4400	–12388.0	0.0036	–0.0035	Berhard *et al.* 2002
4	52522.4432	–12388.0	0.0068	–0.0003	Pejcha 2005
5	52576.3098	–12257.5	–0.0008	–0.0093	Pejcha 2005
6	55405.0525	–5405.5	0.0331	–0.0014	Kazuo O–C Gateway
7	57614.6837	–53.0	–0.0064	0.0024	This Paper
8	57634.4925	–5.0	–0.0134	–0.0039	This Paper
9	57636.5626	0.0	–0.0074	0.0021	This Paper

Table 4. V1695 Aql light curve characteristics.

Filter	*Phase*	*Magnitude Max. I*	*Phase*	*Magnitude Max. II*
	0.25		0.75	
B		–1.408 ± 0.019		–1.406 ± 0.010
V		–1.408 ± 0.016		–1.431 ± 0.005
R_c		–1.386 ± 0.015		–1.401 ± 0.007
I_c		–1.406 ± 0.017		–1.432 ± 0.005

Filter	*Phase*	*Magnitude Min. II*	*Phase*	*Magnitude Min. I*
	0.0		0.5	
B		–0.993 ± 0.002		–1.077 ± 0.014
V		–1.040 ± 0.004		–1.108 ± 0.013
R_c		–0.993 ± 0.004		–1.078 ± 0.015
I_c		–1.040 ± 0.003		–1.108 ± 0.013

Filter	*Min. I – Max. I*	*Min. I – Min. II*
B	0.415 ± 0.021	0.084 ± 0.016
V	0.368 ± 0.020	0.068 ± 0.016
R_c	0.393 ± 0.019	0.085 ± 0.018
I_c	0.366 ± 0.020	0.068 ± 0.016

Filter	*Max. I – Max. II*	*Filter*	*Min. II – Max. I*
B	–0.002 ± 0.030	B	0.331 ± 0.033
V	0.023 ± 0.021	V	0.300 ± 0.028
R_c	0.015 ± 0.022	R_c	0.308 ± 0.030
I_c	0.026 ± 0.022	I_c	0.298 ± 0.029

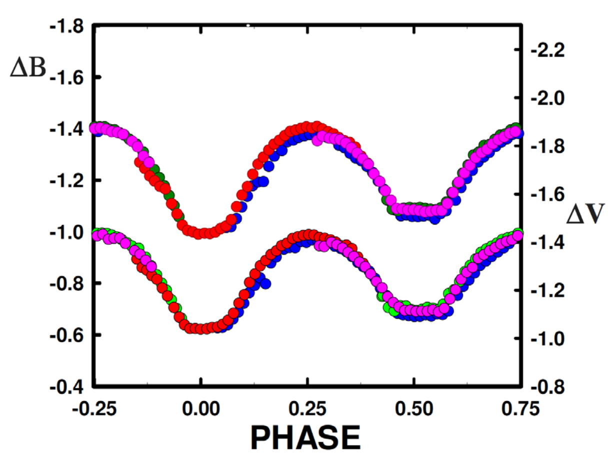

Figure 6. Each night's observations in B and V are plotted to show night to night variations in observations. Blue = night 1, Green = night 2, Red = night 3, Pink = night 4.

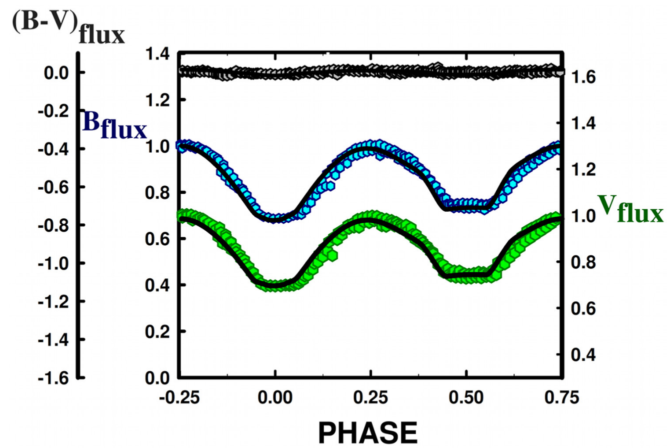

Figure 7a. V1695 Aql B, V normalized fluxes overlaid by our solution of V1695 Aql.

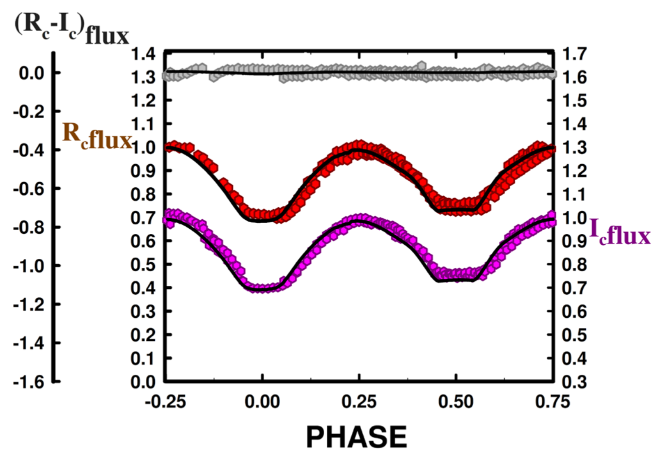

Figure 7b. V1695 Aql R_c, I_c normalized fluxes overlaid by our solution of V1695 Aql.

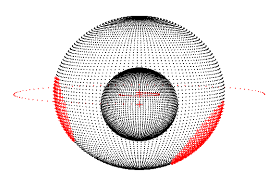

Figure 8a. V1695 Aql, geometrical representation at phase 0.00.

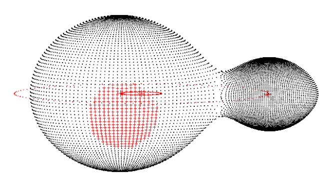

Figure 8b. V1695 Aql, geometrical representation at phase 0.25.

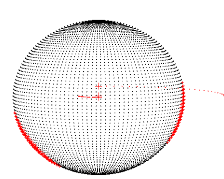

Figure 8c. V1695 Aql, geometrical representation at phase 0.50.

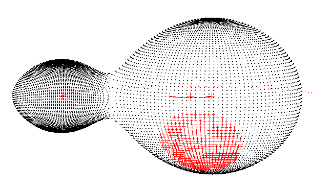

Figure 8d. V1695 Aql, geometrical representation at phase 0.75.

Table 5. Synthetic curve solution for V1695 Aql. Terms with errors are iterated values.

Parameter	*Value*
λ_B, λ_V, λ_{Rc}, λ_{Ic} (nm)	440, 550, 640, 790
$x_{bol1,2}$, $y_{bol1,2}$	0.649, 0.649, 0.193, 0.193
$x_{1Ic,2Ic}I$, $y_{1Ic,2Ic}$	0.623, 0.623, 0.230, 0.230
$x_{1Rc,2Rc}$, $y_{1Rc,2Rc}$	0.708, 0.708, 0.229, 0.229
$x_{1V,2V}$, $y_{1V,2V}$	0.778, 0.778, 0.108, 0.108
$x_{1B,2B}$, $y_{1B,2B}$	0.847, 0.847 –0.018, –0.018
g_1 , g_2	0.32
A_1 , A_2	0.5
Inclination (°)	85.6 ± 0.2
T_1, T_2 (K)	5500, 5649 ± 3
Ω_1, Ω_2	2.049 ± 0.001
$q(m_2 / m_1)$	0.1622 ± 0.0002
Fill–outs: $F_1 = F_2$	83% ± 1%
$L_1 / (L_1 + L_2)_{Ic}$	0.805 ± 0.001
$L_1 / (L_1 + L_2)_{Rc}$	0.803 ± 0.002
$L_1 / (L_1 + L_2)_V$	0.800 ± 0.001
$L_1 / (L_1 + L_2)_B$	0.792 ± 0.001
r_1, r_2 (pole)	0.525 ± 0.002, 0.246 ± 0.003
r_1, r_2 (side)	0.586 ± 0.003, 0.260 ± 0.004
r_1, r_2 (back)	0.613 ± 0.003, 0.340 ± 0.019
Spot 1	*Star 1*
Colatitude	125 ± 1
Longitude	80.6 ± 0.4
Spot radius	29.5 ± 0.1
T–Factor	0.812 ± 0.003
Spot 2	*Star 1*
Colatitude	102.2 ± 0.4
Longitude	275.4 ± 0.3
Spot radius	23.9 ± 0.01
T–Factor	0.803 ± 0.003
Pshift	0.0
JD_0 (days)	2457634.7038 ± 0.0003
Period (days)	0.412755 ± 0.000006
$\Sigma(res)^2$	0.1468

Table 6. Unspotted synthetic curve solution for V1695 Aql. Terms with errors are iterated values. The values not listed are identical as those in Table 4.

Parameter	*Value*
Inclination (°)	87.1 ± 0.5
T_1, T_2 (K)	5500, 5252 ± 4
Ω_1, Ω_2	2.114 ± 0.002
$q(m_2 / m_1)$	0.1684 ± 0.0004
Fill–outs: $F_1 = F_2$	34.8 ± 0.2%,
$L_1 / (L_1 + L_2)_I$	0.849 ± 0.010
$L_1 / (L_1 + L_2)_R$	0.852 ± 0.015
$L_1 / (L_1 + L_2)_V$	0.856 ± 0.010
$L_1 / (L_1 + L_2)_B$	0.866 ± 0.011
r_1, r_2 (pole)	0.509 ± 0.002, 0.232 ± 0.003
r_1, r_2 (side)	0.561 ± 0.003, 0.243 ± 0.003
r_1, r_2 (back)	0.585 ± 0.004, 0.287 ± 0.008
$\Sigma(res)^2$	0.1932

Table 7. Comparison of KIC 9832227 to V1685 Aql.

Star	*q*	T_1	T_2	*P*	$\dot{P}$
KIC 9832227	0.227957	5800 K	5920 K	0.4579615 d	2.0×10^{-6}
V1685 Aql	0.1622	5500 K	5649 K	0.4128296 d	1.7×10^{-6}

9. Acknowledgements

We thank the Southeastern Association for Research in Astronomy for providing observing time, as well as the Emmanuel College Natural Sciences Department for its continued support of student research projects. Student researcher Christopher R. Gray would also like to personally thank Dr. Ron Samec for his mentorship and providing the opportunity to work on the project. Finally, Gray would like to also thank Dr. Brian Peek for his leadership in overseeing the 2016–2017 Research Symposium at Emmanuel College.

References

Bernhard, K., Kiyota, S., and Pejcha, O. 2002, *Inf. Bull. Var. Stars*, No. 5318, 1.
Bradstreet, D. H., and Steelman, D. P., 2002, *Bull. Amer. Astron. Assoc.*, **34**, 1224.
Gazeas, K., and Stępień, K. 2008, *Mon. Not. Roy. Astron. Soc.*, **390**, 1577.
Hoffman, D. I., Harrison, T. E., and McNamara, B. J. 2009, *Astron. J.*, **138**, 466.
Høg, E., *et al.* 2000, *Astron. Astrophys.*, **355**, L27.
Kazarovets, E. V., Samus, N. N., Durlevich, O. V., Kireeva, N. N, and Pastukhova, E. N. 2006, *Inf. Bull. Var. Stars*, No. 5721, 1.
Kreiner, J. M. 2004, *Acta Astron.*, **54**, 207.
Kwee, K. K., and Van Woerden, H. 1956, *Bull. Astron. Inst. Netherlands*, **12**, 327.
Molnar, L. A. 2017, private communication (June 26).
Molnar, L. A., *et al.* 2017, *Astrophys. J.*, **840**, 1.
Nelson, R. 2016, Nelson Database of Times of Minima (https://www.aavso.org/bob-nelsons-o-c-files).
Paschke, A. 1994, observations of V1695 Aql in O–C Gateway (http://var2.astro.cz/ocgate/).
Paschke, A. 2002, observations of V1695 Aql in O–C Gateway (http://var2.astro.cz/ocgate/).
Pejcha, O. 2005, *Inf. Bull. Var. Stars*, No. 5645, 1.
Rasio, F. A. 1995, *Astrophys. J., Lett.*, **444**, L41.
Szczygiel, D. M., Socrates, A., Paczynski, B., Pojmanski, G., and Pilecki, B. 2008, *Acta Astron.*, **58**, 405.
Van Hamme, W., and Wilson, R. E. 1998, *Bull. Amer. Astron. Soc.*, **30**, 1402.
Van Hamme, W., and Wilson, R. E. 2003, in *GAIA Spectroscopy: Science and Technology*, ed. U. Munari, ASP Conf. Ser. 298, Astronomical Society of the Pacific, San Francisco, 323.
Wilson, R. E. 1990, *Astrophys. J.*, **356**, 613 .
Wilson, R. E. 1994, *Publ. Astron. Soc. Pacific*, **106**, 921 .
Wilson, R. E. 2001, *Inf. Bull. Var. Stars*, No. 5076, 1.
Wilson, R. E. 2004, *New Astron. Rev.*, **48**, 695 .
Wilson, R. E., and Devinney, E. J. 1971, *Astrophys. J.*, **166**, 605.

BVRI Photometric Study of the High Mass Ratio, Detached, Pre-contact W UMa Binary GQ Cancri

Ronald G. Samec
Amber Olson
Natural Sciences Department, Emmanuel College,181 Springs Street, Franklin Springs, GA 30639; ronaldsamec@gmail.com

Daniel Caton
Dark Sky Observatory, Department of Physics and Astronomy, Appalachian State University, 525 Rivers Street, Boone, NC 28608

Danny R. Faulkner
Johnson Observatory, 1414 Bur Oak Court, Hebron, KY 41048

Walter Van Hamme
Department of Physics, Florida International University,11200 SW 8th Street, CP 204, Miami, FL 33199

Received June 30, 2017; revised August 8, August 18, 2017; accepted August 18, 2017

Abstract CCD BVR_cI_c light curves of GQ Cancri were observed in April 2013 using the SARA North 0.9-meter Telescope at Kitt Peak National Observatory in Arizona in remote mode. It is a high-amplitude (V ~ 0.9 magnitude) K0–V type eclipsing binary (T_1 ~ 5250 K) with a photometrically-determined mass ratio of $M_2 / M_1 = 0.80$. Its spectral color type classifies it as a pre-contact W UMa Binary (PCWB). The Wilson-Devinney Mode 2 solutions show that the system has a detached binary configuration with fill-outs of 94% and 98% for the primary and secondary component, respectively. As expected, the light curve is asymmetric due to spot activity. Three times of minimum light were calculated, for two primary eclipses and one secondary eclipse, from our present observations. In total, some 26 times of minimum light covering nearly 20 years of observation were used to determine linear and quadratic ephemerides. It is noted that the light curve solution remained in a detached state for every iteration of the computer runs. The components are very similar with a computed temperature difference of only 4 K, and the flux of the primary component accounts for 53–55% of the system's light in B, V, R_c, and I_c. A 12-degree radius high latitude white spot (faculae) was iterated on the primary component.

1. Introduction

Contact binaries with mass ratios near unity are very rare. In this study, we analyze a near contact solar type binary (a pre-contact W UMa binary) with a mass ratio near that of unity. The Wilson-Devinney (WD) program was used for this calculation. This paper represents the first precision BVR_cI_c study of GQ Cnc. A mass ratio (q) search was needed since a number of solutions may be generated with different values of q. However, in this case, the deep, knife-like, nearly identical eclipses are possible only when q is near one.

The formation of contact binaries may happen in one of three evolutionary channels (Jiang *et al.* 2014). One is nuclear expansion of the primary component, two others involve loss or exchange of angular momentum via magnetic braking or by interacting with a third body. Magnetic braking occurs since solar type stars are highly magnetic in nature, due to their convective envelopes and fast rotation. They undergo magnetic braking as plasma winds leave the stars on stiff rotating dipole fields. This action torques the binary, eventually bringing them into contact and finally, following a red novae event (Molnar *et al.* 2017), leaves a single, fast-rotating star.

2. History and observations

The variable NSV 4411 (GQ Cnc) was discovered by Rigollet (1953) and classified as a RR Lyrae variable star with a photographic magnitude of 13.1 to 13.7. It was observed in 1996 with a CCD camera (Vidal-Sainz and Garcia-Melendo 1996) and found to be an eclipsing binary with an ephemeris of:

$$\text{Min. I.} = \text{HJD } 2450154.2091 + 0.42228\text{ d} \times E. \qquad (1)$$

They gave seven eclipse timings in their paper. Their light curve fit (BINARY MAKER 2.0; Bradstreet 1993) gave a mass ratio of 0.9 and an inclination of 86° and a component temperature difference of 150 K. They included a cool spot on the primary component. Their V filter CCD curve is given as Figure 1.

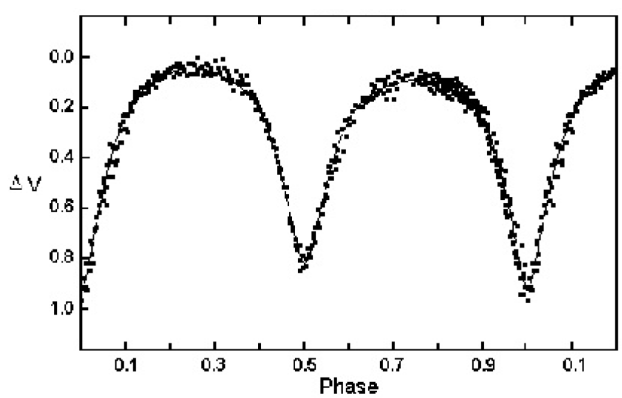

Figure 1. V-filtered CCD Light curve (Vidal-Sainz and Garcia-Melendo 1996).

Table 1. Information on the stars used in this study.

Star	*Name*	*R.A. (2000)* h m s	*Dec. (2000)* ° ′ ″	*V*	*J–K*	*B–V*
V	GQ Cnc 3UC234-096892* 2MASS J09120836+2650180 NSV 4411 GSC 01954 00180	09 12 08.386	+26 50 18.20[1]	12.96	0.51	0.81
C	BD +27.1722	09 12 23.58	+26 52 44.6[2]	9.76	—	0.815
K (Check)	TYCHO 1954 642	09 12 08.7879	+26 46 33.966[3]	10.622	0.625 (K3)	1.006 (K4)

[1] *UCAC3 (USNO 2012).* [2] *Perryman et al. (1997).* [3] *Høg, E., et al. (2000).*

GQ Cnc was included in the "75th Name-list of Variable Stars" (Kazarovets *et al.* 2000). Times of minimum light are given by Hübscher and Monninger (2011), Zejda (2004), Diethelm (2003, 2012, 2010, 2009), and Locher (2005). An updated ephemeris was given by Kreiner (2004):

$$\text{Min. I.} = \text{HJD } 2452500.0108\ (4) + 0.4222087\ \text{d}\ (1) \times E. \quad (2)$$

It is listed in the automated variable star classification using the NSVS (Hoffman *et al.* 2009) as an Algol/EB type and W UMa, with a period of 0.42221 day and J–H = 0.396, H–K = 0.114, a ROTSE magnitude of 12.702, and an amplitude of 0.865. It is listed in the Fourier region where β Lyr stars are expected (http://vizier.u-strasbg.fr/viz-bin/VizieR).

CCD BVR_cI_c light curves of GQ Cnc were observed in April 2013 on the SARA North 0.9-meter Telescope at Kitt Peak National Observatory in Arizona in remote mode by Samec with a –110° C cooled 2 K × 2 K, ARC-E2V42-40 chip CCD camera. Standard B, V, R_c, and I_c Johnson-Cousins filters were used. Reduction and analyses were mostly done by authors Samec, Olson, and Caton. Individual observations included 203 in B, 236 in V, 259 in R, and 260 in I. The standard error of a single observation was ~14 mmag. in B, 12 mmag. in V, 8 mmag. in R, and 9 mmag. in I. Images were calibrated from biases, 10–300-second darks and a minimum of five B, V, R_c, and I_c flat frames taken nightly. The nightly C–K values stayed constant throughout the observing run with a precision of 1%. Exposure times varied from 250–275 seconds in B, 80–100 seconds in V, and 30–50 seconds in R_c and I_c.

3. Finding charts and stellar identifications

The finding chart, given here for future observers, is shown as Figure 2. The coordinates and magnitudes of the variable star, comparison star, and check star are given in Table 1. The C–K values stayed constant throughout the observing run to better than 1%. Figures 3 and 4 show sample observations of B, V, and B–V color curves on the night of 24 April 2013, and R_c, I_c, and R_c–I_c color curves on 8 April 2013. Our observations are given in Table 2, in delta magnitudes, ΔB, ΔV, ΔR_c, and ΔI_c, in the sense of variable minus comparison star.

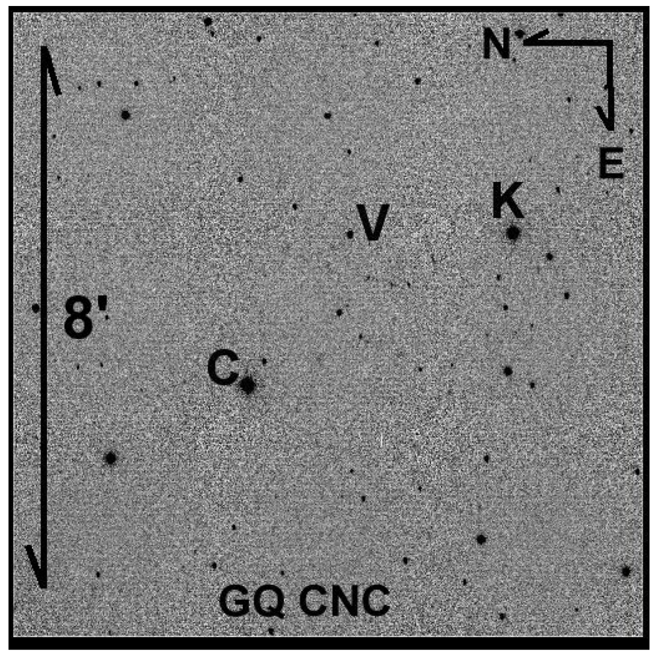

Figure 2. Finder chart for GQ Cnc. V: variable star, C: comparison star, K: check star.

4. Period study

Three times of minimum light were calculated for two primary eclipses and one secondary eclipse from our present observations with the Kwee van Woerden (1956) method:

$$\text{HJD I} = 2456390.66196 \pm 0.00002, 2456406.7056 \pm 0.0001 \quad (1)$$

$$\text{HJD II} = 2456405.6505 \pm 0.0002 \quad (2)$$

In total, some 26 times of minimum light covering 17 years of observation (Table 3) were used to determine the following linear ephemeris:

$$\text{HJD MinI} = 2456406.7057 \pm 0.0007 + 0.422208807 \pm 0.00000074\ \text{d} \times E \quad (3)$$

A negative quadratic ephemeris was also calculated:

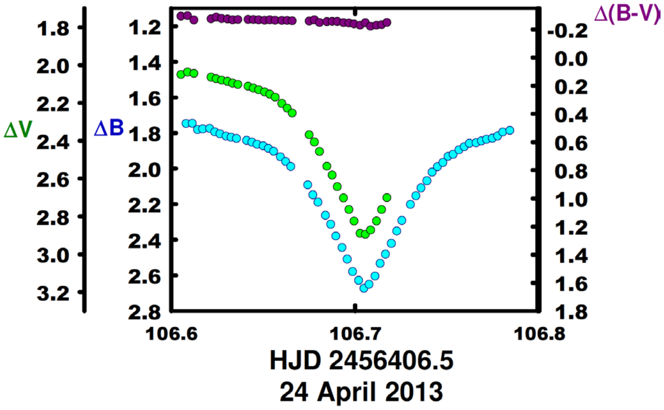

Figure 3. GQ Cnc B, V observations from 24 April 2013.

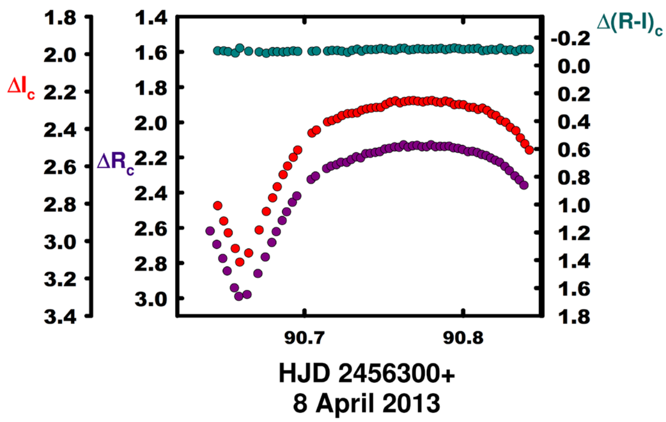

Figure 4. GQ Cnc R_c, I_c observations from 8 April 2013.

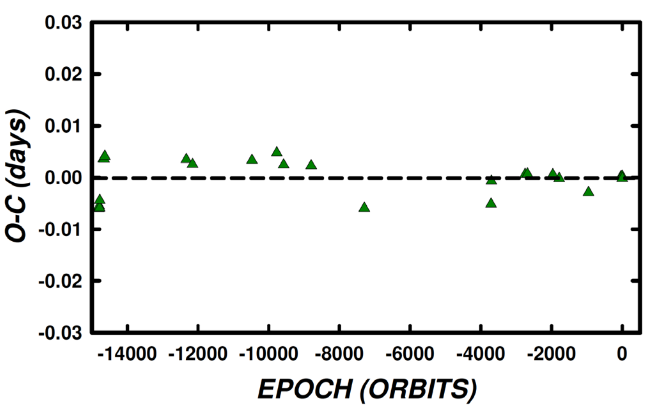

Figure 5. O–C residuals from the linear ephemeris of GQ Cnc from equation (3).

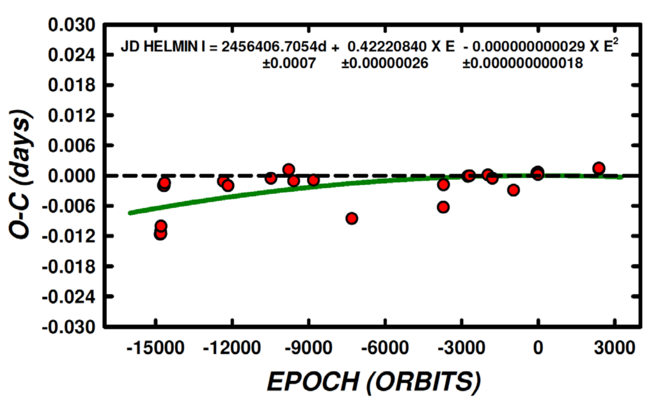

Fiigure 6. O–C Residuals from the quadratic term compared to the linear terms of GQ Cnc from equation (4). This shows that the period may be slowly decreasing at a rate near that theoretically expected for magnetic braking (for example, Molnar *et al.* 2017).

$$\text{HJD Min I} = 2456406.7054\text{d} + 0.42220840 \pm 0.0007 \pm 0.00000026 \times E - 2.9 \times 10^{-11} \pm 1.8 \times 10^{-11} \times E^2. \quad (4)$$

The O–C residuals, both linear and quadratic calculations, are given in Table 3. The linear and quadratic residuals are shown in Figures 5 and 6. The rms residuals for the linear and quadratic ephemerides were 1.15×10^{-5} and 1.13×10^{-5}, respectively. This means that both are very similar and no conclusion may be made of which best describes the data.

The light curves phased using equation (3) of GQ Cnc, delta mag vs. phase, are shown in Figures 7 and 8. Light curve amplitudes and the differences in magnitudes at various quadratures are given in Table 4.

5. Light curve characteristics

The light curves are of good precision, 0.014 magnitude in ΔB, 0.011 in ΔV, 0.008 in ΔR_c, and 0.009 in ΔI_c. The amplitude of the light curve is ~ 0.85 magnitude in all filters. This is quite large for a W UMa binary. This could mean the inclination is high and/or the mass ratio is near unity. The O'Connell effect, which is classically an indication of spot activity, varies 3–4%. This means that solar type spots are probably active, as expected. The differences in minima are small, 0.08 magnitude in all filters, pointing to the nearly equal temperatures of the components.

6. Temperature and light curve solution

2MASS (Skrutskie *et al.* 2006) gives J–K = 0.51 (K0V) or a temperature ~ 5250 K (Cox 2000), which was used in the light curve solution. This is a typical temperature of a short period (< 0.3 d) W UMa contact binary. This gives us a hint that we are observing a precursor to a W UMa Binary and that the evolution is following a detached to contact channel (Jiang *et al.* 2014).

The B, V, R_c, and I_c light curves were carefully pre-modeled with BINARY MAKER 3.0 (Bradstreet and Steelman 2002) and light curve fits were determined in all filter bands. The hand modeling revealed that both semidetached and detached models would fit the data (both with spots). The parameters from these two results were then averaged and input into a four-color simultaneous light curve calculation using the Wilson-Devinney (WD) program (Wilson and Devinney 1971; Wilson 1990, 1994; Van Hamme and Wilson 1998). The present solution was computed in Mode 2; which allows WD to determine the configuration. Convective parameters, g = 0.32, A = 0.5, were used. The program iterations remained and converged in a detached configuration. A mass ratio very nearly unity was determined with the first solution. We preserve this computation by including it in Table 5 (q = 0.95). Iterated parameters included both surface potentials, mass ratio, all spot parameters, inclination, T_2 (T_1 fixed), the ephemeris, and the relative monochromatic luminosity (L_1). Both a hot spot and a dark spot were used in BINARY MAKER modeling, but only a white spot (faculae) persisted in the WD modeling. Next we determined solutions with q-values fixed and noted the sum of square residuals given by the program for each. We show the

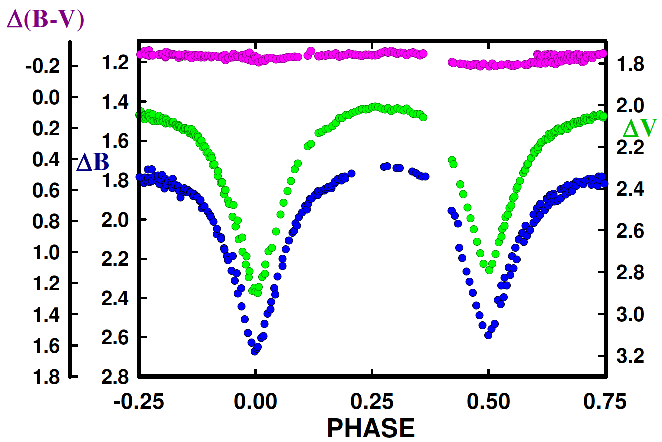

Figure 7. B, V phases calculated from Equation 3.

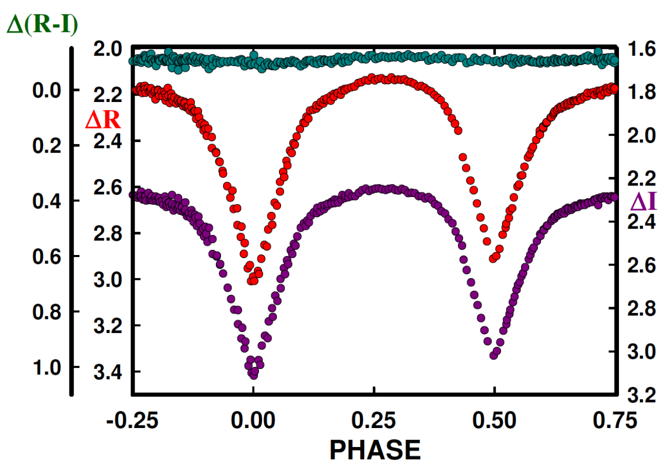

Figure 8. R_c, I_c phases calculated from Equation 3.

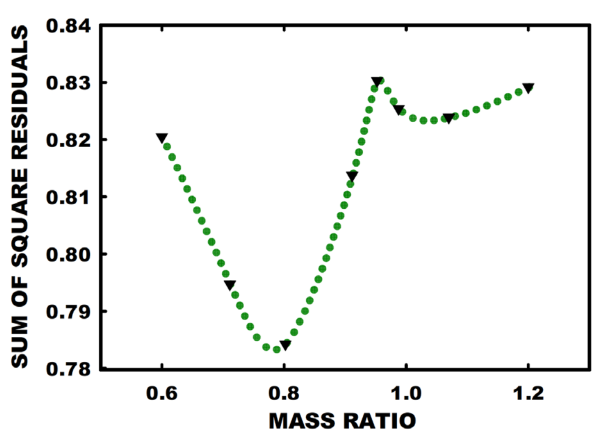

Figure 9. Goodness-of-fit values versus various values of mass ratio (q). The residual minimizes at about 0.8.

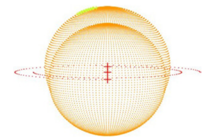

Figure 10a. Geometrical representation at phase 0.00 of GQ Cnc.

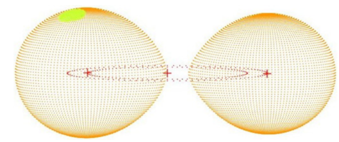

Figure 10b. Geometrical representation at phase 0.25 of GQ Cnc.

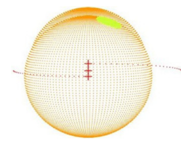

Figure 10c. Geometrical representation at phase 0.50 of GQ Cnc.

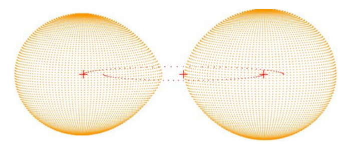

Figure 10d. Geometrical representation at phase 0.75 of GQ Cnc.

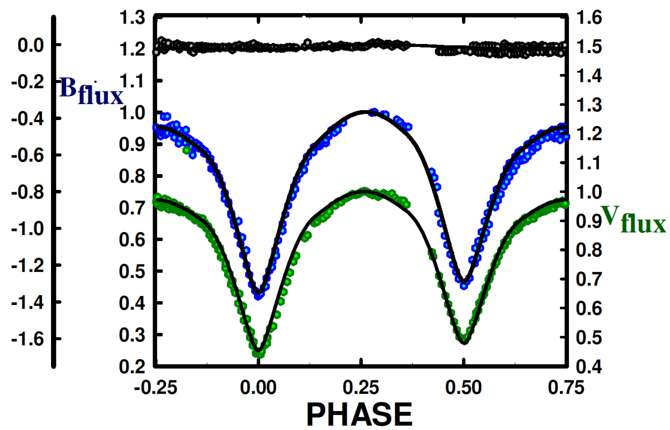

Figure 11a. B,V normalized fluxes overlaid by our solution of GQ Cnc.

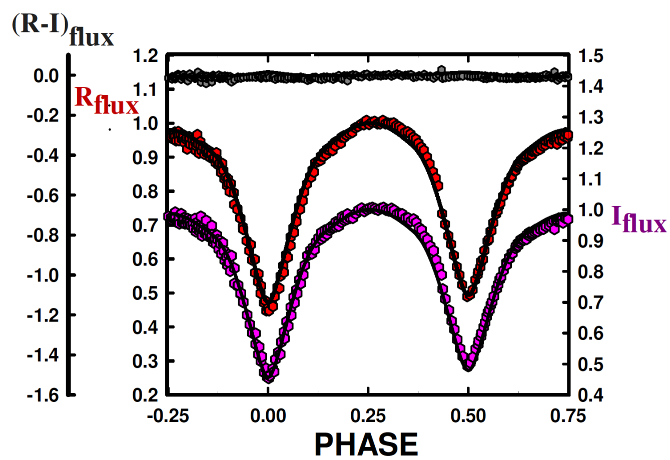

Figure 11b. R_c,I_c normalized fluxes overlaid by our solution of GQ Cnc.

results of that analysis in Figure 9. The best solution occurred at about q = 0.8. This was surprising since we thought the mass ratio would be nearer unity due to the near equal temperatures. A geometrical (Roche-lobe) representation of the system is given in Figure 10 (a, b, c, d) at the light curve quadratures so that the reader may see the placement of the spot and the relative size of the stars as compared to the orbit. As seen, the system is detached. The normalized curves overlain by our light curve solutions are shown as Figures 11a and 11b.

7. Discussion

Our model of GQ Cnc is a precontact W UMa binary. In addition, the stars are virtually the same in temperature. Since contact is not yet attained, we suspect the components began as nearly identical stars. The components' temperatures are within 4 K of each other. The mass ratio is 0.80, even though the fill-outs are nearly identical, 97 and 99% for the primary and secondary components, respectively. This may indicate that component 2 is slightly more evolved than component 1. The lights, 53% and

47%, for the primary and secondary components, respectively, are very similar. Even though the stars are near duplicates of each other, the curves are not symmetrical, with distortions that are probably due to spots. This betrays the fact that the nature of these are solar type, magnetic stars. Contact W UMa binaries with the q > 0.72 are called H-subtype systems (Csizmadia and Klagyivik 2004). GQ Cnc may be a precursor of this type of contact binary. Extreme examples of this subtype of contact binary are V803 Aql (Samec *et al.* 1993) and WZ And (Zhang and Zhang 2006), with mass ratios equal to unity.

8. Conclusion

GQ Cnc is apparently approaching contact for the first time with a mass ratio near unity and fill-outs less than critical contact. Solar type binaries, over time, should steadily lose angular momentum and spin down as the ion winds stream outward on stiff magnetic field lines rotating with the binary (out to the Alfvén radius). The natural tendency is for mass ratios to become more extreme with time (move away from unity) and coalesce into a contact binary. The system evidently will come into contact as a H sub-type W UMa binary (mass ratio > 0.72). Ultimately, one expects the binary will coalesce, producing a rather normal, fast rotating, single F2V-type ($m = 1.5\,M_\odot$) field star, assuming a $0.1\,M_\odot$ mass loss. The weakly negative quadratic ephemeris found in the period study may indicate that the binary is following this pattern.

9. Future work

Radial velocity curves are needed to obtain absolute (not relative) system parameters, including a firm determination of the mass ratio. Continued monitoring of eclipses could confirm or disaffirm the period evolution scenario given here.

10. Acknowledgements

Dr. Samec wishes to thank Emmanuel College and its vice president, Dr. John Henzel, President for Academic Affairs, for their past support for travel, and membership fees and meeting expenses.

References

Blättler, E., Diethelm, R., and Guilbault, P. 2001, *BBSAG Bull.*, No. 125, 1.
Bradstreet, D. H. 1993, in *Light Curve Modeling of Eclipsing Binary Stars*, IAU Symp. 151, Springer-Verlag, Berlin, 151.
Bradstreet, D. H., and Steelman, D. P. 2002, *Bull. Amer. Astron. Soc.*, **34**, 1224.
Cox, A. N., ed. 2000, *Allen's Astrophysical Quantities*, 4th ed., Springer, New York.
Csizmadia, Sz., and Klagyivik, P. 2004, *Astron. Astrophys.*, **426**, 1001.
Diethelm, R. 2003, *Inf. Bull. Var. Stars*, No. 5438, 1.
Diethelm, R. 2009, *Inf. Bull. Var. Stars*, No. 5894, 1.
Diethelm, R. 2010, *Inf. Bull. Var. Stars*, No. 5945, 1.
Diethelm, R. 2012, *Inf. Bull. Var. Stars*, No. 6029, 1.
Høg, E., *et al.* 2000, *Astron. Astrophys.*, **355**, L27.
Hoffman, D. I., Harrison, T. E., and McNamara, B. J. 2009, *Astron. J.*, **138**, 466.
Hübscher, J. 2017, *Inf. Bull. Var. Stars*, No. 6196, 1.
Hübscher, J., and Monninger, G. 2011, *Inf. Bull. Var. Stars*, No. 5959, 1.
Jaing, D., Han, Z., and Lifang, L. 2014, *Mon. Not. Roy. Astron. Soc.*, **438**, 859.
Kazarovets, E. V., Samus, N. N., and Durlevich, O. V. 2000, *Inf. Bull. Var. Stars*, No. 4870, 1.
Kreiner, J. M. 2004, *Acta Astron.*, **54**, 207.
Kwee, K. K., and van Woerden, H. 1956, *Bull. Astron. Inst. Netherlands*, **12**, 327.
Locher, K. 2005, *Open Eur. J. Var. Stars*, **3**, 1.
Locher, K., Blättler, E., and Diethelm, R. 2002, *BBSAG Bull.*, No. 128, 1.
Molnar, L. A., *et al.* 2017, *Astrophys. J.*, **840**, 1.
Paschke, A. 1999, observation of GQ Cnc in O–C Gateway (http://var2.astro.cz/ocgate/).
Perryman, M. A. C., European Space Agency Space Science Department, and the Hipparcos Science Team. 1997, *The Hipparcos and Tycho Catalogues, ESA SP-1200* (VizieR On-line Data Catalog: I/239), ESA Publications Division, Noordwijk, The Netherlands.
Rigollet, R. 1953, *IAU Circ.*, No. 1387, 1.
Samec, R. G., Su, W., and Dewitt, J. R. 1993, *Publ. Astron. Soc. Pacific*, **105**, 1441.
Skrutskie, M. F., *et al.* 2006, *Astron. J.*, **131**, 1163.
U.S. Naval Observatory. 2012, UCAC-3 (http://www.usno.navy.mil/USNO/astrometry/optical-IR-prod/ucac). [VizieR On-line Data Catalog: I/315.]
Van Hamme, W. V., and Wilson, R. E. 1998, *Bull. Amer. Astron. Soc.*, **30**, 1402.
Vidal-Sainz, J., and Garcia-Melendo, E. 1996, *Inf. Bull. Var. Stars*, No. 4393, 1.
Wilson, R. E. 1990, *Astrophys. J.*, **356**, 613.
Wilson, R. E. 1994, *Publ. Astron. Soc. Pacific*, **106**, 921.
Wilson, R. E., and Devinney, E. J. 1971, *Astrophys. J.*, **166**, 605.
Wolf, M., and Diethelm, R. 1999, *BBSAG Bull.*, No. 125, 1.
Zejda, M. 2004, *Inf. Bull. Var. Stars*, No. 5583, 1.
Zhang, X. B., and Zhang, R. X. 2006, *New Astron.*, **11**, 339 (http://www.sciencedirect.com/science/article/pii/S1384107605001375).

Table 2. Observations of GQ CNC, ΔB, ΔV, ΔR_c, ΔI_c, variable-comparison.

ΔB	HJD 2457270+	ΔB	HJD 2457270+	ΔB	HJD 2457270+	ΔB	HJD 2457270+	ΔB	HJD 2457270+
2.189	90.6383	2.592	105.6499	1.748	106.6082	2.022	106.7419	1.789	108.7166
2.277	90.6420	2.560	105.6527	1.747	106.6116	1.991	106.7448	1.784	108.7087
2.353	90.6461	2.534	105.6556	1.778	106.6173	1.991	106.7448	1.791	108.7197
2.660	90.6601	2.434	105.6610	1.776	106.6210	1.933	106.7506	1.789	108.7227
2.596	90.6662	2.398	105.6638	1.795	106.6238	1.921	106.7534	1.793	108.7286
2.460	90.6726	2.338	105.6666	1.806	106.6266	1.856	106.7658	1.802	108.7317
2.385	90.6768	2.285	105.6698	1.819	106.6299	1.846	106.7687	1.807	108.7347
2.240	90.6836	2.251	105.6727	1.825	106.6327	1.837	106.7715	1.813	108.7405
2.061	90.6938	2.206	105.6755	1.832	106.6356	1.831	106.7747	1.825	108.7436
2.034	90.6966	2.117	105.6820	1.843	106.6411	1.818	106.7775	1.837	108.7467
1.951	90.7056	2.085	105.6849	1.853	106.6440	1.796	106.7803	1.853	108.7522
1.897	90.7084	2.057	105.6877	1.865	106.6468	1.787	106.7842	1.851	108.7552
1.878	90.7154	2.020	105.6909	1.873	106.6501	1.794	106.7870	1.866	108.7583
1.855	90.7216	2.001	105.6937	1.888	106.6529	2.413	108.6144	1.885	108.7637
1.844	90.7244	1.980	105.6966	1.904	106.6558	2.339	108.6175	1.910	108.7668
1.843	90.7280	1.955	105.7009	1.935	106.6594	2.299	108.6205	1.938	108.7699
1.811	90.7309	1.932	105.7038	1.962	106.6623	2.247	108.6242	1.981	108.7759
1.804	90.7369	1.915	105.7066	1.990	106.6651	2.190	108.6273	2.014	108.7790
1.784	90.7400	1.911	105.7098	2.093	106.6743	2.147	108.6303	2.050	108.7821
1.769	90.7461	1.907	105.7127	2.149	106.6771	2.104	108.6335	2.101	108.7859
1.734	90.7755	1.895	105.7155	2.190	106.6799	2.072	108.6366	2.157	108.7889
1.732	90.7783	1.875	105.7200	2.264	106.6839	2.035	108.6396	2.210	108.7920
1.741	90.7868	1.862	105.7229	2.314	106.6868	1.977	108.6468	1.934	119.6316
1.741	90.7897	1.858	105.7257	2.380	106.6896	1.945	108.6499	1.900	119.6383
1.758	90.8010	1.825	105.7432	2.445	106.6930	1.922	108.6529	1.886	119.6411
1.767	90.8045	1.821	105.7460	2.510	106.6958	1.896	108.6587	1.885	119.6443
1.779	90.8073	1.831	105.7489	2.580	106.6987	1.878	108.6618	1.844	119.6560
1.784	90.8102	1.820	105.7551	2.629	106.7020	1.871	108.6648	1.831	119.6649
1.784	90.8130	1.817	105.7601	2.674	106.7049	1.849	108.6712	1.823	119.6710
1.958	90.8368	1.809	105.7635	2.651	106.7077	1.843	108.6743	1.805	119.6766
1.983	90.8397	1.806	105.7673	2.605	106.7109	1.828	108.6774	1.802	119.6856
2.024	90.8425	1.806	105.7720	2.534	106.7137	1.824	108.6823	1.795	119.6943
2.147	105.6235	1.845	105.7787	2.482	106.7166	1.809	108.6854	1.806	119.6976
2.199	105.6263	1.795	105.7861	2.422	106.7198	1.810	108.6884	1.812	119.7004
2.267	105.6301	1.846	105.7904	2.352	106.7227	1.804	108.6939	1.822	119.7092
2.319	105.6329	1.890	105.7931	2.293	106.7255	1.795	108.6969	1.826	119.7153
2.376	105.6358	1.861	105.7959	2.203	106.7302	1.795	108.7000	1.842	119.7209
2.440	105.6389	1.863	105.7992	2.154	106.7331	1.784	108.7056	1.857	119.7272
2.490	105.6418	1.862	105.8019	2.110	106.7359	1.784	108.7087	1.945	119.7476
2.541	105.6446	1.883	105.8047	2.070	106.7391	1.786	108.7118	2.078	119.7613

Table continued on following pages

Table 2. Observations of GQ CNC, ΔB, ΔV, ΔR_c, ΔI_c, variable-comparison, cont.

ΔV	HJD 2457270+	ΔV	HJD 2457270+	ΔV	HJD 2457270+	ΔV	HJD 2457270+	ΔV	HJD 2457270+
2.480	90.6390	2.045	90.8053	2.078	105.7728	2.403	108.6313	2.165	119.6391
2.554	90.6428	2.046	90.8081	2.089	105.7795	2.364	108.6344	2.155	119.6419
2.636	90.6470	2.060	90.8110	1.866	105.7869	2.327	108.6375	2.129	119.6451
2.726	90.6508	2.265	105.6169	2.097	105.7912	2.288	108.6406	2.114	119.6479
2.798	90.6536	2.285	105.6182	2.109	105.7939	2.227	108.6477	2.126	119.6507
2.876	90.6581	2.381	105.6243	2.111	105.7966	2.203	108.6508	2.104	119.6540
2.901	90.6609	2.428	105.6271	2.117	105.8000	2.179	108.6539	2.116	119.6568
2.810	90.6675	2.492	105.6309	2.138	105.8027	2.160	108.6596	2.099	119.6596
2.685	90.6739	2.543	105.6337	2.133	105.8054	2.146	108.6627	2.093	119.6629
2.607	90.6776	2.596	105.6366	2.051	106.6054	2.136	108.6658	2.088	119.6657
2.525	90.6816	2.656	105.6397	2.038	106.6090	2.114	108.6721	2.086	119.6685
2.469	90.6844	2.712	105.6426	2.045	106.6125	2.105	108.6752	2.079	119.6718
2.413	90.6881	2.762	105.6454	2.053	106.6182	2.100	108.6783	2.072	119.6746
2.365	90.6910	2.792	105.6507	2.065	106.6218	2.083	108.6832	2.074	119.6774
2.309	90.6946	2.762	105.6535	2.073	106.6246	2.083	108.6863	2.051	119.6807
2.281	90.6974	2.715	105.6564	2.081	106.6275	2.076	108.6894	2.052	119.6835
2.199	90.7064	2.632	105.6618	2.087	106.6307	2.068	108.6948	2.046	119.6864
2.187	90.7092	2.580	105.6646	2.097	106.6335	2.062	108.6979	2.054	119.6895
2.135	90.7162	2.526	105.6674	2.103	106.6364	2.060	108.7009	2.031	119.6923
2.129	90.7190	2.481	105.6707	2.113	106.6419	2.055	108.7066	2.051	119.6951
2.116	90.7224	2.439	105.6735	2.123	106.6448	2.061	108.7097	2.051	119.6984
2.114	90.7253	2.392	105.6764	2.131	106.6476	2.057	108.7127	2.068	119.7012
2.102	90.7289	2.313	105.6828	2.143	106.6509	2.060	108.7175	2.078	119.7040
2.087	90.7317	2.282	105.6857	2.155	106.6537	2.054	108.7206	2.072	119.7071
2.064	90.7349	2.255	105.6885	2.171	106.6566	2.055	108.7236	2.079	119.7100
2.063	90.7377	2.234	105.6917	2.204	106.6602	2.065	108.7295	2.081	119.7128
2.049	90.7408	2.215	105.6946	2.229	106.6631	2.076	108.7326	2.086	119.7161
2.051	90.7436	2.185	105.6974	2.255	106.6659	2.066	108.7357	2.090	119.7189
2.038	90.7469	2.163	105.7017	2.370	106.6751	2.084	108.7414	2.082	119.7217
2.033	90.7497	2.140	105.7046	2.408	106.6779	2.096	108.7445	2.105	119.7252
2.027	90.7528	2.136	105.7074	2.458	106.6807	2.102	108.7476	2.110	119.7280
2.020	90.7556	2.125	105.7107	2.536	106.6847	2.111	108.7531	2.122	119.7308
2.022	90.7590	2.114	105.7135	2.583	106.6876	2.115	108.7562	2.118	119.7340
2.019	90.7618	2.120	105.7163	2.644	106.6904	2.117	108.7592	2.137	119.7368
2.012	90.7646	2.098	105.7209	2.704	106.6938	2.147	108.7646	2.144	119.7397
2.009	90.7675	2.096	105.7237	2.765	106.6967	2.171	108.7677	2.157	119.7427
2.011	90.7703	2.088	105.7265	2.826	106.6995	2.198	108.7708	2.185	119.7456
2.018	90.7731	2.079	105.7311	2.891	106.7028	2.244	108.7769	2.203	119.7484
2.023	90.7763	2.076	105.7350	2.896	106.7057	2.285	108.7799	2.229	119.7519
2.016	90.7791	2.064	105.7369	2.873	106.7085	2.318	108.7830	2.252	119.7547
2.029	90.7820	2.061	105.7393	2.825	106.7117	2.371	108.7868	2.288	119.7575
2.023	90.7848	2.061	105.7440	2.765	106.7145	2.408	108.7899	2.341	119.7621
2.017	90.7876	2.054	105.7469	2.702	106.7174	2.474	108.7929	2.374	119.7649
2.023	90.7905	2.054	105.7497	2.658	108.6153	2.312	119.6186	2.428	119.7678
2.027	90.7933	2.049	105.7557	2.595	108.6184	2.219	119.6268		
2.018	90.7961	2.070	105.7607	2.538	108.6215	2.205	119.6296		
2.033	90.7990	2.054	105.7640	2.494	108.6251	2.184	119.6325		
2.043	90.8018	2.076	105.7678	2.448	108.6282	2.169	119.6363		

Table continued on following pages

Table 2. Observations of GQ CNC, ΔB, ΔV, ΔR_c, ΔI_c, variable-comparison, cont.

ΔR_c	HJD 2457270+	ΔR_c	HJD 2457270+	ΔR_c	HJD 2457270+	ΔR_c	HJD 2457270+	ΔR_c	HJD 2457270+
2.618	90.6406	2.203	90.8173	2.237	105.7980	2.248	106.7608	2.350	108.7775
2.694	90.6448	2.216	90.8202	2.242	105.8008	2.235	106.7645	2.386	108.7806
2.774	90.6486	2.227	90.8230	2.258	105.8035	2.224	106.7673	2.455	108.7844
2.845	90.6514	2.251	90.8263	2.166	106.6069	2.218	106.7701	2.494	108.7875
2.941	90.6559	2.275	90.8291	2.167	106.6097	2.208	106.7733	2.544	108.7905
2.990	90.6587	2.305	90.8326	2.164	106.6105	2.199	106.7761	2.358	119.6247
2.979	90.6639	2.328	90.8354	2.175	106.6131	2.194	106.7790	2.340	119.6275
2.860	90.6707	2.358	90.8383	2.175	106.6160	2.183	106.7828	2.325	119.6303
2.766	90.6754	2.473	105.6221	2.184	106.6196	2.184	106.7857	2.302	119.6341
2.683	90.6795	2.520	105.6250	2.185	106.6224	2.809	108.6129	2.281	119.6369
2.622	90.6823	2.574	105.6287	2.190	106.6253	2.761	108.6160	2.269	119.6397
2.559	90.6860	2.616	105.6316	2.200	106.6285	2.705	108.6191	2.263	119.6429
2.509	90.6888	2.673	105.6344	2.206	106.6314	2.647	108.6227	2.255	119.6458
2.455	90.6924	2.734	105.6375	2.213	106.6342	2.600	108.6258	2.238	119.6486
2.419	90.6952	2.781	105.6404	2.229	106.6398	2.553	108.6289	2.244	119.6519
2.325	90.7042	2.838	105.6432	2.229	106.6426	2.514	108.6320	2.228	119.6547
2.306	90.7070	2.913	105.6485	2.239	106.6454	2.474	108.6351	2.229	119.6575
2.263	90.7140	2.901	105.6514	2.254	106.6487	2.440	108.6382	2.224	119.6608
2.249	90.7168	2.870	105.6542	2.260	106.6516	2.370	108.6453	2.213	119.6636
2.241	90.7202	2.778	105.6596	2.273	106.6544	2.344	108.6484	2.195	119.6664
2.227	90.7231	2.736	105.6624	2.300	106.6581	2.321	108.6515	2.195	119.6696
2.228	90.7267	2.694	105.6653	2.325	106.6609	2.287	108.6572	2.204	119.6724
2.212	90.7295	2.591	105.6713	2.350	106.6637	2.269	108.6603	2.186	119.6753
2.196	90.7327	2.551	105.6742	2.451	106.6729	2.255	108.6634	2.206	119.6785
2.203	90.7355	2.461	105.6807	2.492	106.6757	2.249	108.6697	2.193	119.6814
2.178	90.7387	2.428	105.6835	2.532	106.6786	2.231	108.6728	2.192	119.6842
2.176	90.7415	2.399	105.6863	2.598	106.6826	2.231	108.6759	2.168	119.6874
2.171	90.7447	2.376	105.6895	2.648	106.6854	2.214	108.6808	2.175	119.6902
2.167	90.7475	2.348	105.6924	2.697	106.6883	2.210	108.6839	2.184	119.6930
2.152	90.7507	2.324	105.6952	2.767	106.6916	2.209	108.6870	2.177	119.6962
2.148	90.7535	2.300	105.6996	2.819	106.6945	2.191	108.6924	2.195	119.6990
2.140	90.7569	2.275	105.7024	2.892	106.6973	2.193	108.6955	2.194	119.7019
2.142	90.7597	2.262	105.7053	2.954	106.7007	2.186	108.6985	2.189	119.7050
2.128	90.7625	2.257	105.7085	3.010	106.7035	2.180	108.7042	2.201	119.7078
2.141	90.7653	2.246	105.7113	3.009	106.7063	2.181	108.7072	2.223	119.7106
2.134	90.7682	2.244	105.7142	2.966	106.7095	2.184	108.7103	2.207	119.7139
2.131	90.7710	2.228	105.7187	2.913	106.7124	2.182	108.7151	2.210	119.7168
2.139	90.7741	2.225	105.7215	2.853	106.7152	2.178	108.7182	2.228	119.7196
2.139	90.7770	2.218	105.7244	2.786	106.7185	2.176	108.7212	2.238	119.7231
2.128	90.7798	2.188	105.7418	2.728	106.7213	2.187	108.7271	2.229	119.7259
2.139	90.7826	2.181	105.7447	2.670	106.7242	2.190	108.7302	2.241	119.7287
2.137	90.7855	2.173	105.7475	2.580	106.7289	2.186	108.7333	2.237	119.7318
2.138	90.7883	2.173	105.7542	2.537	106.7317	2.190	108.7390	2.252	119.7347
2.136	90.7912	2.186	105.7590	2.489	106.7345	2.174	108.7421	2.257	119.7375
2.145	90.7939	2.181	105.7625	2.445	106.7377	2.198	108.7452	2.271	119.7406
2.148	90.7968	2.177	105.7664	2.412	106.7406	2.222	108.7507	2.279	119.7434
2.155	90.7996	2.182	105.7708	2.383	106.7434	2.231	108.7538	2.307	119.7462
2.167	90.8031	2.181	105.7775	2.351	106.7464	2.234	108.7568	2.331	119.7497
2.165	90.8059	2.212	105.7849	2.323	106.7493	2.236	108.7622	2.357	119.7526
2.172	90.8089	2.218	105.7892	2.298	106.7521	2.273	108.7653	2.381	119.7554
2.183	90.8117	2.215	105.7920	2.271	106.7551	2.274	108.7684	2.434	119.7600
2.189	90.8145	2.225	105.7947	2.267	106.7580	2.332	108.7744		

Table continued on next page

Table 2. Observations of GQ CNC, ΔB, ΔV, ΔR, ΔI, variable-comparison, cont.

ΔI_c	*HJD 2457270+*	ΔI_c	*HJD 2457270+*	ΔI_c	*HJD 2457270+*	ΔI_c	*HJD 2457270+*	ΔI_c	*HJD 2457270+*
2.811	90.6454	2.329	90.8207	2.340	105.7953	2.339	106.7614	2.379	108.7690
2.893	90.6492	2.354	90.8235	2.334	105.7986	2.330	106.7651	2.426	108.7750
2.956	90.6520	2.365	90.8268	2.354	105.8013	2.327	106.7679	2.431	108.7781
3.040	90.6565	2.392	90.8297	2.367	105.8041	2.320	106.7707	2.483	108.7812
3.113	90.6593	2.410	90.8332	2.264	106.6074	2.312	106.7739	2.559	108.7850
3.064	90.6649	2.448	90.8360	2.281	106.6109	2.300	106.7767	2.598	108.7880
2.941	90.6715	2.480	90.8389	2.270	106.6137	2.302	106.7795	2.461	119.6252
2.842	90.6760	2.513	90.8417	2.284	106.6166	2.280	106.7834	2.438	119.6281
2.769	90.6800	2.578	105.6227	2.287	106.6202	2.283	106.7862	2.420	119.6309
2.710	90.6829	2.626	105.6255	2.292	106.6230	2.271	106.7891	2.400	119.6347
2.645	90.6866	2.683	105.6293	2.305	106.6259	2.906	108.6135	2.389	119.6375
2.599	90.6894	2.741	105.6321	2.304	106.6291	2.856	108.6166	2.375	119.6403
2.552	90.6930	2.788	105.6350	2.315	106.6320	2.809	108.6196	2.367	119.6435
2.513	90.6958	2.848	105.6381	2.320	106.6348	2.749	108.6233	2.364	119.6463
2.422	90.7048	2.904	105.6410	2.329	106.6404	2.694	108.6264	2.339	119.6491
2.406	90.7076	2.955	105.6438	2.335	106.6432	2.655	108.6294	2.347	119.6524
2.363	90.7146	3.021	105.6491	2.347	106.6460	2.613	108.6326	2.337	119.6553
2.355	90.7174	3.000	105.6519	2.361	106.6493	2.576	108.6357	2.334	119.6581
2.345	90.7208	2.960	105.6548	2.366	106.6521	2.534	108.6387	2.327	119.6613
2.329	90.7237	2.877	105.6602	2.383	106.6550	2.460	108.6459	2.325	119.6641
2.319	90.7273	2.829	105.6630	2.411	106.6587	2.441	108.6490	2.316	119.6670
2.317	90.7301	2.774	105.6659	2.435	106.6615	2.420	108.6521	2.312	119.6702
2.314	90.7333	2.717	105.6691	2.459	106.6643	2.420	108.6521	2.304	119.6730
2.300	90.7361	2.681	105.6719	2.564	106.6735	2.381	108.6578	2.326	119.6758
2.293	90.7392	2.640	105.6748	2.601	106.6763	2.366	108.6609	2.293	119.6791
2.289	90.7421	2.556	105.6812	2.642	106.6791	2.360	108.6639	2.294	119.6820
2.285	90.7453	2.522	105.6841	2.708	106.6831	2.351	108.6703	2.302	119.6848
2.285	90.7481	2.493	105.6869	2.760	106.6860	2.340	108.6734	2.285	119.6879
2.269	90.7513	2.469	105.6901	2.809	106.6888	2.328	108.6765	2.279	119.6908
2.257	90.7541	2.442	105.6930	2.876	106.6922	2.322	108.6814	2.284	119.6936
2.250	90.7574	2.422	105.6958	2.942	106.6951	2.318	108.6845	2.287	119.6968
2.261	90.7602	2.392	105.7001	2.988	106.6979	2.313	108.6875	2.300	119.6996
2.254	90.7631	2.378	105.7030	3.068	106.7012	2.300	108.6930	2.305	119.7024
2.250	90.7659	2.366	105.7058	3.101	106.7041	2.295	108.6960	2.302	119.7056
2.248	90.7687	2.357	105.7091	3.093	106.7069	2.296	108.6991	2.305	119.7084
2.252	90.7715	2.346	105.7119	3.042	106.7101	2.290	108.7048	2.306	119.7112
2.256	90.7747	2.343	105.7147	2.975	106.7130	2.285	108.7078	2.311	119.7145
2.251	90.7775	2.333	105.7193	2.929	106.7158	2.290	108.7109	2.324	119.7173
2.248	90.7804	2.330	105.7221	2.863	106.7191	2.292	108.7157	2.335	119.7201
2.256	90.7832	2.319	105.7250	2.802	106.7219	2.290	108.7187	2.333	119.7236
2.259	90.7860	2.291	105.7424	2.744	106.7247	2.300	108.7218	2.351	119.7264
2.251	90.7889	2.286	105.7453	2.667	106.7294	2.295	108.7277	2.343	119.7293
2.257	90.7917	2.286	105.7481	2.617	106.7323	2.295	108.7308	2.352	119.7324
2.271	90.7945	2.287	105.7546	2.581	106.7351	2.295	108.7338	2.357	119.7352
2.269	90.7974	2.282	105.7595	2.535	106.7383	2.287	108.7396	2.377	119.7381
2.271	90.8002	2.285	105.7629	2.505	106.7411	2.314	108.7427	2.384	119.7412
2.285	90.8037	2.284	105.7668	2.471	106.7440	2.279	108.7458	2.404	119.7440
2.285	90.8065	2.303	105.7714	2.430	106.7470	2.294	108.7513	2.423	119.7468
2.296	90.8094	2.309	105.7781	2.409	106.7498	2.332	108.7543	2.450	119.7503
2.289	90.8122	2.324	105.7855	2.397	106.7527	2.313	108.7574	2.471	119.7531
2.301	90.8151	2.326	105.7898	2.376	106.7557	2.349	108.7628		
2.321	90.8179	2.330	105.7925	2.359	106.7586	2.371	108.7659		

Table 3. O–C residuals, linear and quadratic period study, GQ Cnc.

	Epoch	*Cycles*	*Lineal Residuals*	*Quadratic Residuals*	*Wt.*	*Reference*
1	50154.4206	–14808.5	–0.0060	–0.0054	1.0	Vidal-Sainz and Garcia-Melendo 1996
2	50159.4876	–14796.5	–0.0055	–0.0049	1.0	Vidal-Sainz and Garcia-Melendo 1996
3	50164.3426	–14785.0	–0.0059	–0.0053	1.0	Vidal-Sainz and Garcia-Melendo 1996
4	50165.3996	–14782.5	–0.0044	–0.0038	1.0	Vidal-Sainz and Garcia-Melendo 1996
5	50207.4174	–14683.0	0.0036	0.0042	1.0	Vidal-Sainz and Garcia-Melendo 1996
6	50218.3948	–14657.0	0.0036	0.0041	1.0	Vidal-Sainz and Garcia-Melendo 1996
7	50226.4173	–14638.0	0.0041	0.0047	1.0	Vidal-Sainz and Garcia-Melendo 1996
8	51199.6080	–12333.0	0.0035	0.0032	1.0	Wolf and Diethelm 1999
9	51274.3380	–12156.0	0.0025	0.0022	1.0	Paschke 1999
10	51984.4940	–10474.0	0.0033	0.0026	1.0	Blättler *et al.* 2001
11	52279.6194	–9775.0	0.0048	0.0039	1.0	Zejda 2004
12	52362.3700	–9579.0	0.0024	0.0015	1.0	Locher *et al.* 2002
13	52691.2705	–8800.0	0.0023	0.0013	1.0	Diethelm 2003
14	53325.6310	–7297.5	–0.0060	–0.0071	0.5	Locher 2005
15	54839.8837	–3711.0	–0.0051	–0.0059	1.0	Diethelm 2009
16	54842.8436	–3704.0	–0.0007	–0.0015	1.0	Diethelm 2009
17	55245.8432	–2749.5	0.0006	0.0000	1.0	Diethelm 2010
18	55275.3979	–2679.5	0.0007	0.0001	1.0	Hübscher and Monninger 2011
19	55577.9104	–1963.0	0.0006	0.0002	1.0	Diethelm 2009
20	55652.6406	–1786.0	–0.0002	–0.0005	1.0	Diethelm 2009
21	56002.6490	–957.0	–0.0029	–0.0029	0.5	Diethelm 2012
22	56390.6620	–38.0	0.0002	0.0005	1.0	Present Observations
23	56405.6505	–2.5	0.0003	0.0006	1.0	Present Observations
24	56406.7056	0.0	–0.0002	0.0002	1.0	Present Observations
25	57414.3070	2386.5	0.0000	0.0014	1.0	Hübscher 2017
26	57414.5183	2387.0	0.0001	0.0016	1.0	Hübscher 2017

Table 4. Light curve characteristics, GQ Cnc.

Filter	*Phase*	*Magnitude Min. I*	*Phase*	*Magnitude Max. II*
	0.0		0.25	
B		2.991 ± 0.005		2.135 ± 0.005
V		3.092 ± 0.003		2.252 ± 0.003
R_c		2.991 ± 0.026		2.135 ± 0.005
I_c		3.092 ± 0.027		2.252 ± 0.003
Filter	*Phase*	*Magnitude Min. II*	*Phase*	*Magnitude Max. I*
	0.50		0.75	
B		2.907 ± 0.026		2.179 ± 0.005
V		3.011 ± 0.027		2.286 ± 0.003
R_c		2.907 ± 0.026		2.179 ± 0.005
I_c		3.011 ± 0.027		2.286 ± 0.003
Filter		*Min. I – Max. II*		*Min. I – Min. II*
B		0.856 ± 0.009		0.084 ± 0.031
V		0.840 ± 0.007		0.081 ± 0.031
R_c		0.856 ± 0.031		0.084 ± 0.053
I_c		0.840 ± 0.031		0.081 ± 0.054
Filter		*Max. I – Max. II*		
B		0.044 ± 0.009		
V		0.034 ± 0.007		
R_c		0.044 ± 0.009		
I_c		0.034 ± 0.007		

Table 5. GQ Cnc light curve solutions.

Parameters	*Best Solution*	*Initial Solution*
λ_B, λ_V, λ_R, λ_I (nm)	440, 550, 640, 790	—
$x_{bol1,2}$, $y_{bol1,2}$	0.648 0 .647, 0.207, 0 .176	—
$x_{1I,2I}$, $y_{1I,2I}$	0.590, 0. 590, 0.260, 0.260	—
$x_{1R,2R}$, $y_{1R,2R}$	0. 674, 0.674, 0. 269, 0. 269	—
$x_{1V,2V}$, $y_{1V,2V}$	0.745, 0.745, 0. 256, 0. 256	—
$x_{1B,2B}$, $y_{1B,2B}$	0. 829, 0.829, 0.185, 0.185	—
g_1 , g_2	0.320,0.320	—
A_1 , A_2	0.5, 0.5	—
Inclination (°)	85.6 ± 0.1	85.21 ± 0.15
T_1, T_2 (K)	5250*, 5247 ± 2	5250, 5225 ± 1
Ω_1, Ω_2 pot	3.529 ± 0.002, 3.442 ± 0.002	3.7549 ± 0.0013, 3.804 ± 0.002
q (m_2 / m_1)	0.802 ± 0.001	0.9877 ± 0.0004
Fill-outs: F_1, F_2 (%)	97, 99	94, 98
L_1 / (L_1 + L_2)I	0.5326 ± 0.00009	0.518 ± 0.001
L_1 / (L_1 + L_2)R	0.5327 ± 0.0010	0.519 ± 0.001
L_1 / (L_1 + L_2)V	0.5326 ± 0.0011	0.5199 ± 0.0006
L_1 / (L_1 + L_2)B	0.5327 ± 0.0008	0.5218 ± 0.0008
JD_o (days)	2456406.70555 ± .000011	2456406.70552 ± .000005
Period (days)	0. 4222380 ± 0.0000003	0. 42223823 ± 0.0000003
r_1, r_2 (pole)	0. 3604 ± 0.0035, 0.335 ± 0.004	0. 354 ± 0.001, 0.346 ± 0.004
r_1, r_2 (point)	0.439 ± 0.011, 0.4405 ± 0.0256	0.463 ± 0.024, 0.433 ± 0.017
r_1, r_2 (side)	0.377 ± 0.004, 0.351 ± 0.004	0.372 ± 0.004, 0.362 ± 0.005
r_1, r_2 (back)	0.402 ± 0.006, 0.381 ± 0.006	0.401 ± 0.006, 0.389 ± 0.007
Spot Parameters	*Star 1*	*Hot Spot*
Colatitude (°)	24 ± 1	94 ± 2
Longitude (°)	238 ± 1	224 ± 1
Spot radius (°)	11.7 ± 0.2	15.1 ± 0.5
Tfact	1.47 ± 0.01	1.106 ± 0.006
$\Sigma(res)^2$	0.7842	0.8303

**The primary temperature is an estimate from 2MASS results ± 150 K.*

Multi-color Photometry of the Hot R Coronae Borealis Star, MV Sagittarii

Arlo U. Landolt
Department of Physics and Astronomy, Louisiana State University, Baton Rouge, LA 70803; landolt@phys.lsu.edu

Visiting astronomer, Cerro Tololo Inter-American Observatory, National Optical Astronomical Observatory, which is operated by the Association of Universities for Research in Astronomy, Inc., under contract with the National Science Foundation.

James L. Clem
Department of Physics and Astronomy, Louisiana State University, Baton Rouge, LA 70803 (Current address: Department of Physics, Grove City College, Grove City, PA 16127); jclem@phys.lsu.edu

Visiting astronomer, Cerro Tololo Inter-American Observatory, National Optical Astronomical Observatory, which is operated by the Association of Universities for Research in Astronomy, Inc., under contract with the National Science Foundation.

Received July 3, 2017; revised September 20, October 10, 2017; accepted November 29, 2017

Abstract A long term program of photoelectric UBVRI photometry has been combined with AAVSO archival data for the hot, R CrB-type hydrogen deficient star MV Sgr. A deep minimum and a trend of decreasing brightness over time at maximum light thereby become evident. Variations seen via monitoring with a CCD detector also are described.

1. Introduction

The variable star now known as MV Sgr was discovered by Woods (1928), who quoted a range in magnitude of 12.7 to fainter than 15.0. Woods's discovery note does not state the kind of emulsion utilized, and hence the type of magnitude. (History describing the Harvard College Observatory (HCO) telescopes, leading to an enhanced understanding of the kinds of magnitudes produced by the HCO patrol telescopes, may be found at the Digital Access to a Sky Century @ Harvard (DASCH), dasch.rc.fas.harvard.edu/photometry.php, leading to dasch.rc.fas.harvard.edu/lightcurve.php.) Additional insight is located in Laycock *et al.* (2010). MV Sgr was determined to be of the R Coronae Borealis (R CrB) type by Hoffleit (1958). Hoffleit (1959) provided the first light curve, where she found "two groups of minima." Herbig (1964) discussed in detail spectra of MV Sgr taken at maximum light. He found the strongest lines "to be due to He I with no sign of hydrogen in absorption, and with the presence of C II." Herbig called MV Sgr a "very hot carbon star." He reported a radial velocity of -68 km s^{-1}. Finally, Herbig reported photoelectric photometry carried out by B. Paczynski on 1963 July 26 and August 10. The mean values of the single measurements made on each of those two nights were $V = 12.70$, $(B-V) = +0.26$, and $(U-B) = -0.60$. Since no exact times of observation were reported by Herbig, a straight average of, say, twelve hours UT, of the Julian Dates for July 26th and August 10th, 1963, gives a mean time of observation of JD 2438244.5. Percy and Fu (2012) announced an approximate eight-day pulsation period from their study of AAVSO data.

MV Sgr, whose UCAC4 coordinates (Zacharias *et al.* 2013) are R.A. $18^h 44^m 31.968^s$, Dec. $-20° 57' 12.87''$ (J2000), is a member of a small subset of four hot hydrogen-deficient stars. These four stars, MV Sgr, V348 Sgr, DY Cen, and HV 2671, possess the R CrB-type of light curve, that is, they spend the majority of the time at maximum brightness, with occasional excursions to fainter magnitudes (De Marco *et al.* 2000, and references therein). They differ from most R CrB stars in that on average their effective temperatures are 10,000 K to 15,000 K hotter.

MV Sgr also appears in the literature as HV 4168, UCAC4 346-161178, AAVSO 1838-21, 2MASS J18443197-2057127, and ASASJ184432-2057.2. The UCAC4 catalogue lists its proper motions as $\mu_\alpha = -3.2 \pm 3.2$ and $\mu_\delta = -8.7 \pm 4.1$ mas yr^{-1}. The related AAVSO Photometric All-Sky Survey (APASS; Henden *et al.* 2009) photometry, Data Release 6 (DR 6), lists a brightness of $V = 13.387$ and $B = 13.565$, for a combined $(B-V) = +0.178$. This magnitude and color index are a combination of measures taken on 2012 April 3rd, April 15th, and September 21st.

A finding chart for MV Sgr is given in Figure 1. The chart is based on a digitized version of the Palomar Sky Survey I (POSS I) blue survey (Palomar Observatory 1950–1957). The size of the field as presented in the chart is about ten arc minutes on a side.

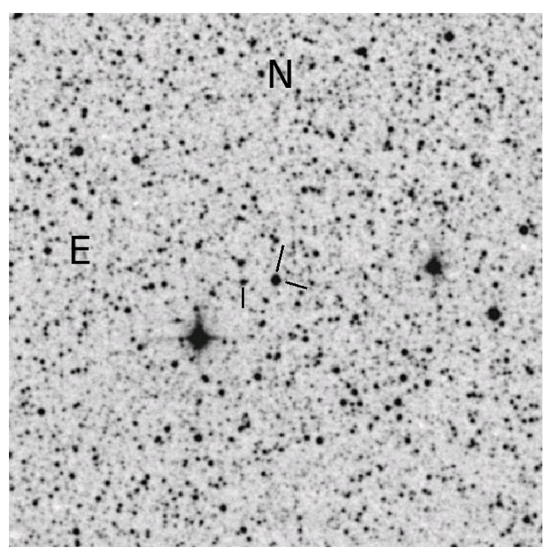

Figure 1. Finding Chart for MV Sgr identified between two lines, and a nearby faint star UCAC4 346–161204 identified by one line. The field of view is approximately 10 arc minutes on a side.

Excellent and definitive summaries of the characteristics of R CrB stars, including the four stars listed above, have appeared in Clayton (1996, 2012). De Marco *et al.* (2002) thoroughly describe this four-member subset of R CrB stars. They write that these four stars are quite different from each other as evidenced by their spectra. They indicate that the "only common characteristics are their temperatures and light variation." Finally, they found that MV Sgr, V348 Sgr, and DY Cen all exhibit a long-term downward trend in brightness over the time frame under study. Schaefer (2016) has searched archival files and also has discussed the long term behavior of this four-star group of hot R CrB stars.

2. Observations

Photoelectric observations of MV Sgr were carried out by AUL in the interval 1977 June 5 to 2001 October 15 (2443299.82217 ≤ *HJD* ≤ 2452197.58510), a range of 8,898 days, or 24.4 years. The data were collected at Cerro Tololo Inter-American Observatory's (CTIO) 0.6-meter (Lowell), 0.9-meter, 1.0-meter (Yale), and 1.5-meter telescopes. A "quick look at the telescope" measurement was reported by Landolt (1979). The June 1977 data were collected at the CTIO (Lowell) 0.6-meter telescope. The detector was a 1P21 photomultiplier in cold box no. 62. The filters were *UBV* set no. 2. These data were tied into standard stars defined by Johnson (1963) and by Landolt (1973). Data acquired between 1979 and including 1997 were tied into *UBVRI* standard stars as defined in Landolt (1983). All R and I measures herein are on the Kron-Cousins system. The 1998 through 2001 data were tied into Landolt (1992). The 1979 through 2001 data, using detectors described in Landolt (1983, 1992), were reduced following precepts outlined in Landolt (2007).

Some doubt exists concerning the photoelectric measures of 1979 October and 1980 March. The raw data printout at the telescope for 1979 October 28 *UT* (HJD 2444474.5) provided a record indicating that the observer found MV Sgr to be below visibility that night at the CTIO 0.9-meter telescope. This perhaps was to be expected given the variable and poor seeing of approximately 4 arc seconds at the time of non-detection, 00:25 *UT* (HJD 2444174.51736). Also, five nights earlier, the star was found to be at $V = 15.167$ on 1979 October 23 *UT* as measured at the CTIO 1.5-meter telescope. The data for 1979 October 23 *UT* (HJD 2444169.51798) were $V = 15.167$, $(B–V) = +0.871$, $(U–B) = +0.254$. However, these data are a close match for UCAC4 346-161204; that star's photometry is $V = 15.118$, and $(B–V) = +0.855$, taken from APASS photometry (Henden *et al.* 2009), Data Release 6 (DR 6).

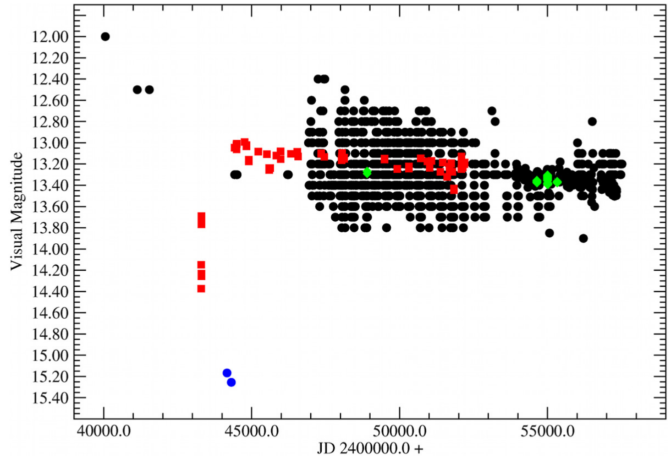

Figure 2. Visual AAVSO database magnitudes plus *V* photoelectric and CCD magnitudes from this paper for MV Sgr. Black color coding indicates AAVSO data, red photoelectric data, green CCD data, and blue two photoelectric possible MV Sgr data points.

A supposed measurement of MV Sgr taken 1980 March 17 *UT* (HJD 2444315.87955) also provided photometry $V = 15.255$ and $(B–V) = +0.886$, which may be the same star which was observed 1979 October 23. However, a note in AUL's log book for 1980 March 17 *UT* specifically said that "if the star just observed was not MV Sgr, then MV Sgr is fainter than 16th magnitude."

A problem with verifying that the above measures are of MV Sgr arises from the apparent lack of measurements in the literature anywhere near this time frame, and with which the authors could compare these suspicious data points. MV Sgr never has been seen that faint. At that time in observational history, observers at the telescope visually located a program star with a finder chart nearby. There is a possibility that a star other than MV Sgr was observed, as it may have been on 1979 October 23. There is evidence from the log book on 1980 March 17 that MV Sgr was not visible that night. Therefore, was it also below visibility on 1979 October 23?

The three 1992 October (HJD 2448905.6) CCD data points, shown in Figure 2 as a green symbol, were obtained by AUL and A. K. Uomoto at the Las Campanas Observatory (LCO) Swope 1.0-meter telescope. The detector was a Texas Instrument (TI #1) 800 × 800 pixel chip whose plate scale was 0.435" pixel^{-1}. The field size was 5.8' on a side. The data were binned 2 × 2. A 2 × 2-inch *UBVRI* filter set borrowed from CTIO meant that the same filter set was used for AUL's CTIO and LCO programs at that time. The composition of the filter set is described in Table 1. The third column provides the effective wavelength for the filter and the fourth column gives the full width at half

Table 1. CTIO CCD filter set used at LCO's Swope Telescope.

Filter	*CTIO ID*	λ_{eff} *Å*	*fwhm* *Å*	*Thickness* *mm*	*Comments*
U	Hamilton No.1	3570	0660	8.78	1 mm UG1 + 1 mm WG295 + 6.78 mm $CuSO_4$
B	B13	4440	1123	5.68	2 mm GG385 + 1 mm BG12 + 2 mm BG39
V	V16	5460	1118	5.72	2 mm GG495 + 3 mm BG39
R	R11	6477	1239	5.80	2 mm GG570 + 3 mm KG3
I	I11	8227	1865	4.62	3 mm RG9 + 1 mm WG295

maximum (fwhm), both in Angstroms. The fifth column lists the total thickness of the filters in millimeters. The final column, Comments, provides the combination of filters employed to define the filters' effective wavelengths and full width at half maximum.

The CTIO data, calendar years 2008 through 2010, were obtained at the CTIO Yale 1.0-meter telescope by JLC, using the Y4KCam CCD. The equipment, data acquisition, and reduction processes were described in Clem and Landolt (2013).

3. Discussion

The reduction process recovered the magnitudes and color indices of the standard stars observed each night. The rms errors calculated from those recovered magnitudes and color indices are listed in Table 2. Columns one and two give the *UT* date of observation and the corresponding Julian Date, respectively. The telescope at which the data were collected is given in the third column, and the filters through which the data were taken are in the fourth column. The last six columns list the rms errors of the recovered standard stars' magnitude and color indices for that night. The last two lines in Table 2 show that the accuracy of the recovered standard star photometry was one percent or less, except for (*U–B*). MV Sgr itself most often was on the order of 1.5 magnitudes fainter than the standard stars.

At the time of initial writing in 2016 May, all available visual and *V*-magnitude data for MV Sgr were downloaded from the AAVSO International Database (Kafka 2015). These data covered the time interval 1968 July 21 to 2016 May 11 *UT* (2440058.700 ≤ JD ≤ 2457520.2958). Visual observations indicating "fainter than" and those taken through filters other than "Johnson *V*" then were eliminated from the listing. The remaining AAVSO observations have been displayed in Figure 2 as black circles. Johnson *V*-magnitude photoelectric data from the observations reported in this manuscript, Table 3, then were overlayed in Figure 2 onto the AAVSO-based observations. Our photoelectric observations are plotted in red. The two possible measurements, described above, of MV Sgr are shown as blue circles. The first two observations in Table 3 were obtained on a marginally photometric night at the CTIO (Lowell) 0.6-meter telescope, hence the discrepancy. An average of those two measures, $\overline{V}$ = 14.261, agrees with the trend of the measures taken on the following photometric nights. One is reminded that the AAVSO database observations are in Julian Days (JDs), whereas the authors' are in Heliocentric Julian Days (HJDs).

CCD data for MV Sgr, from Table 4 and plotted with green symbols in Figure 2, were obtained by JLC at the CTIO Yale 1.0-meter telescope in the interval 2008 June 29 to 2010 May 13 *UT* (2454646.7 ≤ HJD ≤ 2455329.7).

Figure 2 shows MV Sgr coming out of a minimum in light in the Johnson *V* band on HJD2443302.9, having reached *V* = 14.256, roughly 1.2 magnitudes fainter than its average brightness in the following year. Depending on the veracity of the data points on HJD 2444169.51798 and 2444315.87955, one could deduce that a second dimming had taken place, coming to a swift end about HJD 2444316 at *V* = 15.255. These dates, the first certainly, and the second more problematic, were the first deep minima found and measured since those described

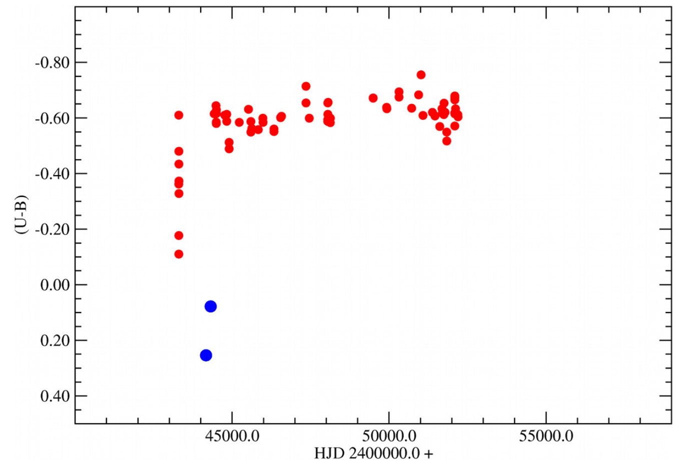

Figure 3. Photoelectric (*U–B*) color index data for MV Sgr from this paper. Data point colors are the same as in Figure 2.

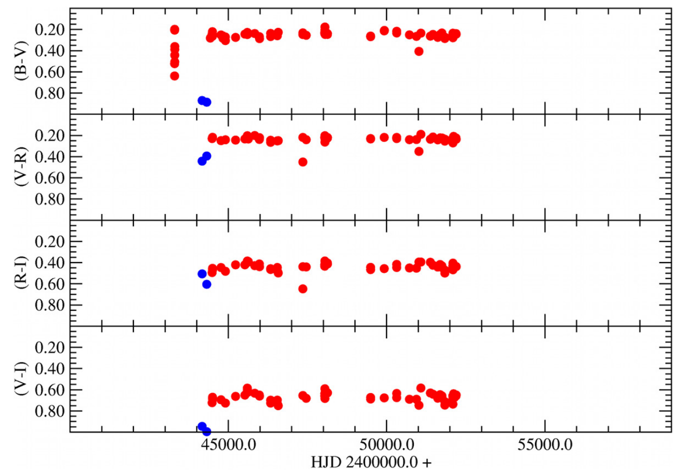

Figure 4. Photoelectric (*B–V*), (*V–R*), (*R–I*), and (*V–I*) color index data for MV Sgr from this paper. Data point colors are the same as in Figure 2.

by Hoffleit (1958, 1959), which minima were on the order of, or greater than, two magnitudes in depth as measured in a photographic *B* magnitude.

More precisely, perusal of data plotted in Figure 4, and taken from Table 3, provide the results in Table 5. The final magnitudes and color indices have been grouped into two "windows," for convenience: window 1 averages results between HJD 2444486 and HJD 2446574; window 2 averages data between HJD 2447352 and HJD 2452197. Rounded off, MV Sgr dropped 0.13 magnitude in brightness in *V* over 7,711 days, following the certain minimum prior to or about HJD 2443299.

If the data taken on HJD 2444169.51798 and 2444315.87955 truly were of MV Sgr, then MV Sgr reached (*B–V*) = +0.88 and (*U–B*) = +0.25 when faintest. The *R* and *I* filter data for these nights' data also show a more red color index in (*V–R*), (*R–I*) and (*V–I*) by some 0.2, 0.1, and 0.2 magnitude, respectively. These values are in line with, or are reasonable for what one might expect for a R CrB star at minimum brightness. Otherwise, as illustrated in Figures 3 and 4, the color indices following minimum essentially are constant, except for (*U–B*), which becomes more blue with time, with large variations.

Table 2. RMS photometric errors per night recovered from standard stars.

UT	*HJD*	*Telescope*	*Filter*	*RMS Errors Recovered Standards*					
(mmddyy)	*2400000.0+*			*V*	*(B–V)*	*(U–B)*	*(V–R)*	*(R–I)*	*(V–I)*
060577	43299.5	CTIO 0.6-m	UBV	0.008	0.005	0.018	—	—	—
060877	43302.5	CTIO 0.6-m	UBV	0.011	0.008	0.016	—	—	—
060977	43303.5	CTIO 0.6-m	UBV	0.015	0.006	0.016	—	—	—
061177	43305.5	CTIO 0.6-m	UBV	0.015	0.007	0.012	—	—	—
090480	44486.5	CTIO 1.5-m	UBVRI	0.023	0.011	0.033	0.009	0.007	0.014
091280	44494.5	CTIO 0.9-m	UBV	0.014	0.007	0.011	—	—	—
091680	44498.5	CTIO 0.9-m	UBVRI	0.010	0.011	0.023	0.007	0.006	0.008
061081	44765.5	CTIO 1.5-m	UBVRI	0.011	0.013	0.044	0.011	0.017	0.022
081181	44827.5	CTIO 0.9-m	UBV	0.011	0.016	0.023	—	—	—
102681	44903.5	CTIO 0.9-m	UBV	0.013	0.016	0.025	—	—	—
102881	44905.5	CTIO 0.9-m	UBVRI	0.014	0.009	0.023	0.007	0.004	0.007
091482	45226.5	CTIO 1.5-m	UBVRI	0.016	0.014	0.050	0.008	0.008	0.008
070583	45520.5	CTIO 1.5-m	UBVRI	0.006	0.007	0.006	0.003	0.004	0.004
092083	45597.5	CTIO 1.5-m	UBVRI	0.003	0.010	0.037	0.005	0.010	0.010
102183	45628.5	CTIO 0.9-m	UBVRI	0.005	0.007	0.012	0.002	0.004	0.005
051384	45833.5	CTIO 1.5-m	UBVRI	0.007	0.013	0.056	0.007	0.009	0.015
100584	45978.5	CTIO 0.9-m	UBVRI	0.010	0.006	0.015	0.008	0.005	0.007
101184	45984.5	CTIO 0.9-m	UBVRI	0.016	0.005	0.027	0.005	0.003	0.004
092585	46333.5	CTIO 1.5-m	UBVRI	0.012	0.011	0.032	0.014	0.011	0.018
042586	46545.5	CTIO 1.5-m	UBVRI	0.007	0.011	0.045	0.006	0.010	0.011
052486	46574.5	CTIO 1.5-m	UBVRI	0.004	0.008	0.025	0.006	0.017	0.017
071088	47352.5	CTIO 1.5-m	UBVRI	0.009	0.007	0.017	0.008	0.005	0.007
102388	47457.5	CTIO 1.5-m	UBVRI	0.009	0.010	0.042	0.008	0.006	0.009
060290	48044.5	CTIO 1.5-m	UBVRI	0.012	0.009	0.026	0.006	0.012	0.013
060690	48048.5	CTIO 1.0-m	UBVRI	0.009	0.009	0.028	0.006	0.005	0.009
060890	48050.5	CTIO 1.0-m	UBVRI	0.006	0.011	0.028	0.006	0.010	0.012
061390	48055.5	CTIO 1.5-m	UBVRI	0.006	0.009	0.023	0.005	0.006	0.010
061690	48058.5	CTIO 1.5-m	UBVRI	0.007	0.009	0.033	0.008	0.011	0.018
082490	48127.5	CTIO 1.5-m	UBVRI	0.011	0.009	0.032	0.006	0.005	0.006
082690	48129.5	CTIO 1.5-m	UBVRI	0.010	0.008	0.029	0.005	0.008	0.009
052094	49492.5	CTIO 1.5-m	UBVRI	0.004	0.003	0.012	0.003	0.003	0.005
072495	49922.5	CTIO 1.5-m	UBVRI	0.007	0.009	0.020	0.004	0.010	0.011
073195	49929.5	CTIO 1.0-m	UBV	0.004	0.008	0.020	—	—	—
082196	50316.5	CTIO 1.0-m	UBVRI	0.006	0.009	0.029	0.004	0.004	0.007
092997	50720.5	CTIO 1.5-m	UBVRI	0.006	0.009	0.031	0.004	0.007	0.008
050898	50941.5	CTIO 1.5-m	UBVRI	0.008	0.009	0.014	0.004	0.005	0.004
072598	51019.5	CTIO 1.5-m	UBVRI	0.015	0.014	0.020	0.006	0.011	0.014
092598	51081.5	CTIO 1.5-m	UBVRI	0.008	0.009	0.032	0.007	0.011	0.014
072199	51380.5	CTIO 1.5-m	UBVRI	0.008	0.007	0.020	0.004	0.007	0.008
101299	51463.5	CTIO 1.5-m	UBVRI	0.005	0.006	0.033	0.004	0.008	0.008
031100	51614.5	CTIO 1.5-m	UBVRI	0.006	0.010	0.020	0.005	0.004	0.007
052300	51687.5	CTIO 1.5-m	UBVRI	0.008	0.010	0.019	0.006	0.012	0.015
052900	51693.5	CTIO 1.5-m	UBVRI	0.008	0.012	0.023	0.004	0.006	0.007
071900	51744.5	CTIO 1.5-m	UBVRI	0.007	0.007	0.020	0.004	0.004	0.007
072500	51750.5	CTIO 1.5-m	UBVRI	0.005	0.008	0.020	0.003	0.004	0.006
082500	51781.5	CTIO 1.5-m	UBVRI	0.010	0.011	0.036	0.005	0.008	0.009
102000	51837.5	CTIO 1.5-m	UBVRI	0.008	0.009	0.033	0.003	0.005	0.006
102100	51838.5	CTIO 1.5-m	UBVRI	0.007	0.010	0.031	0.003	0.006	0.006
062801	52088.5	CTIO 1.5-m	UBVRI	0.007	0.011	0.022	0.006	0.004	0.008
070301	52093.5	CTIO 1.5-m	UBVRI	0.004	0.006	0.010	0.004	0.007	0.008
072501	52115.5	CTIO 1.5-m	UBVRI	0.007	0.007	0.023	0.004	0.008	0.010
082101	52142.5	CTIO 1.5-m	UBVRI	0.008	0.010	0.033	0.003	0.009	0.011
100701	52189.5	CTIO 1.5-m	UBVRI	0.010	0.010	0.034	0.005	0.014	0.015
101501	52197.5	CTIO 1.5-m	UBVRI	0.007	0.010	0.037	0.007	0.029	0.031
			ave.	0.009	0.009	0.026	0.006	0.008	0.010
			±	0.004	0.003	0.010	0.002	0.005	0.005

Table 3. UBVRI photoelectric data for MV Sgr.

UT (mmddyy)	HJD	V m	(B–V) m	(U–B) m	(V–R) m	(R–I) m	(V–I) m
060577	2443299.82217	14.373	+0.523	–0.610	—	—	—
060577	2443299.82442	14.148	+0.639	–0.362	—	—	—
060877	2443302.90741	14.256	+0.206	–0.177	—	—	—
060877	2443302.90924	14.233	+0.199	–0.110	—	—	—
060977	2443303.88910	13.768	+0.442	–0.434	—	—	—
060977	2443303.89093	13.740	+0.506	–0.480	—	—	—
061177	2443305.88507	13.689	+0.361	–0.328	—	—	—
061177	2443305.88707	13.700	+0.387	–0.373	—	—	—
090480	2444486.51589	13.024	+0.242	–0.644	+0.230	+0.494	+0.722
091280	2444494.64401	13.009	+0.264	–0.580	—	—	—
091280	2444494.64613	13.062	+0.221	–0.585	—	—	—
091680	2444498.52265	13.009	+0.250	–0.616	+0.220	+0.469	+0.688
091680	2444498.52510	13.011	+0.250	–0.629	+0.218	+0.454	+0.671
061081	2444765.86108	12.992	+0.252	–0.610	+0.249	+0.447	+0.695
081181	2444827.61518	13.032	+0.261	–0.588	—	—	—
081181	2444827.61730	13.021	+0.283	–0.613	—	—	—
102681	2444903.53541	13.176	+0.271	–0.512	—	—	—
102881	2444905.54671	13.158	+0.305	–0.489	+0.241	+0.482	+0.726
091482	2445226.52759	13.083	+0.275	–0.584	+0.244	+0.421	+0.663
070583	2445520.72851	13.107	+0.244	–0.631	+0.233	+0.421	+0.651
092083	2445597.56996	13.238	+0.228	–0.549	+0.207	+0.399	+0.603
092083	2445597.57513	13.255	+0.248	–0.587	+0.203	+0.385	+0.585
102183	2445628.56142	13.238	+0.237	–0.562	+0.234	+0.390	+0.621
051384	2445833.86878	13.120	+0.238	–0.558	+0.201	+0.429	+0.633
100584	2445978.57635	13.081	+0.268	–0.599	+0.238	+0.413	+0.650
101184	2445984.55183	13.154	+0.286	–0.584	+0.221	+0.439	+0.660
092585	2446333.54524	13.104	+0.267	–0.560	+0.246	+0.458	+0.699
092585	2446333.54891	13.104	+0.237	–0.551	+0.265	+0.465	+0.726
042586	2446545.79576	13.085	+0.259	–0.602	+0.251	+0.477	+0.728
042586	2446545.80049	13.093	+0.239	–0.601	+0.252	+0.446	+0.698
052486	2446574.87069	13.129	+0.227	–0.606	+0.250	+0.498	+0.751
071088	2447352.78055	13.098	+0.248	–0.654	+0.219	+0.439	+0.655
071088	2447352.78498	13.103	+0.232	–0.714	+0.451	+0.648	+1.097
102388	2447457.55773	13.132	+0.255	–0.599	+0.240	+0.441	+0.681
060290	2448044.87654	13.165	+0.228	–0.588	+0.223	+0.434	+0.659
060290	2448044.88185	13.155	+0.238	–0.594	+0.216	+0.419	+0.637
060690	2448048.77037	13.130	+0.206	–0.654	+0.203	+0.385	+0.591
060890	2448050.71535	13.153	+0.177	–0.613	+0.263	+0.423	+0.682
061390	2448055.71465	13.113	+0.238	–0.587	+0.232	+0.411	+0.640
061690	2448058.73850	13.097	+0.247	–0.656	+0.221	+0.411	+0.633
082490	2448127.66543	13.152	+0.247	–0.583	+0.226	+0.404	+0.630
082690	2448129.68335	13.139	+0.240	–0.599	+0.220	+0.413	+0.629
052094	2449492.88803	13.158	+0.262	–0.671	+0.230	+0.445	+0.673
052094	2449492.89161	13.149	+0.268	–0.672	+0.233	+0.466	+0.688
072495	2449922.68955	13.247	+0.213	–0.638	+0.219	+0.457	+0.677
073195	2449929.51290	13.245	+0.209	–0.633	—	—	—
082196	2450316.50323	13.223	+0.233	–0.694	+0.219	+0.417	+0.635
082196	2450316.50670	13.244	+0.217	–0.675	+0.230	+0.446	+0.675
092997	2450720.54775	13.147	+0.251	–0.635	+0.240	+0.451	+0.690
050898	2450941.79774	13.174	+0.265	–0.683	+0.239	+0.453	+0.690
072598	2451019.75696	13.236	+0.407	–0.755	+0.351	+0.395	+0.747
092598	2451081.55383	13.170	+0.235	–0.609	+0.190	+0.395	+0.584
072199	2451380.72017	13.273	+0.263	–0.620	+0.236	+0.397	+0.631
101299	2451463.52822	13.186	+0.247	–0.607	+0.215	+0.425	+0.642
031100	2451614.86820	13.322	+0.274	–0.569	+0.242	+0.442	+0.680
052300	2451687.83956	13.224	+0.261	–0.633	+0.231	+0.418	+0.647
052900	2451693.76138	13.261	+0.247	–0.617	+0.223	+0.430	+0.652
071900	2451744.69523	13.191	+0.233	–0.612	+0.224	+0.431	+0.658
072500	2451750.68494	13.197	+0.251	–0.653	+0.234	+0.446	+0.679
082500	2451781.53115	13.273	+0.263	–0.620	+0.229	–0.085	+0.145
102000	2451837.55127	13.430	+0.273	–0.549	+0.236	+0.472	+0.713
102100	2451838.55956	13.446	+0.285	–0.517	+0.254	+0.499	+0.745
062801	2452088.80147	13.248	+0.250	–0.618	+0.227	+0.433	+0.658
070301	2452093.66246	13.198	+0.278	–0.672	+0.234	+0.446	+0.677
070301	2452093.66693	13.198	+0.256	–0.615	+0.228	+0.462	+0.686
070301	2452093.67873	13.239	+0.235	–0.665	+0.236	+0.433	+0.666
070301	2452093.70532	13.224	+0.257	–0.679	+0.229	+0.431	+0.657
070301	2452093.70988	13.232	+0.247	–0.672	+0.254	+0.405	+0.657
070301	2452093.71508	13.231	+0.248	-0.675	+0.254	+0.405	+0.657
070301	2452093.72151	13.129	+0.263	-0.571	+0.271	+0.468	+0.736
072501	2452115.63344	13.226	+0.238	-0.633	+0.209	+0.428	+0.638
082101	2452142.61772	13.233	+0.241	-0.613	+0.232	+0.442	+0.673
100701	2452189.55720	13.202	+0.239	-0.612	+0.224	+0.438	+0.659
101501	2452197.58510	13.184	+0.244	-0.604	+0.236	+0.438	+0.650

Without any available spectroscopic data concurrent with our photometry, one can only conjecture the meaning of these color changes; see, for example, Cottrell *et al.* (1990a, 1990b), and Cottrell and Lawson (1990).

Data from Table 3, illustrated in Figures 3 and 4, show that as MV Sgr became brighter in the interval between HJD 2443299 and HJD 2443305 (1977 June 5 to 1977 June 11) it showed variations in both (*B–V*) and (*U–B*). Neither *R* nor *I* filter data were available for those dates. Figures 5 and 6 further illustrate these changes. Figure 7, the (*U–B*), (*B–V*) color-color plot, more than Figure 8, the (*V–R*), (*R–I*) color-color plot, shows considerable scatter with some tendency that when one color index is redder, so is the other. The (*V–R*), (*R–I*) color-color plot shows a more modest correlation between (*V–R*) and (*R–I*). If the two faint *V* measures, whose corresponding color index measures are indicated by the blue data points in Figures 7 and 8, are of MV Sgr, then the correlations of color with brightness and color are more robust.

Following the minimum, MV Sgr returned to its more normal magnitude and color indices, but continued its long term decline in brightness. From the first day in window 1, and the last day of observation in window 2, MV Sgr dropped by 0.13 magnitude in *V* over 7,711 days (21.1 years, 0.21 century). This change in brightness, then, was at a rate of 0.62 magnitude per century. Since (*B–V*) does not change between these two windows, the rate of change in *B* is the same. This short time interval result is to be compared with the value of 1.29 magnitudes per century in *B* found by Schaefer (2016) for the much longer time interval of 29,547 days (80.895 years). This is about half the rate of decline and indicates a recent slowing down of MV Sgr's rate of evolutionary change. Again, see De Marco *et al.* (2002) for a thorough discussion of a variety of possible scenarios, followed by confirmation in Schaefer (2016).

Evidence from Table 5, illustrated in Figures 5 and 6, shows that the long term diminution in brightness documented by Schaefer (2016) continued, but there was no change in the (*B–V*), (*V–R*), (*R–I*), or (*V–I*) color indices. The (*U–B*) color index did, however, become more blue by 0.05 magnitude. A more complete understanding is on the horizon, and additional current speculation is premature since such will be laid to rest with the appearance of the Large Synoptic Survey Telescope (LSST) data-set in the not so distant future.

Table 4, including the three LCO data points from Landolt and Uomoto, lists the new CCD data obtained by JLC. These data are plotted in Figure 9, which illustrates the average *V* magnitude for each night of CCD data, together with the

Table 4. CCD data for MV Sgr.

HJD 2400000.0+	*V* *m*	*RMS* *error*	*HJD* 2400000.0+	*V* *m*	*RMS* *error*	*HJD* 2400000.0+	*V* *m*	*RMS* *error*
48905.610645	13.270	0.0230	54646.737859	13.372	0.0193	54646.843571	13.364	0.0134
48905.611108	13.291	0.0230	54646.739430	13.373	0.0190	54646.845146	13.370	0.0150
48905.611664	13.266	0.0230	54646.740994	13.364	0.0187	54646.846715	13.370	0.0147
54646.567589	13.359	0.0125	54646.742570	13.364	0.0158	54646.848277	13.366	0.0142
54646.575431	13.360	0.0149	54646.744135	13.362	0.0160	54646.849839	13.367	0.0126
54646.577006	13.356	0.0127	54646.745707	13.364	0.0210	54646.851408	13.368	0.0127
54646.578570	13.358	0.0144	54646.747256	13.365	0.0169	54646.852973	13.364	0.0123
54646.580141	13.361	0.0132	54646.748834	13.365	0.0152	54646.854543	13.363	0.0135
54646.581706	13.362	0.0121	54646.750409	13.366	0.0185	54646.856117	13.366	0.0139
54646.583274	13.359	0.0145	54646.751985	13.367	0.0154	54646.857692	13.367	0.0138
54646.584856	13.363	0.0140	54646.753555	13.371	0.0168	54646.859276	13.366	0.0143
54646.586435	13.356	0.0132	54646.755122	13.365	0.0149	54646.860846	13.364	0.0133
54646.588010	13.361	0.0171	54646.756701	13.368	0.0203	54646.862472	13.365	0.0121
54646.589583	13.361	0.0137	54646.758301	13.366	0.0141	54646.864041	13.364	0.0129
54646.591164	13.353	0.0140	54646.759873	13.372	0.0174	54646.865652	13.366	0.0130
54646.592736	13.371	0.0145	54646.761453	13.371	0.0155	54646.867230	13.371	0.0127
54646.594305	13.361	0.0153	54646.763026	13.374	0.0207	54646.868801	13.369	0.0148
54646.595885	13.363	0.0164	54646.764601	13.372	0.0192	54646.870377	13.363	0.0124
54646.597467	13.359	0.0136	54646.766170	13.374	0.0193	54646.871946	13.365	0.0135
54646.599039	13.359	0.0124	54646.767888	13.374	0.0191	54646.873513	13.361	0.0122
54646.600609	13.360	0.0161	54646.769470	13.378	0.0197	54646.875092	13.365	0.0144
54646.602184	13.368	0.0181	54646.771044	13.372	0.0196	54646.876663	13.370	0.0133
54646.603755	13.366	0.0163	54646.772614	13.376	0.0198	54646.878235	13.368	0.0132
54646.605329	13.362	0.0154	54646.774179	13.368	0.0177	54646.879807	13.370	0.0132
54646.606923	13.361	0.0144	54646.775750	13.373	0.0177	54646.881379	13.363	0.0125
54646.608496	13.366	0.0175	54646.777321	13.371	0.0155	54646.882958	13.366	0.0131
54646.610073	13.365	0.0184	54646.778899	13.373	0.0173	54646.884535	13.361	0.0121
54646.611665	13.372	0.0182	54646.780466	13.371	0.0167	54646.886106	13.368	0.0121
54646.613248	13.374	0.0185	54646.782042	13.370	0.0187	54646.887673	13.372	0.0126
54646.614827	13.368	0.0184	54646.783620	13.375	0.0174	54646.889240	13.366	0.0123
54646.616408	13.369	0.0150	54646.785192	13.375	0.0174	54646.890803	13.366	0.0141
54646.617981	13.371	0.0173	54646.786776	13.378	0.0181	54646.892379	13.368	0.0133
54646.619550	13.371	0.0189	54646.788340	13.372	0.0179	55003.742459	13.311	0.0213
54646.621118	13.369	0.0197	54646.789915	13.373	0.0193	55003.744505	13.315	0.0193
54646.622683	13.365	0.0161	54646.791485	13.374	0.0193	55003.746072	13.315	0.0194
54646.624251	13.369	0.0177	54646.793062	13.374	0.0184	55003.747651	13.319	0.0168
54646.625828	13.370	0.0180	54646.794633	13.370	0.0170	55003.749226	13.317	0.0177
54646.627395	13.367	0.0183	54646.796208	13.368	0.0143	55003.750803	13.318	0.0197
54646.628972	13.366	0.0177	54646.797784	13.372	0.0181	55003.752386	13.321	0.0165
54646.630543	13.374	0.0205	54646.799406	13.371	0.0185	55003.753957	13.318	0.0170
54646.632116	13.369	0.0160	54646.801014	13.370	0.0185	55003.755506	13.303	0.0264
54646.633686	13.371	0.0205	54646.802590	13.364	0.0168	55003.758662	13.317	0.0198
54646.635249	13.370	0.0192	54646.804162	13.376	0.0180	55003.760227	13.318	0.0208
54646.636817	13.367	0.0205	54646.805727	13.372	0.0164	55003.761806	13.317	0.0174
54646.639121	13.364	0.0192	54646.807304	13.372	0.0159	55003.763382	13.317	0.0197
54646.640692	13.362	0.0171	54646.808877	13.372	0.0176	55003.765037	13.316	0.0185
54646.642263	13.367	0.0191	54646.810448	13.373	0.0179	55003.766698	13.318	0.0176
54646.643831	13.368	0.0174	54646.812017	13.371	0.0163	55003.768330	13.318	0.0204
54646.645405	13.370	0.0178	54646.813590	13.376	0.0176	55003.769901	13.321	0.0177
54646.646979	13.367	0.0192	54646.815174	13.372	0.0176	55003.771473	13.317	0.0177
54646.648549	13.368	0.0178	54646.816746	13.371	0.0160	55003.773047	13.320	0.0160
54646.650111	13.363	0.0169	54646.818317	13.372	0.0158	55003.774624	13.317	0.0182
54646.651688	13.367	0.0167	54646.819889	13.371	0.0157	55003.776199	13.321	0.0164
54646.653259	13.368	0.0180	54646.821463	13.371	0.0165	55003.777773	13.319	0.0166
54646.654836	13.367	0.0172	54646.823027	13.372	0.0139	55003.779340	13.319	0.0174
54646.656414	13.364	0.0165	54646.824600	13.374	0.0155	55003.780914	13.304	0.0172
54646.657997	13.364	0.0168	54646.826177	13.373	0.0151	55003.782488	13.319	0.0181
54646.659572	13.365	0.0159	54646.827748	13.371	0.0152	55003.784073	13.318	0.0148
54646.661152	13.365	0.0133	54646.829325	13.370	0.0172	55003.785648	13.317	0.0159
54646.662734	13.359	0.0153	54646.830955	13.367	0.0140	55003.787230	13.322	0.0160
54646.664307	13.359	0.0160	54646.832524	13.367	0.0128	55003.788810	13.322	0.0159
54646.665880	13.360	0.0147	54646.834135	13.371	0.0160	55003.790377	13.320	0.0168
54646.667453	13.362	0.0170	54646.835719	13.375	0.0141	55003.791969	13.320	0.0166
54646.669036	13.357	0.0148	54646.837287	13.374	0.0158	55003.793546	13.321	0.0159
54646.670628	13.357	0.0200	54646.838853	13.367	0.0153	55003.795116	13.318	0.0159
54646.672199	13.358	0.0192	54646.840422	13.369	0.0147	55003.796700	13.317	0.0142
54646.736295	13.367	0.0170	54646.841996	13.368	0.0139	55003.798277	13.325	0.0153

Table continued on next page

Table 4. CCD data for MV Sgr, cont.

HJD 2400000.0+	*V* *m*	*RMS* *error*
55003.799850	13.313	0.0176
55003.801413	13.321	0.0170
55003.802989	13.313	0.0173
55003.804563	13.324	0.0164
55003.806136	13.315	0.0187
55003.807712	13.321	0.0160
55003.809285	13.315	0.0181
55003.810858	13.318	0.0156
55003.812425	13.317	0.0183
55003.813999	13.317	0.0164
55003.815571	13.321	0.0168
55003.817144	13.316	0.0177
55003.818710	13.318	0.0185
55003.820276	13.320	0.0219
55003.821854	13.319	0.0179
55003.823434	13.318	0.0163
55003.825007	13.322	0.0157
55003.826571	13.318	0.0149
55003.828144	13.318	0.0172
55003.829718	13.315	0.0159
55003.831296	13.326	0.0164
55003.832881	13.323	0.0174
55003.834454	13.317	0.0174
55003.836026	13.321	0.0162
55003.837606	13.325	0.0151
55003.839374	13.320	0.0182
55003.840945	13.318	0.0202
55003.842517	13.317	0.0181
55003.844081	13.315	0.0177
55003.845660	13.317	0.0197
55003.847233	13.313	0.0202
55003.848798	13.317	0.0179
55003.850365	13.318	0.0213
55003.851935	13.321	0.0223
55003.853500	13.318	0.0204
55003.855077	13.307	0.0205
55003.856650	13.317	0.0210
55003.858226	13.318	0.0194
55003.859790	13.328	0.0244
55003.861362	13.310	0.0196
55003.862970	13.314	0.0275
55004.696693	13.355	0.0171
55004.698799	13.350	0.0137
55004.700372	13.354	0.0134
55004.701945	13.351	0.0132
55004.703517	13.352	0.0145
55004.705088	13.346	0.0144
55004.706658	13.354	0.0130
55004.708241	13.353	0.0149
55004.709814	13.347	0.0137
55004.711388	13.349	0.0138
55004.712963	13.347	0.0134
55004.714529	13.349	0.0145
55004.716099	13.352	0.0147
55004.717674	13.345	0.0160
55004.719249	13.354	0.0136
55004.720823	13.351	0.0120
55004.722388	13.353	0.0150
55004.723966	13.353	0.0140
55004.725535	13.350	0.0151
55004.727110	13.351	0.0149
55004.728692	13.348	0.0143
55004.730264	13.342	0.0192
55004.731839	13.341	0.0174
55004.733414	13.335	0.0237
55004.734986	13.338	0.0219
55004.736548	13.340	0.0218
55004.738126	13.332	0.0204
55004.739700	13.345	0.0168
55004.741265	13.336	0.0231
55004.742841	13.338	0.0202
55004.744414	13.345	0.0158
55004.747132	13.346	0.0161
55004.748710	13.350	0.0158
55004.750282	13.349	0.0155
55004.751855	13.350	0.0145
55004.753436	13.348	0.0140
55004.755007	13.350	0.0180
55004.756585	13.346	0.0155
55004.758148	13.339	0.0173
55004.759726	13.328	0.0293
55004.762872	13.339	0.0225
55004.764447	13.341	0.0282
55004.766021	13.338	0.0287
55004.767597	13.336	0.0211
55004.769162	13.337	0.0196
55004.770733	13.342	0.0211
55004.772307	13.344	0.0202
55004.773899	13.339	0.0222
55004.775551	13.341	0.0184
55004.777174	13.339	0.0187
55004.778744	13.334	0.0267
55004.780323	13.332	0.0278
55004.781897	13.334	0.0238
55004.783470	13.337	0.0236
55004.786604	13.330	0.0253
55004.788167	13.342	0.0210
55004.789745	13.336	0.0218
55004.791311	13.341	0.0222
55004.792882	13.331	0.0229
55005.687939	13.346	0.0223
55005.689154	13.347	0.0190
55005.690389	13.346	0.0224
55005.691606	13.351	0.0198
55005.692830	13.343	0.0231
55005.694058	13.350	0.0207
55005.695275	13.349	0.0204
55005.696494	13.356	0.0208
55005.697721	13.351	0.0205
55005.698944	13.352	0.0216
55005.700177	13.357	0.0229
55005.701406	13.350	0.0232
55005.702628	13.345	0.0252
55005.703856	13.350	0.0238
55005.705083	13.355	0.0200
55005.706312	13.345	0.0218
55005.707534	13.349	0.0225
55005.708770	13.350	0.0222
55005.709995	13.353	0.0228
55005.711220	13.349	0.0226
55005.712446	13.349	0.0224
55005.713663	13.343	0.0179
55005.714891	13.345	0.0199
55005.716123	13.349	0.0206
55005.717349	13.343	0.0205
55005.718577	13.346	0.0207
55005.719800	13.344	0.0213
55005.721024	13.343	0.0218
55005.722251	13.351	0.0225
55005.723469	13.348	0.0185
55005.724716	13.346	0.0211
55005.725940	13.348	0.0201
55005.727158	13.349	0.0201
55005.728392	13.343	0.0216
55005.729618	13.347	0.0216
55005.730843	13.345	0.0213
55005.732068	13.347	0.0195
55005.733292	13.348	0.0202
55005.734511	13.353	0.0210
55005.735734	13.346	0.0194
55007.599466	13.377	0.0264
55007.602624	13.383	0.0267
55007.605771	13.387	0.0214
55007.607334	13.390	0.0216
55007.608911	13.382	0.0274
55007.610475	13.385	0.0213
55007.612046	13.393	0.0204
55007.615197	13.396	0.0280
55007.616771	13.382	0.0251
55007.618344	13.383	0.0214
55007.619913	13.387	0.0195
55007.621487	13.384	0.0268
55007.623058	13.390	0.0214
55007.624633	13.394	0.0280
55007.626205	13.381	0.0245
55007.629745	13.390	0.0203
55007.632019	13.388	0.0200
55007.634284	13.384	0.0201
55007.636546	13.380	0.0163
55007.638815	13.376	0.0284
55329.739310	13.374	0.0150
55329.740713	13.369	0.0163
55329.742121	13.372	0.0174
55329.743525	13.375	0.0163
55329.744927	13.375	0.0151
55329.746337	13.378	0.0158
55329.747733	13.376	0.0178
55329.749137	13.377	0.0150
55329.750542	13.371	0.0167
55329.751946	13.370	0.0142
55329.753349	13.372	0.0175
55329.754756	13.370	0.0247
55329.756159	13.366	0.0260
55329.757557	13.366	0.0267
55329.761777	13.364	0.0266
55329.763174	13.372	0.0188
55329.764580	13.366	0.0256
55329.765986	13.371	0.0170
55329.767383	13.370	0.0163
55329.768785	13.371	0.0207
55329.770190	13.366	0.0247
55329.771594	13.375	0.0187
55329.772989	13.372	0.0190
55329.774385	13.371	0.0199
55329.775789	13.365	0.0238
55329.777192	13.372	0.0191
55329.778599	13.377	0.0149
55329.779995	13.370	0.0178
55329.781543	13.369	0.0200
55329.782954	13.370	0.0191
55329.784348	13.369	0.0188
55329.785752	13.369	0.0219
55329.787151	13.368	0.0270
55329.791750	13.364	0.0219
55329.795954	13.363	0.0213
55329.797359	13.369	0.0181
55329.798763	13.372	0.0200
55329.800169	13.366	0.0217
55329.801564	13.370	0.0173
55329.808585	13.369	0.0278

Table 5. UBVRI photoelectric photometry near maximum.

Filter	*HJD Window 1* 2444486–2446574	*HJD Window 2* 2447352–2452197	*n*
V	$13^{\mathrm{m}}.099 \pm 0.077$	$13^{\mathrm{m}}.229 \pm 0.069$	32
(B–V)	+0.254 ± 0.021	+0.255 ± 0.033	32
(U–B)	–0.584 ± 0.037	–0.635 ± 0.046	32
(V–R)	+0.234 ± 0.018	+0.236 ± 0.026	31
(R–I)	+0.444 ± 0.034	+0.437 ± 0.024	30
(V–I)	+0.676 ± 0.047	+0.671 ± 0.034	30

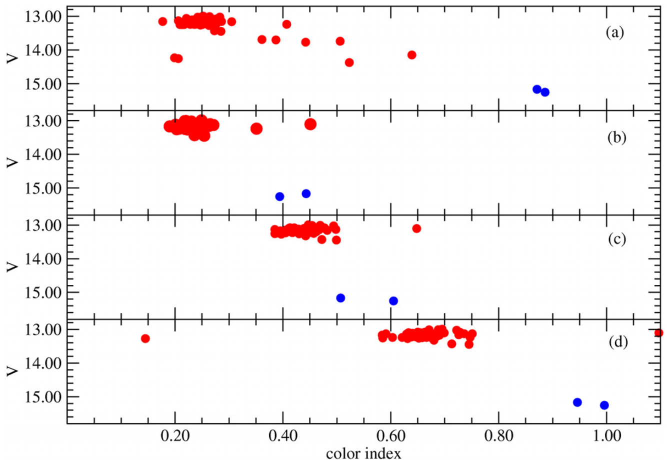

Figure 5. V magnitude vs color indices for MV Sgr, with these photoelectric data point colors identical to those in Figure 2.: (a) (*B–V*), (b) (*V–R*), (c) (*R–I*), and (d) (*V–I*).

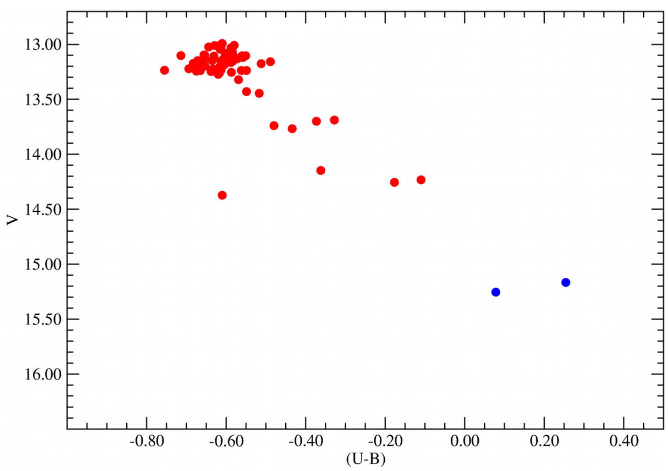

Figure 6. *V* magnitudes vs (*U–B*) color index for the photoelectric data for MV Sgr for this paper. Data point colors are the same as in Figure 2.

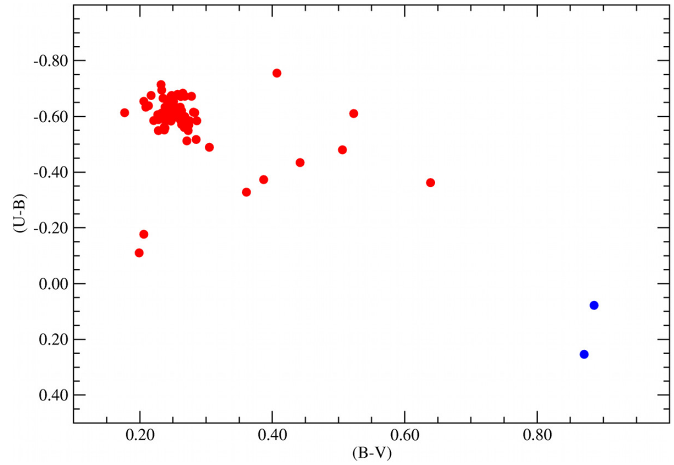

Figure 7. (*U–B*) vs. (*B–V*) photoelectric data herein for MV Sgr. Data point colors are the same as in Figure 2.

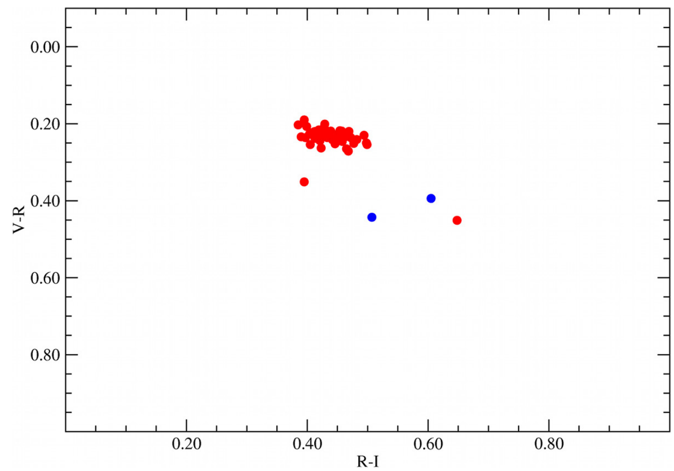

Figure 8. (*V–R*) vs. (*R–I*) photoelectric data herein for MV Sgr. Data point colors are the same as in Figure 2.

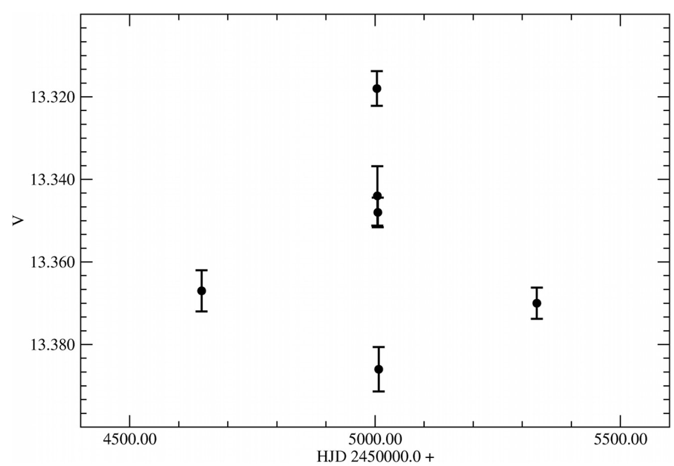

Figure 9. The average *V* magnitude and standard deviation for each night's CCD data for MV Sgr.

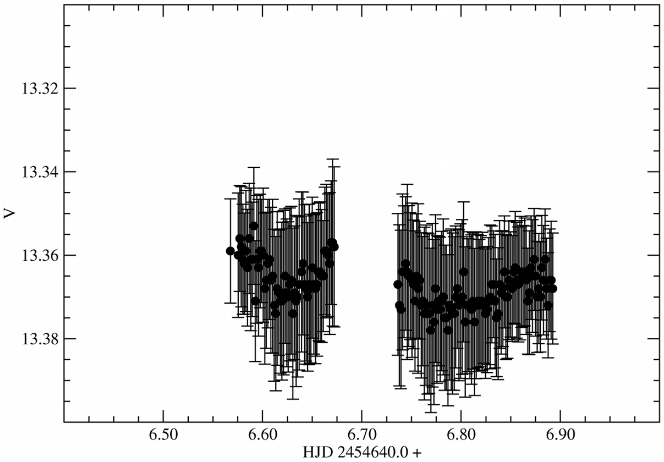

Figure 10. *V* magnitude CCD data for MV Sgr for 2008 June 29 *UT* (HJD 2454646.5+).

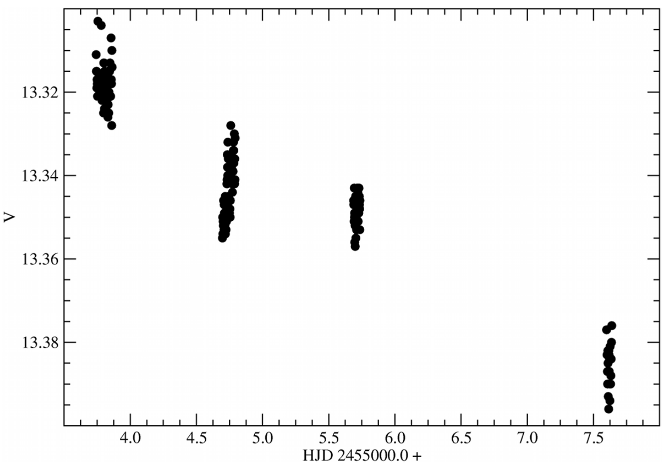

Figure 11. *V* magnitude CCD data for MV Sgr obtained in the time interval 2009 June 20–24 UT (2455003.7 ≤ HJD ≤ 2455007.64).

average deviation for each night's average *V* magnitude. The Heliocentric Julian Day is tabulated in column one, the *V* magnitude in column two, and the corresponding error in the third column. From this data set, the values of the observed magnitudes fall in the range of 13.303 ≤ *V* ≤ 13.396, with an average magnitude of *V* = 13.354 ± 0.021. The average error for the individual error measurements in the third column is 0.0181 ± 0.0036.

Figure 10 presents the CCD data through the *V* filter that were obtained on HJD 2454646.6 (2008 June 29). It illustrates the longest CCD-based data string for a monitoring interval of just under eight hours. The seeing varied between 1.0 and 1.5 arc-seconds. The error for each data point essentially is equivalent to the total scatter visible in the figure. Plots of the CCD data in Table 4 from all other nights are similar in appearance, with the size of the error bars being equivalent to the scatter in the nightly data strings. Application of the PERIOD04 program (Lenz and Breger 2005) in a search for possible short-term variability was inconclusive.

Figure 11 provides the CCD data taken through a *V* filter in the time interval 2455003.7 ≤ HDJ ≤ 2455007.6 (2009 June 20–24). A total range in the *V* magnitude of 0.093 is evident. The time elapsed during which data were taken varied a bit from night to night. The total variation was 0.025, 0.027, 0.014, and 0.020 magnitude for the nights of HJD 2455003.7, 2455004.6, 2455005.6, and 2455007.5, encompassing time durations of 173.5, 138.5, 68.8, and 56.7 minutes, respectively. Figure 11 illustrates that over this particular five-night interval, MV Sgr steadily declined in brightness by approximately 0.07 magnitude. It may be interpreted that this decline is the downward leg of the approximate eight-day period, but with a somewhat larger amplitude, than found by Percy and Fu (2012). However, the shortness of the data strings within individual nights preclude definitive statements about intra-night variations.

4. Summary

Calibrated photometric photoelectric and CCD data of MV Sgr obtained by the authors over an interval of 32.9 years confirm a long term downward trend in brightness and the CCD data are consistent with an approximate eight-day pulsation period. These new data have provided the first and only deep minimum identified since those described by Hoffleit (1958, 1959). Since the individual errors of the individual CCD data points are similar in size to any variation among those data points, nothing definitive can be said about possible short term changes in light over the course of a night. Night-to-night changes, however, do occur.

At least one observing season completely devoted to thoroughly photometrically calibrated night-long monitoring of MV Sgr no doubtedly will elucidate the reality of these light variations plus most probably additional light variations at other frequencies. Since the intra-nightly light variations are small, only a couple percent, highly accurate photometric data are required. Data should be acquired, preferentially, through a Johnson *V*-filter to better enable robust comparison with most extant photometric data for MV Sgr. Accompanying spectroscopy would be exceedingly useful. Such an observing program would be a challenging, fun, and rewarding endeavor!

5. Acknowledgements

It is a pleasure to thank the staffs of CTIO and LCO for their help in making the observing runs a success. Daniel Maturana recently reminded AUL of the filter prescriptions. The authors note with appreciation G. Clayton's comments, and recognize with gratitude the long term observation efforts of the AAVSO community. The authors acknowledge with thanks the input from the referee.

The data reported in this paper came from observing runs supported by AFOSR grants 77-3218 and 82-0192, Space Telescope Science Institute grant STScI CW-0004-85, and NSF grants MPS 75-01890 and AST 9114457, 9313868, 9528177, 0097895, and 0803158.

References

Clayton, G.C. 1996, *Publ. Astron. Soc. Pacific*, **108**, 225.

Clayton, G.C. 2012, *J. Amer. Assoc. Var. Star Obs.*, **40**, 539.

Clem, J. L., and Landolt, A. U. 2013, *Astron. J.*, **146**, 88.

Cottrell, P. L., and Lawson, W. A. 1990, in *Confrontation between Stellar Pulsation and Evolution; Proceedings of the Conference,* Bologna, Italy, May 28–31, 1990, ASP Conf. Ser. 11, Astronomical Society of the Pacific, San Francisco, 570.

Cottrell, P. L., Lawson, W. A., and Buchhorn, M. 1990a, *Mon. Not. Roy. Astron. Soc.*, **244**, 149.

Cottrell, P. L., Lawson, W. A., and Buchhorn, M. 1990b, in *Cambridge Workshop on Cool Stars, Stellar Systems, and the Sun. Sixth Cambridge Workshop*, 1989, ed. G. Wallerstein, ASP Conf. Ser. 9, Astronomical Society of the Pacific, San Francisco, 456.

De Marco, O., Clayton, G. C., Herwig, F., Pollacco, D. L. Clark, J. S., and Kilkenny, D. 2002, *Astron. J.*, **123**, 3387.

Henden, A. A., Welch, D. L., Terrell, D., and Levine, S. E. 2009, *Bull. Amer. Astron. Soc.*, **41**, 669.

Herbig, G. H. 1964, *Astrophys. J.*, **140**, 1317.

Hoffleit, D. 1958, *Astron. J.*, **63**, 50.

Hoffleit, D. 1959, *Astron. J.*, **64**, 241.

Johnson, H. L. 1963, in *Basic Astronomical Data: Stars and Stellar Systems*, ed. K. Aa. Strand, University of Chicago Press, 204.

Kafka, S. 2015, variable star observations from the AAVSO International Database (https://www.aavso.org/aavso-international-database).

Landolt, A. U. 1973, *Astron. J.*, **78**, 959.

Landolt, A. U. 1979, *IAU Circ.*, No. 3419, 1.

Landolt, A. U. 1983, *Astron. J.*, **88**, 439.

Landolt, A. U. 1992, *Astron. J.*, **104**, 340.

Landolt, A. U. 2007, in *The Future of Photometric, Spectrophotometric, and Polarimetric Standardization*, ed. C. Sterken, ASP Conf. Ser. 364, Astronomical Society of the Pacific, San Francisco, 27.

Laycock, S., Tang, S., Grindlay, J., Los, E., Simcoe, R., and Mink, D. 2010, *Astron. J.*, **140**, 1062.

Lenz, P., and Breger, M. 2005, *Commun. Astroseismology*, **146**, 53.

Percy, J. R., and Fu, R. 2012, *J. Amer. Assoc. Var. Star Obs.*, **40**, 900.

Schaefer, B. E. 2016, *Mon. Not. Roy. Astron. Soc.*, **460**, 1233.

Woods, I. E. 1928, *Bull. Harvard College Obs.*, No. 855, 22.

Zacharias, N., Finch, C. T., Girard, T. M., Henden, A., Bartlett, J. L., Monet, D. G., and Zacharias, M. I. 2013, *Astron. J.*, **145**, 44.

New Observations of AD Serpentis

Samantha Raymond
Ximena Morales
Badger High School, Lake Geneva, Wisconsin
Yerkes Observatory, 260 W. Geneva Williams Bay, WI 53169; address email correspondence to wayne.osborn@cmich.edu

Wayne Osborn
Yerkes Observatory, 260 W. Geneva Williams Bay, WI 53169

Received September 4, 2017; revised October 6, October 11, 2017; accepted October 31, 2017

Abstract The little-studied star AD Ser has been investigated utilizing archival data as well as new CCD observations. AD Ser is found to be a semiregular variable with a V range of about 1.5 mag and a persistent, but likely somewhat variable, period of 90 d.

1. Introduction

Yerkes Observatory offers a number of activities for students with the goal of stimulating interest in science and engineering. Premier among these is the McQuown Scholars Program for high school students. Those named as McQuown Scholars assume leadership roles in the Yerkes educational program, helping to organize and run activities for younger students, while also selecting a project in computer science, engineering, or astronomy that allows an in-depth investigation of a topic that makes use of the resources of the observatory. One project area in astronomy is to investigate a poorly studied variable star, starting with Yerkes' collection of archival photographic plates. In brief, the selected star is identified and its variation followed on available plates. What is learned from the plate observations suggests additional data that would be useful, typically additional observations. The task is then to gather sufficient additional data, within the ever-present time and other constraints of student projects, for some new conclusions to be drawn about the star. The process demonstrates how a scientific study takes place. The goal is to produce a paper suitable for publication in a scientific journal, but this is not always achieved. This paper describes a study of the variable star AD Ser carried out as a McQuown Scholar project.

The Ross Variable Stars were discovered by F. Ross of Yerkes Observatory. Ross compared photographs he took in the 1920s and 1930s to plates that had been taken earlier by E. E. Barnard. He found 379 suspected variables. Most of these have been confirmed as variables, but many remain poorly studied. One of these is Ross 27 (Ross 1925), now known as AD Ser.

AD Ser is located at RA = 17 39 01.5, Dec = -15 07 16 (2000). The AAVSO International Database (AID) has only three old observations from the work of Ross (Kafka 2016); the AAVSO Photometric All-Sky Survey Data Release 9 (APASS; Henden *et al.* 2015) lists four observations. The star has been extensively observed by the All Sky Automated Survey (ASAS) monitoring program (Pojmański 1997). These indicated it is a semiregular variable with a V amplitude of 1.25 magnitudes and a period given as 92.70682 days. On the other hand, the *General Catalogue of Variable Stars* (GCVS; Samus *et al.* 2017) has AD Ser as a Mira with a period of 175.4 days and a photographic magnitude range of 13.5 to 16, with these values apparently from an unpublished manuscript.

The archival information on AD Ser is summarized in Table 1. The three ASAS values are from the ASAS web page (http://www.astrouw.edu.pl/asas/?page=catalogues) link to information in the ASAS variable star catalog (ACVS/variables), the link to the photometry (AASC/photometry), and our mean from the downloaded ASAS data. The inconsistencies in the published material for AD Ser indicate additional study of the star is warranted.

2. Observations

For our investigation three different sets of observations of AD Ser were collected. First, we made use of the V observations from the ASAS program. Second, we searched the Yerkes Observatory's archive for photographic plates showing the star's field. Finally, we obtained some CCD images of AD Ser using the Skynet System (Smith *et al.* 2016).

The ASAS is a program for monitoring the sky for variable stars and other objects. Over 1,300,000 stars brighter than V = 15 magnitude were observed. A catalogue of the observations is available online (http://www.astrouw.edu.pl/asas/?page=aasc), and AD Ser was found to be one of the stars listed. We downloaded the ASAS data, each observation having five magnitudes representing aperture photometry with different apertures (Pojmański *et al.* 2005). We adopted the MAG_0 values (2 pixel = 28.4 arcsec aperture, Pojmański 2002) as recommended.

Table 1. Information on AD Ser from various databases.

Data Source	*Number of Observations*	*Years*	*m(pg)*	*B*	*V*
GCVS		~1929	14.8[1]		
AID (AAVSO web page)	3	1908–1925		14.8:	13.9:
APASS (DR9)	4	2009–2013		14.629	12.726[2]
ASAS (ACVS/Variables)		2001–2009			13.52[3]
ASAS (AASC/Photometry)	15	2001–2009			13.396
ASAS (on-line data files)	335	2001–2009			13.263

1. Mean of listed photographic maximum and minimum.
2. The APASS coordinates are for AD Ser, but the V magnitude may refer to a star 4 seconds east that has V = 12.80 from ASAS.
3. The listed V(maximum) plus half the listed amplitude.

Yerkes Observatory has the original plates taken by Ross on which he discovered AD Ser = Ross Variable 27. We were able to locate those plates and confirm the change in brightness he found. We also found fifty-eight additional plates showing the field of AD Ser. Forty of the plates reached deep enough to be useful. We made eye estimates of the variable's magnitude on these plates using the comparison sequence given in Table 2 where the adopted magnitudes are based on our CCD results and may have a significant zero point error. While our CCD measures are consistent differentially to a few hundredths of a magnitude, the published photographic B magnitudes needed to set the zero point are uncertain, with differences between different catalog values up to a magnitude. Each plate was estimated at least twice, and most more times, and the results averaged. Often there are two plates taken simultaneously with co-mounted 10-inch (10B) and 6-inch (6B) cameras. The contemporaneous results as well as the standard deviation of the magnitudes derived from the separate eye estimates indicate the typical error of a given magnitude is less than 0.20 magnitude, but the error depends significantly on how well the variable was exposed on the plate and may reach 0.30 magnitude in the worst cases. Our photographic plate results are given in Table 3. In those cases when the variable was not seen we determined "less than" measures based on the faintest comparison star visible.

Finally, we obtained CCD observations using the Skynet system (Smith *et al.* 2016) on ten nights from February to May 2016. We used a B filter to allow comparison with our plate results. We performed aperture photometry using the Skynet Afterglow program to obtain magnitudes relative to the same set of comparison stars used for the plates. The magnitudes of AD Ser from our CCD observations are given in Table 4.

3. Results

The ASAS data show a range of approximately 1.5 magnitudes from about 12.8 to 14.3 in the V band. A period search over the range 50 to 500 days was carried out using the VSTAR software available online from the AAVSO (Benn 2012). As shown in Figure 1 from VSTAR, the only periodicity showing power was centered on 90.23 days. The phased light curve for the ASAS data with this period is shown in Figure 2. The full-width at half maximum of the power spectrum peak is 3.0 days, indicating the derived period is uncertain by ±1.5 days. Periods outside this range, including the 92.7-day period given by ASAS, gave significantly less smooth light curves. The GCVS 175.4-day period is close to an alias of 90.23 days.

The plate observations show a B range from about 14.0 to 16.5, consistent with the photographic range given in the GCVS. The light curve, which spans over 50 years, is shown in Figure 3. A period search on the photographic data yielded most power at 90.4 days.

Our CCD photometry, taken over two months, showed a rise in B from 14.8 to 14.4 over about 25 days followed by a slow decline. The light curve is consistent with the 90-day period but the variation over the 58-day span is less than seen in the other observation sets, as shown in Figure 4.

Table 2. Comparison stars and adopted magnitudes.

Identification	*R.A. (2000)*	*Dec. (2000)*	*B**
	h m s	*° ′ ″*	
A = Nomad 0748-0430533	17 39 05.6	–15 07 20	13.85
B = Nomad 0748-0430001	17 38 58.4	–15 06 17	15.05
C = Nomad 0749-0430405	17 39 03.8	–15 08 30	15.96
D = Nomad 0748-0419986	17 38 58.7	–15 05 51	16.69

**From our CCD photometry with a B filter but not transformed to UBV system.*

Table 3. Magnitudes from photographic plates.

Plate No.	*Date*	*Julian Date*	*B**	*Note*
6B-12	1899-06-07	2414813.708	14.8	
10B-90	1904-07-12	2416674.731	14.3	
6B-90	1904-07-12	2416674.731	14.1	
10B-99	1904-07-31	2416693.635	14.2	
6B-99	1904-07-31	2416693.635	14.3	
10B-100	1904-08-02	2416695.7	14.4	
6B-100	1904-08-02	2416695.7	14.3	
10B-194	1905-05-08	2416974.908	14.8	
10B-224	1905-06-20	2417017.717	15.2	
6B-224	1905-06-20	2417017.717	<15.05	Variable fainter than Star B
3B-224	1905-06-20	2417017.717	<15.05	Variable fainter than Star B
10B-255	1905-07-25	2417052.764	14.6	
6B-255	1905-07-25	2417052.764	14.5	
10B-457	1908-06-29	2418122.720	14.2	
6B-457	1908-06-29	2418122.720	14.1	
10B-689	1911-05-01	2419158.816	16.4	
6B-689	1911-05-01	2419158.816	16.7	
6B-810	1912-08-11	2419626.619	<13.85	Variable fainter than Star A
10B-979	1915-07-05	2420684.697	15.4	
6B-979	1915-07-05	2420684.697	15.0	
10B-1340	1919-03-02	2422020.930	14.9	
6B-1340	1919-03-02	2422020.930	14.6	
10B-1345	1919-03-27	2422045.887	<15.05	Variable fainter than Star B
6B-1345	1919-03-27	2422045.887	15.6	
10B-1355	1919-05-09	2422088.852	15.0	
6B-1355	1919-05-09	2422088.852	14.8	
10R-44	1925-06-19	2424320.766	16.0	
6R-44	1925-06-19	2424320.766	16.1	
10R-229	1927-04-28	2424998.869	15.8	
6R-229	1927-04-28	2424998.869	15.7	
5R-927	1931-06-11	2426504.750	16.7	
5R-1125	1933-06-21	2427244.805	13.9	
CR-1125	1933-06-21	2427244.805	14.1	
5R-1126	1933-06-22	2427245.792	13.7	
CR-1126	1933-06-22	2427245.792	14.1	
IL-RF-512	1941-05-24	2430138.808	<15.05	Variable fainter than Star B
IL-RF-518	1941-05-25	2430139.803	<13.85	Variable fainter than Star A
IL-RF-558	1941-06-25	2430170.738	14.5	
IL-RF-573	1941-07-17	2430192.668	<13.85	Variable fainter than Star A
Cook 1-103	1950-09-10	2433527.649	16.5	

**Based on our adopted magnitudes in Table 2 and not strictly on the UBV system.*

No mean period was found that fits all the data well, likely reflecting changes in period and light curve shape from cycle to cycle or over time. From many trials, the 90.23-day period seemed the best, and the phased light curve using it is shown in Figure 4. The plate observations are plotted as open circles and our CCD observations as dots. The phases of maximum from ASAS data and the GCVS are shown as filled and open arrows, respectively, plotted at magnitude 13.0. As an example of the incongruency in the data, modifying the period to align the plate

Table 4. CCD observations of AD Ser.

2016 date	*Julian Date*	*Exposure (seconds)*	*B* (magnitude)*
February 23	2457441.826	10	14.82
February 23	2457441.826	20	14.76
February 23	2457441.827	40	14.87
February 27	2457445.823	30	14.74
February 27	2457445.824	60	14.77
February 27	2457445.825	120	14.75
March 17	2457464.752	90	14.40
March 17	2457464.757	90	14.40
March 21	2457468.733	90	14.36
March 21	2457468.734	90	14.41
March 22	2457469.729	90	14.52
March 22	2457469.730	90	14.47
March 30	2457469.710	90	14.51
March 30	2457469.711	90	14.51
April 2	2457480.701	90	14.47
April 2	2457480.702	90	14.43
April 6	2457484.892	90	14.49
April 6	2457484.893	90	14.44
April 7	2457485.825	90	14.43
April 7	2457485.826	90	14.41
April 21	2457499.863	90	14.52
April 21	2457499.865	90	14.53

**Based on our adopted magnitudes in Table 2 and not strictly on the UBV system.*

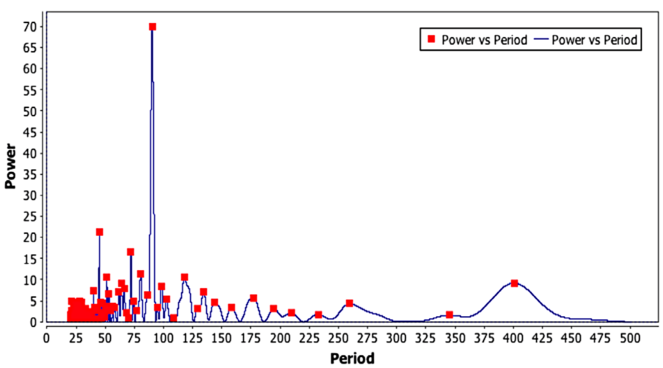

Figure 1. The power spectrum produced by VSTAR from a search on the ASAS data set for periodicities in the range 20 to 500 days. The only period with significant power is 90.23 days.

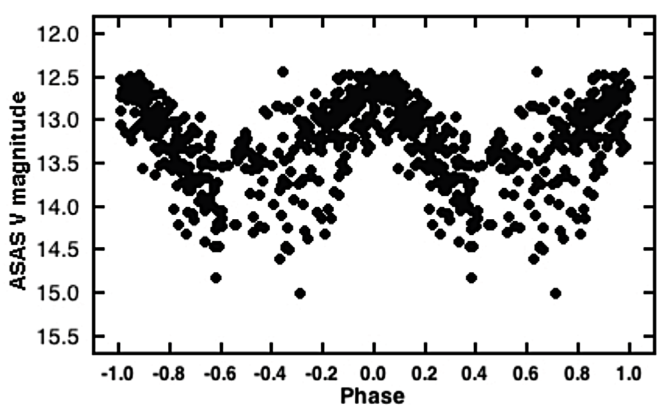

Figure 2. The phased light curve of ASAS data for AD Ser using the elements JD (Maximum) = 2452704.848 + 90.23 E.

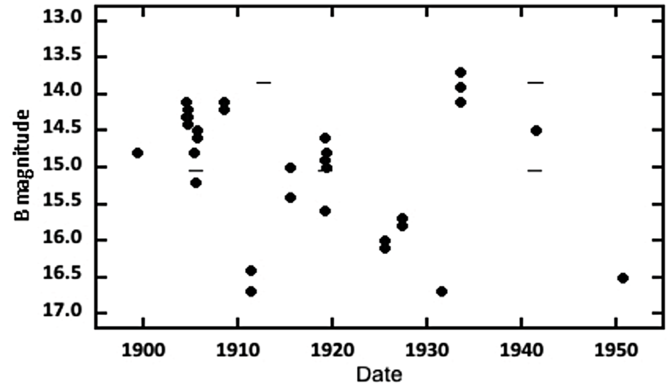

Figure 3. The light curve from magnitude estimates of AD Ser on photographic plates. Dots are observed magnitudes. Lines indicate the faintest magnitude seen in those cases where one or more comparison stars were visible but not the variable.

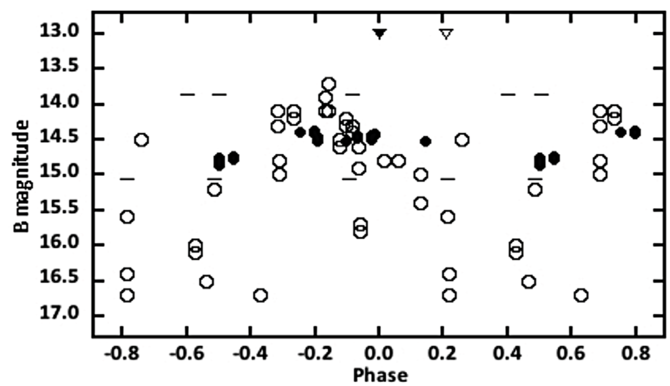

Figure 4. A phased light curve using the same ephemeris as in Figure 2. Plate observations are shown as open circles and CCD observations as dots. The phases of maximum from the ASAS data and from the GCVS are indicated by the filled and open arrows, respectively, at B = 13.0.

and ASAS maxima in Figure 4 leaves the CCD data—which seem to cover a maximum—shifted to the minima of the other observation sets.

4. Conclusions

Our results indicate that AD Ser should be classified as a semiregular variable, not a Mira, based on the GCVS variable type definitions (http://www.sai.msu.su/gcvs/gcvs/vartype.htm). We find variation amplitudes of about 1.5 magnitudes in V and ~2.5 magnitudes in B and a persistent, but likely somewhat variable, period of 90.23 days. A more systematic CCD study would be worthwhile.

Acknowledgements

We thank the anonymous referee for helpful comments that significantly improved the paper. The lead authors thank Yerkes Observatory for use of its resources and its McQuown Scholars Program for high school students that allowed this study to take place. We acknowledge with thanks the variable star observations from the AAVSO International Database contributed by observers worldwide. This research has made use of the SIMBAD database, operated at CDS, Strasbourg, France, and the Skynet Robotic Telescope Network.

References

Benn, D. 2012, *J. Amer. Assoc. Var. Star Obs.*, **40**, 852.

Henden, A. A., *et al*. 2015, AAVSO Photometric All-Sky Survey, data release 9 (http://www.aavso.org/apass).

Kafka, S. 2016, variable star observations from the AAVSO International Database (https://www.aavso.org/aavso-international-database).

Pojmański, G. 1997, *Acta Astron.*, **47**, 467.

Pojmański, G. 2002, *Acta Astron.*, **52**, 397.

Pojmański, G., Pilecki, B., and Szczygiel, D. 2005, *Acta Astron.*, **55**, 275.

Ross, F. E. 1925, *Astron. J.*, **36**, 99.

Samus, N. N., Kazarovets, E. V., Durlevich, O. V., Kireeva, N. N., and Pastukova, E. N. 2017, *General Catalogue of Variable Stars: Version GCVS 5.1*, *Astron. Rep.*, **61**, 80 (http://www.sai.msu.su/gcvs/).

Smith, A. B., Caton D. B., and Hawkins R. L. 2016, *Publ. Astron. Soc. Pacific*, **128e**, 055002.

BVR$_c$I$_c$ Study of the Short Period Solar Type, Near Contact Binary, NSVS 10083189

Ronald G. Samec
Amber Olsen
Department of Natural Sciences, Emmanuel College, 181 Springs Street, Franklin Springs, GA 30639; ronaldsamec@gmail.com

Daniel B. Caton
Dark Sky Observatory, Physics and Astronomy Department, Appalachian State University, 525 Rivers Street, Boone, NC, 28608-2106

Danny R. Faulkner
Johnson Observatory, 1414 Bur Oak Court, Hebron, KY 41048

Robert L. Hill
Department of Chemistry and Physics, Bob Jones University, 1700 Wade Hampton Boulevard, Greenville, SC 29614

Received September 14, 2017; revised October 31, 2017; accepted October 31, 2017

Abstract The first precision BVR$_c$I$_c$ light curves of NSVS 10083189 were taken on eight nights in 2015 at Dark Sky Observatory in North Carolina with the 0.81-m reflector of Appalachian State University and on one night on the SARA 1-m reflector at Kitt Peak National Observatory in remote mode. It is an ~F8V eclipsing binary with a short period of 0.4542238 (2) d. Seven times of minimum light were calculated. In addition, seven observations at minima were determined from archived NSVS Data. A statistically significant negative quadratic ephemeris was calculated. A light curve analysis with the Wilson-Devinney program led to a semidetached-near contact configuration (larger component filling its critical lobe and the secondary just under filing). This may indicate that NSVS 10083189 is near the end of its Detached to Contact Binary Channel. Our synthetic light curve solution gave a mass ratio of 0.58, with component temperatures of 6250 and 4573 K. A 15° radius cool spot with a T-factor of 0.85 was determined on the primary star. Thus, magnetic braking may be its main process acting in the orbital evolution. The fill-out of the secondary star has apparently reached ~99%.

1. Introduction

In this study, we continue our analysis of solar-type binaries in transition. Such transitions include the detached-to-contact binary channel and the contact-to-single star channel. The critical nature of these studies was recently highlighted by the phenomena of Red Novae, a violent event which appears to be the final coalescence a contact binary into fast rotating, blue straggler-like single star. The recovery of archived observations of a contact binary with high fill-out at the site of the red nova V1309 Sco (Tylenda *et al.* 2011; Tylenda and Kamiński 2016) has underlined the need for study of the characterization and continued patrol of such binaries in transition.

The detached-to-contact binary channel (Jiang *et al.* 2014) may be accomplished by several means, including evolutionary expansion of the components through ordinary core nuclear processes, interaction with a third component, or magnetic braking. Exponentially decaying orbital periods are easiest to explain by the magnetic braking process. In this paper, we find NSV 10083189 is a main sequence binary with its smoothly changing light curve and a large amplitude difference, possibly indicating that it is very near contact but still unattached. This binary appears to fall into the probable category of being near the end of the detached-to-contact binary channel. This makes the binary's observation and analysis important in the understanding of contact binary formation. Its study also fits our program of binaries in transition. We have undertaken a complete photometric investigation of this binary and present the results in this paper.

2. History and observations

NSVS 1083189 is listed in the All Sky Automated Survey (ASAS; Pojmański 2002). Light curve data are given at the SkyDOT NSVS website (Los Alamos Natl. Lab. 2017). The binary is in the constellation of Cancer. ASAS-3 categorizes it as a semi-detached eclipsing binary (ESD) type. VSX gives a V = 13.07 (0.72) magnitude and an ephemeris of

$$\text{HJD} = 2452623.12\ \text{d} + 0.454224 \times E \quad (1)$$

NSVS data from the SkyDOT catalog, object 10083189 (Los Alamos Natl. Lab. 2017), are plotted with Equation (1) and are given as Figure 1. This system was observed as a part of our student/professional collaborative studies of near-contact binaries at Emmanuel College using data taken from DSO and SARA observations. The observations were taken by Dr. Ron Samec, Dr. Daniel Caton, Danny Faulkner, and Robert Hill. Reduction and analyses were done by Dr. Samec and Amber Olsen.

Our 2012 light curves were taken with the Dark Sky Observatory 0.81-meter reflector at Philips Gap, North Carolina, on 21, 22, 23 February, 07, 08, 16 March, and 02 and 06 May 2013 with a thermoelectrically cooled (–40° C) 2KX2K Apogee Alta by D. Caton and R. Samec, and remotely, with the SARA

Table 1. Information on the stars used in this study.

Star	Name	R.A. (2000) h m s	Dec. (2000) ° ′ ″	V	J–K
V	NSVS 10083189 GSC 1388 0132 ASAS 080441+2124.3 UCAC3 3UC223-096945 UCAC4 558-044873	08 04 41.300	+21 24 20.06	13.15[1]	0.32[1]
C	3UC223-096984	08 05 00.1835	+21 24 29.370	14.25[2]	0.30[2]
K (Check)	3UC223-096989	08 04 17.8266	+21 21 34.359	14.36[2]	0.28[2]

[1] 2MASS (Skrutskie et al. 2006). [2] UCAC3 (Zacharias et al. 2012a).

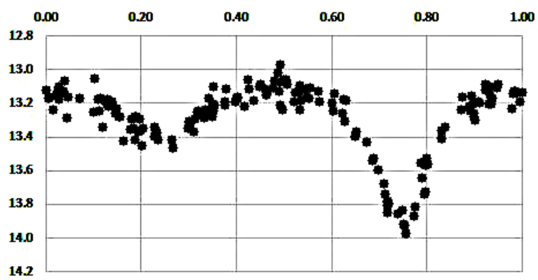

Figure 1. NSVS light curves phased with Equation 1.

North 0.91-meter reflector at KPNO, on 17 March 2015 by R. Samec with the ARC 2KX2K camera cooled to –110° C and both with standard BVR_cI_c filters. Individual observations include 527 in B, 536 in V, 540 in R_c, and 544 in I_c. The probable error of a single observation was 7 mmag in B, 9 mmag in V and R_c, and 10 mmag in I_c. The nightly C–K values stayed constant throughout the observing interval within a precision of 1%. Exposure times varied from 100–200s in B, 40–60s in V, and 30–40s in R_c and I_c. Nightly images were calibrated with twenty-five bias frames, at least five flat frames in each filter, and ten 300-second dark frames.

3. Stellar identifications and finding chart

The coordinates and magnitudes of the variable star, comparison star, and check star are given in Table 1.

The finding chart, given here for future observers, is shown as Figure 2. Figures 3a and 3b show sample observations of B, V, and B–V color curves on the night of 7 and 17 March 2015. Our observations are given in Table 2, in delta magnitudes, ΔB, ΔV, ΔR_c and ΔI_c, in the sense of variable minus comparison star.

4. Period study

Seven times of minimum light were calculated, five primary and two secondary eclipses, from our present observations in the form of Heliocentric Julian Day (HJD):

$$
\begin{aligned}
\text{HJD I} = \; & 2457067.7545 \pm 0.0003 \\
& 2457088.64907 \pm 0.00001 \\
& 2457089.5571 \pm 0.0001 \\
& 2457098.6416 \pm 0.0004 \\
& 2457113.63117 \pm 0.0002 \\
\text{HJD II} = \; & 2457066.6187 \pm 0.0011 \\
& 2457067.5233 \pm 0.0017.
\end{aligned}
$$

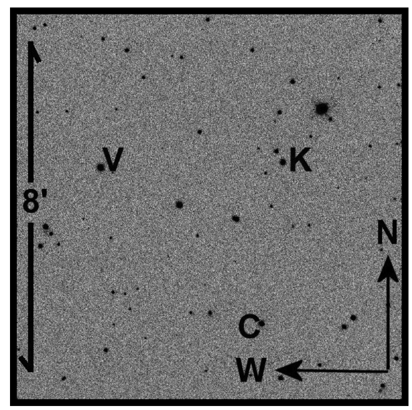

Figure 2. Finding chart of NSVS 10083189 (V), Comparison (C), and Check Stars (K).

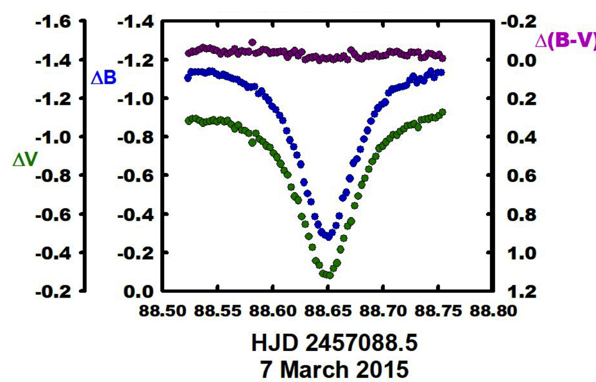

Figure 3 a. B,V and B-V color curves of NSVS 10083189 on the night of 7 March, 2015.

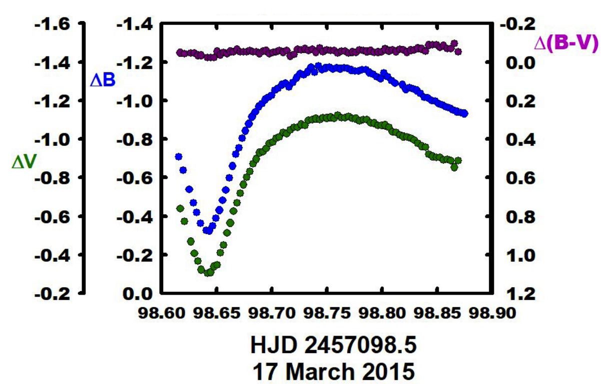

Figure 3 a, b. B,V and B-V color curves of NSVS 10083189 on the night of 17 March, 2015.

In addition, seven more times of low light (points chosen within ±0.01 of phases 0.0 and 0.5) were taken from an earlier light curve phased from data (ASAS J080441+2124.3) from the all All Sky Automated Survey (Figure 1) were used to obtain these timings. Two additional minima are given by Diethelm (2011, 2012).

A linear ephemeris and quadratic ephemerides were determined from these data, respectively:

$$\text{HJD Min I} = 2457089.5588 + 0.45422383\,\text{d} \quad \pm 0.0023 \;\; \pm 0.00000034 \times E \qquad (2)$$

$$\text{HJD Min I} = 2457089.55665\,\text{d} + 0.45421797 \times E - 0.000000000486 \times E^2 \quad \pm 0.00080 \;\; \pm 0.00000085 \;\; \pm 0.000000000070 \qquad (3)$$

This period study covers a 15.4-year interval and shows a period that is apparently decreasing (at about the 7-sigma level). A plot of the residuals for Equation 2 is given as Figure 4. Also, a plot of the quadratic term overlying the linear residuals of Equation 3 is shown in Figure 5. O–C residuals, both linear and quadratic calculations, are given in Table 3. The quadratic ephemeris yields a $\dot{P} = -7.816 \times 10^{-7}$ d/yr, or a mass exchange rate of

$$\frac{dM}{dt} = \frac{\dot{P} M_1 M_2}{3P\,(M_1 - M_2)} = \frac{-9.98 \times 10^{-7}\,M_\odot}{d.} \qquad (4)$$

in a conservative mass scenario.

From the archived records of Bob Nelson on the AAVSO website (Nelson 2016), a very early timing is listed, HJD = 2440273.8663. With this data point added to our study, a simple quadratic fit does not fit two recent timings very well (residuals 0.009 and 0.0065 d) for precision timings. The quadratic term including the new timing becomes $-1.10(8) \times 10^{-10}$. However, a cubic fit or a large amplitude sinusoidal ephemeris (with a 158.8-year period and an a sin(i) = 14.2 AU, $M_\odot$ sin(i) ≈ 0.11) does fit quite well. The cubic fit with its slightly smaller RMSE is shown in Figure 6. Both the quadratic and the cubic terms of this fit are negative. Further timings are needed to determine the orbital evolution of this binary.

Presently, there are not enough timings are available to distinguish between the cubic and quadratic fits.

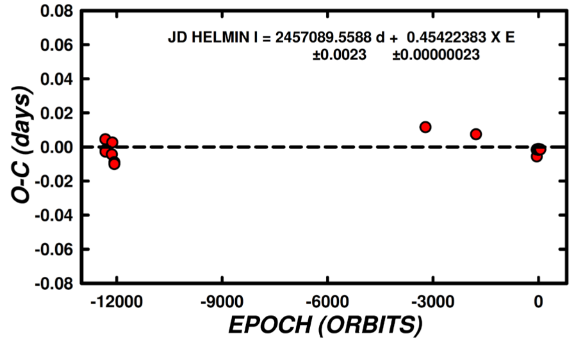

Figure 4. A plot of the linear residuals calculated from Equation 2.

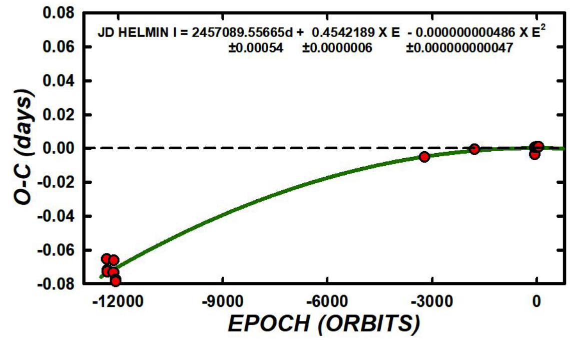

Figure 5. A plot of the quadratic term overlying the linear residuals of Equation 3.

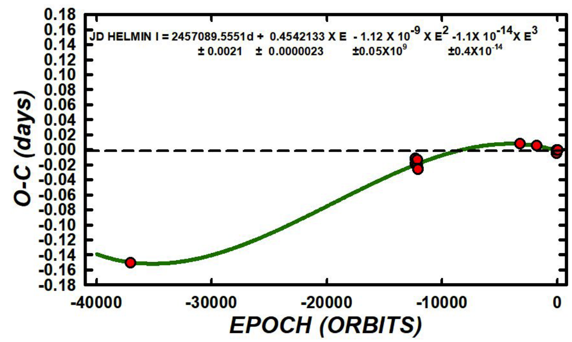

Figure 6. A cubic fit of the residuals shown in Figure 3 including the earliest minima.

5. Light curve characteristics

The phased B,V and R_c,I_c light curves folded using Equation (2) of NSVS 10083189, delta mag vs. phase, are shown in Figures 7a, and 7b, respectively. Light curve characteristics are tabulated by quadratures (averaged magnitudes about Phase 0.0, 0.25, 0.50, and 0.75) in Table 4. As noted in the table, averaged data about phase 0.0 (primary eclipse) are denoted as "Min I", phase 0.5 (secondary eclipse) as "Min II", phase 0.25 as "Max I", and phase 0.250.75 as "Max II". The curves are of good photometric precision, averaging 0.98% in B and 1.2% in V, 1.1% in R_c, and 1.3% in I_c. The amplitudes of the light curves vary from 0.86 to 0.74 magnitude in B to I_c. The O'Connell effect (|Max II–Max I|), a classic indicator of spot activity, averages several times the noise level, 0.02–0.04 magnitude. The differences in minima are large, 0.5–0.6 magnitude, indicating a noncontact binary, since thermal contact is not attained (which means the depths of eclipse should be more similar). Some interesting trends are noted. The $(R–I)_c$ color curves dip at phase 0.0, which is characteristic of a contact binary, however, the rising color curves' rise at phase 0.5 may indicate that the secondary component is under-filling its Roche Lobe. Despite these apparent signs, synthetic light curve modeling is needed to disclose the characteristics of the binary.

6. Temperature and light curve solution

The 2MASS, J–K = 0.32 for the binary. This corresponds to an ~F8V eclipsing binary which yields a temperature of 6250 K. Fast rotating binary stars of this type are noted for having convective atmospheres, so spots are expected.

The B, V, R_c, and I_c curves were pre-modeled with BINARY MAKER 3.0 (Bradstreet and Steelman 2002) and program fits were determined in all filter bands. The result of the best fit was that of a shallow contact binary (fill-out 1%). The parameters were then averaged and input into a four-color simultaneous light curve calculation using the Wilson-Devinney Program (WD;

Wilson and Devinney 1971; Wilson 1990; Wilson 1994; Van Hamme and Wilson 1998). Convective parameters, g = 0.32, A = 0.5 were used. The initial iterations were computed in contact mode (Mode 3). After about ten iterations the potentials went slightly under contact and persisted in that state. We then switched to Mode 2, which has no constraints on the Roche Lobe configuration. The primary component then iterated into fill-outs of 0–1% with the secondary component under-filling (<0.0%). This also persisted. This indicates that the binary was in a semidetached mode computed in Mode 4 (primary filling its critical lobe and the secondary component under-filling its Roche Lobe). The computation converged in that configuration.

The eclipses were not total, so a number of solutions were generated with fixed mass ratios (q). The sum of square residuals was tabulated with each q-value. Solutions were obtained with q-values from 0.38 to 0.8, where the minimization clearly occurred between 0.5 and 0.6. Allowing the q value to adjust along with the other iterated values from our best solution, the residuals minimized at q ~ 0.58. The residual vs. mass ratio plot is given as Figure 8. A single spot was iterated along with the other parameters. A cool spot resulted. In running the WD program, when the absolute values of all of the corrections became less than their associated uncertainties, i.e. convergence was achieved, which is the solution. A geometrical (Roche-lobe) representation of the system is given in Figures 9a, b, c, d at light curve quadratures so that the reader may see the placement of the spot and the relative size of the stars as compared to the orbit. As seen, the system is semi-detached and very near contact, within 0.1% potential-wise. The normalized curves overlain by our light curve solutions are shown as Figures 10a and 10b. The light curve solution parameters are given in Table 5.

7. Discussion

Due to its temperature, configuration, and evolution, NSVS 10083189 is a *precontact* W UMa binary (i.e., a W UMa progenitor) in a V1010 Oph (primary, more massive component is filling its critical Roche Lobe and the secondary is underfilling) configuration (Samec *et al.* 2016). This binary system can result when a binary is coming into contact for the first time. Considering this and its decreasing (and perhaps accelerating decreasing) orbital period, it is near the end of the detached to contact channel (Jiang *et al.* 2014, here after, JHL). JHL found that the ratio of the birth rate of the progenitors of contact binaries to that of contact binaries is greater than about 1.2. This suggests that for the detached-binary channel, the progenitors are sufficient in number to produce the observed contact binaries. NSVS 10083189 is evidently an example of this process taking place. Its spectral type indicates a surface temperature of 6250 K for the primary component. The secondary component has a temperature of ~4570 K (K4V), which means that it is near the values expected for single main sequence stars. The mass ratio is 0.6, with an amplitude of 0.9–0.7 magnitude in B to I, respectively. The fill-out of the secondary component is 99% by potential, which means it is very near critical contact. The inclination is 79°, which allows only 3% of the light of the system to be contributed by the secondary component at phase 0.5.

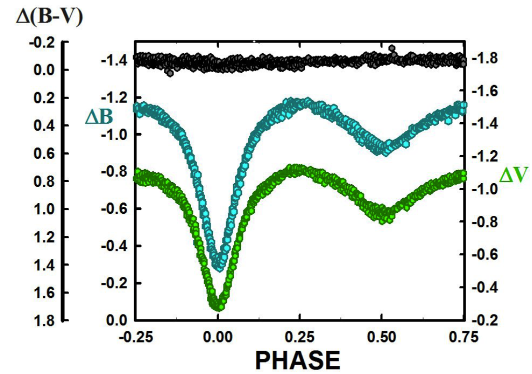

Figure 7a. B,V Δ mag. of NSVS 10083189 phased with Equation 2.

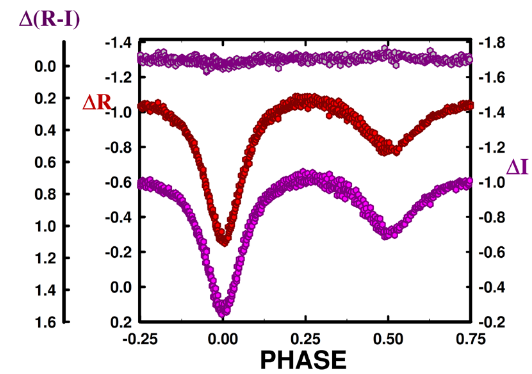

Figure 7b. R,I Δ mag. of NSVS 10083189 phased with Equation 2.

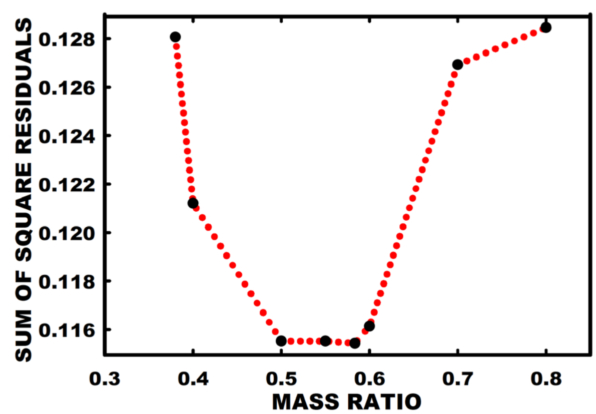

Figure 8. Q-search: plot of mass ratios verses the sum of square residual for each solution.

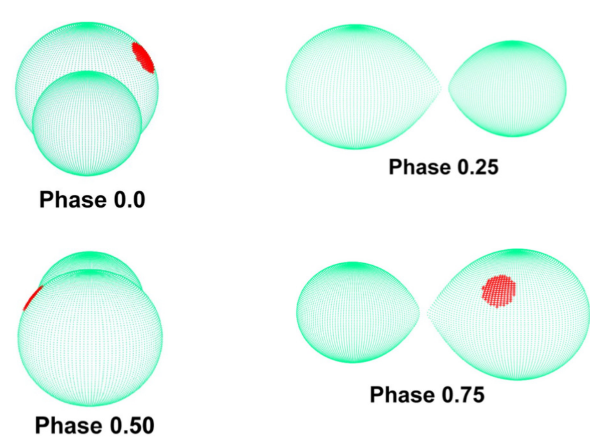

Figure 9. Geometrical representation of the surface of the binary at phases, 0.0, 0.25, 0,50, and 0.75 for NSVS 10083189.

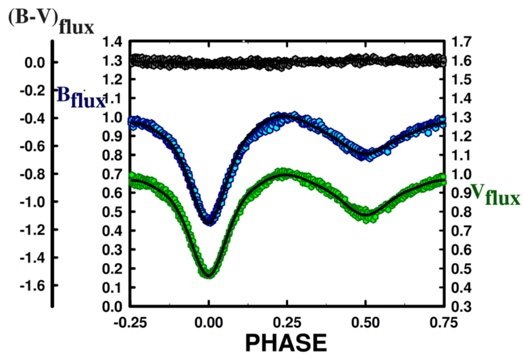

Figure 10a. B,V Normalized Fluxes overlaid by our solution of NSVS 10083189.

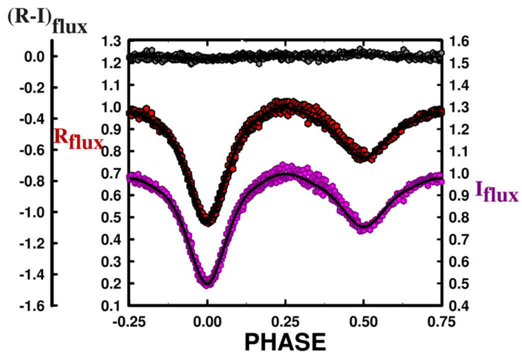

Figure 10b. R_c,I_c Normalized Fluxes overlaid by our solution of NSVS 10083189.

The primary component has an iterated cool spot region of ~15° with a mean T-factor of ~0.86 (T~5360 K). This spot fits the small observed asymmetries in the light curves.

8. Conclusions

The period study of this apparent pre-contact W UMa binary has a ~15-year time duration. The period is found to be decreasing at about the 7 sigma level. This calculated decrease is not unusual for a solar type binary undergoing magnetic braking. The presence of a cool magnetic spot supports this scenario. If this is the case, the system should soon become a contact (W UMa) binary and eventually coalesce over time as it loses angular momentum (AML) due to ionized winds moving radially outward on stiff magnetic field lines rotating with the binary (out to the Alfvén radius). We note that AML due to gravitational radiation also plays a role at this stage. One would expect, eventually, that the binary will coalesce into a rather normal, fast rotating, single A5V type field star after a red novae coalescence event (Tylenda and Kamiński 2016). FK Comae Berenices stars are believed to be a result of such a coalescence event. Finally, radial velocity curves are needed to obtain absolute (not relative) system parameters.

9. Acknowledgements

Dr. Samec wishes to thank Emmanuel College for providing travel expenses as well as some publication costs, and for encouraging undergraduate research with their annual research symposium which was led by Dr. Peek. We wish to thank the college for our association over the past two years.

References

Bradstreet, D. H., and Steelman, D. P. 2002, *Bull. Amer. Astron. Soc.*, **34**, 1224.

Diethelm, R. 2011, *Inf. Bull. Var. Stars*, No. 5992, 1.

Diethelm, R. 2013, *Inf. Bull. Var. Stars*, No. 6042, 1.

Jiang, D., Han, Z., and Li, L. 2014, *Mon. Not. Roy. Astron. Soc.*, **438**, 859.

Los Alamos National Laboratory. 2017, SkyDOT Northern Sky Variability Survey database (http://skydot.lanl.gov/).

Nelson, R. 2016, Eclipsing Binary O–C Files (https://www.aavso.org/bob-nelsons-o-c-files).

Pojmański, G. 2002, *Acta Astron.*, **52**, 397.

Samec, R. G., Nyaude, R., Caton, D., and Van Hamme, W. 2016, *Astron. J.*, **152**, 199.

Skrutskie, M. F., *et al.* 2006, *Astron. J.*, **131**, 1163.

Space Telescope Science Institute 2001, The Guide Star Catalog, Version 2.2 (VizieR On–line Data Catalog: I/271), STScI, Baltimore.

Tylenda, R., and Kamiński, T. 2016, *Astron. Astrophys.*, **592**, A134.

Tylenda, R., *et al.* 2011, *Astron. Astrophys.*, **528**, 114.

Van Hamme, W. V., and Wilson, R. E. 1998, *Bull. Amer. Astron. Soc.*, **30**, 1402.

Wilson, R. E. 1990, *Astrophys. J.*, **356**, 613.

Wilson, R. E. 1994, *Publ. Astron. Soc. Pacific*, **106**, 921.

Wilson, R. E., and Devinney, E. J. 1971, *Astrophys. J.*, **166**, 605.

Wozniak, P. R., *et al.* 2004, *Astron. J.*, **127**, 2436.

Zacharias, N., *et al.* 2012a, The Third U.S. Naval Observatory CCD Astrograph Catalog (UCAC3; http://www.usno.navy.mil/USNO/astrometry/optical-IR-prod/ucac).

Zacharias, N., Finch C., Girard, T., Henden A., Bartlett J., Monet D., and Zacharias M. 2012b, The Fourth U.S. Naval Observatory CCD Astrograph Catalog (UCAC4; http://www.usno.navy.mil/USNO/astrometry/optical-IR-prod/ucac).

Table 2. CW Scl observations ΔB, ΔV, ΔR, and ΔI, variable minus comparison star (Epoch 2400000+).

ΔB	HJD 2457000+	ΔB	HJD 2457000+	ΔB	HJD 2457000+	ΔB	HJD 2457000+	ΔB	HJD 2457000+
–1.129	66.5259	–0.933	67.5262	–1.125	88.5485	–0.884	89.5159	–1.079	89.7288
–1.127	66.5290	–0.932	67.5302	–1.116	88.5517	–0.872	89.5191	–1.072	89.7320
–1.129	66.5322	–0.942	67.5334	–1.121	88.5549	–0.830	89.5223	–1.044	89.7352
–1.107	66.5382	–0.937	67.5366	–1.114	88.5581	–0.788	89.5255	–1.047	89.7383
–1.109	66.5414	–1.128	67.6606	–1.105	88.5613	–0.725	89.5286	–1.021	89.7415
–1.099	66.5447	–1.120	67.6638	–1.099	88.5645	–0.676	89.5318	–1.018	89.7447
–1.088	66.5493	–1.125	67.6670	–1.096	88.5677	–0.606	89.5350	–1.004	89.7479
–1.106	66.5525	–1.122	67.6714	–1.083	88.5708	–0.565	89.5382	–0.984	89.7510
–1.093	66.5557	–1.103	67.6746	–1.072	88.5741	–0.508	89.5413	–0.999	89.7542
–1.067	66.5601	–1.104	67.6778	–1.058	88.5773	–0.446	89.5445	–0.971	89.7574
–1.063	66.5633	–1.091	67.6823	–1.056	88.5804	–0.396	89.5477	–0.990	89.7606
–1.052	66.5665	–1.074	67.6855	–1.060	88.5836	–0.299	89.5540	–0.958	89.7637
–1.048	66.5726	–1.065	67.6887	–1.023	88.5868	–0.294	89.5572	–0.954	89.7669
–1.017	66.5759	–1.044	67.6954	–1.034	88.5900	–0.300	89.5604	–0.941	89.7701
–1.028	66.5791	–1.025	67.6986	–1.007	88.5932	–0.339	89.5636	–0.940	89.7733
–0.993	66.5844	–1.016	67.7018	–0.988	88.5964	–0.376	89.5667	–0.948	89.7765
–0.973	66.5876	–0.976	67.7062	–0.956	88.5996	–0.433	89.5699	–0.912	89.7796
–0.958	66.5908	–0.952	67.7094	–0.939	88.6028	–0.500	89.5731	–0.920	89.7828
–0.986	66.5952	–0.920	67.7126	–0.911	88.6060	–0.563	89.5763	–0.921	89.7860
–0.957	66.5984	–0.816	67.7215	–0.883	88.6092	–0.630	89.5795	–0.915	89.7891
–0.938	66.6016	–0.762	67.7248	–0.830	88.6124	–0.684	89.5826	–0.916	89.7923
–0.931	66.6065	–0.712	67.7280	–0.782	88.6156	–0.733	89.5858	–0.952	97.5158
–0.931	66.6097	–0.631	67.7326	–0.747	88.6188	–0.785	89.5890	–0.928	97.5188
–0.916	66.6129	–0.577	67.7358	–0.705	88.6220	–0.818	89.5922	–0.946	97.5218
–0.914	66.6205	–0.504	67.7391	–0.656	88.6252	–0.871	89.5953	–0.942	97.5247
–0.902	66.6237	–0.419	67.7437	–0.563	88.6283	–0.885	89.5985	–0.951	97.5279
–0.956	66.6388	–0.370	67.7469	–0.506	88.6315	–0.934	89.6017	–0.968	97.5311
–0.961	66.6421	–0.331	67.7501	–0.463	88.6348	–0.957	89.6049	–0.961	97.5343
–0.968	66.6453	–0.323	67.7573	–0.386	88.6380	–0.996	89.6081	–0.975	97.5375
–0.985	66.6495	–0.347	67.7606	–0.344	88.6412	–1.007	89.6112	–0.985	97.5407
–0.994	66.6527	–0.388	67.7638	–0.304	88.6443	–1.030	89.6144	–0.995	97.5439
–0.993	66.6559	–0.474	67.7683	–0.289	88.6475	–1.034	89.6176	–1.012	97.5471
–1.002	66.6600	–0.533	67.7715	–0.281	88.6507	–1.048	89.6208	–1.024	97.5503
–1.028	66.6633	–0.600	67.7747	–0.302	88.6539	–1.044	89.6240	–1.036	97.5535
–1.034	66.6665	–0.777	67.7854	–0.339	88.6571	–1.082	89.6271	–1.042	97.5567
–1.038	66.6705	–0.820	67.7886	–0.388	88.6603	–1.113	89.6303	–1.052	97.5599
–1.054	66.6737	–0.868	67.7918	–0.483	88.6635	–1.088	89.6335	–1.057	97.5631
–1.061	66.6769	–0.934	67.7976	–0.510	88.6667	–1.102	89.6367	–1.047	97.5663
–1.062	66.6811	–0.967	67.8008	–0.583	88.6699	–1.107	89.6399	–1.071	97.5695
–1.079	66.6843	–0.998	67.8040	–0.663	88.6731	–1.144	89.6430	–1.069	97.5728
–1.079	66.6875	–1.027	67.8098	–0.685	88.6762	–1.128	89.6462	–1.078	97.5760
–1.088	66.6945	–1.048	67.8130	–0.734	88.6794	–1.142	89.6494	–1.069	97.5791
–1.100	66.6977	–1.059	67.8162	–0.787	88.6826	–1.136	89.6526	–1.092	97.5823
–1.095	66.7010	–1.066	67.8222	–0.832	88.6858	–1.160	89.6557	–1.106	97.5855
–1.101	66.7059	–1.090	67.8254	–0.879	88.6890	–1.169	89.6589	–1.103	97.5887
–1.112	66.7091	–1.115	67.8287	–0.916	88.6922	–1.139	89.6621	–1.109	97.5919
–1.134	66.7124	–1.124	67.8320	–0.948	88.6954	–1.173	89.6652	–1.123	97.5951
–1.129	66.7196	–1.125	67.8352	–0.966	88.6986	–1.170	89.6684	–1.127	97.5983
–1.159	66.7228	–1.137	67.8384	–0.978	88.7018	–1.157	89.6716	–1.127	97.6015
–1.134	66.7258	–1.143	67.8416	–1.025	88.7049	–1.171	89.6748	–1.128	97.6047
–1.123	66.7298	–1.134	67.8448	–1.044	88.7081	–1.162	89.6780	–1.134	97.6079
–1.150	66.7331	–1.153	67.8480	–1.049	88.7113	–1.180	89.6811	–1.140	97.6111
–1.142	66.7363	–1.150	67.8513	–1.056	88.7145	–1.167	89.6843	–1.150	97.6143
–1.139	66.7406	–1.153	67.8545	–1.059	88.7177	–1.152	89.6875	–1.128	97.6174
–1.132	66.7438	–1.167	67.8577	–1.067	88.7209	–1.150	89.6907	–1.152	97.6207
–1.123	66.7470	–1.153	67.8610	–1.093	88.7241	–1.136	89.6938	–1.135	97.6270
–1.127	66.7513	–1.172	67.8642	–1.111	88.7273	–1.150	89.6970	–1.146	97.6302
–1.134	66.7545	–1.151	67.8674	–1.081	88.7305	–1.134	89.7002	–1.138	97.6334
–1.128	66.7577	–1.104	88.5229	–1.097	88.7337	–1.129	89.7034	–1.134	97.6366
–1.132	66.7618	–1.134	88.5261	–1.091	88.7369	–1.120	89.7066	–1.127	97.6398
–1.069	66.7683	–1.136	88.5293	–1.118	88.7401	–1.138	89.7097	–1.122	97.6430
–0.947	67.5092	–1.135	88.5325	–1.137	88.7433	–1.121	89.7129	–1.109	97.6462
–0.934	67.5124	–1.136	88.5357	–1.106	88.7464	–1.099	89.7161	–1.112	97.6494
–0.921	67.5156	–1.129	88.5389	–1.133	88.7496	–1.112	89.7193	–1.096	97.6526
–0.909	67.5198	–1.137	88.5421	–1.132	88.7528	–1.102	89.7225	–1.090	97.6558
–0.918	67.5230	–1.140	88.5453	–0.930	89.5127	–1.087	89.7256	–1.075	97.6590

Table continued on following pages

Table 2. CW Scl observations ΔB, ΔV, ΔR, and ΔI, variable minus comparison star (Epoch 2400000+), cont.

ΔB	HJD 2457000+	ΔB	HJD 2457000+	ΔB	HJD 2457000+	ΔB	HJD 2457000+	ΔB	HJD 2457000+
–1.061	97.6622	–1.081	98.7090	–1.012	98.8413	–0.870	113.6695	–1.134	117.6072
–1.053	97.6686	–1.090	98.7123	–1.000	98.8447	–0.924	113.6727	–1.110	117.6102
–1.035	97.6718	–1.070	98.7156	–0.995	98.8479	–0.926	113.6759	–1.149	117.6131
–1.007	97.6749	–1.092	98.7189	–0.983	98.8512	–0.981	113.6791	–1.155	117.6161
–0.999	97.6782	–1.117	98.7223	–0.977	98.8545	–0.983	113.6823	–1.128	117.6190
–0.996	97.6814	–1.140	98.7256	–0.967	98.8579	–1.004	113.6855	–1.137	117.6220
–0.965	97.6846	–1.133	98.7289	–0.959	98.8612	–1.027	113.6887	–1.141	117.6249
–0.957	97.6878	–1.147	98.7322	–0.949	98.8644	–1.051	113.6919	–1.121	117.6279
–0.914	97.6910	–1.172	98.7355	–0.942	98.8678	–1.054	113.6951	–1.134	117.6308
–0.880	97.6942	–1.145	98.7388	–0.937	98.8711	–1.054	113.6983	–1.105	117.6337
–0.843	97.6973	–1.178	98.7421	–0.932	98.8744	–1.088	113.7015	–1.106	117.6367
–0.792	97.7005	–1.159	98.7454	–1.046	113.5735	–1.080	113.7047	–1.119	117.6396
–0.707	98.6157	–1.167	98.7487	–0.995	113.5767	–0.948	117.5247	–1.093	117.6426
–0.639	98.6196	–1.173	98.7520	–1.011	113.5799	–0.999	117.5276	–1.074	117.6455
–0.538	98.6251	–1.162	98.7553	–0.975	113.5831	–1.005	117.5306	–1.077	117.6485
–0.469	98.6287	–1.170	98.7587	–0.915	113.5863	–1.033	117.5335	–1.057	117.6514
–0.420	98.6319	–1.164	98.7620	–0.918	113.5895	–1.018	117.5365	–1.054	117.6544
–0.362	98.6351	–1.168	98.7653	–0.877	113.5927	–1.031	117.5394	–1.040	117.6573
–0.325	98.6405	–1.165	98.7686	–0.828	113.5959	–1.031	117.5424	–1.016	117.6602
–0.324	98.6435	–1.157	98.7719	–0.790	113.5991	–1.037	117.5453	–0.992	117.6632
–0.349	98.6465	–1.153	98.7752	–0.782	113.6023	–1.062	117.5482	–0.986	117.6661
–0.388	98.6494	–1.153	98.7785	–0.676	113.6055	–1.058	117.5512	–1.001	117.6690
–0.430	98.6524	–1.159	98.7818	–0.623	113.6087	–1.072	117.5541	–0.957	117.6720
–0.482	98.6554	–1.159	98.7851	–0.581	113.6119	–1.091	117.5571	–0.938	117.6749
–0.535	98.6583	–1.144	98.7884	–0.513	113.6151	–1.087	117.5600	–0.906	117.6779
–0.599	98.6613	–1.135	98.7917	–0.469	113.6183	–1.080	117.5630	–0.854	117.6808
–0.659	98.6643	–1.122	98.7950	–0.392	113.6215	–1.103	117.5659	–0.840	117.6838
–0.720	98.6672	–1.114	98.7984	–0.334	113.6279	–1.111	117.5689	–0.792	117.6867
–0.755	98.6702	–1.113	98.7984	–0.339	113.6311	–1.110	117.5718	–0.739	117.6897
–0.803	98.6732	–1.142	98.8017	–0.308	113.6343	–1.111	117.5748	–0.674	117.6926
–0.878	98.6791	–1.122	98.8050	–0.321	113.6375	–1.118	117.5777	–0.662	117.6955
–0.915	98.6821	–1.102	98.8083	–0.375	113.6407	–1.110	117.5807	–0.593	117.6985
–0.939	98.6850	–1.089	98.8116	–0.465	113.6439	–1.073	117.5836	–0.574	117.7014
–0.968	98.6880	–1.081	98.8182	–0.520	113.6471	–1.129	117.5866	–0.481	117.7043
–0.983	98.6909	–1.058	98.8215	–0.582	113.6503	–1.129	117.5895	–0.438	117.7073
–1.004	98.6939	–1.066	98.8248	–0.643	113.6535	–1.134	117.5925	–0.380	117.7102
–1.016	98.6969	–1.059	98.8281	–0.701	113.6567	–1.143	117.5954	–0.349	117.7132
–1.025	98.6999	–1.051	98.8314	–0.764	113.6599	–1.158	117.5984		
–1.052	98.7028	–1.035	98.8347	–0.807	113.6631	–1.140	117.6013		
–1.063	98.7058	–1.015	98.8380	–0.835	113.6663	–1.159	117.6043		

ΔV	HJD 2457000+	Δv	HJD 2457000+	ΔV	HJD 2457000+	ΔV	HJD 2457000+	ΔV	HJD 2457000+
–1.060	66.5269	–1.060	66.6108	–1.060	66.6886	–1.060	67.5178	–0.752	67.7237
–1.060	66.5301	–1.060	66.6140	–1.060	66.6956	–1.060	67.5219	–0.693	67.7269
–1.060	66.5333	–1.060	66.6184	–1.060	66.6988	–1.060	67.5251	–0.636	67.7301
–1.060	66.5393	–1.060	66.6216	–1.060	66.7020	–1.060	67.5283	–0.561	67.7348
–1.060	66.5425	–1.060	66.6248	–1.060	66.7070	–1.060	67.5323	–0.502	67.7380
–1.060	66.5457	–1.060	66.6290	–1.060	66.7102	–1.060	67.5355	–0.445	67.7412
–1.060	66.5503	–1.060	66.6320	–1.060	66.7134	–1.060	67.5387	–0.377	67.7459
–1.060	66.5536	–1.060	66.6350	–1.060	66.7206	–1.060	67.6627	–0.320	67.7491
–1.060	66.5568	–1.060	66.6399	–1.060	66.7238	–1.060	67.6660	–0.310	67.7523
–1.060	66.5612	–1.060	66.6431	–1.060	66.7268	–1.060	67.6692	–0.320	67.7595
–1.060	66.5644	–1.060	66.6463	–1.060	66.7309	–1.060	67.6736	–0.354	67.7627
–1.060	66.5676	–1.060	66.6505	–1.060	66.7341	–1.060	67.6768	–0.396	67.7659
–1.060	66.5737	–1.060	66.6538	–1.060	66.7373	–1.060	67.6800	–0.491	67.7704
–1.060	66.5769	–1.060	66.6570	–1.060	66.7416	–1.060	67.6844	–0.533	67.7737
–1.060	66.5801	–1.060	66.6611	–1.060	66.7449	–1.060	67.6876	–0.610	67.7769
–1.060	66.5854	–1.060	66.6643	–1.060	66.7481	–1.060	67.6908	–0.783	67.7875
–1.060	66.5887	–1.060	66.6675	–1.060	66.7523	–1.060	67.6975	–0.820	67.7908
–1.060	66.5919	–1.060	66.6715	–1.060	66.7555	–1.060	67.7007	–0.862	67.7940
–1.060	66.5962	–1.060	66.6748	–1.060	66.7588	–1.060	67.7039	–0.916	67.7998
–1.060	66.5995	–1.060	66.6780	–1.060	66.7629	–1.060	67.7083	–0.944	67.8030
–1.060	66.6027	–1.060	66.6821	–1.060	67.5114	–0.894	67.7115	–0.966	67.8062
–1.060	66.6075	–1.060	66.6854	–1.060	67.5146	–0.857	67.7148	–1.007	67.8120

Table continued on following pages

Table 2. CW Scl observations ΔB, ΔV, ΔR, and ΔI, variable minus comparison star (Epoch 2400000+), cont.

ΔV	HJD 2457000+	ΔV	HJD 2457000+	ΔV	HJD 2457000+	ΔV	HJD 2457000+	ΔV	HJD 2457000+
–1.016	67.8152	–0.750	88.6805	–1.089	89.6473	–1.030	97.5770	–0.984	98.7008
–1.024	67.8184	–0.785	88.6837	–1.096	89.6504	–1.041	97.5802	–1.003	98.7038
–1.044	67.8244	–0.832	88.6869	–1.103	89.6536	–1.035	97.5834	–1.010	98.7067
–1.053	67.8276	–0.871	88.6901	–1.092	89.6568	–1.045	97.5866	–1.034	98.7101
–1.064	67.8308	–0.897	88.6932	–1.110	89.6599	–1.061	97.5898	–1.026	98.7134
–1.080	67.8341	–0.939	88.6964	–1.090	89.6631	–1.066	97.5930	–1.047	98.7167
–1.086	67.8373	–0.952	88.6996	–1.104	89.6663	–1.063	97.5962	–1.061	98.7200
–1.095	67.8405	–0.972	88.7028	–1.099	89.6695	–1.079	97.5994	–1.059	98.7233
–1.096	67.8438	–0.990	88.7060	–1.125	89.6727	–1.070	97.6026	–1.075	98.7266
–1.105	67.8470	–1.011	88.7092	–1.107	89.6758	–1.079	97.6057	–1.071	98.7299
–1.113	67.8502	–1.009	88.7124	–1.112	89.6790	–1.091	97.6089	–1.097	98.7332
–1.129	67.8534	–1.027	88.7156	–1.093	89.6822	–1.081	97.6121	–1.099	98.7366
–1.122	67.8566	–1.040	88.7188	–1.102	89.6854	–1.090	97.6153	–1.105	98.7399
–1.131	67.8598	–1.058	88.7220	–1.085	89.6885	–1.097	97.6185	–1.101	98.7432
–1.130	67.8631	–1.060	88.7252	–1.105	89.6917	–1.108	97.6217	–1.109	98.7465
–1.126	67.8663	–1.065	88.7284	–1.102	89.6949	–1.081	97.6249	–1.108	98.7498
–1.127	67.8695	–1.049	88.7316	–1.086	89.6981	–1.090	97.6281	–1.112	98.7531
–1.082	88.5239	–1.086	88.7347	–1.083	89.7013	–1.098	97.6313	–1.106	98.7564
–1.094	88.5271	–1.089	88.7379	–1.074	89.7044	–1.093	97.6345	–1.124	98.7597
–1.094	88.5303	–1.092	88.7411	–1.062	89.7076	–1.079	97.6377	–1.110	98.7630
–1.083	88.5335	–1.099	88.7443	–1.068	89.7108	–1.080	97.6409	–1.111	98.7663
–1.072	88.5367	–1.096	88.7475	–1.048	89.7140	–1.079	97.6441	–1.117	98.7696
–1.077	88.5399	–1.109	88.7507	–1.060	89.7171	–1.062	97.6472	–1.106	98.7729
–1.080	88.5431	–1.126	88.7539	–1.038	89.7203	–1.078	97.6504	–1.105	98.7762
–1.085	88.5463	–0.867	89.5138	–1.041	89.7235	–1.071	97.6536	–1.093	98.7795
–1.076	88.5495	–0.835	89.5170	–1.040	89.7267	–1.038	97.6568	–1.101	98.7828
–1.087	88.5527	–0.812	89.5202	–1.044	89.7299	–1.039	97.6600	–1.101	98.7861
–1.077	88.5559	–0.762	89.5233	–1.021	89.7330	–1.040	97.6632	–1.084	98.7895
–1.082	88.5591	–0.729	89.5265	–0.987	89.7362	–1.021	97.6664	–1.082	98.7928
–1.064	88.5623	–0.671	89.5297	–0.985	89.7394	–1.008	97.6696	–1.069	98.7961
–1.042	88.5655	–0.612	89.5329	–0.977	89.7426	–0.997	97.6728	–1.071	98.7994
–1.061	88.5687	–0.563	89.5360	–0.955	89.7458	–0.995	97.6760	–1.068	98.8027
–1.034	88.5719	–0.497	89.5392	–0.966	89.7489	–0.975	97.6792	–1.071	98.7994
–1.030	88.5751	–0.440	89.5424	–0.948	89.7521	–0.936	97.6824	–1.072	98.8027
–1.017	88.5783	–0.376	89.5456	–0.919	89.7553	–0.934	97.6856	–1.059	98.8060
–0.969	88.5815	–0.331	89.5487	–0.912	89.7584	–0.899	97.6888	–1.037	98.8093
–1.017	88.5847	–0.309	89.5519	–0.902	89.7616	–0.875	97.6920	–1.034	98.8126
–0.987	88.5879	–0.278	89.5551	–0.892	89.7648	–0.821	97.6952	–1.020	98.8159
–0.973	88.5911	–0.274	89.5583	–0.893	89.7680	–0.819	97.6984	–1.012	98.8193
–0.952	88.5943	–0.290	89.5614	–0.860	89.7711	–0.782	97.7016	–1.010	98.8226
–0.944	88.5975	–0.319	89.5646	–0.852	89.7743	–0.638	98.6170	–1.004	98.8259
–0.914	88.6007	–0.352	89.5678	–0.868	89.7775	–0.573	98.6209	–0.994	98.8292
–0.893	88.6038	–0.415	89.5710	–0.862	89.7807	–0.468	98.6264	–0.976	98.8325
–0.859	88.6070	–0.493	89.5742	–0.850	89.7839	–0.407	98.6298	–0.962	98.8358
–0.825	88.6102	–0.557	89.5773	–0.855	89.7870	–0.367	98.6330	–0.958	98.8391
–0.801	88.6134	–0.601	89.5805	–0.858	89.7902	–0.322	98.6360	–0.922	98.8424
–0.739	88.6166	–0.657	89.5837	–0.856	89.7934	–0.303	98.6415	–0.909	98.8457
–0.690	88.6198	–0.710	89.5869	–0.854	97.5169	–0.309	98.6444	–0.904	98.8490
–0.670	88.6230	–0.760	89.5900	–0.862	97.5198	–0.339	98.6474	–0.905	98.8523
–0.587	88.6262	–0.798	89.5932	–0.880	97.5228	–0.348	98.6504	–0.891	98.8556
–0.546	88.6294	–0.822	89.5964	–0.882	97.5258	–0.409	98.6533	–0.895	98.8589
–0.483	88.6326	–0.861	89.5996	–0.902	97.5290	–0.450	98.6563	–0.887	98.8622
–0.427	88.6358	–0.895	89.6028	–0.902	97.5322	–0.513	98.6593	–0.853	98.8655
–0.357	88.6390	–0.912	89.6059	–0.923	97.5354	–0.564	98.6622	–0.888	98.8688
–0.334	88.6422	–0.950	89.6091	–0.926	97.5386	–0.626	98.6652	–0.867	98.8721
–0.291	88.6454	–0.952	89.6123	–0.932	97.5418	–0.668	98.6682	–0.944	113.5745
–0.284	88.6486	–0.977	89.6155	–0.948	97.5450	–0.719	98.6711	–0.933	113.5778
–0.280	88.6518	–0.999	89.6186	–0.959	97.5482	–0.763	98.6741	–0.932	113.5810
–0.316	88.6550	–0.999	89.6218	–0.959	97.5514	–0.802	98.6770	–0.887	113.5842
–0.345	88.6582	–1.023	89.6250	–0.979	97.5546	–0.831	98.6800	–0.863	113.5874
–0.415	88.6614	–1.021	89.6282	–0.990	97.5578	–0.870	98.6830	–0.822	113.5906
–0.472	88.6645	–1.036	89.6314	–1.003	97.5610	–0.896	98.6860	–0.787	113.5938
–0.535	88.6677	–1.038	89.6346	–1.002	97.5642	–0.929	98.6889	–0.755	113.5970
–0.561	88.6709	–1.060	89.6377	–1.017	97.5674	–0.935	98.6919	–0.726	113.6002
–0.643	88.6741	–1.066	89.6409	–1.023	97.5706	–0.951	98.6948	–0.655	113.6034
–0.693	88.6773	–1.073	89.6441	–1.036	97.5738	–0.976	98.6978	–0.607	113.6066

Table continued on following pages

Table 2. CW Scl observations ΔB, ΔV, ΔR, and ΔI, variable minus comparison star (Epoch 2400000+), cont.

ΔV	*HJD 2457000+*	ΔV	*HJD 2457000+*	ΔV	*HJD 2457000+*	ΔV	*HJD 2457000+*	ΔV	*HJD 2457000+*
–0.556	113.6098	–0.861	113.6738	–0.987	117.5522	–1.050	117.6112	–0.897	117.6701
–0.489	113.6130	–0.868	113.6770	–0.998	117.5551	–1.056	117.6141	–0.889	117.6730
–0.434	113.6162	–0.927	113.6802	–0.989	117.5581	–1.060	117.6171	–0.836	117.6759
–0.399	113.6194	–0.935	113.6834	–1.011	117.5610	–1.062	117.6200	–0.812	117.6789
–0.308	113.6226	–0.955	113.6866	–1.009	117.5640	–1.043	117.6230	–0.819	117.6818
–0.301	113.6258	–0.985	113.6898	–1.015	117.5669	–1.057	117.6259	–0.748	117.6848
–0.277	113.6290	–0.965	113.6929	–1.025	117.5699	–1.039	117.6289	–0.718	117.6877
–0.276	113.6322	–0.983	113.6961	–1.026	117.5728	–1.040	117.6318	–0.679	117.6906
–0.281	113.6354	–0.986	113.6993	–1.022	117.5758	–1.040	117.6347	–0.598	117.6936
–0.317	113.6386	–1.001	113.7025	–1.039	117.5787	–1.036	117.6377	–0.569	117.6965
–0.370	113.6418	–1.022	113.7057	–1.034	117.5817	–1.019	117.6406	–0.513	117.6995
–0.423	113.6450	–0.886	117.5257	–1.045	117.5846	–1.017	117.6436	–0.469	117.7024
–0.468	113.6482	–0.917	117.5286	–1.048	117.5876	–0.991	117.6465	–0.418	117.7053
–0.523	113.6514	–0.915	117.5315	–1.048	117.5905	–0.984	117.6495	–0.329	117.7083
–0.592	113.6546	–0.932	117.5345	–1.051	117.5935	–0.982	117.6524	–0.296	117.7112
–0.640	113.6578	–0.952	117.5375	–1.054	117.5964	–0.973	117.6553	–0.284	117.7142
–0.698	113.6610	–0.952	117.5404	–1.056	117.5994	–0.959	117.6583		
–0.754	113.6642	–0.970	117.5434	–1.067	117.6023	–0.949	117.6612		
–0.794	113.6674	–0.974	117.5463	–1.063	117.6053	–0.930	117.6642		
–0.829	113.6706	–0.977	117.5492	–1.060	117.6082	–0.923	117.6671		

ΔR_c	*HJD 2457000+*	ΔR_c	*HJD 2457000+*	ΔR_c	*HJD 2457000+*	ΔR_c	*HJD 2457000+*	ΔR_c	*HJD 2457000+*
–1.035	66.5245	–0.978	66.6860	–0.857	67.7077	–1.045	68.7726	–0.745	88.6141
–1.041	66.5275	–0.985	66.6930	–0.833	67.7109	–1.036	68.7759	–0.685	88.6173
–1.023	66.5307	–1.006	66.6962	–0.795	67.7141	–1.020	68.7791	–0.643	88.6205
–1.023	66.5367	–1.026	66.6995	–0.694	67.7231	–1.041	68.7827	–0.579	88.6237
–1.012	66.5399	–1.009	66.7076	–0.647	67.7263	–1.040	68.7859	–0.546	88.6269
–1.018	66.5431	–1.008	66.7109	–0.608	67.7295	–1.067	68.7891	–0.485	88.6301
–1.003	66.5477	–1.044	66.7181	–0.517	67.7341	–1.040	68.7942	–0.422	88.6333
–0.984	66.5510	–1.048	66.7213	–0.459	67.7373	–1.029	68.8012	–0.390	88.6365
–0.984	66.5542	–1.041	66.7244	–0.409	67.7406	–0.979	68.8083	–0.327	88.6397
–0.982	66.5586	–1.045	66.7283	–0.333	67.7452	–1.019	68.8132	–0.276	88.6429
–0.951	66.5618	–1.031	66.7315	–0.291	67.7484	–0.997	68.8187	–0.265	88.6460
–0.963	66.5650	–1.020	66.7348	–0.277	67.7516	–0.988	68.8229	–0.275	88.6492
–0.941	66.5711	–1.031	66.7391	–0.274	67.7588	–0.994	68.8276	–0.263	88.6524
–0.918	66.5744	–1.019	66.7423	–0.309	67.7620	–0.979	68.8325	–0.280	88.6556
–0.919	66.5776	–1.004	66.7455	–0.344	67.7653	–0.966	68.8347	–0.332	88.6588
–0.902	66.5828	–1.038	66.7498	–0.429	67.7698	–1.031	88.5246	–0.387	88.6620
–0.874	66.5861	–1.027	66.7530	–0.483	67.7730	–1.029	88.5278	–0.447	88.6652
–0.863	66.5893	–1.054	66.7562	–0.543	67.7762	–1.030	88.5310	–0.486	88.6684
–0.854	66.5937	–1.026	66.7603	–0.706	67.7869	–1.045	88.5342	–0.552	88.6716
–0.837	66.5969	–1.032	66.7636	–0.705	67.7901	–1.039	88.5374	–0.605	88.6748
–0.812	66.6050	–0.969	66.7668	–0.782	67.7933	–1.047	88.5406	–0.650	88.6779
–0.782	66.6082	–0.815	67.5107	–0.842	67.7991	–1.030	88.5438	–0.696	88.6811
–0.777	66.6114	–0.790	67.5139	–0.872	67.8023	–1.021	88.5470	–0.741	88.6843
–0.773	66.6158	–0.772	67.5171	–0.899	67.8055	–1.026	88.5502	–0.770	88.6875
–0.793	66.6190	–0.767	67.5213	–0.932	67.8113	–1.019	88.5534	–0.834	88.6907
–0.782	66.6222	–0.786	67.5245	–0.941	67.8145	–1.019	88.5566	–0.857	88.6939
–0.779	66.6266	–0.777	67.5277	–0.955	67.8177	–1.003	88.5598	–0.877	88.6971
–0.790	66.6296	–0.795	67.5317	–0.980	67.8237	–0.998	88.5662	–0.899	88.7003
–0.820	66.6373	–0.781	67.5349	–0.987	67.8269	–0.972	88.5694	–0.915	88.7035
–0.822	66.6406	–0.768	67.5381	–1.006	67.8302	–0.976	88.5726	–0.940	88.7066
–0.859	66.6438	–1.015	67.6621	–1.005	67.8335	–0.963	88.5758	–0.957	88.7098
–0.852	66.6480	–1.003	67.6653	–1.023	67.8367	–0.957	88.5790	–0.968	88.7130
–0.874	66.6512	–1.010	67.6685	–1.013	67.8399	–0.959	88.5822	–0.965	88.7162
–0.884	66.6544	–0.998	67.6729	–1.025	67.8431	–0.953	88.5853	–0.966	88.7194
–0.892	66.6585	–0.982	67.6761	–1.034	67.8463	–0.921	88.5885	–0.973	88.7226
–0.901	66.6618	–0.982	67.6793	–1.039	67.8495	–0.924	88.5917	–1.006	88.7258
–0.914	66.6650	–0.972	67.6838	–1.029	67.8528	–0.904	88.5949	–1.008	88.7290
–0.938	66.6690	–0.966	67.6870	–1.048	67.8560	–0.883	88.5981	–1.015	88.7322
–0.938	66.6722	–0.942	67.6902	–1.053	67.8592	–0.856	88.6013	–1.016	88.7354
–0.965	66.6754	–0.930	67.6969	–1.058	67.8625	–0.839	88.6045	–1.021	88.7386
–0.984	66.6796	–0.906	67.7001	–1.045	67.8657	–0.816	88.6077	–1.029	88.7418
–0.975	66.6828	–0.889	67.7033	–1.061	67.8689	–0.776	88.6109	–1.038	88.7450

Table continued on following pages

Table 2. CW Scl observations ΔB, ΔV, ΔR, and ΔI, variable minus comparison star (Epoch 2400000+), cont.

ΔR_c	HJD 2457000+	ΔR_c	HJD 2457000+	ΔR_c	HJD 2457000+	ΔR_c	HJD 2457000+	ΔR_c	HJD 2457000+
–1.048	88.7481	–0.994	89.7178	–0.974	97.6575	–1.062	98.7902	–0.961	113.7063
–1.056	88.7513	–1.006	89.7210	–0.980	97.6607	–1.050	98.7935	–0.883	117.5262
–1.045	88.7544	–0.993	89.7242	–0.935	97.6639	–1.048	98.7968	–0.886	117.5292
–0.812	89.5145	–0.976	89.7273	–0.938	97.6671	–1.062	98.8001	–0.907	117.5321
–0.778	89.5176	–0.967	89.7305	–0.943	97.6703	–1.045	98.8034	–0.905	117.5351
–0.748	89.5208	–0.962	89.7337	–0.940	97.6735	–1.035	98.8068	–0.923	117.5380
–0.707	89.5240	–0.969	89.7369	–0.929	97.6767	–1.025	98.8101	–0.935	117.5410
–0.677	89.5272	–0.933	89.7401	–0.903	97.6799	–1.005	98.8134	–0.933	117.5439
–0.627	89.5303	–0.927	89.7432	–0.876	97.6831	–1.006	98.8167	–0.952	117.5469
–0.565	89.5335	–0.900	89.7464	–0.851	97.6863	–0.989	98.8200	–0.968	117.5498
–0.526	89.5367	–0.881	89.7496	–0.827	97.6895	–0.981	98.8233	–0.974	117.5528
–0.450	89.5399	–0.888	89.7527	–0.796	97.6927	–0.960	98.8266	–0.976	117.5557
–0.413	89.5430	–0.873	89.7559	–0.784	97.6959	–0.964	98.8299	–0.979	117.5587
–0.363	89.5462	–0.850	89.7591	–0.725	97.6991	–0.937	98.8332	–0.982	117.5616
–0.304	89.5494	–0.837	89.7623	–0.670	98.6140	–0.918	98.8365	–0.992	117.5646
–0.269	89.5526	–0.821	89.7654	–0.584	98.6179	–0.905	98.8398	–1.000	117.5675
–0.264	89.5557	–0.823	89.7686	–0.490	98.6234	–0.888	98.8431	–1.012	117.5705
–0.269	89.5589	–0.813	89.7718	–0.442	98.6273	–0.884	98.8464	–1.009	117.5734
–0.320	89.5653	–0.792	89.7750	–0.402	98.6306	–0.879	98.8497	–1.004	117.5764
–0.355	89.5685	–0.798	89.7782	–0.352	98.6338	–0.853	98.8530	–1.029	117.5793
–0.408	89.5716	–0.796	89.7813	–0.315	98.6392	–0.849	98.8563	–1.028	117.5823
–0.468	89.5748	–0.781	89.7845	–0.343	98.6481	–0.839	98.8596	–1.019	117.5852
–0.525	89.5780	–0.775	97.5175	–0.385	98.6511	–0.822	98.8629	–1.021	117.5882
–0.582	89.5812	–0.791	97.5204	–0.417	98.6541	–0.823	98.8662	–1.041	117.5911
–0.634	89.5843	–0.823	97.5234	–0.478	98.6570	–0.824	98.8695	–1.033	117.5941
–0.679	89.5875	–0.830	97.5264	–0.528	98.6600	–0.923	113.5752	–1.026	117.5970
–0.717	89.5907	–0.834	97.5296	–0.578	98.6630	–0.881	113.5784	–1.040	117.6000
–0.762	89.5939	–0.849	97.5328	–0.637	98.6659	–0.880	113.5816	–1.050	117.6029
–0.785	89.5970	–0.855	97.5360	–0.670	98.6689	–0.856	113.5848	–1.036	117.6059
–0.845	89.6002	–0.874	97.5393	–0.728	98.6719	–0.829	113.5880	–1.045	117.6088
–0.854	89.6034	–0.885	97.5424	–0.771	98.6748	–0.823	113.5912	–1.042	117.6118
–0.888	89.6066	–0.902	97.5456	–0.795	98.6778	–0.758	113.5944	–1.046	117.6147
–0.894	89.6098	–0.907	97.5488	–0.838	98.6808	–0.726	113.5976	–1.021	117.6177
–0.918	89.6129	–0.937	97.5520	–0.855	98.6837	–0.677	113.6008	–1.040	117.6206
–0.941	89.6161	–0.931	97.5552	–0.897	98.6867	–0.635	113.6040	–1.020	117.6236
–0.948	89.6193	–0.945	97.5584	–0.911	98.6896	–0.587	113.6072	–1.028	117.6265
–0.954	89.6225	–0.967	97.5616	–0.935	98.6926	–0.514	113.6104	–1.022	117.6294
–0.965	89.6257	–0.965	97.5648	–0.950	98.6956	–0.461	113.6136	–1.008	117.6324
–0.982	89.6288	–0.973	97.5681	–0.972	98.6986	–0.415	113.6168	–1.016	117.6353
–0.985	89.6320	–0.974	97.5713	–0.980	98.7015	–0.352	113.6200	–1.013	117.6383
–1.001	89.6352	–0.990	97.5745	–0.997	98.7045	–0.322	113.6232	–0.999	117.6412
–1.011	89.6384	–0.993	97.5777	–1.001	98.7075	–0.297	113.6264	–0.974	117.6442
–1.012	89.6415	–0.989	97.5808	–1.005	98.7108	–0.259	113.6296	–0.988	117.6471
–1.027	89.6447	–0.998	97.5840	–1.020	98.7141	–0.249	113.6329	–0.958	117.6501
–1.028	89.6479	–1.004	97.5872	–1.025	98.7174	–0.283	113.6360	–0.961	117.6530
–1.038	89.6511	–1.007	97.5904	–1.031	98.7207	–0.333	113.6393	–0.942	117.6559
–1.054	89.6543	–1.017	97.5936	–1.052	98.7240	–0.378	113.6424	–0.934	117.6589
–1.049	89.6574	–1.021	97.5968	–1.045	98.7273	–0.399	113.6456	–0.932	117.6618
–1.036	89.6606	–1.014	97.6000	–1.056	98.7307	–0.486	113.6488	–0.913	117.6647
–1.030	89.6638	–1.018	97.6032	–1.069	98.7340	–0.519	113.6520	–0.876	117.6677
–1.045	89.6670	–1.025	97.6064	–1.065	98.7373	–0.590	113.6552	–0.863	117.6706
–1.061	89.6701	–1.033	97.6096	–1.089	98.7406	–0.638	113.6584	–0.852	117.6736
–1.055	89.6733	–1.047	97.6128	–1.089	98.7439	–0.673	113.6616	–0.833	117.6765
–1.063	89.6765	–1.037	97.6160	–1.083	98.7472	–0.708	113.6648	–0.794	117.6795
–1.072	89.6797	–1.033	97.6192	–1.084	98.7505	–0.756	113.6681	–0.749	117.6824
–1.053	89.6828	–1.028	97.6224	–1.087	98.7538	–0.818	113.6712	–0.727	117.6854
–1.055	89.6860	–1.034	97.6255	–1.088	98.7571	–0.827	113.6744	–0.684	117.6883
–1.051	89.6892	–1.029	97.6287	–1.087	98.7604	–0.858	113.6776	–0.631	117.6912
–1.054	89.6924	–1.031	97.6319	–1.074	98.7637	–0.883	113.6808	–0.580	117.6942
–1.038	89.6955	–1.029	97.6351	–1.088	98.7670	–0.895	113.6840	–0.531	117.6971
–1.040	89.6987	–1.017	97.6383	–1.080	98.7703	–0.940	113.6872	–0.515	117.7001
–1.039	89.7019	–1.009	97.6415	–1.073	98.7737	–0.965	113.6904	–0.435	117.7030
–1.032	89.7051	–1.016	97.6447	–1.066	98.7770	–0.944	113.6936	–0.404	117.7059
–1.002	89.7083	–1.008	97.6479	–1.073	98.7803	–0.947	113.6968	–0.336	117.7089
–1.005	89.7114	–0.995	97.6511	–1.073	98.7835	–0.981	113.7000	–0.303	117.7118
–1.011	89.7146	–0.996	97.6543	–1.059	98.7869	–0.986	113.7032	–0.283	117.7147

Table continued on following pages

Table 2. CW Scl observations ΔB, ΔV, ΔR, and ΔI, variable minus comparison star (Epoch 2400000+), cont.

ΔI_c	HJD 2457000+	ΔI_c	HJD 2457000+	ΔI_c	HJD 2457000+	ΔI_c	HJD 2457000+	ΔI_c	HJD 2457000+
–0.988	66.5250	–0.715	67.5166	–1.002	68.7896	–0.880	88.7040	–0.992	89.6707
–0.978	66.5280	–0.715	67.5208	–0.995	68.7954	–0.885	88.7072	–1.006	89.6738
–0.964	66.5312	–0.720	67.5240	–0.992	68.8024	–0.895	88.7104	–1.011	89.6770
–0.952	66.5372	–0.695	67.5272	–0.976	68.8089	–0.938	88.7136	–1.022	89.6802
–0.959	66.5404	–0.728	67.5312	–0.970	68.8139	–0.923	88.7168	–1.008	89.6834
–0.965	66.5437	–0.710	67.5343	–0.924	68.8193	–0.927	88.7200	–1.004	89.6865
–0.965	66.5483	–0.728	67.5375	–0.984	68.8236	–0.946	88.7232	–1.016	89.6897
–0.926	66.5515	–0.968	67.6616	–0.957	68.8283	–0.963	88.7263	–1.009	89.6929
–0.919	66.5547	–0.957	67.6648	–0.953	68.8331	–0.954	88.7295	–0.977	89.6961
–0.904	66.5591	–0.948	67.6680	–0.949	68.8353	–0.965	88.7327	–0.977	89.6992
–0.930	66.5623	–0.951	67.6724	–1.000	88.5251	–0.976	88.7359	–0.981	89.7024
–0.928	66.5656	–0.942	67.6756	–0.972	88.5283	–0.980	88.7391	–0.971	89.7056
–0.880	66.5717	–0.934	67.6788	–1.003	88.5315	–0.977	88.7423	–0.975	89.7088
–0.891	66.5749	–0.919	67.6832	–0.976	88.5347	–0.984	88.7455	–0.962	89.7120
–0.870	66.5781	–0.915	67.6864	–1.008	88.5379	–0.972	88.7487	–0.963	89.7151
–0.815	66.5834	–0.922	67.6896	–0.991	88.5411	–1.013	88.7519	–0.951	89.7183
–0.807	66.5866	–0.891	67.6963	–1.004	88.5443	–0.981	88.7549	–0.953	89.7215
–0.803	66.5899	–0.872	67.6995	–0.989	88.5475	–0.775	89.5150	–0.959	89.7247
–0.786	66.5942	–0.865	67.7027	–0.981	88.5507	–0.757	89.5181	–0.955	89.7279
–0.766	66.5974	–0.824	67.7072	–0.982	88.5539	–0.719	89.5213	–0.932	89.7310
–0.762	66.6007	–0.797	67.7104	–0.992	88.5571	–0.683	89.5245	–0.915	89.7342
–0.728	66.6055	–0.769	67.7136	–0.984	88.5603	–0.635	89.5277	–0.896	89.7374
–0.729	66.6087	–0.656	67.7225	–0.980	88.5635	–0.593	89.5309	–0.874	89.7406
–0.710	66.6120	–0.630	67.7257	–0.957	88.5667	–0.541	89.5340	–0.878	89.7438
–0.690	66.6163	–0.578	67.7289	–0.940	88.5699	–0.500	89.5372	–0.859	89.7469
–0.712	66.6228	–0.493	67.7336	–0.959	88.5731	–0.457	89.5404	–0.841	89.7501
–0.696	66.6271	–0.463	67.7368	–0.938	88.5763	–0.387	89.5436	–0.848	89.7533
–0.743	66.6301	–0.404	67.7400	–0.925	88.5795	–0.347	89.5467	–0.807	89.7564
–0.725	66.6330	–0.323	67.7447	–0.926	88.5827	–0.301	89.5499	–0.791	89.7596
–0.752	66.6379	–0.271	67.7479	–0.926	88.5859	–0.271	89.5531	–0.787	89.7628
–0.759	66.6411	–0.254	67.7511	–0.884	88.5891	–0.272	89.5563	–0.773	89.7660
–0.800	66.6443	–0.271	67.7583	–0.882	88.5922	–0.258	89.5594	–0.749	89.7691
–0.817	66.6485	–0.299	67.7615	–0.859	88.5955	–0.289	89.5626	–0.740	89.7723
–0.825	66.6517	–0.324	67.7647	–0.835	88.5986	–0.325	89.5658	–0.742	89.7755
–0.844	66.6549	–0.391	67.7693	–0.814	88.6018	–0.348	89.5690	–0.687	89.7787
–0.854	66.6591	–0.432	67.7725	–0.794	88.6050	–0.418	89.5722	–0.716	89.7818
–0.864	66.6623	–0.507	67.7757	–0.762	88.6082	–0.472	89.5753	–0.717	89.7850
–0.872	66.6655	–0.669	67.7863	–0.733	88.6114	–0.533	89.5785	–0.730	89.7882
–0.882	66.6695	–0.702	67.7896	–0.691	88.6146	–0.560	89.5817	–0.722	89.7914
–0.907	66.6727	–0.747	67.7928	–0.663	88.6178	–0.616	89.5849	–0.729	89.7945
–0.872	66.6760	–0.810	67.7986	–0.615	88.6210	–0.656	89.5880	–0.727	97.5179
–0.910	66.6801	–0.833	67.8018	–0.570	88.6242	–0.699	89.5912	–0.739	97.5209
–0.936	66.6833	–0.823	67.8050	–0.506	88.6274	–0.729	89.5944	–0.762	97.5238
–0.931	66.6866	–0.883	67.8108	–0.470	88.6306	–0.782	89.5976	–0.759	97.5270
–0.969	66.6935	–0.911	67.8140	–0.409	88.6338	–0.811	89.6008	–0.785	97.5302
–0.960	66.6968	–0.916	67.8172	–0.365	88.6370	–0.825	89.6039	–0.785	97.5334
–0.963	66.7000	–0.936	67.8232	–0.318	88.6402	–0.854	89.6071	–0.808	97.5366
–0.978	66.7049	–0.933	67.8264	–0.273	88.6434	–0.869	89.6103	–0.826	97.5398
–0.983	66.7082	–0.933	67.8296	–0.243	88.6466	–0.878	89.6135	–0.854	97.5430
–0.956	66.7114	–0.952	67.8329	–0.274	88.6498	–0.912	89.6166	–0.857	97.5462
–0.975	66.7186	–0.963	67.8361	–0.256	88.6529	–0.901	89.6198	–0.855	97.5494
–0.989	66.7218	–0.967	67.8393	–0.305	88.6561	–0.916	89.6230	–0.876	97.5526
–0.988	66.7249	–0.988	67.8426	–0.325	88.6593	–0.946	89.6262	–0.901	97.5558
–0.983	66.7289	–0.966	67.8458	–0.381	88.6625	–0.931	89.6294	–0.913	97.5590
–0.987	66.7321	–0.991	67.8490	–0.447	88.6657	–0.958	89.6325	–0.920	97.5622
–0.988	66.7353	–0.986	67.8522	–0.481	88.6689	–0.941	89.6357	–0.918	97.5654
–0.969	66.7396	–0.996	67.8554	–0.536	88.6721	–0.986	89.6389	–0.940	97.5686
–0.972	66.7428	–1.010	67.8587	–0.598	88.6753	–0.971	89.6421	–0.945	97.5718
–0.963	66.7460	–1.000	67.8619	–0.632	88.6785	–0.990	89.6453	–0.948	97.5750
–0.987	66.7503	–0.999	67.8651	–0.689	88.6817	–0.980	89.6484	–0.965	97.5782
–0.966	66.7535	–1.001	67.8683	–0.702	88.6849	–0.987	89.6516	–0.947	97.5814
–0.966	66.7567	–1.008	68.7732	–0.748	88.6880	–1.000	89.6548	–0.965	97.5846
–0.953	66.7609	–0.992	68.7764	–0.772	88.6912	–0.993	89.6579	–0.979	97.5878
–0.934	66.7641	–1.006	68.7796	–0.814	88.6944	–0.988	89.6611	–0.974	97.5910
–0.734	67.5102	–0.998	68.7832	–0.834	88.6976	–1.013	89.6643	–0.976	97.5942
–0.724	67.5134	–1.010	68.7864	–0.841	88.7008	–0.996	89.6675	–0.988	97.5974

Table continued on following pages

Table 2. CW Scl observations ΔB, ΔV, ΔR, and ΔI, variable minus comparison star (Epoch 2400000+), cont.

ΔI_c	HJD 2457000+	ΔI_c	HJD 2457000+	ΔI_c	HJD 2457000+	ΔI_c	HJD 2457000+	ΔI_c	HJD 2457000+
–0.996	97.6005	–0.456	98.6575	–0.998	98.7941	–0.446	113.6494	–1.006	117.5975
–1.005	97.6037	–0.516	98.6604	–1.006	98.7974	–0.511	113.6526	–0.994	117.6004
–1.000	97.6069	–0.558	98.6634	–1.013	98.8007	–0.560	113.6558	–1.008	117.6034
–0.999	97.6101	–0.612	98.6664	–1.010	98.8040	–0.608	113.6590	–1.001	117.6063
–0.993	97.6133	–0.668	98.6693	–0.986	98.8073	–0.644	113.6622	–1.001	117.6093
–0.993	97.6165	–0.703	98.6723	–0.988	98.8106	–0.685	113.6654	–0.991	117.6122
–0.999	97.6197	–0.746	98.6753	–0.983	98.8139	–0.748	113.6686	–1.000	117.6152
–1.007	97.6229	–0.772	98.6782	–0.944	98.8173	–0.796	113.6718	–0.986	117.6181
–0.997	97.6261	–0.805	98.6812	–0.945	98.8205	–0.793	113.6750	–0.987	117.6211
–1.006	97.6293	–0.829	98.6842	–0.953	98.8239	–0.828	113.6782	–0.971	117.6240
–1.013	97.6325	–0.850	98.6871	–0.927	98.8272	–0.859	113.6814	–0.977	117.6270
–0.994	97.6357	–0.867	98.6901	–0.905	98.8305	–0.865	113.6845	–0.953	117.6299
–0.983	97.6389	–0.899	98.6931	–0.896	98.8338	–0.904	113.6877	–0.957	117.6329
–0.979	97.6421	–0.903	98.6960	–0.874	98.8371	–0.901	113.6909	–0.955	117.6358
–0.972	97.6452	–0.925	98.6990	–0.824	98.8404	–0.928	113.6941	–0.948	117.6387
–0.959	97.6484	–0.931	98.7020	–0.853	98.8437	–0.912	113.6973	–0.942	117.6417
–0.968	97.6516	–0.947	98.7050	–0.816	98.8470	–0.934	113.7005	–0.936	117.6446
–0.944	97.6548	–0.949	98.7080	–0.802	98.8503	–0.958	113.7037	–0.928	117.6476
–0.965	97.6580	–0.972	98.7113	–0.792	98.8536	–0.972	113.7068	–0.935	117.6505
–0.926	97.6612	–0.969	98.7147	–0.790	98.8569	–0.827	117.5267	–0.907	117.6535
–0.937	97.6676	–0.988	98.7180	–0.756	98.8602	–0.852	117.5297	–0.921	117.6564
–0.926	97.6708	–0.995	98.7213	–0.870	113.5757	–0.870	117.5326	–0.891	117.6593
–0.914	97.6740	–1.009	98.7246	–0.842	113.5789	–0.875	117.5356	–0.876	117.6623
–0.895	97.6772	–1.014	98.7279	–0.830	113.5821	–0.887	117.5385	–0.872	117.6652
–0.863	97.6804	–1.014	98.7312	–0.788	113.5886	–0.913	117.5415	–0.856	117.6682
–0.856	97.6836	–1.022	98.7346	–0.741	113.5918	–0.897	117.5444	–0.823	117.6711
–0.831	97.6868	–1.029	98.7378	–0.697	113.5950	–0.916	117.5474	–0.790	117.6740
–0.806	97.6900	–1.039	98.7412	–0.673	113.5982	–0.906	117.5503	–0.783	117.6770
–0.761	97.6932	–1.043	98.7445	–0.625	113.6014	–0.929	117.5533	–0.757	117.6799
–0.705	97.6964	–1.043	98.7478	–0.578	113.6046	–0.933	117.5562	–0.733	117.6829
–0.717	97.6996	–1.059	98.7511	–0.611	113.6078	–0.963	117.5591	–0.695	117.6858
–0.658	98.6146	–1.042	98.7544	–0.479	113.6110	–0.949	117.5621	–0.666	117.6888
–0.601	98.6185	–1.048	98.7577	–0.446	113.6142	–0.956	117.5650	–0.626	117.6917
–0.498	98.6240	–1.029	98.7610	–0.343	113.6174	–0.971	117.5680	–0.537	117.6946
–0.436	98.6278	–1.053	98.7643	–0.298	113.6206	–0.971	117.5709	–0.504	117.6976
–0.391	98.6310	–1.040	98.7676	–0.284	113.6238	–0.982	117.5739	–0.475	117.7005
–0.352	98.6342	–1.032	98.7709	–0.261	113.6270	–0.986	117.5768	–0.404	117.7035
–0.306	98.6397	–1.036	98.7742	–0.275	113.6302	–0.986	117.5798	–0.338	117.7064
–0.301	98.6427	–1.030	98.7775	–0.266	113.6334	–0.983	117.5827	–0.305	117.7093
–0.314	98.6456	–1.033	98.7808	–0.267	113.6366	–0.988	117.5857	–0.297	117.7123
–0.327	98.6486	–1.018	98.7841	–0.305	113.6398	–0.991	117.5886	–0.271	117.7152
–0.372	98.6516	–1.044	98.7874	–0.360	113.6430	–1.001	117.5916		
–0.405	98.6545	–1.020	98.7908	–0.418	113.6462	–0.997	117.5946		

Table 3. O–C residuals from NSVS 10083189 period study.

No.	*HJD 2400000+*	*Cycle*	*Linear Residual*	*Quadratic Residual*	*Weight*	*Reference*
1	51492.3901	–12322.5	0.0045	0.0082	0.2	NSVS (Wozniak et al. 2004)
2	51494.4278	–12318.0	–0.0018	0.0019	0.2	NSVS (Wozniak et al. 2004)
3	51494.4268	–12318.0	–0.0028	0.0009	0.2	NSVS (Wozniak et al. 2004)
4	51576.1855	–12138.0	–0.0044	–0.0018	0.2	NSVS (Wozniak et al. 2004)
5	51581.1890	–12127.0	0.0026	0.0051	0.2	NSVS (Wozniak et al. 2004)
6	51608.2037	–12067.5	–0.0090	–0.0069	0.2	NSVS (Wozniak et al. 2004)
7	51608.2026	–12067.5	–0.0100	–0.0079	0.2	NSVS (Wozniak et al. 2004)
8	55629.6950	–3214.0	0.0116	0.0030	1.0	Diethelm 2011
9	56282.8654	–1776.0	0.0074	0.0007	1.0	Diethelm 2013
10	57066.6187	–50.5	–0.0017	0.0001	1.0	Present Observations
11	57067.5233	–48.5	–0.0056	–0.0038	1.0	Present Observations
12	57067.7545	–48.0	–0.0015	0.0003	1.0	Present Observations
13	57088.6491	–2.0	–0.0013	0.0009	1.0	Present Observations
14	57089.5571	0.0	–0.0017	0.0004	1.0	Present Observations
15	57098.6416	20.0	–0.0016	0.0006	1.0	Present Observations
16	57113.6312	53.0	–0.0015	0.0010	1.0	Present Observations

Table 4. NSVS 1083189 light curve characteristics ΔB, ΔV, ΔR_c, and ΔI_c, variable minus comparison star.

Filter	*Phase*	*Magnitude Max. I*	*Phase*	*Magnitude Max. II*
	0.25		0.75	
ΔB		–1.165 ± 0.008		–1.137 ± 0.013
ΔV		–1.113 ± 0.014		–1.071 ± 0.017
ΔR_c		–1.058 ± 0.017		–1.037 ± 0.008
ΔI_c		–1.015 ± 0.023		–0.996 ± 0.010
Filter	*Phase*	*Magnitude Min. II*	*Phase*	*Magnitude Min. I*
	0.50		0.00	
ΔB		–0.926 ± 0.012		–0.307 ± 0.020
ΔV		–0.850 ± 0.019		–0.287 ± 0.014
ΔRc		–0.793 ± 0.018		–0.241 ± 0.092
ΔIc		–0.751 ± 0.014		–0.272 ± 0.019

Filter	*Min. I – Max. I*	*Max. I – Max. II*	*Min. I – Min. II*
ΔB	0.858 ± 0.028	–0.028 ± 0.021	0.619 ± 0.033
ΔV	0.826 ± 0.028	–0.042 ± 0.032	0.564 ± 0.033
ΔRc	0.817 ± 0.109	–0.021 ± 0.025	0.552 ± 0.110
ΔIc	0.743 ± 0.043	–0.019 ± 0.033	0.479 ± 0.034

Filter	*Max. II – Max. I*	*Min. II – Max. I*
ΔB	0.028 ± 0.021	0.239 ± 0.020
ΔV	0.042 ± 0.032	0.263 ± 0.034
ΔRc	0.021 ± 0.025	0.265 ± 0.035
ΔIc	0.019 ± 0.033	0.264 ± 0.038

Table 5. NSVS 1083189 synthetic light curve solution.

Parameters	*Values*
λ_B, λ_V, λ_R, λ_I (nm)	440, 550, 640, 790
$x_{bol1,2}$, $y_{bol1,2}$	0.642, 0. 828, 0.242, -0.167
$x_{1Ic,2Ic}$, $y_{1Ic,2Ic}$	0. 569, 0.668, 0. 271, 0.144
$x_{1Rc,2Rc}$, $y_{1Rc,2Rc}$	0.652, 0.754, 0. 278, 0.096
$x_{1V,2V}$, $y_{1V,2V}$	0.725, 0.799, 0. 266, 0.006
$x_{1B,2B}$, $y_{1B,2B}$	0. 815, 0.840, 0.206, -0.155
g_1 , g_2	0.32
A_1 , A_2	0.5
Inclination (°)	78.60 ± 0.04
T_1, T_2 (K)	6250, 4573 ± 2
Ω_1, Ω_2	3.031, 3.054 ± 0.002
q (m_2 / m_1)	0.584 ± 0.001
Fill-outs: $F_1 = F_2$	100%,99.3 ± 0.1%
$L_1 / (L_1 + L_2)_{Ic}$	0.8480 ± 0.0005
$L_1 / (L_1 + L_2)_{Rc}$	0.8732 ± 0.0006
$L_1 / (L_1 + L_2)_V$	0.9027 ± 0.0008
$L_1 / (L_1 + L_2))_B$	0.9385 ± 0.0014
JDo (days)	2457098.642242 ± 0.000054
Period (days)	0.4542195 ± 0.0000015
r_1, r_2 (pole)	0. 40135 ± 0.00076, 0.309 ± 0.002
r_1, r_2 (point)	0.555 ± 0.002, 0.405 ± 0.014
r_1, r_2 (back)	0.4250 ± 0.0009, 0.322 ± 0.003
r_1, r_2 (back)	0.4537 ± 0.008, 0.352 ± 0.004
Spot	
Co-latitude (˚)	58.3 ± 0.4
Longitude (˚)	76 ± 1
Spot Radius	14.7 ± 0.2
Temperature Factor	0.858 ± 0.004

Evidence for High Eccentricity and Apsidal Motion in the Detached Eclipsing Binary GSC 04052-01378

Riccardo Furgoni
Keyhole Observatory MPC K48, Via Fossamana 86, San Giorgio di Mantova (MN), Italy; riccardo.furgoni@gmail.com

Gary Billings
Monument Hill Observatory, P.O. Box 263, Rockyford, AB T0J 2R0, Canada; obs681@gmail.com

Received September 27, 2017; revised November 21, 2017; accepted December 4, 2017

Abstract We observed the recently discovered eccentric eclipsing binary GSC 04052-01378 in order to improve the light curve parameters and to find further evidence of its probable high eccentricity and of apsidal motion. Furthermore, we propose a basic stellar model that fits very well the observations of our dataset and where the eccentricity is found to be e = 0.538(6), which corresponds to an high value among this group of binaries.

1. Eccentric detached eclipsing binaries: some considerations about this type of system and serendipitous photometric discovery

Detached eclipsing binary systems (β Persei or "EA" type) are one of the largest groups in any catalog of variable stars. Both in the *General Catalogue of Variable Stars* (GCVS; Samus *et al.* 2017), and in the more recently created International Variable Star Index (VSX; Watson *et al.* 2014), there are thousands of members and at least a few hundred more that are strongly suspected to be of this type. This is not surprising: stellar multiplicity (systems with two or more components) is common, with the frequency declining with the number of components present (Tokovinin 2014).

Whether single star systems are more common than multiple systems is still unresolved. Mathieu (1994, p. 517) in his careful analysis of the stellar multiplicity in the pre-main sequence stars, said that the formation of binary stars is the primary branch of the star-forming processes. More recently Lada (2006) observed on the contrary that "most stellar systems formed in the Galaxy are likely single and not binary, as has been often asserted. Indeed, in the current epoch two-thirds of all main-sequence stellar systems in the Galactic disk are composed of single stars."

That this question is unresolved is probably associated with the lack of a definitive theory for the formation of multiple systems. According to Tohline (2002), one of the most promising theories explaining formation of multiple systems is the fragmentation of the pre-stellar core in the early stages of its collapse, controlled by factors such as pressure, rotation, turbulence, and magnetic fields (Commerçon *et al.* 2010). Alternately, Bonnel (1994) presents the option of early fragmentation of a circumstellar disk, especially when the mass of the disk itself is higher than that of the protostar in the early stages of its formation.

In a recent review of the literature about this subject, Duchêne and Kraus (2013) concluded that the degree of multiplicity is directly related to the mass of the primary component, according to the results shown in Table 1.

Table 1. Multiplicity properties for Population I main sequence stars and field brown dwarfs (Duchêne and Kraus 2013).

Category	*Mass Range ($M_\odot$)*	*Multiple System / Companion Frequency*
VLM/BD	$\lesssim 0.1$	MF = 22 % CF = 22 %
M	0.1–0.5	MF = 26 ± 3% CF = 33 ± 5%
FGK	0.7–1.3	MF = 44 ± 2% CF = 62 ± 3%
A	1.5–5	MF ≥ 50% CF = 100 ± 10%
Early B	8–16	MF ≥ 60% CF = 100 ± 20%
O	$\gtrsim 16$	MF ≥ 80% CF = 130 ± 20%

Note: MF is the frequency of multiple systems and CF the companion frequency, whereas it must be noted that this last can exceed 100%.

All these data justify the large number of detached eclipsing systems in variable star catalogs, and lead us to examine the nature of the orbits of those systems, in particular systems showing a marked orbital eccentricity.

Only a small fraction of known detached eclipsing binary systems have a detectable eccentricity, while for most the eccentricity is near zero (essentially circular orbits). Amongst short period systems (more easily discovered and studied) it is most likely that the orbit has already been circularized by tidal interactions.

Since tidal interactions will circularize orbits that were initially more eccentric, we should expect to see greater eccentricity, and more frequent occurrence of eccentric systems, amongst younger stellar systems, and systems of "earlier" spectral type (see on this subject Mazeh 2008).

To determine the orbital radii (and the related quantity, orbital period) corresponding to circularized orbits is not straightforward. But empirically, orbits are usually circularized in systems with periods shorter than ~7.1 days for pre-main sequence stars with an age between ~1 and ~10 Myr, up to

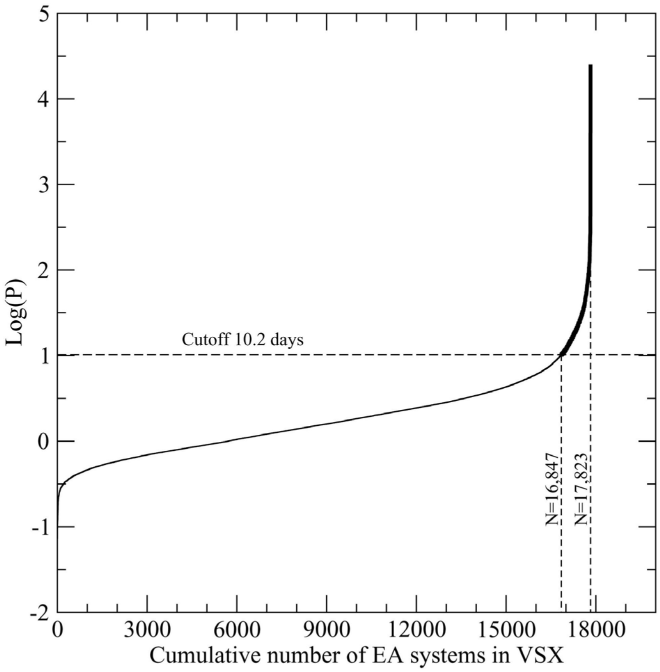

Figure 1. The graph shows the cumulative number of EA systems in VSX with specified period (excluding systems with unknown or uncertain period) in relation to the logarithm of the orbital period. The horizontal dashed line represents 10.2 days, the value of the circularization period used for this analysis.

~15.6 days for the stars of the Galactic Halo with estimated age of ~10 Gyr (Meibom and Mathieu 2005). For main sequence stars (in M35), the same authors showed that orbits with periods shorter than ~10.2 days are circularized. We apply this latter period as a cutoff to the entire population of detached binaries found in VSX to get an estimate the population of the number of eccentric (non-circularized) systems. The result is shown in Figure 1.

Of the 17,823 EA systems listed in VSX with a defined orbital period, only 976 (5.47%) exceed our circularization cutoff period of 10.2 days. No correction has been attempted for selection effects (longer period systems are less likely to be discovered). Thus, we expect eccentric systems to be rare.

2. GSC 04052-01378

This binary system was discovered by R. Furgoni and S. Otero and then added to VSX on April 4, 2014. Subsequently, complete information about the system has appeared in Furgoni (2014). The variable was classified as a β Persei (EA) after evaluation of the phase plot. The basic data of this system as well as the stars used for comparison in the paper published by Furgoni (2014) are presented in Table 2.

The system was immediately identified as eccentric, and with probable apsidal motion. The eccentricity was recognized by the large difference in duration between primary and secondary eclipses while the apsidal motion was suggested by a better matching of the secondary eclipse observations using a slightly shorter period than for primary eclipses. Both conclusions can be assessed by examining the data originally published in Furgoni (2014).

The interesting difference in the primary and secondary eclipse durations, where the secondary is more than three times longer than the primary, led to the planning of a new observational campaign aimed at a better characterization of the light curve for subsequent modeling.

3. Instrumentation used and observation details

The observations were made in two observatories at a great distance in longitude corresponding to a time difference of 8 hours. This was advantageous to observing more eclipses, in light of the long period and the period being a non-integer number of days.

At the observatory managed by R. Furgoni, two different telescopes were used. The main instrument was a TS Optics APO906 Carbon apochromatic refractor with 90 mm aperture and f/6.6 focal ratio, and in the last observational sessions, a Celestron C8 Starbright Schmidt-Cassegrain with aperture of 203 mm and Baader Planetarium Alan Gee II focal reducer, yielding f/6. With both telescopes photometry was done with a CCD SBIG ST8300m equipped with a Kodak KAF8300m monochromatic sensor. The Johnson V passband photometry was performed with an Astrodon Photometrics Johnson-V 50 mm round filter.

At the observatory managed by G. Billings, observations were made using a Celestron C-14 (14" f/11 Schmidt-Cassegrain) telescope and an SBIG STL-6303E CCD camera and a Bessell-prescription Johnson V filter. Image processing was conventional dark subtraction and flat fielding, performed using Starlink software (Currie *et al.* 2014). Photometry was performed using the Starlink operation "photom" with measurement apertures that varied night-to-night depending on the seeing-limited PSF.

The log of the authors' observations used in the graphs and analysis is presented in Table 3.

Table 2. Position, identification, and light elements of GSC 04052-01378 as presented in Furgoni (2014).

Position (UCAC4)[1]	R.A. (J2000) = $02^h\ 53^m\ 08.34^s$, Dec. (J2000) = +62° 06' 10.5"
Cross Identification	UCAC4 761-021922; NSVS 1888562; 1SWASP J025308.36+620610.7
Variability Type	EA
Magnitude Range	Max. = 11.76 V, Min. = 12.08: V
Spectral type	B2
Period	18.3024(1) d
Epoch	2451403.83(1) HJD
Ensemble Comparison Stars	UCAC4 761-021906 (APASS 12.498 V); UCAC 4 761-021905 (APASS 12.566 V)
Check Star	UCAC4 761-022036

1. *Zacharias et al. 2012.*

Table 3. Log of observations used in the analysis and that were fit by modeling.

Observer	*RJD*[1]	*Start Time (UT)*	*End Time (UT)*	*Telescope*	*Notes*
RF	6630	03/12/2013 17:28	03/12/2013 23:53	Celestron 8	Non-eclipse
RF	6631	04/12/2013 17:17	04/12/2013 22:43	Celestron 8	Non-eclipse
RF	6632	05/12/2013 17:03	05/12/2013 21:39	Celestron 8	Non-eclipse
RF	6706	17/02/2014 17:43	17/02/2014 21:45	Celestron 8	Non-eclipse
RF	6958	27/10/2014 19:42	27/10/2014 23:28	TS 906 APO	(s) ingress
RF	6959	28/10/2014 17:15	28/10/2014 22:11	TS 906 APO	(s) egress
RF	7022	30/12/2014 22:09	31/12/2014 00:50	TS 906 APO	(p) ingress
RF	7114	01/04/2015 19:13	01/04/2015 21:25	TS 906 APO	(p) egress
GB	7699	07/11/2016 03:36	07/11/2016 13:59	Celestron 14	(p) ingress and egress
GB	7702	10/11/2016 05:38	10/11/2016 06:17	Celestron 14	Non-eclipse
GB	7725	03/12/2016 07:05	03/12/2016 07:31	Celestron 14	Non-eclipse
GB	7726	04/12/2016 05:57	04/12/2016 09:02	Celestron 14	(s) ingress
GB	7745	23/12/2016 01:45	23/12/2016 12:48	Celestron 14	(s) egress
GB	7781	28/01/2017 06:25	28/01/2017 13:56	Celestron 14	(s) ingress
GB	7782	29/01/2017 04:29	29/01/2017 08:00	Celestron 14	(s) egress

1. Reduced Julian date, viz., JD – 2450000.

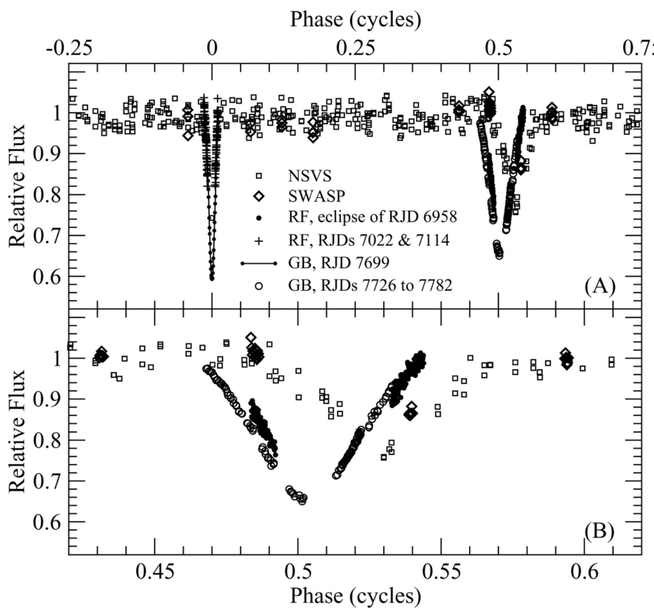

Figure 2. The upper panel (A) shows the full cycle phased light curve using elements from Furgoni (2014). The NSVS data, which span the whole cycle, are relatively noisy but show no out-of-eclipse variation. The lower panel (B) is an enlargement of the secondary eclipse. The different datasets have minima at different phases. Each data source is clustered around a different epoch, so each is showing the secondary eclipse at a different point in the rotation of the apse. The difference between the NSVS data and the observations by GB of RJD 7726 - 7782 also suggests a different eclipse depth, but this is not certain as the two datasets are not transformed to a common photometric system.

For this star we made use of observations obtained by the Northern Sky Variability Survey (NSVS) (Wozniak *et al.* 2004) and by the Wide Angle Search for Planets (SuperWASP) (Butters *et al.* 2010), in addition to those made by the authors at their private observatories. The authors' data are untransformed V-filtered differential aperture photometry. The authors' data are attributed using the authors' intials (RF or GB), and the time series are referred to using reduced Julian data (RJD), that is, the last four digits of the Julian date, 7699, for example, for the time series from Julian date 2457699.

RF's differential photometry was performed using ensemble photometry as described in Table 2 and Furgoni (2014). GB used single comparison and check stars (GSC 4052-1048 and 4052-0634) selected for having similar color to the target, as determined from the AAVSO Photometric All-Sky Survey (APASS DR9; Henden *et al.* 2015).

These datasets were not inter-calibrated or transformed to a standard system, except for zeropoint shifts determined by graphical comparison. Only one, constant, shift was used for each data source. Thus, inter-night zero-point offsets from each observer were not removed. Visual inspection of the light curves (at larger scale) suggests such offsets are occasionally present at the level of as much as a few percent. This level of uncertainty inevitably limits the precision and accuracy of the modeling that follows.

Finally, each dataset was converted from magnitude to flux, so the light curves could be displayed along with the modeling results in the program BINARYMAKER3 (Bradstreet and Steelman 2004).

The data used here have been deposited in the AAVSO International Database (Kafka 2017; observer codes FRIC and BGW, and star AUID 000-BLH-415).

4. Analysis and modeling

Figure 2(A) is the phased light curve for this star. It shows the NSVS and SWASP data used in Furgoni's earlier paper, as well as new time-series concentrated on the minima, taken by the present authors. All the data in Figure 2 are "phased" using elements that give a best fit to the times of all primary eclipses (period 18.3024 d). These data confirm the dramatically different eclipse widths noted by Furgoni (2014), and show that the narrow eclipse is the primary (deepest) eclipse.

Figure 2(B). An enlargement of the data around the secondary eclipse. The different datasets are clustered in time around different dates. The NSVS data ranges from RJD 1370 to 1609 (midpoint RJD 1490), and SWASP data from 3196 to 3226 (midpoint RJD 3212). Furgoni (2014) determined a time of (secondary) minimum from these data, with the NSVS data dominating the result. RF's data from around RJD 6958 (about

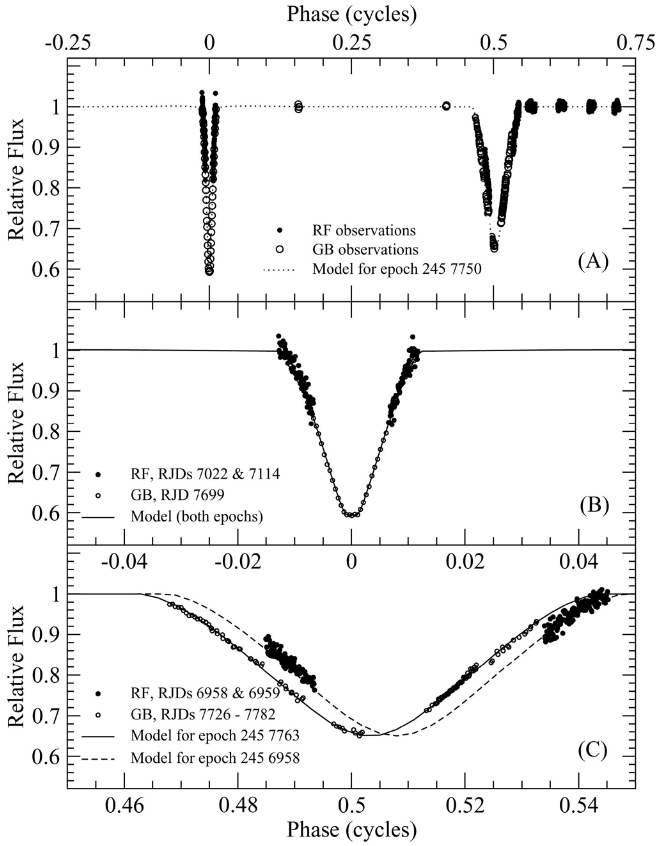

Figure 3: Data used in fitting a model to the observations, and the resulting modeled light curve. The upper panel (A) shows the full cycle. Several sets of observations from out-of-eclipse are shown; these were used to establish the relative zeropoints between the observers, and to set the level for flux=1.0. The middle panel (B) is an enlargement of the primary eclipse. The elements used to phase all three panels were chosen to perfectly phase the primary eclipse in the GB and RF datasets (from two epochs, about two years apart). The lower panel (C) is an enlargement of the secondary eclipse. The horizontal scale, but not its range, is the same as for the middle panel, to demonstrate the difference in eclipse widths. The GB and RF datasets are each from a short range of dates about 2 years apart, and show a distinctly different phase for the eclipse. A second model (dashed line) was created so both datasets could be fit; the only difference between the models is longitude of perihelion, viz., rotation of the apse.

15 years later than the NSVS observations) come at an earlier phase, and GB's data from around 7763 (about 2 years later still) comes even earlier. Thus, the secondary eclipse is consistently shifting to be closer in time to the preceding primary eclipse, indicating apsidal rotation.

The data during the secondary eclipse also suggest that the eclipse depth is changing (see Guilbault *et al.* 2001 for an example of another system showing changing eclipse depths). However, this is not entirely proven because the datasets are not inter-calibrated.

In the following, we describe the steps used to "model" the light curve. This type of model is not merely "curve fitting." Rather, it is the development of a set of numerical values for physical properties of this star system, such as the separation of the stars, their relative sizes, orbital eccentricity, and so on (see, for example, Wilson 1994b). Using these quantities, appropriate software generates the predicted light-curve for such a star system, in this case the program BINARYMAKER3. The numerical "parameters" are manually adjusted to achieve a good fit of the predicted light curve to the observations.

Figure 3 shows the data used as the goal to be fit by the model, as well as the full cycle light curve predicted by the model. It consists of the data listed in Table 3, during primary and secondary eclipses, as well as some nights of out-of-eclipse observations that were used to compute the zeropoint shift between the observers, and establish flux = 1 for modeling.

Figure 3(A) shows all the data that were fit, and the final model.

Figure 3(B) is an enlargement around the primary eclipse. It shows that we have just one observing run through the primary eclipse (GB's data of RJD 7699). It is complemented by a pair of nights during ingress and egress by RF (7022 and 7114). A time of minimum was determined for the night of RJD 7699 (HJD 2457699.8739(2)) using the Kwee and van Woerden (1956) algorithm as implemented by the program AVE (Barberà 1996). A "synthetic" time of minimum was determined from RF's ingress and egress observations of RJDs 7022 and 7114 using "the digital tracing paper method." In this method, all the data are first "moved" to a single cycle by adding an integral number of periods to the time of each observation. The data are then plotted against the time away from a trial minimum, and then over-plotted with the same data time-reversed around the trial minimum. The trial time of minimum that gives the best visual match between the forward and reversed data is taken as the time of the eclipse—in this case, 2457059.269(2). The process is iterated if the resulting time of minimum implies a different period than was used to first move the observations to a single common cycle.

These two times of primary minima were used to determine the elements used to phase the data shown in Figure 3 (epoch 2457699.8739, period 18.3030 d). These elements perfectly "phase" the data in the primary eclipse (Figure 3(B)), but not the secondary eclipses (Figure 3(C)). The secondary eclipse data are grouped around two epochs. RF's data from RJDs 6958 and 6959 are just one night apart (epoch 2456958). GB's data from RJDs 7726–7782 span 56 days (epoch 2457763), centred 805 days after RF's data. These two epochs show a different phase for the secondary eclipse, and we fit them with two different models, differing only in the longitude of periastron.

From these data (plotted at larger scale) we observed that the primary eclipse is flat-bottomed, with duration 0.0022 of the cycle (0.0403 d), and flux 0.595 during the primary eclipse, and 0.655 during the secondary (the out-of-eclipse brightness defines flux of 1.0).

Times of minima were also estimated for two secondary eclipses corresponding to the aforementioned epochs RJD 6958 and 7763. Once again, "synthetic" minima were analysed using the digital tracing paper method, with the results listed in Table 4. The O–C (observed minus computed) values in Table 4 are the difference between observed eclipse times and the times predicted by a mean ephemeris with epoch 2457699.8739, period 18.3017, and a secondary eclipse phase of 0.5035. The deviations of the primary and eclipse times from a single linear ephemeris is shown in the O–C diagram of Figure 4.

To generate a modeled light curve, we must supply the modeling program with parameters that describe the two

Table 4. Times of minima for primary and secondary eclipses.

Time of Minimum (RJD)	*Cycle*	*Notes*	*O–C (days)*
1403.83(1)	–344	(p), fit to NSVS and SuperWASP data by Furgoni (2014)	0.26(1)
7059.269(2)	–35	(p), fit to RF observations, this paper	–0.045(2)
7699.8739(2)	0	(p), GB observations, this paper	0
1486.75(1)	–340	(s), fit to NSVS and SuperWASP data by Furgoni (2014)	0.24(1)
6958.76(5)	–41	(s), fit to RF observations, this paper	0.041(5)
7763.993(5)	3	(s), fit to GB observations, this paper	0.001(5)

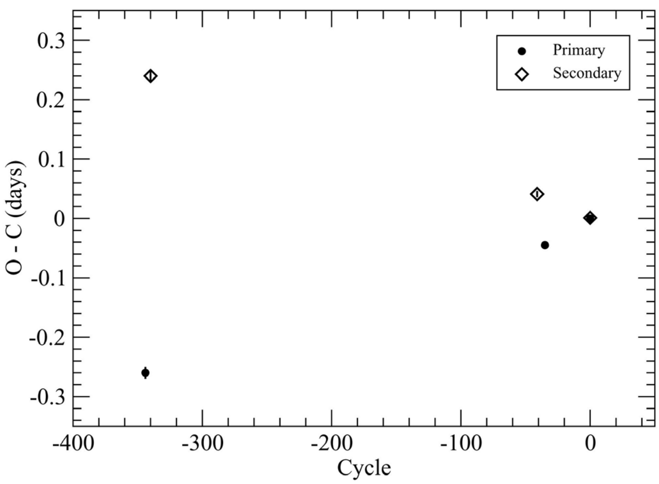

Figure 4. O–C ("observed minus calculated") diagram showing the observed eclipse times of Table 4 relative to time calculated using mean (of primary and secondary) elements (epoch 2457699.873, period 18.3017), and a secondary eclipse phase of 0.5035.

stars and their orbits. We start with initial estimates of these parameters and adjust them to improve the model fit.

4.1. Initializing parameters: temperature

Effective temperature (T_{eff}) is a key parameter describing a star, but our modeling is based on only single color data, so we cannot tune stellar temperatures based on the model fit. In other words, the model is independent of stellar temperatures, and assumes both stars have the same T_{eff}. We use T_{eff} = 22000, corresponding to the spectral type B2 and luminosity class V (Schmidt-Kaler 1982, p. 456). The spectral class used was taken from the *Catalogue of Stellar Spectral Classifications* (Skiff 2009–2016) compiled after a systematic review of the literature. In particular this spectral classification was originally provided by Voroshilov (Voroshilov *et al.* 1985). In any case, the spectral type considered will not affect our determination of the key orbital parameters of eccentricity and changing longitude of periastron.

4.2. Initializing parameters: geometric factors

Inspection of the light curve reveals some general properties of the system, as follows. During primary eclipse, a smaller star must be entirely behind, or transiting the face of a larger star (to give the flat-bottomed (total) eclipse). Inclination must be near 90° (to give the total primary eclipse), but different from 90° so as to produce the round-bottomed (partial) secondary eclipse. We must be observing an eccentric system with our line-of-

Table 5. Resulting model parameters for GSC 04052-01378.

Mass ratio	Not determined[1]
Radius of star 1[2,3,7]	0.0643(3)[7]
Radius of star 2[3,7]	0.0788(4)[7]
Temperature of star 1	22000 K[4]
Temperature of star 2	22000 K[4]
Gravity brightening exponent of star 1	1.0[5]
Gravity brightening exponent of star 2	1.0[5]
Limb darkening coefficient for star 1	0.255[5]
Limb darkening coefficient for star 2	0.255[5]
Reflection coefficient for star 1	1.0[5]
Reflection coefficient for star 2	1.0[5]
Third light	0.0[6]
Inclination	88.77(5)°[7]
Longitude of periastron for epoch 245 7763	89.54(4)°[7]
Longitude of periastron for epoch 245 6958	88.82(4)°[7]
Eccentricity	0.538(6)[7]

1. *Modeling results were insensitive to large variations in mass ratio. A value of 1.0 was used in modeling. Wilson (1994a, p. 930) states "for a detached binary…a light curve ordinarily carries insufficient information to fix the mass ratio reliably."*
2. *Star 1 is eclipsed during the primary eclipse.*
3. *The radii are r_{back}: "the radius of the star directed away from the other star, along the axis containing their mass centers," expressed as a fraction of the semimajor axis of the relative orbit of the two stars. See the BINARYMAKER3 documentation.*
4. *Temperatures are fixed, to correspond to the spectral type B2.*
5. *Values recommended by BINARYMAKER3 documentation, based on T_{eff}*
6. *Assumed.*
7. *Adjusted to achieve model fit.*

sight nearly along its semi-major axis (longitude of periastron near 90°), so that the secondary eclipse occurs at near phase 0.50, and is of different duration than the primary. None of the data suggest brightness variations outside of the eclipses, so we expect a detached system with nearly spherical stars. With these qualitative guides as a starting point, the relative radii of the two stars, system eccentricity, and longitude of perihelion were determined by trial and error. The resulting parameters are listed in Table 5.

5. Results

Figure 3(A) shows the resulting model fit to the whole cycle, and 3(B) shows an enlargement at primary minimum. The modeled light curve is flat-bottomed in the primary eclipse, that is, star 1 passes entirely behind star 2 during this eclipse. Figure 3(C) shows an enlargement around the secondary eclipse (at the same horizontal scale as Figure 3(B)). The solid line is the fit to epoch 7763; the dashed line is a fit to epoch 6958. Only the longitude of periastron was changed to accomplish

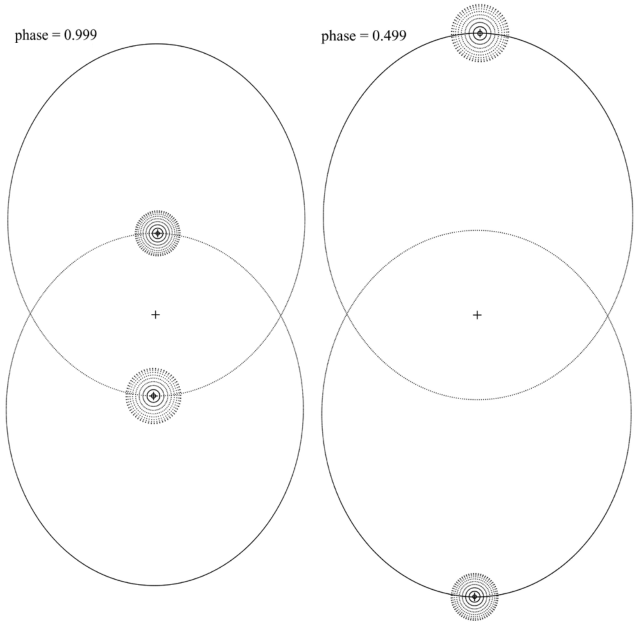

Figure 5. The binary system as viewed from above the plane of orbits, i.e. perpendicular to the line-of-sight from earth. Earth is towards the bottom of the page, in the plane of the page. The ellipses are the eccentric (non-circular) orbits of the stars. In the left image, the system is at primary eclipse, and the two stars are at their nearest approach to each other. In the right-hand image, the stars are at their maximum separation, and at secondary eclipse. When the stars are at maximum separation, i.e. maximum distance from the foci of their orbits, they move much more slowly—this is the cause of the greater duration of the secondary eclipse.

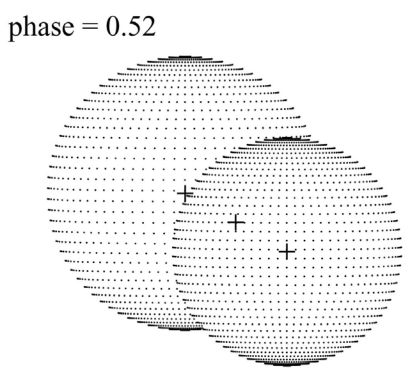

Figure 6. The binary system as viewed along the line-of-sight from earth, as the stars leave secondary eclipse. The smaller star is passing (from left to right) in front of the larger star, but the eclipse is partial (the smaller star does not cross directly in front of the larger star). In the primary eclipse (not shown), only the larger star is visible—the smaller star is hidden behind it. This is possible because the inclination is not exactly 90° and the orbit is eccentric (the stars are closer together at the time of primary eclipse).

this second fit from the first one, consistent with rotation of the line of apses.

The longitude of periastron changes 0.72(6)° between epochs 6958 and 7763 (Table 5); that is, in 44 cycles of the binary orbit. The rate of change is therefore $1.6(1) \times 10^{-2}$ °/orbit, $8.9(7) \times 10^{-4}$ °/day or $1.1(1) \times 10^{3}$ years/apsidal rotation. (See, for example, Martynov 1973.) This determination should be revisited once data over a longer time span are available—the observations used in this analysis span 17 years—just 1.5% of one rotation of the apse!

For planning future observations, the following elements are recommended. Note: the durations of the eclipses are approximately 10 hours and 31 hours, respectively.

$$\text{Min I: HJDmin} = 245\ 7699.8739 + 18.3030 \times E$$

$$\text{Min II: HJDmin} = 245\ 7709.086 + 18.3009 \times E$$

In Figures 5 and 6 we propose two different views of this high-eccentricity system: from above the plane of obits, perpendicular to the line-of-sight from Earth (Figure 5) and along the line-of-sight from Earth, as the stars leave secondary eclipse (Figure 6).

6. Conclusions

We only varied radii, inclination, eccentricity, and longitude of perihelion to make the model fit. The T^{eff} used was adopted based on spectral type—it does not affect key results such as eccentricity, longitude of periastron, and apsidal motion. The gravity brightening exponent and limb-darkening coefficients were not varied from the values recommended for the spectral type of the star (see the BINARYMAKER3 documentation). Because we have no radial velocity data, and no out-of-eclipse brightness variation, we cannot derive stellar masses, nor the mass ratio, nor the absolute radii or separation of the two stars.

The resulting model parameters are listed in Table 5. BINARYMAKER3 is a forward-modeling program only: it does not adjust the parameters automatically, and provides no estimates of the uncertainty or standard error of the parameters. Nevertheless, in the process of manually performing trial-and-error fits, a one can observe how much of a change in a parameter makes a noticeable difference in the quality of fit, as assessed by visual inspection of residuals, and the computed sum of squared residuals between the observed light curve points and the fitted model. Once the parameters were determined, as reported in Table 5, perturbations were applied to one parameter at a time. A perturbation large enough to make a noticeable deterioration in the quality of fit was taken to be a 2-sigma error. The standard errors reported in Table 5 are half of those values. This process is, of course, subjective, and takes no account of the well-known correlation (non-independence) of the parameters of such models (Kallrath and Milone 2009, p. 174). It is likely that these standard errors significantly underestimate the difference between these parameters and those that might be derived from higher-quality multi-color photometry and radial velocity observations.

This star system's eccentricity of 0.538(6) identifies it as a high-eccentricity system. We have observed apsidal motion, and plan to observe more minima to permit a more confident analysis of the apsidal rotation rate. The system may also be showing a varying depth of secondary eclipse due to the apsidal rotation—this could be confirmed by monitoring with more precise (transformed) photometry. Finally, radial-velocity observations would permit determination of masses and absolute radii, thereby confirming and refining the spectral type.

7. Acknowledgements

This work has made use of the VizieR catalogue access tool, CDS, Strasbourg, France, and the International Variable Star Index (VSX) operated by the AAVSO, Cambridge, Massachusetts.

This work has made use of NSVS data obtained from the Sky Database for Objects in Time-Domain operated by the Los Alamos National Laboratory, and data from the DR1 of the WASP data (Butters *et al.* 2010) as provided by the WASP consortium, and the computing and storage facilities at the CERIT Scientific Cloud, reg. no. CZ.1.05/3.2.00/08.0144 which is operated by Masaryk University, Czech Republic.

References

Barberà, R. 1996. "Introducing AVE", translated to English by J. Iparraguirre (http://astrogea.org/soft/ave/aveint.htm).

Bonnel, I. A. 1994, *Mon. Not. Roy. Astron. Soc.*, **269**, 837.

Bradstreet, D. H., and Steelman, D. P. 2004, BINARYBAKER3, Contact Software (http://www.binarymaker.com).

Butters, O. W., *et al.* 2010, *Astron. Astrophys.*, **520**, L10.

Commerçon, B., Hennebelle, P., Audit, E., Chabrier, G., and Teyssier, R. 2010, *Astron. Astrophys.*, **510**, L3.

Currie, M. J., Berry, D. S., Jenness, T., Gibb, A. G., Bell, G. S., and Draper, P. W. 2014, in *Astronomical Data Analysis Software and Systems XXIII*, eds. N. Manset, P. Forshay, ASP Conf. Ser. 485, Astronomical Society of the Pacific, San Francisco, 391.

Duchêne, G., and Kraus, A. 2013, *Ann. Rev. Astron. Astrophys.*, **51**, 269.

Furgoni, R. 2014, *J. Amer. Assoc. Var. Star Obs.*, **42**, 364.

Guilbault, P. R., Lloyd, C., and Paschke, A. 2001, *Inf. Bull. Var. Stars*, No. 5090, 1.

Henden, A. A., *et al.* 2015, AAVSO Photometric All-Sky Survey, data release 9 (http://www.aavso.org/apass).

Kafka, S. 2017, variable star observations from the AAVSO International Database (https://www.aavso.org/aavso-international-database).

Kallrath, J., and Milone, E.F. 2009, *Eclipsing Binary Stars: Modeling and Analysis*, 2nd ed., Springer, New York.

Kwee, K. K., and van Woerden, H. 1956, *Bull. Astron. Inst. Netherlands*, **12**, 327.

Lada, C. J. 2006, *Astrophys. J.*, **640**, L63.

Mathieu, R. D. 1994, *Ann. Rev. Astron. Astrophys.*, **32**, 465.

Mazeh, T. 2008, in EAS Publication Series 29, EDP Sciences, Paris, 1.

Meibom, S., and Mathieu, R. D. 2005, *Astrophys. J.*, **620**, 970.

Martynov, D. Ya. 1973, in *Eclipsing Variable Stars*, ed. V. P. Tsesevich, Wiley, New York, Chapter 9.

Samus, N. N. Kazarovets, E. V., Durlevich, O. V., Kireeva, N. N., and Pastukhova, E. N. 2017, *Astron. Rep.*, **61**, 80.

Schmidt-Kaler, Th. 1982, in *Landolt-Börnstein: Numerical Data and Functional Relationships in Science and Technology*, ed. K. Schaifers, H. H. Voight. Springer-Verlag, Berlin, VI/2b.

Skiff, B. A. 2009-2016, General Catalogue of Stellar Spectral Classifications, CDS/ADC Collection of Electronic Catalogues, 1, 2023 (2014), Lowell Observatory, Flagstaff, AZ (http://cdsarc.u-strasbg.fr/viz-bin/Cat?B/mk).

Tohline, J. E. 2002, *Ann. Rev. Astron. Astrophys.*, **40**, 349.

Tokovinin, A. 2014, *Astron. J.*, **147**, 87.

Voroshilov, V. I., Guseva N.G., Kalandadze N. B., Kolesnik L. N., Kuznetsov V. I., Metreveli M. D., and Shapovalov A. N. 1985, *Catalogue of BV Magnitudes and Spectral Classes for 6000 Stars* (http://cdsarc.u-strasbg.fr/viz-bin/Cat?III/230), Ukrainian Acad. Nauk, 1.

Watson, C., Henden, A. A., and Price, C. A. 2014, AAVSO International Variable Star Index VSX (Watson+, 2006-2014; http://www.aavso.org/vsx).

Wilson, R. E. 1994a, *Publ. Astron. Soc. Pacific*, **106**, 921.

Wilson, R. E. 1994b, *I.A.P.P.P. Commun.*, **55**, 1.

Wozniak, P. R. *et al.* 2004, *Astron. J.*, **127**, 2436.

Zacharias, N., Finch, C., Girard, T., Henden, A., Bartlett, J., Monet, D., and Zacharias, M. 2012, The Fourth US Naval Observatory CCD Astrograph Catalog (UCAC4; http://arxiv.org/abs/1212.6182).

Preliminary Modeling of the Eclipsing Binary Star GSC 05765-01271

Sara Marullo
Astronomical Observatory, DSFTA - University of Siena (K54), via Roma 56, Siena, 53100, Italy; sara.marullo@student.unisi.it

Alessandro Marchini
Astronomical Observatory, DSFTA - University of Siena (K54), via Roma 56, Siena, 53100, Italy; alessandro.marchini@unisi.it

Lorenzo Franco
Balzaretto Observatory (A81), Rome, Italy

Riccardo Papini
Wild Boar Remote Observatory (K49), via Potente 52, San Casciano in val di Pesa, Florence, 50026, Italy

Fabio Salvaggio
Wild Boar Remote Observatory (K49), via Potente 52, San Casciano in val di Pesa, Florence, 50026, Italy

Received October 31, 2017; revised December 9, 2017; accepted December 11, 2017

Abstract The authors discovered the eclipsing binary star system GSC 05765-01271 on August 19, 2015; here a preliminary model is presented. Lacking spectroscopic radial velocity data, period-based empirical relations have been used in order to constrain physical parameters as masses and radii. The effective temperature has been evaluated using color index (V–R) and spectral type estimated from a composite spectrum. These parameters were used as input to obtain a preliminary model of this binary system with BINARY MAKER 3 and PHOEBE software.

1. Introduction

Photometric observations to determine synodic rotational period of (9801) 1997 FX3 asteroid (Marchini *et al.* 2016) led us to discover the binary star system GSC 05765-01271 (Marullo *et al.* 2015). The discovery was made by Sara Marullo, an undergraduate student in Physics and Advanced Technologies at the DSFTA Department (Siena, Italy), and we thought it would be stimulating to go over the analysis of this system, aware of the important role played by eclipsing binary star systems in the knowledge of the universe. Eclipsing binaries are direct indicators of distance between galaxies; moreover, the analysis of the spatial distribution of these systems in an external galaxy gives an estimate of the size and the structure of the galaxy itself (Southworth 2012). Low mass eclipsing systems are an important subject because the vast majority of known extrasolar planets are hosted by low mass systems (Lopez-Morales 2007). Moreover, if radial velocities are known, it is possible to univocally determine masses and radii of eclipsing binaries.

2. Methods

2.1. Instrumentation

New filtered photometric data were acquired on October 11, 2015, using a 300-mm Maksutov-Cassegrain telescope equipped with a SBIG STL-6303E CCD camera and Custom Scientific Johnson-Cousins V and R filters at the Astronomical Observatory of the University of Siena, Italy. Exposures were taken in sequence with 4 minutes and 3 minutes, respectively, in V and R bands. All the images were calibrated with dark and flat-field frames. Differential aperture photometry was performed with MAXIM DL (Diffraction Limited 2012). V and R magnitudes were standardized using the method described by Dymock and Miles (2009) with selected reference stars from the CMC15 catalogue (Copenhagen Univ. Obs. 2013; Figure 1, Table 1).

In order to acquire the composite spectrum, we had a collaboration with Siding Spring Observatory, Australia (LCOGT network). The instruments used were a 2-m Ritchey-Chrétien telescope with e2v CCD42-10 and Andor Newton 9401 CCD cameras, on altazimuth mount. The spectrum was acquired on October 15, 2015, and reduced with the custom IRAF pipeline "floydsspec" (Valenti *et al.* 2013); an Hg-Ar lamp was used for wavelength calibration, and the white-dwarf Feige 110 was used for flux calibration. The wavelength coverage was 320–1000 nm. Spectrum inspection and analysis were made with VISUAL SPEC (Desnoux 2015) and ISIS (Buil 2015) software tools.

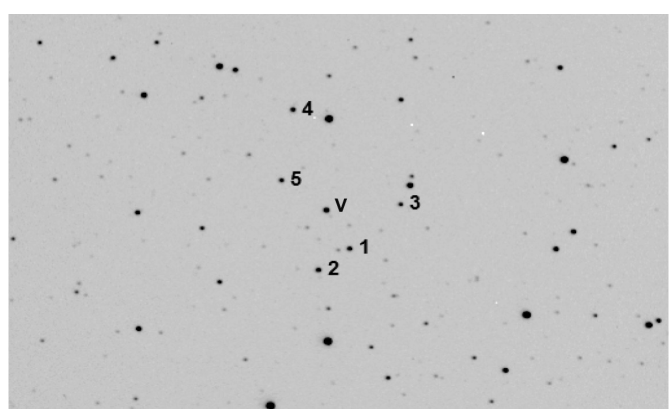

Figure 1. Star field with the binary star GSC 05765-01271 (V) and the reference stars used in differential photometry.

Table 1. Photometry.

Star	*CMC15 Designation*	*R.A. (J2000) h m s*	*Dec. (J2000) ° ′ ″*	*V*	*R*	*V–R*
GSC 05765–0127	204933.2–120851	20 49 33.3	–12 08 52	—	—	—
Reference 1	204930.4–121003	20 49 30.4	–12 10 03	13.661	13.280	0.381
Reference 2	204934.1–121044	20 49 34.1	–12 10 44	13.549	13.110	0.439
Reference 3	204924.5–120838	20 49 24.5	–12 08 38	14.147	13.743	0.404
Reference 4	204937.4–120543	20 49 37.4	–12 05 43	13.600	13.174	0.426
Reference 5	204938.6–120756	20 49 38.6	–12 07 56	13.936	13.523	0.413

2.2. Results

Period analysis gave an orbital period P = 0.382878 ± 0.00002 day with an epoch E = 2457254.5065 ± 0.0001 based on the first observed primary minimum (Papini *et al.* 2015). In the following we present the main results that led us to the preliminary model of this binary system.

2.2.1. Color index

Exposure times were a lot shorter than rotational period, so we assumed that taking an image with V filter and, immediately after it, another one in R-band was equivalent to taking them at the same time. This allowed us to measure the color index (V–R) = 0.37 ± 0.02, using the values of the magnitudes at the minima of the R and V light curves, determined with a 4th-order polynomial fit in PERANSO (Vanmunster 2007). The color index was dereddened using the NASA/IPAC Extragalactic Database—Coordinate Transformation and Galactic Extinction Calculator (NASA/IED 2015). This service gave us the total galactic visual extinction along the line of sight. At the object coordinates the service reports (Schlafly and Finkbeiner 2011), for Landolt bandpass, a color excess

$$E(B–V) = A_B – A_v = 0.174 – 0.132 = 0.042$$

and

$$E(V–R) = A_v – A_R = 0.132 – 0.104 = 0.028$$

Then, using experimental (V–R) color index and assuming an error of 0.02 for A_v and A_r as reported in Schlafly and Finkbeiner (2011), we derived the dereddened color index:

$$(V–R)_0 = (V–R) – E(V–R) = (0.37 – 0.03) \pm 0.03 = 0.34 \pm 0.03$$

where the error is evaluated as the quadratic sum of the uncertainties of the components (color index and color excess). This color index fits with spectral types G0/1V at effective temperature of ~5900 K (Mamajek 2016).

2.2.2. Spectrum Analysis

The reduced composite spectrum was dereddened applying a color excess E(B–V) = 0.042 (value obtained as shown in the previous section), by using the specific function implemented in the ISIS software tool. The resulting dereddened spectrum is close to an F8V type star (Figure 2) at an effective temperature of ~6100 K (Mamajek 2016).

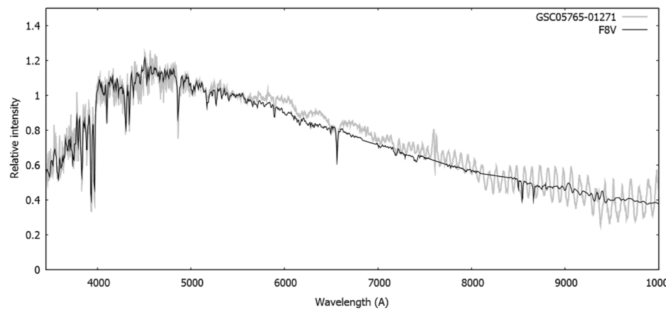

Figure 2. Comparison between GSC 05765-01271 dereddened spectrum and F8V synthetic spectrum.

2. 2. 3. Light curve modeling

Since radial velocities of this binary system weren't known, we used widely adopted empirical relations obtained by regression from the analysis of experimental data (including radial velocities) of several eclipsing binary systems.

Relations 4–5 reported in Gazeas and Stepień (2008) gave an estimate of the masses of the components. By applying Kepler's Third Law we estimated the semimajor axis. An estimate of radii was computed thanks to relations Eq. 8–9 in Gazeas and Stepień (2008).

In order to estimate temperatures, in agreement with previous works, we assumed the temperature of the hotter component equal to 6100 K and determined the other one with Bronstein's relation reported in Eq. 2 (Ivanov *et al.* 2010).

The distance of the system from Earth was figured out using

$$D = 10^{\{0,2\,(m_V - M_V + 5)\}} = 606 \text{ parsec},$$

where M_V = 3.81 was given by Eq. (3) in Gazeas and Stepień (2008) and m_V = 12.73 was derived by V-band maximum light (12.86 V) corrected for galactic extinction value A_V = 0.132.

We used these parameters as inputs in PHOEBE (Prša and Zwitter 2005), in addition to the following parameters: albedos (assumed 0.5 for both components—stars with convective envelopes, T < 7200 K); gravity darkening coefficients (assumed 0.32 for both components—convective envelopes, in agreement with Von Zeipel's Law); limb darkening coefficients (obtained by interpolating Van Hamme's tables).

We also assumed a low light scatter, because of the low magnitude of the system. Moreover, we interpreted the different depths of the minima in the light curve as due to different temperatures of the components; setting the lower temperature

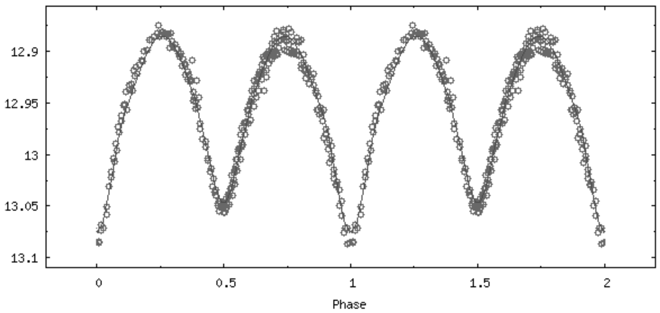

Figure 3. Fit of the light curve performed with PHOEBE.

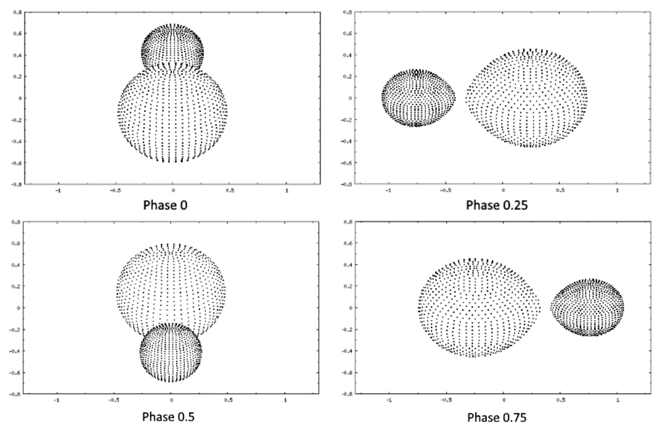

Figure 4. Graphical representation of the system (PHOEBE software).

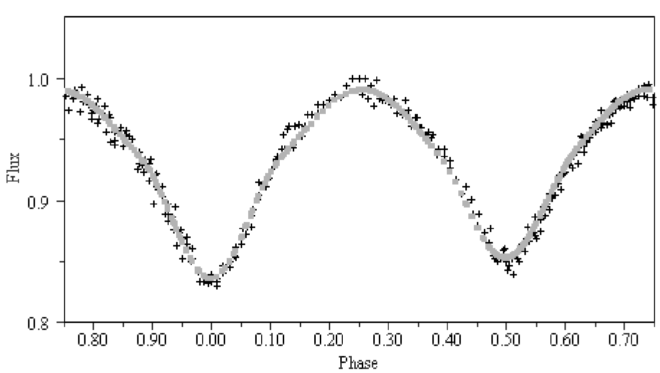

Figure 5. Fit of the light curve from BINARY MAKER 3.

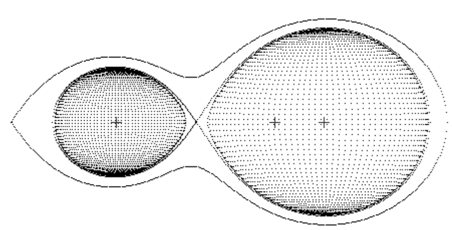

Figure 6. Equipotential curves (BINARY MAKER 3 tool).

for the more massive star was required in order to produce a good fit. The result of the fit is shown in Figure 3. In Figure 4 a possible graphic representation of the system is shown.

Moreover, an independent model of the system was realized using BINARY MAKER 3 (Bradstreet and Steelman 2002), starting from the mass ratio obtained by the empirical relations and adjusting the model parameters (q, T_1, i, Omega) in order to minimize the sum square of the residual of the model fit. Fillout factors returned by BINARY MAKER 3 (–0.01 for both components) allowed us to classify better the system type: according to the initial classification, reported in Marullo *et al.* (2015), based only on period and light curve shape, the system should have been an EW-type member, but fillout factors clearly show that the system has to be considered as "near-contact." Fit of the light curve and equipotential curves are shown in Figure 5 and Figure 6, respectively.

Values obtained with PHOEBE, BINARY MAKER 3, and empirical relations are compared in Table 2.

Table 2. Results and comparison among PHOEBE, BINARY MAKER 3 and EMPIRICAL RELATIONS.

Parameter	*PHOEBE*	*BINARYMAKER3*	*EMPIRICAL REL.*
M_1	1.12 $M_\odot$	1.26 $M_\odot$	1.26 $M_\odot$
M2	0.36 $M_\odot$	0.40 $M_\odot$	0.40 $M_\odot$
q = (M_2 / M_1)	0.32	0.32	0.32
R_1	1.20 $R_\odot$	1.25 $R_\odot$	1.26 $R_\odot$
R_2	0.70 $R_\odot$	0.72 $R_\odot$	0.74 $R_\odot$
T_1	5832 K	5850 K	5855 K
T_2	6100 K	6100 K	6100 K
a (semi-major axis)	2.53 $R_\odot$	2.63 $R_\odot$	2.63 $R_\odot$
i (inclination)	57.1°	57.5°	——
x_1 (limb darkening coeff.)	0.50	0.50	——
x_2 (limb darkening coeff.)	0.49	0.50	——
Distance from Earth (1977 ly)	——	——	606 pc

3. Discussion

In this preliminary work, either the best fit obtained with PHOEBE or the best fit obtained with BINARY MAKER 3 minimizes the chi-squared, but we can't exclude that the proposed solutions are only local minima. However, the good agreement between empirical relations and the best fits supports the proposed analysis. A better way to proceed would be using the Wilson-Devinney code implemented in PHOEBE only as a likelihood function for a Bayesian model. A noise model of the data would need to be added to the likelihood function. With the aid of a MCMC (Markov chain Monte Carlo) sampler, it would then be possible to correctly search the best possible solution to the problem.

4. Conclusions

We think this work supports the claim that even with limited instrumentation it is possible to do quite complete binary system analysis. In this case, the object is also faint and there wasn't any support from historical records. A more accurate model (including spectral types) could be obtained with high-resolution spectroscopy and analysis of disentangled spectra of the two components. We want to remark that the present work, a little contribution to the astrophysical knowledge, was made possible thanks to the great deal of effort made in Observational

Astrophysics by astrophysicists like Gazeas, Stępień, and Bronstein during many years of hard work. The widely adopted empirical relations used in this work are recognized as good starting points in the process of modeling an eclipsing binary star system.

5. Acknowledgements

The authors are sincerely grateful to Todd Boroson and Griffin Hosseinzadeh, Australian Siding Spring Observatory-LCOGT Network, for their willingness and speed in replying to the request for the GSC 05765-01271 spectrum.

References

Bradstreet, D. H., and Steelman, D. P. 2002, *Bull. Amer. Astron. Soc.*, **34**, 1224.

Buil, C. 2015, ISIS Integrated Spectrographic Innovative Software (http://www.astrosurf.com/buil/isis/isis_en.htm).

Copenhagen Univ. Obs., *et al.* 2013, Carlsberg Meridian Catalogues La Palma 15, (http://svo2.cab.inta-csic.es/vocats/cmc15/).

Desnoux, V. 2015, VISUAL SPEC software (http://www.astrosurf.com/vdesnoux/).

Diffraction Limited. 2012, MAXIMDL image processing software (http://www.cyanogen.com).

Dymock, R., and Miles, R. 2009, *J. Br. Astron. Assoc.*, **119**, 149.

Gazeas, K. D., and Stępień, K. 2008, *Mon. Not. Roy. Astron. Soc.*, **390**, 1577 (arXiv:0803.0212v2 [astro-ph]).

Ivanov, V., Kjurkchieva, D., and Srinivasa Rao, M. 2010, *Bull. Astron. Soc. India*, **38**, 83.

Lopez-Morales, M. 2007, *Astrophys. J.*, **660**, 732.

Mamajek, E. 2016, "A Modern Mean Dwarf Stellar Color and Effective Temperature Sequence" (http://www.pas.rochester.edu/~emamajek/EEM_dwarf_UBVIJHK_colors_Teff.txt).

Marchini, A., Marullo, S., Bacci, P., Franco, L., Papini, R., and Salvaggio, F. 2016, *Minor Planet Bull.*, **43**, 7.

Marullo, S., Marchini, A., Papini, R., and Salvaggio, F. 2015, AAVSO VSX (https://www.aavso.org/vsx/index.php?view=detail.top&oid=409960).

NASA/IPAC Extragalactic Database (NED). 2015, Coordinate Transformation and Galactic Extinction Calculator (https://ned.ipac.caltech.edu/forms/calculator.html).

Papini, R., Franco, L., Marchini, A., and Salvaggio, F. 2015, *J. Amer. Assoc. Var. Star Obs.*, **43**, 207.

Prša, A., and Zwitter, T. 2005, *Astrophys. J.*, **628**, 426.

Schlafly, E., and Finkbeiner D. P. 2011, *Astrophys. J.*, **737**, 103.

Southworth, J. 2012, arXiv:1201.1388v1 [astro-ph.SR].

Valenti, S., Sand, D., and Howell, D. A. 2013, Authorea, *FLOYDS Manual and Pipeline* (https://www.authorea.com/users/598/articles/6566).

Vanmunster, T. 2007, Light Curve and Period Analysis Software PERANSO (http://www.peranso.com).

Amplitude Variations in Pulsating Red Giants. II. Some Systematics

John R. Percy
Department of Astronomy and Astrophysics, and Dunlap Institute of Astronomy and Astrophysics, University of Toronto, Toronto, ON M5S 3H4, Canada; john.percy@utoronto.ca

Jennifer Laing
Department of Astronomy and Astrophysics, University of Toronto, Toronto, ON M5S 3H4, Canada; jen.laing@mail.utoronto.ca

Received September 22, 2017; revised October 16, 2017; accepted October 19, 2017

Abstract In order to extend our previous studies of the unexplained phenomenon of cyclic amplitude variations in pulsating red giants, we have used the AAVSO time-series analysis package VSTAR to analyze long-term AAVSO visual observations of 50 such stars, mostly Mira stars. The relative amount of the variation, typically a factor of 1.5, and the time scale of the variation, typically 20–35 pulsation periods, are not significantly different in longer-period, shorter-period, and carbon stars in our sample, and they also occur in stars whose period is changing secularly, perhaps due to a thermal pulse. The time scale of the variations is similar to that in smaller-amplitude SR variables, but the *relative* amount of the variation appears to be larger in smaller-amplitude stars, and is therefore more conspicuous. The cause of the amplitude variations remains unclear, though they may be due to rotational modulation of a star whose pulsating surface is dominated by the effects of large convective cells.

1. Introduction

Percy and Abachi (2013) showed that, in almost all pulsating red giants (PRGs), the pulsation *amplitude* varied by a factor of up to 10, on a time scale of 20–40 pulsation periods. The authors were initially concerned that the variation might be an artifact of wavelet analysis, but it can be confirmed by Fourier analysis of individual sections of the dataset. Similar amplitude variations were found in pulsating red supergiants (Percy and Khatu 2014) and yellow supergiants (Percy and Kim 2014). There were already sporadic reports in the literature of amplitude variations in PRGs (e.g. Templeton *et al.* 2008; Price and Klingenberg 2005), but these stars tended to be the rare few which also showed large changes in period, and which may be undergoing thermal pulses (Uttenthaler *et al.* 2011). Furthermore, it is well known that stars such as Mira do not repeat exactly from cycle to cycle. Percy and Abachi (2013), however, was the first *systematic* study of this phenomenon. Since these amplitude variations remain unexplained, we have examined the behavior of more PRGs to investigate some of the systematics of this phenomenon.

We have analyzed samples of *large-amplitude* PRGs, mostly Mira stars, in each of four groups: A: 17 shorter-period stars; B: 20 longer-period stars; C: 15 carbon stars; D: 8 stars with significant secular period changes (Templeton *et al.* 2005). The stars in groups A, B, and C were drawn randomly from among the 547 studied by Templeton *et al.* (2005) and which did not show significant secular period changes. As did Templeton *et al.* (2005), we used visual observations from the American Association of Variable Star Observers (AAVSO) International Database. We did not analyze stars for which the data were sparse, or had significant gaps. Note that Templeton *et al.* (2005) specifically studied Mira variables, which, by definition, have full ranges greater than 2.5 in visual light—an arbitrary limit.

The purposes of this paper are: (1) to present our analyses of these 50 PRGs, and (2) to remind the astronomical community, once again, that the amplitude variations in PRGs require an explanation.

2. Data and analysis

We analyzed visual observations from the AAVSO International Database (AID; Kafka 2017) using the AAVSO's VSTAR software package (Benn 2013). It includes both a Fourier and wavelet analysis routine; we used primarily the latter. The wavelet analysis uses the Weighted Wavelet Z-Transform (WWZ) method (Foster 1996). The "wavelet" scans along the dataset, estimating the most likely value of the period and amplitude at each point in time, resulting in graphs which show the best-fit period and amplitude versus time.

For each star, we noted the Modified Julian Date MJD(1) after which the data were suitable for analysis—not sparse, no significant gaps. The datasets are typically a century long so, for these mostly-Mira stars, there are typically at least a hundred pulsation cycles in the dataset. From the WWZ wavelet plots, we determined the maximum (Amx), minimum (Amn), and average ($\bar{A}$) amplitude, the number of cycles N of amplitude increase and decrease, and the average length L of these cycles. See Percy and Abachi (2013) for a discussion of these quantities and their uncertainties; N and therefore L can be quite uncertain because the cycles are irregular, and few in number, especially if they are long. This is doubly true for the few stars in which the length of the dataset is shorter than average. The maximum and minimum amplitudes are also uncertain since they are determined over a limited interval of time.

We then calculated the ratio of L in days to the pulsation period P in days, the ratio of maximum to minimum amplitude, the difference ΔA between the maximum and minimum amplitude, and the ratio of this to the average amplitude $\bar{A}$. The periods were taken from the VSX catalog, and rounded off; the periods of stars like these "wander" by several percent, due to random cycle-to-cycle fluctuations. All this information is listed in Tables 1–4. In the "Notes" column, the symbols are as

Table 1. Pulsation properties of shorter-period PRGs.

Name	*P(d)*	*MJD(1)*	*N*	*L/P*	*Amn*	*Amx*	*Amx/Amn*	*Å*	*ΔA*	*ΔA/Å*	*Note*
T And	281	16000	8	18	2.38	2.78	1.17	2.60	0.40	0.15	s
V And	256	20000	5	29	2.17	2.63	1.21	2.40	0.46	0.19	s
UW And	237	39000	1	80	1.68	2.21	1.32	2.00	0.53	0.27	d
YZ And	207	40000	3	28	2.00	2.51	1.26	2.25	0.51	0.23	—
S Car	151	20000	10	25	1.03	1.46	1.42	1.25	0.43	0.34	—
U Cas	277	20000	6	22	2.50	3.50	1.40	3.30	1.00	0.30	s
SS Cas	141	27500	5	43	1.28	1.78	1.39	1.55	0.50	0.32	—
Z Cet	184	25000	7	25	2.00	2.45	1.23	2.25	0.45	0.20	—
T Phe	282	20000	3	44	2.00	3.10	1.55	2.50	1.10	0.44	d
W Psc	188	40000	4	23	1.75	2.15	1.23	1.95	0.40	0.21	s
RZ Sco	160	25000	5	41	0.80	1.70	2.13	1.30	0.90	0.69	d*
T Scl	205	32000	2	63	1.40	2.40	1.71	1.70	1.00	0.59	d
V Scl	296	30000	3	31	2.05	2.85	1.39	2.50	0.80	0.32	g
X Scl	265	33000	6	15	1.60	2.03	1.27	1.80	0.43	0.24	—
S Tuc	242	23000	6	24	2.35	2.85	1.21	2.65	0.50	0.39	s
U Tuc	262	20000	6	24	2.35	2.85	1.21	2.70	0.50	0.19	g
R Vir	149	20000	8	31	1.56	2.25	1.44	1.95	0.69	0.35	—

Table 2. Pulsation properties of longer-period PRGs.

Star	*P(d)*	*MJD(1)*	*N*	*L/P*	*Amn*	*Amx*	*Amx/Amn*	*Å*	*ΔA*	*ΔA/Å*	*Note*
R And	410	20000	7	13	3.19	3.60	1.13	3.38	0.41	0.12	g
X And	343	16000	6	20	1.90	3.00	1.58	2.60	1.10	0.42	d
RR And	331	20000	5	22	2.68	3.18	1.19	3.00	0.50	0.17	s
RW And	430	15000	4	25	2.45	3.50	1.43	3.10	1.05	0.34	—
SV And	313	15500	6	22	2.15	2.80	1.30	2.45	0.65	0.27	—
TU And	313	37000	2	33	1.85	2.30	1.24	2.15	0.45	0.21	—
R Aqr	386	28000	4	19	1.80	2.20	1.22	1.95	0.40	0.21	—
R Car	310	20000	6	20	2.23	2.60	1.17	2.40	0.38	0.16	—
R Cas	430	15000	5	20	2.60	2.98	1.14	2.73	0.38	0.14	—
T Cas	445	20000	2	42	1.15	1.97	1.71	1.75	0.82	0.47	d
Y Cas	414	14500	4	26	1.80	2.28	1.27	2.05	0.48	0.23	g
RV Cas	332	20000	9	12	2.50	3.25	1.30	2.90	0.75	0.26	s
TY Cas	645	40000	1	27	2.28	3.20	1.40	2.90	0.92	0.32	s
Y Cep	333	15000	5	25	1.50	3.10	2.07	2.80	1.60	0.57	d
o Cet	332	20000	7	16	2.60	3.05	1.17	2.80	0.45	0.16	—
S Cet	321	20000	5	23	2.30	2.87	1.25	2.70	0.57	0.21	—
W Cet	352	32500	2	36	2.35	3.30	1.40	2.80	0.95	0.34	—
R Cyg	434	15000	5	19	2.73	2.98	1.09	2.83	0.25	0.09	—
R Hor	408	25000	5	16	2.95	3.67	1.24	3.45	0.72	0.21	g
Z Peg	320	20000	2	59	1.90	2.40	1.26	2.20	0.50	0.23	d

Table 3. pulsation properties of some carbon PRGs.

Star	*P(d)*	*MJD(1)*	*N*	*L/P*	*Amn*	*Amx*	*Amx/Amn*	*Å*	*ΔA*	*ΔA/Å*	*Note*
AZ Aur	415	40000	2.5	17	1.35	1.75	1.30	1.65	0.40	0.24	s
W Cas	406	20000	3.5	26	1.18	1.45	1.23	1.27	0.27	0.21	d
X Cas	423	20000	5	17	0.70	0.93	1.32	0.80	0.23	0.28	—
RV Cen	457	20000	3.5	23	0.83	1.23	1.48	1.03	0.40	0.39	g
V CrB	358	20000	6	17	1.36	1.75	1.29	1.50	0.39	0.26	—
U Cyg	463	20000	4	20	1.23	1.55	1.26	1.45	0.32	0.22	—
T Dra	422	20000	3	30	0.60	1.55	2.58	1.30	0.95	0.73	gd
R For	386	33000	5	12	1.17	1.53	1.31	1.35	0.36	0.27	d
VX Gem	379	40000	1.5	31	1.65	2.15	1.30	1.85	0.50	0.27	gd
ZZ Gem	315	40000	2.5	22	0.83	1.22	1.47	1.07	0.39	0.36	g
R Lep	445	20000	4	21	0.75	1.27	1.69	1.05	0.52	0.50	d*
T Lyn	406	28000	4	18	1.18	1.53	1.30	1.40	0.35	0.25	—
V Oph	295	25000	5	22	1.03	1.30	1.27	1.13	0.28	0.24	—
RU Vir	434	20000	4.5	19	1.25	1.78	1.42	1.40	0.53	0.38	—
R Vol	453	20000	4	20	0.95	1.65	1.74	1.40	0.70	0.50	gd

Table 4. pulsation properties of some PRGs with rapidly-changing periods.

Star	*P(d)*	*MJD(1)*	*N*	*L/P*	*Amn*	*Amx*	*Amx/Amn*	*Å*	*ΔA*	*ΔA/Å*	*Note*
R Aql	311	20000	4	30	1.83	2.58	1.41	2.20	0.75	0.34	—
R Cen	502	20000	1	75	0.60	1.70	2.83	1.40	1.10	0.79	d*
V Del	543	20000	2	34	2.58	3.30	1.28	2.85	0.72	0.25	s
W Dra	291	20000	4	32	1.62	2.58	1.59	2.20	0.96	0.44	—
R Hya	414	20000	3	30	1.40	2.25	1.61	1.70	0.85	0.50	*
R Leo	319	20000	5	23	1.60	2.05	1.28	1.87	0.45	0.24	—
S Scl	367	20000	4.5	23	2.52	3.13	1.24	2.85	0.61	0.21	g
Z Tau	446	20000	3	28	1.45	2.78	1.92	1.90	1.33	0.70	ds*

follows: "s"—the data were sparse in places; "g"—there were one or more gaps in the data (but not enough to interfere with the analysis); "d"—the star is discordant in one or more graphs mentioned below, but there were no reasons to doubt the data or analysis; asterisk (*)—see Note in section 3.2. Note that the amplitudes that we determine and list are "half-amplitudes" rather than the full ranges, i.e., they are the coefficient of the sine function which fit to the data.

3. Results

We plotted L/P, Amx/Amn, and ΔA/$\bar{A}$ against period for each of the four groups of stars A, B, C, and D. There was no substantial trend in any case, except as noted below (Figures 1–3). We therefore determined the mean M, the standard error SE, and the standard error of the mean SEM, for each of the three quantities, for each of the four groups. (The mean M is more commonly called the average; the standard error SE is a measure of the scatter of the values around the mean; and the standard error of the mean SEM is a measure of the uncertainty of the mean, given the scatter of the values, and the number thereof.) These are given in Table 5. We also flagged any outliers in the graphs, and re-examined the data and analysis. If there was anything requiring comment, that comment is given in section 3.2.

In stars which are undergoing large, secular period changes, possibly as a result of a thermal pulse, the size and length of the amplitude variation cycles is marginally larger, but this may be partly due to the difficulty of separating the cyclic and secular variations. Note that cyclic variations in amplitude are present during the secular ones in these stars.

We also found that, for the shorter-period stars, $\bar{A}$ increased with increasing period (Figure 4), but this is a well-known

Table 5. Properties of the amplitude variation in four samples of PRGs.

Property	*SP*	*LP*	*C*	*CP*
M(ΔA/Å)	0.31	0.26	0.34	0.43
SE(ΔA/Å)	0.15	0.12	0.14	0.22
SEM(ΔA/Å)	0.036	0.028	0.037	0.076
hline				
M(Amx/Amn)	1.38	1.33	1.46	1.65
SE(Amx/Amn)	0.24	0.23	0.35	0.53
SEM(Amx/Amn)	0.058	0.052	0.089	0.188
hline				
M(L/P)	33	25	21	34
SE(L/P)	17	11	5	17
SEM(L/P)	4.1	2.5	1.3	6

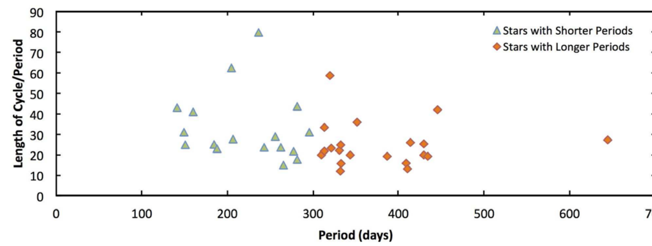

Figure 1. The lengths of the cycles of amplitude increase and decrease, in units of the pulsation period, as a function of pulsation period. At most, there is a slight downward trend, which may be partly due to the fact that the cycles may be more difficult to detect in shorter-period, smaller-amplitude stars.

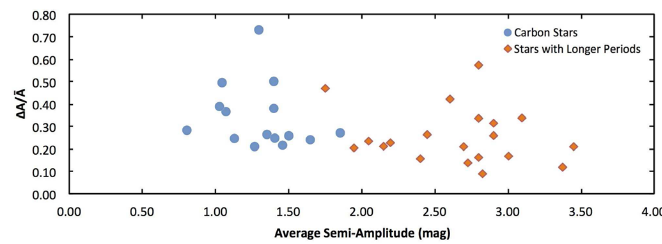

Figure 2. The variation in visual amplitude, relative to the average visual amplitude, as a function of average visual amplitude, for carbon stars (blue filled circles) and non-carbon stars (red filled diamonds). The difference is not significant to the 3σ level (Table 5).

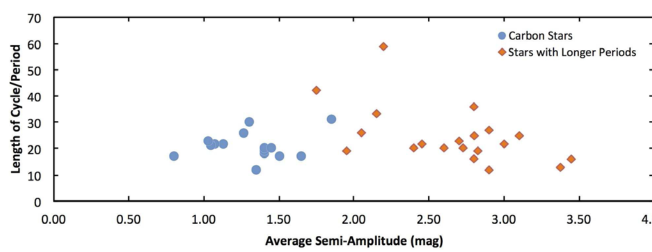

Figure 3. The lengths of the cycles of amplitude increase and decrease, in units of the pulsation period, as a function of average visual amplitude, for carbon stars (blue filled circles) and non-carbon stars (red filled diamonds). There is no trend. The visual amplitudes of the carbon stars are systematically smaller, as is well-known.

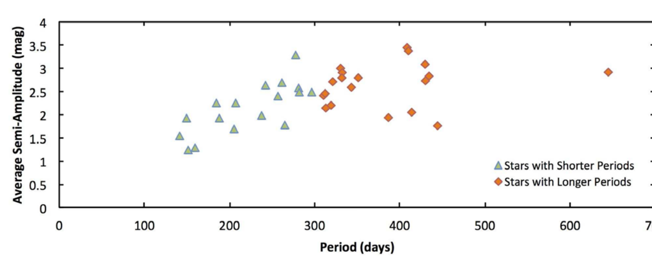

Figure 4. The average visual pulsation amplitude as a function of pulsation period, for shorter- period and longer-period Miras. The amplitude increases with period, up to about 300 days (this is a continuation of a well-known trend), and then levels off.

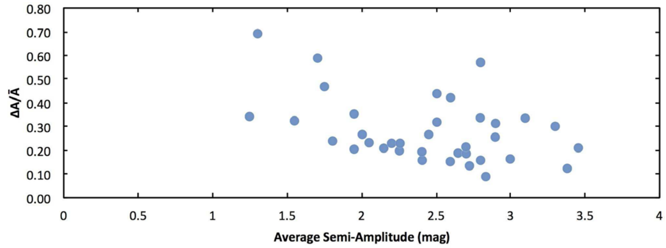

Figure 5. The variation in visual amplitude, relative to the average visual amplitude, as a function of average visual amplitude. There is a downward trend. This trend is consistent with the results of Percy and Abachi (2013), who found values of typically 0.5 to 2.0 for stars with average amplitudes of 1.0 down to 0.1.

correlation. The very shortest-period PRGs have amplitudes of only hundredths of a magnitude. There was no trend in amplitude for the longer-period stars.

The *relative* amount of variation in amplitude is slightly larger in shorter-period, smaller-amplitude stars (Figure 5). This is consistent with the results of Percy and Abachi (2013), as discussed in section 4.

The $\bar{A}$ for the carbon stars are systematically lower than for the oxygen stars (Figures 2 and 3). Again, this is well-known; in the oxygen stars, the visual amplitude is amplified by the temperature sensitivity of TiO bands, which are not present in carbon stars. Note also that the carbon stars have longer periods, since they are in a larger, cooler, and more highly evolved state.

3.1. Stars with secular amplitude variations

Although our main interest was in the cyclic variations in pulsation amplitude, the secular variations in amplitude are also of interest, though they have already been studied and discussed by other authors, as mentioned in the Introduction. We performed a quick wavelet analysis of the 547 Miras in Templeton *et al.*'s (2005) paper, to identify stars in which *secular* amplitude variations might dominate the cyclic ones. Of the 21 stars whose period varied secularly at the three-sigma level or greater, four (T UMi, LX Cyg, R Cen, and RU Sco) seemed to show such secular amplitude variations. There were no other stars in Templeton *et al.*'s (2005) sample which showed *strong* secular variations. Note that, in each case, cyclic amplitude variations were superimposed on the secular ones.

3.2. Notes on individual stars

This section includes notes on two kinds of stars: the ones for which the data or analysis required comments, and ones which appear to be outliers in some of the graphs that we have plotted.

R Cen This star has a secular decrease in amplitude, and period, so it is not surprising that the star is discordant in some of the relationships; see also Templeton *et al.* (2005).

T Dra This star has unusually large cyclic variations in amplitude.

R Lep This star has unusual large variations in mean magnitude.

RZ Sco This star, with a relatively short period, has a secular change in period, but only at the 3σ level (Templeton *et al.* 2005).

Z Tau This star is exceptional in that it is an S-type star. Also, its light curve shows non-sinusoidal variations, and flat minima suggestive that the variable may have a faint companion star. Indeed, SIMBAD lists two faint stars within 5 arc seconds of Z Tau. This star is discussed by Templeton *et al.* (2005).

4. Discussion

Percy and Abachi (2013) obtained a median value of L/P = 44 for 28 monoperiodic smaller-amplitude PRGs. They calculated the median, in part because there were a few stars with very large values of L/P. We have reanalyzed those stars, and realized that Percy and Abachi (2013) adopted a more conservative definition for amplitude variations. Figure 6 shows an example of this: for the smaller-amplitude PRG RY Cam, Percy and Abachi (2013) estimated N = 1.5 whereas, based on our subsequent experience, we would estimate N = 6.7. Based on our reanalysis, the L/P values are now strongly clustered between 20 and 30, with a mean of 26.6. This is consistent with the values which we obtained for shorter- and longer-period PRGs. Figure 7 shows the light curve of RY Cam on which Figure 6 is based.

The values of $\Delta A/\bar{A}$, obtained by Percy and Abachi (2013), for smaller-amplitude (1.0 down to 0.1) variables, are typically about 0.5 to 2.0. This is consistent with the trend shown in Figure 5. The amplitude variations are relatively larger and more conspicuous in small-amplitude stars.

Templeton *et al.* (2008) call attention to three other PRGs with variable amplitudes. The amplitude variations in RT Hya are the largest (0.1 to 1.0) and are cyclic (L/P = 40). The amplitude variations in W Tau are almost as large (0.1 to 0.6) and are also cyclic (L/P = 24). Those in Y Per are less extreme (0.3 to 0.9) and also cyclic (L/P = 29). These three stars therefore behave similarly to PRGs in our sample.

There are therefore at least three unexplained phenomena in the pulsation of PRGs: (1) random, cycle-to-cycle fluctuations which cause the period to "wander"; (2) "long secondary periods," 5 to 10 times the pulsation period; and now (3) cyclic variations in pulsation amplitudes, on timescales of 20 to 30 pulsation periods. PRGs have large outer convective envelopes. Stothers and Leung (1971) proposed that the long secondary periods represented the overturning time of giant convective cells in the outer envelope, and Stothers (2010) amplified this conclusion. Random convective cells may well explain the random cycle-to-cycle period fluctuations, as well. The amplitude variations might then be due to rotational modulation, since the rotation periods of PRGs are significantly longer than the long secondary periods according to Olivier and Wood (2003).

5. Conclusions

Significant cyclic amplitude variations occur in all of our sample of 50 mostly-Mira stars. The relative amount of the variation (typically Amx / Amn = 1.5) and the time scale of the variation (typically 20–35 times the pulsation period) are not significantly different in the shorter-period and longer-period stars, and in the carbon stars. The time scales are consistent with those found by Percy and Abachi (2013) in a sample of mostly smaller-amplitude SR variables, but the *relative* amplitude

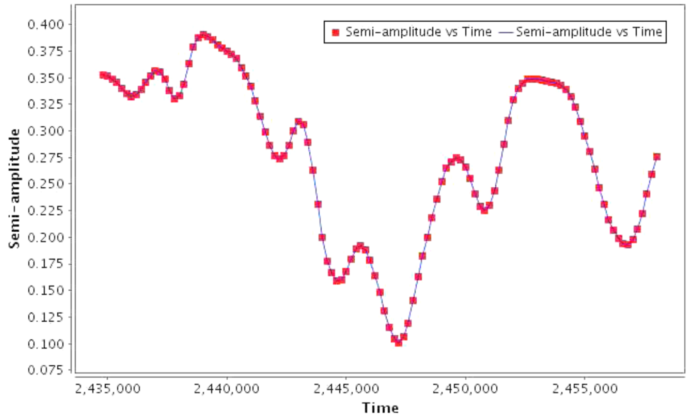

Figure 6. Semi-amplitude versus time for RY Cam, a smaller-amplitude PRG. Percy and Abachi (2013) estimated N conservatively at 1.5 but, based on our subsequent experience, we would estimate N = 6.7. This figure therefore illustrates both the significant amplitude variation, and the somewhat subjective estimate of N and therefore L.

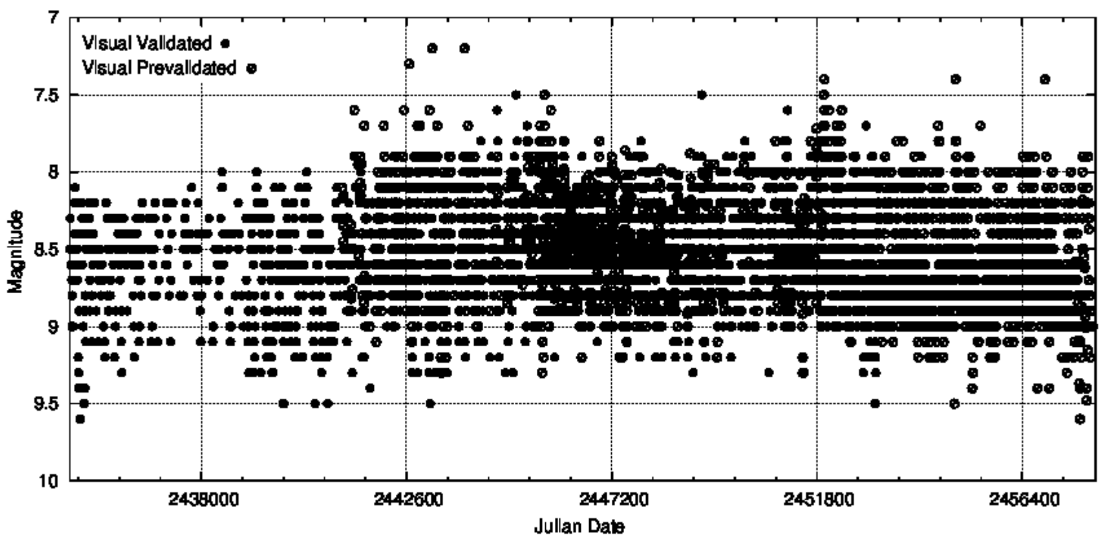

Figure 7. The visual light curve of RY Cam on which Figure 6 is based, taken from the AAVSO International Database. It begins where the data become dense and continuous enough for wavelet analysis.

variations are larger in the smaller-amplitude stars. As was previously known, the average amplitudes increase with period for the shorter-period stars, and the carbon stars have smaller visual amplitudes than the oxygen stars.

6. Acknowledgements

We thank the AAVSO observers who made the observations on which this project is based, the AAVSO staff who archived them and made them publicly available, and the developers of the VSTAR package which we used for analysis. This paper is based, in part, on a short summer research project by undergraduate astronomy and physics student co-author JL. We acknowledge and thank the University of Toronto Work-Study Program for existing, and for financial support. This project made use of the SIMBAD database, maintained in Strasbourg, France.

References

Benn, D. 2013, VSTAR data analysis software (http://www.aavso.org/vstar-overview).

Foster, G. 1996, *Astron. J.*, **112**, 1709.

Kafka, S. 2017, variable star observations from the AAVSO International Database (https://www.aavso.org/aavso-international-database).

Olivier, E. A., and Wood, P. R. 2003, *Astrophys. J.*, **584**, 1035.

Percy, J. R., and Abachi, R. 2013, *J. Amer. Assoc. Var. Star Obs.*, **41**, 193.

Percy, J. R., and Khatu, V. C. 2014, *J. Amer. Assoc. Var. Star Obs.*, **42**, 1.

Percy, J. R., and Kim, R. Y. H. 2014, *J. Amer. Assoc. Var. Star Obs.*, **42**, 267.

Price, A., and Klingenberg, G. 2005, *J. Amer. Assoc. Var. Star Obs.*, **34**, 23.

Stothers, R. B. 2010, *Astrophys. J.*, **725**, 1170.

Stothers, R. B., and Leung, K. C. 1971, *Astron. Astrophys.*, **10**, 290.

Templeton, M. R., Mattei, J. A., and Willson, L. A. 2005, *Astron. J.*, **130**, 776.

Templeton, M. R., Willson, L. A., and Foster, G. 2008, *J. Amer. Assoc. Var. Star Obs.*, **36**, 1.

Uttenthaler, S., *et al.* 2011, *Astron. Astrophys.*, **531**, A88.

Improving the Photometric Calibration of the Enigmatic Star KIC 8462852

Adam J. Lahey
Douglas M. Dimick
Andrew C. Layden
Bowling Green State University, Department of Physics and Astronomy, 104 Overman Hall, Bowling Green, OH 43403; address email correspondence to laydena@bgsu.edu

Received November 3, 2017; revised December 6, 12, 2017; accepted December 12, 2017

Abstract The star KIC 8462852 undergoes dimming events whose origin remains unexplained. Observers from the AAVSO have obtained an impressive amount of data on this challenging, low-amplitude, irregular variable star. We present new, all-sky observations of KIC 8462852 and its surrounding comparison stars in order to refine their photometric calibration, obtaining $V = 11.892$ and $I_C = 11.210$ mag for KIC 8462852 itself. However, our calibration is not definitive and we recommend additional observations that should enable a more precise and accurate recalibration of the AAVSO photometry. We also present our photometric time-series for KIC 8462852 that spans 1.6 years in which we find hints for dimming below its canonical brightness in the days around 2017 May 18.

1. Introduction

The *Kepler* space telescope monitored over 150,000 stars for over four years searching for transiting exoplanets (Borucki *et al.* 2010). Most of the thousands of detections involved the periodic dimming of a host star by $\lesssim$1% as an exoplanet passed between the star and Earth, but one series of dimming events that stood out involved the host star KIC 8462852 (TYC 3162-665-1, 2MASS J20061546+4427248, colloquially referred to as "Boyajian's Star" or "Tabby's Star," and hereafter abbreviated "KIC"). This star was observed to dim, apparently aperiodically, with two main events (denoted D800 and D1500) that reduced the star's flux by $\gtrsim$15% (Boyajian *et al.* 2016). These authors showed that these extraordinary events were astrophysical in origin, not observational, and they considered a variety of explanations for the dimming.

As part of their analysis, Boyajian *et al.* (2016) obtained a variety of observations of KIC, including optical photometry using a 0.9-m Schmidt telescope yielding un-dimmed magnitudes of $V = 11.705 \pm 0.017$ mag, $I_C = 11.051 \pm 0.098$ mag, and $B–V = 0.557$ mag. Other data indicated that KIC is a normal F3-type dwarf star with no apparent infrared excess to indicate the presence of a dust disk.

Searches of the photographic record suggested a gradual dimming of KIC over the last century (Schaefer 2016), though others have questioned this result (Hipke *et al.* 2016, 2017). Additionally, a careful analysis of the *Kepler* data indicated a more pronounced dimming over the four-year duration of the *Kepler* mission, with an accelerated dimming in its last year (Montet and Simon 2016). More recent observations using both space- and ground-based equipment appear to confirm this dimming (Meng *et al.* 2017). Thus, evidence of brightness changes exists on timescales of a century, of years, and of days in this otherwise apparently normal F-type star.

These observational studies have spawned a number of explanations for the brightness variations of KIC, beginning with a series of possibilities entertained by Boyajian *et al.* (2016). They found the most plausible explanation to be obscuration by a swarm of dusty fragments on a comet-like orbit, relaxing dynamically after the break-up of their parent body. Other researchers have hypothesized different explanations for the dimming, including (i) Sun-centered rings of obscuring material in the outer Solar System (Katz 2017) or compact dust clouds in the interstellar medium (Wright and Sigurdsson 2016), (ii) a ringed planet and associated clouds of Trojan objects in orbit around KIC (Ballesteros *et al.* 2017), (iii) the outer layers of KIC cooling and dimming as they dissipate energy from an earlier planetary in-spiral event (Metzger *et al.* 2017), and (iv) transits by a swarm of megastructures near KIC fabricated by an intelligent civilization (Wright *et al.* 2016). Clearly, KIC is a rare and remarkable object worthy of long-term photometric monitoring to detect new dimming events, which may in turn constrain hypotheses of their origin.

In 2015 October, an appeal for observations of KIC by AAVSO observers was placed via *AAVSO Alert Notice 532* (AAVSO 2015a). The AAVSO Variable Star Plotter (AAVSO 2015b; finder chart, X15551E accessed 2015 Oct 27.) provided a finder chart for KIC along with four comparison stars and their APASS magnitudes, which are shown in Table 1, along with the AAVSO Photometric All-Sky Survey (APASS) photometry of KIC itself (Henden and Munari 2014). Specifically, columns 2–3 show the equatorial coordinates of each star, columns 4–5 show the Johnson *V*-band magnitude and its uncertainty, and columns 6–7 show the Johnson *B–V* color and its uncertainty. Columns 8–9 show the APASS Sloan *i*-band magnitude and its uncertainty after conversion to the Cousins I_C system using the transformations for Population I stars in Table 4 of Jordi *et al.* (2006) (see the Appendix for details). These values were from APASS Data Release 9 (Henden *et al.* 2015). Each star in the table was observed five times, though perhaps not in every filter given the zero values in the uncertainty columns for some of the *i*-band entries, a sign that may indicate only a single visit to the field in that filter (as described in the APASS documentation).

Noting the differences between the photometry of Boyajian *et al.* 2016) and of APASS for KIC, and the relatively large uncertainties in the APASS magnitudes for the comparison stars, we became concerned about the quality of the calibrated photometry AAVSO observers are producing. Specifically, systematic offsets might occur between AAVSO work and the

Table 1. APASS Photometry.

Star	*R.A. (J2000)* *h m s*	*Dec. (J2000)* ° ′ ″	V_J	V_{err}	$(B–V)_J$	$(B–V)_{err}$	I_C [a]	I_{err}
KIC	20 06 15.457	+44 27 24.61	11.852	0.046	0.508	0.062	11.132	0.059
113[b]	20 06 48.087	+44 22 48.14	11.263	0.054	0.458	0.068	10.655	0.042
116[b]	20 07 09.068	+44 20 17.06	11.590	0.050	0.543	0.059	10.890	0.008[c]
124[b]	20 06 01.237	+44 29 32.20	12.427	0.029	0.804	0.048	11.429	0.046
128[b]	20 06 21.194	+44 30 51.28	12.789	0.050	0.481	0.067	12.025	0.029
C1	20 07 08.759	+44 24 23.07	10.291	0.067	0.260	0.146	10.036	0.146
C2	20 06 55.880	+44 26 43.35	10.655	0.064	1.328	0.073	9.426	0.021[c]
C3[d]	20 06 36.311	+44 27 03.17	12.415	0.036	0.932	0.050	11.252	0.031
C4	20 06 34.778	+44 27 34.35	12.349	0.045	1.484	0.057	10.880	0.027
C5	20 06 31.134	+44 35 19.35	10.079	0.055	1.231	0.069	8.859	0.008[c]
C6	20 06 23.647	+44 27 38.14	11.698	0.033	1.178	0.047	10.531	0.033
C7	20 06 08.977	+44 24 30.19	11.175	0.038	1.187	0.054	9.994	0.088
C8	20 06 07.757	+44 26 03.71	11.542	0.032	1.208	0.047	10.367	0.097
C9	20 06 00.392	+44 25 54.05	13.327	0.038	1.010	0.048	12.125	0.092
C10	20 06 01.708	+44 34 17.17	10.895	0.060	1.461	0.075	9.524	0.024[c]
C11	20 05 45.056	+44 21 15.85	12.316	0.038	1.469	0.050	10.847	0.083
C12	20 05 25.952	+44 20 35.42	10.877	0.050	1.236	0.062	9.591	0.049
C13	20 05 25.446	+44 31 21.14	11.242	0.039	1.224	0.052	9.977	0.089

a. The original APASS photometry in the Sloan i*-band was transformed to the Cousins* I_C *system using the relations of Jordi* et al. *(2006) shown in the Appendix.*
b. The AAVSO AUID numbers are 113 = 000-BLS-551, 116 = 000-BLS-553, 124 = 000-BLS-549, and 128 = 000-BLS-555.
c. This star had an entry of zero in the APASS i*-error column, suggesting only one* i*-band photometric measure is available for this star; its* I_C *magnitude should be treated with caution.*
d. In 2017 September, 000-BLS-549 was removed from the VSP list of comparison stars for KIC and replaced by this one, 000-BML-045, which also appears as "124" on new VSP finder charts.

Table 2. Photometric Nights.

Date	*Filter*	N_{std}	N_{fld}	c_0	c_1	c_2	*RMS*	N_{KIC}	*Weight*
2016/03/18	*V*	21	7	6.952	0.169	+0.002	0.053	3	1
2016/03/21	*V*	30	9	6.916	0.201	+0.031	0.051	5	2
2016/09/02	*V*	36	11	7.074	0.002	+0.026	0.066	4	1
2017/02/04	I_C	28	10	7.265	0.056	-0.034	0.037	8	1
2017/03/15	I_C	65	15	7.232	0.095	-0.063	0.050	23	2
2017/03/23	I_C	43	14	7.119	0.207	-0.017	0.044	18	1

Table 3. BGSU All-Sky Photometry.

Star	V	SEM_V	N_V	I_C	SEM_I	N_I	$V–I_C$
KIC	11.892	0.006	12	11.210	0.010	49	0.683
113	11.284	0.007	12	10.701	0.010	49	0.584
116	11.616	0.005	10	10.927	0.009	46	0.689
124[a]	12.461	0.009	12	11.492	0.011	49	0.969
128[b]	12.859	0.015	12	12.060	0.014	49	0.800
C1	10.314	0.008	6	10.015	0.014	48	0.299
C2	10.681	0.009	12	9.465	0.038	10	1.216
C3	12.444	0.010	12	11.317	0.015	49	1.127
C4[b]	12.404	0.012	12	10.897	0.016	49	1.507
C5	10.131	0.012	3	9.008	0.033	8	1.122
C6	11.731	0.008	12	10.551	0.014	49	1.180
C7	11.208	0.006	12	10.022	0.016	45	1.186
C8	11.574	0.012	12	10.346	0.014	49	1.228
C9[c]	13.285	0.029	12	12.152	0.015	49	1.133
C10	10.916	0.008	11	9.584	0.037	9	1.332
C11	12.342	0.010	12	10.882	0.014	46	1.460
C12	10.915	0.006	6	—	—	0	—
C13	11.288	0.009	6	—	—	0	—

a. A very low-amplitude rotational variable, KIC~8462696 is not a reliable comparison star.
b. Gary (2017) found a linear trend in brightness over four months, making this a questionable comparison star.
c. We suspect our V*-band photometry for star C9 is in error, and we recommend* $V = 13.35 \pm 0.02$ *and* $V–I_C = 1.20 \pm 0.03$ *mag for this star.*
Note: Comparison stars C5 and C10 were saturated on many of our images, while C12 and C13 were outside the field of view on all of our I*-band images.*

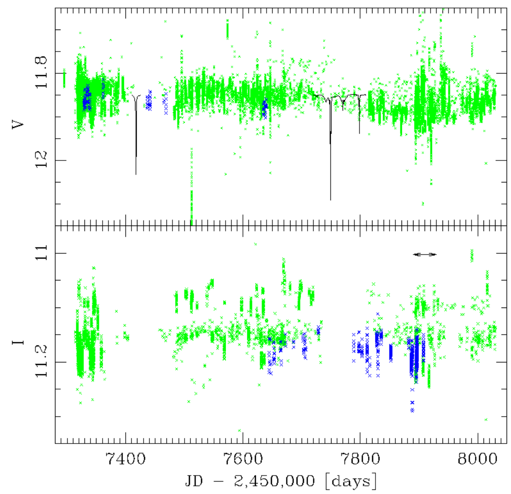

Figure 1. The time-series photometry of KIC 8462852 in the *V* (top panel) and I_C (bottom panel) from the AAVSO International Database, from inception to 2017 Oct 1, is shown as small green crosses. The larger blue crosses show our photometry (see section 2.2). The black curves in the top panel indicate the depth and duration of the first two major dimming events, observed by *Kepler* and presented in Figure 1 of Boyajian *et al.* (2016), at arbitrary times as described in section 1 (D800 is to the left, D1500 is to the right). The arrows in the bottom panel mark the 2017 May dimming episode noted in *AAVSO Alert Notice 579*.

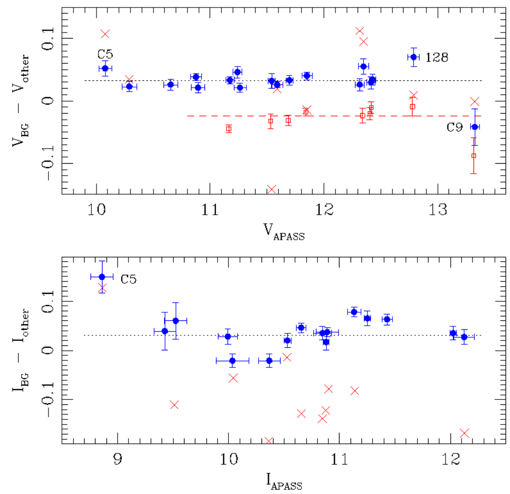

Figure 2. The magnitude difference between our comparison star magnitudes from Table 3 and the APASS photometry from Table 1 (circles), the Pan-STARRS photometry from Chambers *et al.* (2016) (crosses), and photometry from Gary (2017) (squares) is plotted as a function of APASS magnitude for the *V* (top) and I_C (bottom) passbands. The equations of Jordi *et al.* (2006) were used to transform the original APASS and Pan-STARRS photometry to VIC as described in section 2.1, where the labeled outlier points are also discussed. The dashed lines mark the median value for each data set.

standard system defined by Landolt (1992). More importantly, because different AAVSO observers may choose to use a different comparison star among the four available, systematic offsets might occur between the results of different AAVSO observers. Individually, such offsets might be interpreted as low-level dimming events, while collectively, the scatter they inject into the time-series might hinder detection of such dips.

Figure 1 shows the time-series *V* and I_C photometry of KIC downloaded from the AAVSO International Database (Kafka 2017; accessed 2017 Oct 3). In this data set, there are 30,497 measurements in *V*, 4158 in I_C, 7357 in *B*, 2666 in *R*, and including visual observations and measurements in other filter passbands the entire data set comprises an impressive 44,678 entries. Notice that in the lower panel, an "upper tier" of data exists with I_C brighter than 11.12 mag. The AAVSO Light Curve Generator (AAVSO 2017) was employed to recognize that comparison star 124 (AUID 000-BLS-549) was used in calibrating the vast majority of these points, whereas the vast majority of points in the lower tier used either comparison star 113 (000-BLS-551) or an ensemble of comparison stars (also see section 2). This underscores the importance of reliable comparison stars in obtaining a tight time series for KIC.

To further demonstrate the challenge for ground-based observers attempting to detect dimming events like those seen in KIC by the high-precision space-based *Kepler* photometry system, we have taken the large dips D800 and D1500 from Figure 1 of Boyajian *et al.* (2016), converted them from normalized flux into magnitudes, and placed them at arbitrary locations along the time axis of Figure 1 (for convenience of display; the actual dips occurred near Julian dates 2455626 and 2456353 days, respectively). Given the size of the dips in comparison with the photometric scatter, it is clear that every effort—including using precise and accurate comparison star magnitudes—must be made to minimize errors in the final time series of KIC and thereby improve the likelihood of detecting future dimming events, particularly smaller ones at the level of a few hundredths of a magnitude.

The median magnitudes of the AAVSO data shown in Figure 1 are 11.845 mag in *V* and 11.169 mag in I_C, after omitting data taken before the 2017 May dimming event (Boyajian *et al.* 2017) and all I_C data in the "upper tier." Their standard deviations are 0.033 and 0.025 mag in *V* and I_C, respectively. However, the median error the observers associated with their magnitude for KIC was about 0.007 mag for both filters. This represents an "internal" error estimate largely based on the signal and noise in an image, while the standard deviation is an "external" estimate of the typical uncertainty in a single observation that also includes photometric calibration effects. For both *V* and I_C, the relatively large standard deviations suggest that the calibration of the ~1%-level differential photometry obtained by AAVSO observers may be degraded in the calibration process by the standard photometry of the comparison stars, though part may be due to uncertainties in color-term corrections applied by individual observers. This led us to attempt higher quality all-sky photometry of KIC and its comparison stars, along with newly-proposed comparison stars that might be helpful for telescopes with larger apertures and/or smaller fields-of-view (these stars are listed as objects C1–C13 in the lower portion of Table 1).

2. Observations

We obtained images of KIC using the 0.5-m Cassegrain reflector at Bowling Green State University (BGSU) in Bowling Green, Ohio (latitude 41° 22' 42" N, longitude 83° 39' 33" W, elevation 225 m), using an Apogee Ap6e CCD camera having 1024 × 1024 pixels, each 24 µm in size, yielding a 21 × 21 arcmin field of view at a scale of 1.2 arcsec pixel^{-1}. We used custom colored glass filters ANDV4121 and ANDV4123 from the Andover Corporation to replicate the V and I_C passbands, respectively. Due to a malfunction of our filter wheel, we took all of the images on a given night, including flat field images of the clear twilight sky, in either V or I_C, meaning that contemporaneous photometry in the two passbands is not available. Images were processed using the flat field images along with bias and dark frames.

We elected to focus on the V and I_C passbands because of their common usage among AAVSO observers, their wide spectral separation, and the location of their peak throughputs in the redder half of the spectrum where many CCDs (including our own) have their highest quantum efficiency. Unlike the original *Kepler* observations, the use of two or more filters may help to distinguish between sources of dimming events caused by dust obscuration and grey transit events (Meng *et al.* 2017).

2.1. Photometric observations

On six very clear nights, we obtained images of the KIC field over an interval of 1–2 hours, interleaved with images of standard stars from Landolt (1992) or Clem and Landolt (2016) selected to span a wide range in color and airmass. The seeing on these images varied from 3–6 arcsec FWHM with a median of 4 arcsec. Aperture photometry, using a large aperture of 19 arcsec diameter to capture all the light in each star, was performed on the processed images. The resulting instrumental magnitudes (v) of each standard star at airmass (X) on a specific night were employed in a least-squares regression of the form

$$v - V = c_0 + c_1 X + c_2 (B-V), \qquad (1)$$

where V and $(B-V)$ are the standard magnitude and color from Landolt's lists. An analogous equation using i instrumental magnitudes, I_C standard magnitudes, and $(V-I_C)$ standard colors was employed for our long wavelength data. The details of these regressions are summarized in Table 2, in which the columns are (1) date of observation, (2) the filter employed, (3) the number of Landolt standard stars used that night, (4) the number of independent Landolt fields observed, (5)–(7) the coefficient values from Equation 1, (8) the root-mean-squared scatter of the observed magnitudes around the best-fit line for the Landolt standards, (9) the number of independent visits to the KIC field that night, and (10) the weight given to observations from that night (see below). Equatorial standards from Landolt (1992) were used during the first four nights, while standards at declination ~50° from Clem and Landolt (2016), much closer on the sky to the KIC field, were used during the last two nights.

Next, we solved Equation 1 for the standard magnitude (V or I_C) and used the coefficients c_0–c_2 from the fits along with a star's color ($B-V$ or $V-I_C$) from APASS found in Table 1 and our instrumental magnitude (v or i) for each star (comparison star or KIC) on each image taken during each photometric night (This non-standard procedure of assuming known, constant colors was necessitated by our malfunctioning filter wheel. We do not expect the colors of the comparison stars to vary from their values in Table 1, and the color of KIC might only vary if we happened to observe it during a dip. The somewhat large uncertainties on the APASS colors shown in Table 1 are reduced by the small color-term coefficients c_2 in Table 2, so we expect the resulting random errors in our photometry to be less than 0.003 mag in most cases, e.g., $c_2 \times (B-V)_{\rm err} = +0.031 \times 0.1$ mag. Our calibration of the field is thus not strictly independent, and small systematic offsets will be present if the APASS colors have systematic errors.)

We calculated the weighted mean of the N_{KIC} measurements for each star along with its standard error of the mean (SEM). Considering factors in Table 2 and beyond, particularly the values of the c_1 and c_2 coefficients in relation to their historical norms at our observatory, we judged the nights of 2016 March 21 in V and 2017 March 15 in I_C to be significantly better than the other nights, and gave them double weight in determining our final VI_C magnitudes of the comparison stars near KIC, which we list in Table 3. Had we adopted uniform weights, our mean magnitudes would be ~0.002 mag fainter in V and ~0.005 mag fainter in I_C than the values shown in this table. The SEM values in Table 3 describe the random uncertainties in the star-to-star magnitude ranking; uncertainty in the zero-points of our photometry may shift all the magnitudes systematically by an unknown amount. We computed the nightly mean magnitude of each star and calculated their standard deviation as an estimate of the overall uncertainty in our photometric zero-point, finding ~0.02 mag for a typical star. A particular star may have been overexposed or off the CCD field of view on some images, so the number of measurements in Table 3, N_V or N_I, may be less than the number of images available in that filter, N_{KIC}. The right-most column of Table 3 shows our estimate of each star's $V-I_C$ color, obtained by subtracting the non-contemporaneous V and I_C magnitudes in the table. While most of our new stars are redder than KIC itself, some observers who have determined their color-term coefficient c_2 with care may elect to use them because of their brightness or proximity to KIC.

Figure 2 shows the magnitude differences between our values and those found in APASS. In the case of the I-band, we used the I_C magnitudes from Table 1 which were converted from the original APASS Sloan i magnitudes as described in the Appendix. In the V-band panel, we see a flat relationship with a median offset of 0.032 mag and a standard deviation of 0.022 mag. In the I-band panel, the median offset is 0.031 mag with a larger standard deviation of 0.040 mag. The offsets in both V and I_C indicate that our magnitudes are systematically fainter than the APASS ones by about 1.5-times the estimated uncertainty in our photometric zero-point.

The brightest comparison star, C5, is an outlier in both panels of Figure 2, probably because the star was saturated in our images and those of APASS when the seeing was good. The original comparison star 128 and the new star C9 are outliers in V, perhaps because of their lower fluxes, though both are near the median value in I_C at the faint end of that distribution. If we reject these outliers, we obtain a standard deviation of 0.010 mag in V indicating a close correspondence between our magnitudes and those of APASS, though a systematic offset of 0.032 mag remains. Rejecting from the I_C data stars C2 and C10 (both of which are very bright in I_C and may suffer from saturation according to the APASS documentation) along with C5, we find a standard deviation of 0.029 mag and a median offset of 0.026 mag. Thus the star-to-star scatter between our magnitudes and those of APASS remains relatively large in I_C, and substantial zero-point shifts exist between these data sets in both V and I_C.

We require a third-party set of precision photometry to clarify whether the APASS or our photometry better represents the standard system. The Panoramic Survey Telescope and Rapid Response System (Pan-STARRS) project aims to provide high-precision digital photometry in the Sloan *grizy* bandpasses over most of the sky (Chambers *et al.* 2016). We accessed photometry from their recent Data Release 1 (accessed 2017 Oct 11) via the Mikulski Archive for Space Telescopes (Space Telesc. Sci. Inst. 2017) and found close positional matches for many of the stars in Table 1. However, after we transformed these magnitudes to VI_C using the relations in Jordi *et al.* 2006), we found large, random differences with respect to our data and the APASS data (see the crosses in Figure 2), making the Pan-STARRS data unhelpful in answering our question. This is not surprising since most of these stars are brighter than the Pan-STARRS saturation limit of 12–14 mag.

Recently, a post to the AAVSO Forum on the campaign for KIC by Dave Lane (2017) and Brad Walter's reply (Walter 2017) alerted the community to the variability of two of the comparison stars commonly used by AAVSO observers: star 124 (AUID 000-BLS-549) and star 128 (000-BLS-555), based on information in a webpage published by Gary (2017). In a reply post, Brad Walters confirmed that star 124 is identified in the SIMBAD database as a rotational variable with an optical magnitude range <0.01 mag and a period near 17 days (Reinhold *et al.* 2013), while star 128 is not a recognized variable star. Interestingly, star 124 is not an outlier in our Figure 2; the low-amplitude of its variations and that fact that we, and APASS, observed it multiple times at random phases suggests that any deviation from its mean value has been averaged out to below the scatter in this diagram. We also note that the low-amplitude, short-period variability of star 124 cannot by itself explain the 0.06-mag separation of the two "tiers" seen in the *I*-band panel of Figure 1. Since Lane's posting, it appears that the original star 124 (AUID 000-BLS-549) was removed from the VSP and replaced with a new comparison star (000-BML-045, our C3) with a similar magnitude. Unfortunately, this star also receives the label "124" on new VSP charts; users are encouraged to refer to these stars by their AUID number to avoid confusion.

In his unrefereed webpage, Gary (2017) presented all-sky *BV* photometry of 25 potential comparison stars within ~5 arcmin of KIC which he monitored over four months. He was able to detect the photometric variability of star 124 (his #24), and he saw a linear decline of $\Delta V \approx 0.005$ mag in the brightness of star 128 (his #20; he saw similar linear behavior in several other stars in the field). Eight of Gary's comparison stars are in common with our data shown in Table 3; the photometric comparison is shown by the squares in Figure 2. As was the case for the APASS comparison, the star C9 is ~0.07 mag below the other stars, suggesting that the photometric error is in our *V*-band data, and that $V = 13.35 \pm 0.02$ mag (the average of the APASS and Gary values) is a better estimate for this star. Ignoring C9, we see a tight relationship with a standard deviation of 0.013 mag and a median offset of –0.024 mag (–0.031 mag if the questionable stars 124 and 128 are also rejected). This systematic offset, in which Gary's magnitudes are fainter than ours, is in the opposite sense of the comparison with APASS.

While we acknowledge that Gary's description of his all-sky photometry is lacking specifics and has not been subject to scientific review, the fact that Gary's and the APASS photometry sets bracket our own encourages us to think that our *V*-band photometry has the most reliable zero-point calibration and thus may represent the best current estimates for the actual magnitudes of these stars. Unfortunately, third-party photometry in the *I*-band does not yet exist and so we remain uncertain about whether the APASS data or ours are to be preferred. In order to fully resolve the photometric zero-point of the comparison stars at the 0.01-mag level, we recommend new observations of comparison stars in the KIC field, including stars out to ±10 arcmin from KIC to include the commonly-used stars 116 and 113, along with other comparison stars on our list.

2.2. Differential observations

We obtained additional images of the KIC field on non-photometric nights. Together with the photometric images described above, we have 15 nights (102 images) in V and 29 nights (559 images) in I_C with which to study the time-series behavior of KIC. On each of these images, we measured the instrumental aperture magnitude of KIC and each comparison star (using an aperture of 6–9 arcsec diameter to reduce sky noise) and from them determined differentially the standard magnitude of KIC using the equation

$$V_v = V_c + v_v - v_c - c_2\,[(B-V)_v - (B-V)_c], \qquad (2)$$

where the v and c subscripts refer to the variable (KIC) and comparison star, respectively, the capital and lower-case letters again designate standard and instrumental magnitudes, and the $B-V$ colors were taken from Table 1. We used an analogous equation along with $(V-I_C)$ colors from Table 1 for the long wavelength data.

The classical approach to differential photometry of variable stars, practiced by most AAVSO observers, is to select one comparison star for use in the calibration and apply Equation 2 to produce a time series. A check star is then used to confirm the behavior. For the vast majority of variable stars, which exhibit a large amplitude or cyclic variations or both, this procedure is quite satisfactory. In the case of KIC, where the variations are both small and irregular, we need to be particularly careful about the selection of comparison stars, and we can take advantage of averaging over multiple comparison stars to reduce errors. We selected the ten most reliable stars from Table 3 and combined their ten magnitude estimates for KIC from each image using a weighted mean to get a best magnitude for the corresponding time, and used their SEM as a measure of the uncertainty in that ensemble magnitude. We did this for both V and I_C to produce our best data set, and repeated it using the APASS comparison star magnitudes from Table 1 for the same ten comparison stars to get a second time series that better matches the photometric zero-point of the AAVSO data; this data set is shown in Figure 1.

Six nights of our I_C data set are in the time range of the 2017 May dimming events reported in *AAVSO Alert Notice*

Table 4. BGSU Nightly Photometry.

JD[a]	*Date*	*Median* I_C	σ	*SEM*	N_{obs}	Δt
7882.90	May 9	11.189	0.005	0.002	10	0.015
7886.81	May 13	11.224	0.011	0.001	70	0.139
7888.82	May 15	11.215	0.030	0.004	49	0.130
7895.73	May 22	11.220	0.018	0.002	62	0.162
7896.72	May 23	11.207	0.014	0.001	90	0.077
7907.76	June 3	11.204	0.014	0.002	35	0.032
<7852	—	11.207	0.016	0.003	23	207

a. Julian Date after subtraction of 2450000 days. All dates in column 2 are in calendar year 2017.

Note: These data were calculated using BGSU magnitudes from Table 3 for the comparison stars; subtract 0.029 mag to get values equivalent to the APASS system from Table 1.

579 (AAVSO 2017b) and by Boyajian *et al.* (2017). In Table 4 we report the median magnitude from each of these six nights, their standard deviation (σ) and SEM, along with the number of images and the time span of the images that night (Δ*t*, in days). We computed similar nightly median magnitudes for our I_C data previous to 2017 April 9, when KIC was in its undimmed state. The final line of Table 4 reports the median and its statistics for these nightly values, and thus serves as a standard for comparison with our May nights. Only May 13, 15, and 22 are below this value, by 0.017, 0.008, and 0.013 mag, respectively. However, none deviates from the undimmed state by much more than 0.016 mag, the 1-σ level, so none are significantly below the pre-dip median. Nevertheless, it is intriguing that these three nights bracket the ~0.02 mag dip observed on May 18–19 reported by Boyajian *et al.* (2017).

Some of our data points from individual images drop to fainter magnitudes, in particular the six points near I_C = 11.3 mag at JD = 2457888.7 days shown in Figure 1. However, they show random scatter rather than a sequential progression of magnitude with time. Also, the magnitudes brighten by ~0.1 mag within fifteen minutes, much faster than the slopes of the D800 and D1500 events from Boyajian *et al.* (2016). These points are more likely due to poorly-calibrated pixels falling in the star aperture on these images, which suffered from higher than usual dark counts.

3. Conclusions

We obtained all-sky photometry of the enigmatic dimming star KIC 8462852 and its comparison stars in *V* and I_C using the 0.5-m telescope at BGSU. We obtained undimmed magnitudes of *V* = 11.892 and I_C = 11.210 mag for KIC, fainter than the APASS values by 0.04 and 0.08 mag, respectively, and ≳0.15 mag fainter than the *V* and I_C values from Boyajian *et al.* (2016). We estimated the uncertainty in our photometric zero-point to be ~0.02 mag, so these differences are significant. To aid our analysis and those of future studies, we provided photometry of thirteen additional comparison star candidates. Statistical analysis of these magnitudes with respect to their equivalents from APASS (Henden *et al.* 2015) and from unpublished work by Gary (2017) suggests that the star-to-star brightness differences in *V* are small, σ ≈ 0.01 mag, so that differential photometry using these stars will be reliable. However, the star-to-star differences among the I_C magnitudes are larger, σ ≈ 0.03 mag, suggesting that an observer's choice about which comparison star(s) to use in their differential photometry may significantly affect their resulting time-series data; this effect is probably responsible for some of the scatter seen in the current AAVSO *I*-band data shown in Figure 1. Furthermore, comparisons between the available data sets show that the overall photometric zero-points differ at the ~0.03 mag level. There is some evidence suggesting that our *V*-band photometric zero-point is the most reliable of the three, but it remains an open question whether the APASS data our ours provides the better photometric zero-point in I_C. We discuss shortcomings of the photometry for several of the current comparison stars of KIC 8462852 in section 2.1.

To address these problems, we recommend that new all-sky photometry be obtained from a clear, dark site using a low-noise CCD covering a field of view ≳20 arcmin. Multiple observations on at least three independent nights are desirable to reject outliers and average out random noise. Many visits to standard star fields from Clem and Landolt (2016) are needed to ensure a transformation to the standard system accurate to ≲ 0.01 mag. Obtaining such data in $BVRI_C$ will enable the recalibration, using an ensemble of comparison stars to reduce errors, of the full CCD-based AAVSO data set on KIC 8462852, currently over 44,000 measurements.

We also obtained time-series photometry of KIC 8462852 comprising 15 nights in *V* and 29 nights in I_C spanning 1.6 years. Three of these nights are near the 2017 May 18 dimming event reported by Boyajian *et al.* (2017), and while none indicates a dip deeper than 0.02 mag, each of the three measurements is up to 1-σ dimmer than the star's typical, pre-dip brightness. Together with data from other sources, including the recalibrated AAVSO data proposed above, these data may help to trace out the time history of the latest dimming event of this challenging, low-amplitude, irregular variable star.

4. Acknowledgements

We thank the anonymous referee for valuable suggestions that greatly improved this work. In particular, we appreciate the referee's drawing our attention to the AAVSO Forum post by Dave Lane, which in turn led us to the comparison star photometry by Bruce Gary. This work represents partial fulfillment of a Bachelor of Science degree in Physics at BGSU for AJL and DMD. Authors AJL and ACL greatly appreciate funding through BGSU's Center for Undergraduate Research and Scholarship. This research was made possible through the use of the AAVSO Photometric All-Sky Survey (APASS), funded by the Robert Martin Ayers Sciences Fund. The authors gratefully acknowledge the services of the AAVSO International Database (AID); some of the data acquired therefrom were made available by the British Astronomical Association Variable Star Section.

References

AAVSO. 2015a, *AAVSO Alert Notice 532* (October 20; https://www.aavso.org/aavso-alert-notice-532).
AAVSO. 2015b, AAVSO Variable Star Plotter (VSP; https://www.aavso.org/apps/vsp).
AAVSO. 2017a, AAVSO Light Curve Generator (https://www.aavso.org/LCGv2).
AAVSO. 2017b, *AAVSO Alert Notice 579* (May 24; https://www.aavso.org/aavso-alert-notice-579).
Ballesteros, F. J., Arnalte-Mus, P., Fernández-Soto, A., and Martínez, V. I. 2017, arXiv:1705.08427v2.
Borucki, W. J., *et al.* 2010, *Science*, **327**, 977 .
Boyajian, T., Croft, S., Wright, J., Siemion, A., Muterspaught, M., Siegel, M., Gary, B., Wright, S., Maire, J., Duenas, A., Hultgren, C., and Ramos, J. 2017, *Astron. Telegram*, No. 10405, 1.
Boyajian, T. S., *et al.* 2016, *Mon. Not. Roy. Astron. Soc.*, **457**, 3988.
Chambers, K. C., *et al.* 2016, arXiv:1612.05560.
Clem, J. L., and Landolt, A. U. 2016, *Astron. J.*, **152**, 91.
Gary, B. L. 2017, KIC 8462852 Reference Star Analysis (http://www.brucegary.net/ts3/RefStarAnal.html), posted 2017 Sep 10; accessed 2017 Dec 01.
Henden, A. A., and Munari, U. 2014, *Contrib. Astron. Obs. Skalnaté Pleso*, **43**, 518.
Henden, A. A., *et al.* 2015, AAVSO Photometric All-Sky Survey, data release 9 (http://www.aavso.org/apass).
Hippke, M., Angerhausen, D., Lund, M. B., Pepper, J., and Stassun, K. G. 2016, *Astrophys. J.*, **825**, 73.
Hippke, M., *et al.* 2017, *Astrophys. J.*, **837**, 85.
Jordi, K, Grebel, E. K., and Ammon, K. 2006, *Astron. Astrophys.*, **460**, 339.
Kafka, S. 2017, variable star observations from the AAVSO International Database (https://www.aavso.org/aavso-international-database).
Katz, J. I. 2017, *Mon. Not. Roy. Astron. Soc.*, **471**, 3680.
Landolt, A. U. 1992, *Astron. J.*, **104**, 340.
Lane, D. 2017, AAVSO forum posting #31 (2017 Sep 10; https://www.aavso.org/campaign-kic-8462852).
Meng, H. Y. A., *et al.* 2017, *Astrophys. J.*, **847**, 131.
Metzger, B. D., Shen, K. J., and Stone, N. 2017, *Mon. Not. Roy. Astron. Soc.*, **468**, 4399.
Montet, B. T., and Simon, J. D. 2016, *Astrophys. J., Lett.*, **830**, L39.
Reinhold, T., Reiners, A., and Basri, G. 2013, *Astron. Astrophys.*, **560A**, 4.
Schaefer, B. E. 2016, *Astrophys. J., Lett.*, **822**, L34.
Space Telescope Science Institute. 2017, Mikulski Archive for Space Telescopes (http://archive.stsci.edu/panstarrs/search.php).
Walter, B. 2017, AAVSO forum posting #32 (2017 Sep 10; https://www.aavso.org/campaign-kic-8462852).
Wright, J. T., Cartier, K. M. S., Zhao, M., Jontof-Hutter, D., and Ford, E. B. 2016, *Astrophys. J.*, **816**, 17.
Wright, J. T., and Sigurdsson, S. 2016, *Astrophys. J., Lett.*829, L3.

Appendix

To convert APASS photometry into the Cousins I_C equivalent, we utilized the equations in Table 4 of Jordi *et al.* (2006). Specifically, we solved their equation for bluer Population I stars,

$$r - R = 0.275\ (V–R) + 0.086, \qquad (3)$$

for R and entered a star's APASS photometry in the Johnson V and Sloan r bands to get its magnitude on the Cousins R_C system. Then, we solved their equation (also for Population I stars)

$$i - I = 0.251\ (R–I) + 0.325, \qquad (4)$$

for I and used the value of R_C output from the previous equation along with the star's APASS photometry in the Sloan i band to calculate its magnitude on the Cousins I_C system. We propagated the errors in the star's APASS photometry along with the errors in the coefficients for the equations above to obtain the uncertainty in the star's I_C magnitude, I_{err}. Both of these values are shown for each star in Table 1.

We assumed that the stars in the field of KIC are Population I stars because the Galactic latitude is low, $b = +6.64$ deg. If, however, a star belongs to Population II, its inferred I_C magnitude shown in Table 1 will be in error. To quantify the error, we calculated each star's I_C magnitude using the coefficients for the equations above appropriate for Population II stars (Jordi *et al.* 2006). The median difference between the Population I and II photometry is only +0.003 mag, and individual differences range from +0.037 mag for C1 to –0.009 mag for C11, where a positive deviation indicates that the Population II estimate is brighter. Given the relative frequencies of Population I and II stars in the Solar neighborhood, we think it unlikely that more than one or two stars are affected by this ambiguity; this could account for some of the outliers in Figure 2. However, a component of the overall scatter in this diagram is surely due to uncertainties in the transformation from APASS magnitudes in *Vri* to I_C magnitudes. For both these reasons, we advocate direct, high-quality I_C calibration of the comparison stars around KIC.

Visual Times of Maxima for Short Period Pulsating Stars II

Gerard Samolyk

P.O. Box 20677, Greenfield, WI 53220; gsamolyk@wi.rr.com

Received July 20, 2017; accepted July 20, 2017

Abstract This compilation contains 631 times of maxima of 8 short period pulsating stars (primarily RR Lyrae). These were reduced from a portion of the visual observations made from 1966 to 2014 that are included in the AAVSO International Database.

1. Observations

This is the second in a series of papers to publish of times of maxima derived from visual observations reported to the AAVSO International Database as part of the AAVSO RR Lyr committee legacy program. The goal of this project is to fill some historical gaps in the O–C history for these stars. This list contains times of maxima for RR Lyr stars located in the constellation Bootes. This list will be web-archived and made available through the AAVSO ftp site at ftp://ftp.aavso.org/public/datasets/gsamo-452-rrlyr-2.txt.

These observations were reduced by the writer using the PERANSO program (Vanmunster 2007). The linear elements in the *General Catalogue of Variable Stars* (GCVS; Kholopov *et al.* 1985) were used to compute the O–C values for all stars listed.

Figures 1, 2, and 3 are O–C plots for three of the stars listed.

References

Kholopov, P. N., et al. 1985, *General Catalogue of Variable Stars*, 4th ed., Moscow.

Samolyk, G. 2010, *J. Amer. Assoc. Var. Star Obs.,* **38**, 12.

Samolyk, G. 2011, *J. Amer. Assoc. Var. Star Obs.,* **39**, 23.

Samolyk, G. 2012, *J. Amer. Assoc. Var. Star Obs.,* **40**, 923.

Samolyk, G. 2013, *J. Amer. Assoc. Var. Star Obs.,* **41**, 85.

Samolyk, G. 2014, *J. Amer. Assoc. Var. Star Obs.,* **42**, 124.

Samolyk, G. 2015, *J. Amer. Assoc. Var. Star Obs.,* **43**, 74.

Samolyk, G. 2016, *J. Amer. Assoc. Var. Star Obs.,* **44**, 66.

Vanmunster, T. 2007, PERANSO period analysis software (http://www.peranso.com).

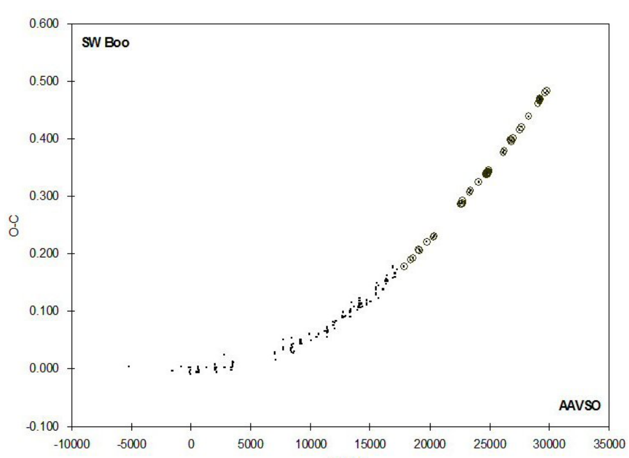

Figure 1. O–C plot for SW Boo. The circled times of maxima are from CCD papers published in *JAAVSO* (Samolyk 2010–2016).

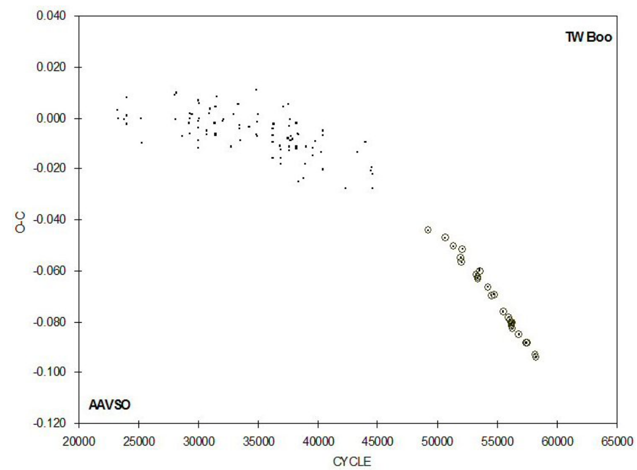

Figure 2. O–C plot for TW Boo. The circled times of maxima are from CCD papers published in *JAAVSO* (Samolyk 2010–2016).

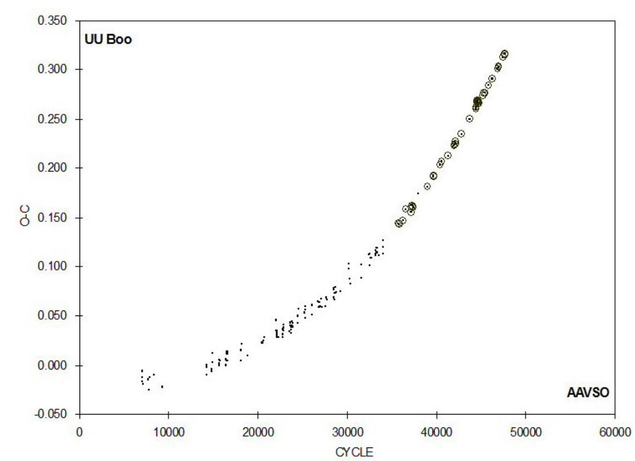

Figure 3. O–C plot for UU Boo. The circled times of maxima are from CCD papers published in *JAAVSO* (Samolyk 2010–2016).

Table 1. Recent times of minima of stars in the AAVSO short period pulsator program.

Star	JD (max) Hel. 2400000 +	Cycle	O–C (day)	Observer	Error (day)	Star	JD (max) Hel. 2400000 +	Cycle	O–C (day)	Observer	Error (day)
RS Boo	39169.880	–6892	0.010	M. Baldwin	0.004	RS Boo	47271.710	14579	–0.005	M. Baldwin	0.005
RS Boo	39197.784	–6818	–0.009	M. Baldwin	0.003	RS Boo	47276.626	14592	0.006	M. Baldwin	0.006
RS Boo	39203.838	–6802	0.008	M. Baldwin	0.006	RS Boo	47648.687	15578	0.011	M. Baldwin	0.007
RS Boo	39288.724	–6577	–0.008	M. Baldwin	0.004	RS Boo	47671.688	15639	–0.006	R. Hill	0.007
RS Boo	39316.664	–6503	0.009	M. Baldwin	0.007	RS Boo	48411.639	17600	–0.017	G. Samolyk	0.001
RS Boo	39319.680	–6495	0.007	M. Baldwin	0.007	RS Boo	48454.687	17714	0.015	M. Baldwin	0.004
RS Boo	39595.892	–5763	0.006	M. Baldwin	0.009	RS Boo	49443.671	20335	–0.007	M. Baldwin	0.003
RS Boo	39668.721	–5570	0.009	M. Baldwin	0.002	RS Boo	49460.662	20380	0.004	M. Baldwin	0.005
RS Boo	39671.733	–5562	0.002	M. Baldwin	0.002	RS Boo	49483.680	20441	0.004	M. Baldwin	0.003
RS Boo	39674.761	–5554	0.012	M. Baldwin	0.002	RS Boo	49529.712	20563	0.001	P. Goodwin	0.003
RS Boo	40400.743	–3630	–0.007	T. Cragg	0.005	RS Boo	49957.620	21697	0.007	M. Baldwin	0.004
RS Boo	40408.665	–3609	–0.009	L. Hazel	0.007	RS Boo	50158.730	22230	–0.005	R. Hill	0.009
RS Boo	40425.646	–3564	–0.008	L. Hazel	0.010	RS Boo	50184.776	22299	0.005	R. Hill	0.004
RS Boo	40437.726	–3532	–0.003	T. Cragg	0.002	RS Boo	50546.637	23258	–0.003	M. Baldwin	0.004
RS Boo	41043.734	–1926	–0.001	T. Cragg	0.005	RS Boo	50967.758	24374	0.008	R. Berg	0.005
RS Boo	41809.738	104	0.005	T. Cragg	0.002	RS Boo	51004.723	24472	–0.006	R. Berg	0.003
RS Boo	42155.763	1021	0.010	M. Baldwin	0.007	RS Boo	51021.698	24517	–0.011	R. Berg	0.003
RS Boo	42157.656	1026	0.016	M. Baldwin	0.004	RS Boo	51281.710	25206	0.014	R. Berg	0.006
RS Boo	42560.639	2094	0.001	M. Baldwin	0.002	RS Boo	51298.676	25251	0.000	R. Berg	0.007
RS Boo	42569.695	2118	0.001	M. Baldwin	0.008	RS Boo	51335.673	25349	0.018	R. Berg	0.006
RS Boo	42572.708	2126	–0.005	M. Baldwin	0.006	RS Boo	51627.698	26123	–0.018	R. Berg	0.007
RS Boo	42863.661	2897	0.020	M. Baldwin	0.005	RS Boo	51633.766	26139	0.013	R. Berg	0.003
RS Boo	42886.662	2958	0.003	M. Baldwin	0.004	RS Boo	51641.691	26160	0.014	R. Berg	0.003
RS Boo	42895.716	2982	0.001	M. Baldwin	0.006	RS Boo	51661.668	26213	–0.008	R. Berg	0.002
RS Boo	42898.737	2990	0.004	M. Baldwin	0.006	RS Boo	51667.719	26229	0.005	R. Berg	0.002
RS Boo	42903.643	3003	0.004	M. Baldwin	0.006	RS Boo	54237.779	33040	0.010	P. Soron	0.007
RS Boo	43244.762	3907	0.009	M. Baldwin	0.002	RS Boo	54649.453	34131	0.007	S. Swierczynski	0.003
RS Boo	43272.689	3981	0.013	M. Baldwin	0.005	RS Boo	54680.395	34213	0.007	S. Swierczynski	0.001
RS Boo	43315.707	4095	0.014	M. Baldwin	0.002	ST Boo	39287.723	32310	0.025	M. Baldwin	0.007
RS Boo	43626.625	4919	0.005	M. Baldwin	0.003	ST Boo	39310.719	32347	–0.004	M. Baldwin	0.006
RS Boo	43630.765	4930	–0.006	M. Baldwin	0.003	ST Boo	39315.696	32355	–0.005	M. Baldwin	0.004
RS Boo	43672.667	5041	0.011	M. Baldwin	0.004	ST Boo	39320.681	32363	0.001	M. Baldwin	0.002
RS Boo	44012.640	5942	0.002	M. Baldwin	0.006	ST Boo	39325.650	32371	–0.008	M. Baldwin	0.007
RS Boo	44335.646	6798	0.006	M. Baldwin	0.001	ST Boo	39343.688	32400	–0.016	M. Baldwin	0.006
RS Boo	44349.604	6835	0.002	M. Baldwin	0.005	ST Boo	39595.735	32805	0.003	M. Baldwin	0.004
RS Boo	44369.616	6888	0.015	M. Baldwin	0.004	ST Boo	39674.763	32932	0.000	M. Baldwin	0.008
RS Boo	44375.644	6904	0.006	M. Baldwin	0.003	ST Boo	39679.726	32940	–0.015	M. Baldwin	0.005
RS Boo	44410.748	6997	0.017	G. Hanson	0.006	ST Boo	39694.677	32964	0.001	M. Baldwin	0.004
RS Boo	44696.757	7755	0.003	M. Baldwin	0.006	ST Boo	39916.820	33321	–0.014	M. Baldwin	0.006
RS Boo	44701.665	7768	0.006	M. Baldwin	0.005	ST Boo	40333.784	33991	0.015	M. Baldwin	0.008
RS Boo	44704.681	7776	0.003	M. Baldwin	0.011	ST Boo	42165.824	36935	0.031	M. Baldwin	0.005
RS Boo	44727.707	7837	0.012	M. Baldwin	0.008	ST Boo	42531.713	37523	0.014	T. Cragg	0.006
RS Boo	45507.665	9904	0.010	G. Chaple	0.001	ST Boo	42567.814	37581	0.022	M. Baldwin	0.003
RS Boo	46173.661	11669	0.003	M. Baldwin	0.004	ST Boo	42569.696	37584	0.037	M. Baldwin	0.006
RS Boo	46176.691	11677	0.014	M. Baldwin	0.003	ST Boo	42887.699	38095	0.049	M. Baldwin	0.006
RS Boo	46193.655	11722	–0.002	M. Baldwin	0.006	ST Boo	42895.773	38108	0.033	M. Baldwin	0.011
RS Boo	46194.784	11725	–0.005	M. Baldwin	0.006	ST Boo	42897.657	38111	0.051	M. Baldwin	0.007
RS Boo	46511.763	12565	0.009	G. Samolyk	0.002	ST Boo	43612.647	39260	0.029	M. Baldwin	0.008
RS Boo	46519.685	12586	0.007	M. Baldwin	0.006	ST Boo	44365.638	40470	0.048	M. Baldwin	0.004
RS Boo	46531.766	12618	0.013	M. Baldwin	0.005	ST Boo	44686.737	40986	0.045	G. Hanson	0.002
RS Boo	46534.783	12626	0.011	M. Baldwin	0.004	ST Boo	44701.673	41010	0.046	M. Baldwin	0.007
RS Boo	46559.687	12692	0.011	R. Hill	0.010	ST Boo	45131.677	41701	0.047	M. Baldwin	0.010
RS Boo	46565.723	12708	0.009	R. Hill	0.006	ST Boo	46210.709	43435	0.027	M. Baldwin	0.006
RS Boo	46591.772	12777	0.022	R. Hill	0.007	ST Boo	46561.703	43999	0.049	M. Baldwin	0.003
RS Boo	46875.873	13530	–0.013	G. Samolyk	0.002	ST Boo	46912.686	44563	0.060	M. Baldwin	0.003
RS Boo	46914.756	13633	0.004	M. Baldwin	0.002	ST Boo	46996.680	44698	0.045	M. Baldwin	0.005
RS Boo	46916.643	13638	0.004	M. Baldwin	0.003	ST Boo	47024.685	44743	0.047	M. Baldwin	0.006
RS Boo	46939.666	13699	0.010	M. Baldwin	0.003	ST Boo	47243.754	45095	0.069	M. Baldwin	0.005
RS Boo	46942.688	13707	0.013	M. Baldwin	0.003	ST Boo	47299.735	45185	0.044	M. Baldwin	0.005
RS Boo	46945.697	13715	0.003	M. Baldwin	0.008	ST Boo	47683.687	45802	0.043	M. Baldwin	0.006
RS Boo	46948.717	13723	0.004	M. Baldwin	0.005	ST Boo	48330.908	46842	0.082	M. Baldwin	0.005
RS Boo	47002.682	13866	0.010	M. Baldwin	0.005	ST Boo	48421.730	46988	0.049	M. Baldwin	0.009
RS Boo	47161.905	14288	–0.004	G. Samolyk	0.003	ST Boo	48454.691	47041	0.029	M. Baldwin	0.006
RS Boo	47231.722	14473	0.005	M. Baldwin	0.005	ST Boo	48749.655	47515	0.027	M. Baldwin	0.009
RS Boo	47268.696	14571	0.000	M. Baldwin	0.006	ST Boo	50553.740	50414	0.091	M. Baldwin	0.002

Table continued on next page

Table 1. Recent times of minima of stars in the AAVSO short period pulsator program, cont.

Star	JD (max) Hel. 2400000 +	Cycle	O–C (day)	Observer	Error (day)
ST Boo	52489.640	53525	0.045	R. Berg	0.004
SW Boo	39916.850	–5168	0.003	M. Baldwin	0.009
SW Boo	41766.571	–1566	–0.004	M. Baldwin	0.004
SW Boo	42155.833	–808	0.004	M. Baldwin	0.006
SW Boo	42476.787	–183	0.003	M. Baldwin	0.005
SW Boo	42509.644	–119	–0.006	M. Baldwin	0.005
SW Boo	42531.735	–76	0.003	T. Cragg	0.003
SW Boo	42569.731	–2	–0.002	M. Baldwin	0.009
SW Boo	42570.763	0	0.003	M. Baldwin	0.006
SW Boo	42571.784	2	–0.003	M. Baldwin	0.006
SW Boo	42572.805	4	–0.009	M. Baldwin	0.005
SW Boo	42836.761	518	–0.007	M. Baldwin	0.003
SW Boo	42871.687	586	0.000	M. Baldwin	0.007
SW Boo	42873.746	590	0.004	M. Baldwin	0.005
SW Boo	42874.771	592	0.002	M. Baldwin	0.004
SW Boo	42891.709	625	–0.006	M. Baldwin	0.004
SW Boo	42895.820	633	–0.003	M. Baldwin	0.006
SW Boo	42907.631	656	–0.003	M. Baldwin	0.004
SW Boo	43272.756	1367	0.003	M. Baldwin	0.004
SW Boo	43610.651	2025	–0.003	M. Baldwin	0.004
SW Boo	43612.716	2029	0.007	M. Baldwin	0.004
SW Boo	43629.658	2062	0.003	M. Baldwin	0.005
SW Boo	43630.685	2064	0.003	M. Baldwin	0.005
SW Boo	43631.708	2066	–0.001	M. Baldwin	0.003
SW Boo	43669.709	2140	–0.001	M. Baldwin	0.003
SW Boo	43670.740	2142	0.003	M. Baldwin	0.005
SW Boo	43672.794	2146	0.003	M. Baldwin	0.009
SW Boo	43688.704	2177	–0.007	M. Baldwin	0.009
SW Boo	44010.716	2804	0.023	M. Baldwin	0.013
SW Boo	44012.749	2808	0.002	M. Baldwin	0.004
SW Boo	44049.723	2880	0.002	M. Baldwin	0.005
SW Boo	44313.677	3394	0.003	M. Baldwin	0.005
SW Boo	44314.699	3396	–0.002	M. Baldwin	0.005
SW Boo	44348.600	3462	0.006	M. Baldwin	0.003
SW Boo	44349.631	3464	0.010	M. Baldwin	0.006
SW Boo	44351.687	3468	0.012	M. Baldwin	0.008
SW Boo	44367.599	3499	0.004	M. Baldwin	0.001
SW Boo	44410.742	3583	0.011	G. Hanson	0.002
SW Boo	46196.811	7061	0.029	M. Baldwin	0.008
SW Boo	46210.672	7088	0.025	M. Baldwin	0.008
SW Boo	46233.771	7133	0.015	M. Baldwin	0.003
SW Boo	46531.652	7713	0.050	M. Baldwin	0.005
SW Boo	46532.667	7715	0.038	M. Baldwin	0.004
SW Boo	46534.720	7719	0.037	M. Baldwin	0.005
SW Boo	46550.639	7750	0.036	M. Baldwin	0.003
SW Boo	46553.717	7756	0.033	M. Baldwin	0.003
SW Boo	46857.728	8348	0.035	M. Baldwin	0.002
SW Boo	46858.751	8350	0.031	M. Baldwin	0.002
SW Boo	46861.833	8356	0.032	M. Baldwin	0.002
SW Boo	46877.754	8387	0.034	M. Baldwin	0.003
SW Boo	46893.668	8418	0.028	M. Baldwin	0.004
SW Boo	46910.639	8451	0.053	M. Baldwin	0.006
SW Boo	46911.648	8453	0.035	M. Baldwin	0.003
SW Boo	46912.680	8455	0.040	M. Baldwin	0.004
SW Boo	46914.736	8459	0.042	M. Baldwin	0.004
SW Boo	46951.705	8531	0.037	G. Samolyk	0.007
SW Boo	46973.777	8574	0.027	M. Baldwin	0.003
SW Boo	46974.820	8576	0.043	M. Baldwin	0.003
SW Boo	47025.646	8675	0.030	M. Baldwin	0.005
SW Boo	47271.643	9154	0.047	M. Baldwin	0.002
SW Boo	47293.722	9197	0.044	M. Baldwin	0.003
SW Boo	47296.809	9203	0.050	M. Baldwin	0.008
SW Boo	47331.723	9271	0.044	M. Baldwin	0.004
SW Boo	47670.668	9931	0.060	M. Baldwin	0.004
SW Boo	47747.686	10081	0.049	M. Baldwin	0.006
SW Boo	47942.832	10461	0.055	M. Baldwin	0.003
SW Boo	47976.726	10527	0.056	M. Baldwin	0.004
SW Boo	48089.706	10747	0.060	M. Baldwin	0.008
SW Boo	48357.774	11269	0.066	M. Baldwin	0.005
SW Boo	48411.684	11374	0.055	M. Baldwin	0.006
SW Boo	48412.728	11376	0.072	M. Baldwin	0.005
SW Boo	48413.753	11378	0.070	M. Baldwin	0.005
SW Boo	48414.772	11380	0.062	M. Baldwin	0.005
SW Boo	48415.802	11382	0.065	M. Baldwin	0.005
SW Boo	48452.777	11454	0.066	M. Baldwin	0.006
SW Boo	48469.720	11487	0.063	M. Baldwin	0.006
SW Boo	48682.853	11902	0.082	M. Baldwin	0.004
SW Boo	48685.928	11908	0.075	M. Baldwin	0.004
SW Boo	48752.686	12038	0.075	M. Baldwin	0.006
SW Boo	48771.682	12075	0.070	M. Baldwin	0.007
SW Boo	48774.773	12081	0.080	M. Baldwin	0.006
SW Boo	48810.724	12151	0.084	M. Baldwin	0.006
SW Boo	49073.658	12663	0.092	M. Baldwin	0.011
SW Boo	49095.737	12706	0.089	M. Baldwin	0.003
SW Boo	49117.828	12749	0.098	M. Baldwin	0.006
SW Boo	49134.764	12782	0.088	M. Baldwin	0.002
SW Boo	49154.793	12821	0.089	M. Baldwin	0.006
SW Boo	49155.820	12823	0.089	M. Baldwin	0.003
SW Boo	49188.687	12887	0.090	M. Baldwin	0.004
SW Boo	49241.582	12990	0.092	M. Baldwin	0.004
SW Boo	49401.810	13302	0.099	M. Baldwin	0.005
SW Boo	49416.693	13331	0.090	M. Baldwin	0.004
SW Boo	49417.729	13333	0.099	M. Baldwin	0.004
SW Boo	49433.640	13364	0.090	M. Baldwin	0.003
SW Boo	49434.667	13366	0.090	M. Baldwin	0.006
SW Boo	49451.623	13399	0.100	M. Baldwin	0.008
SW Boo	49457.788	13411	0.103	M. Baldwin	0.003
SW Boo	49474.747	13444	0.115	M. Baldwin	0.005
SW Boo	49602.608	13693	0.108	M. Baldwin	0.004
SW Boo	49743.822	13968	0.101	M. Baldwin	0.009
SW Boo	49778.746	14036	0.106	M. Baldwin	0.008
SW Boo	49780.803	14040	0.108	M. Baldwin	0.003
SW Boo	49812.647	14102	0.114	M. Baldwin	0.004
SW Boo	49813.678	14104	0.118	M. Baldwin	0.006
SW Boo	49832.683	14141	0.122	M. Baldwin	0.004
SW Boo	49835.754	14147	0.112	M. Baldwin	0.004
SW Boo	49873.749	14221	0.106	M. Baldwin	0.008
SW Boo	49927.676	14326	0.112	M. Baldwin	0.006
SW Boo	49928.699	14328	0.108	M. Baldwin	0.004
SW Boo	50138.737	14737	0.113	M. Baldwin	0.004
SW Boo	50153.627	14766	0.111	M. Baldwin	0.005
SW Boo	50154.661	14768	0.118	M. Baldwin	0.004
SW Boo	50158.770	14776	0.119	M. Baldwin	0.003
SW Boo	50305.636	15062	0.116	M. Baldwin	0.006
SW Boo	50518.775	15477	0.141	M. Baldwin	0.003
SW Boo	50534.682	15508	0.128	M. Baldwin	0.006
SW Boo	50542.902	15524	0.132	M. Baldwin	0.002
SW Boo	50553.692	15545	0.138	M. Baldwin	0.004
SW Boo	50573.732	15584	0.150	M. Baldwin	0.006
SW Boo	50666.675	15765	0.145	M. Baldwin	0.003
SW Boo	50668.707	15769	0.122	M. Baldwin	0.002
SW Boo	50842.809	16108	0.138	M. Baldwin	0.006
SW Boo	50938.853	16295	0.153	M. Baldwin	0.005
SW Boo	50951.687	16320	0.148	M. Baldwin	0.003
SW Boo	50952.721	16322	0.155	M. Baldwin	0.005
SW Boo	50990.729	16396	0.162	M. Baldwin	0.011
SW Boo	50991.748	16398	0.154	M. Baldwin	0.007
SW Boo	50992.774	16400	0.153	M. Baldwin	0.006
SW Boo	51027.693	16468	0.152	M. Baldwin	0.006
SW Boo	51259.813	16920	0.158	M. Baldwin	0.003

Table continued on next page

Table 1. Recent times of minima of stars in the AAVSO short period pulsator program, cont.

Star	JD (max) Hel. 2400000 +	Cycle	O–C (day)	Observer	Error (day)
SW Boo	51273.696	16947	0.175	M. Baldwin	0.005
SW Boo	51275.752	16951	0.177	M. Baldwin	0.004
SW Boo	51368.683	17132	0.160	M. Baldwin	0.004
SW Boo	51370.744	17136	0.166	M. Baldwin	0.004
SW Boo	51423.643	17239	0.172	M. Baldwin	0.004
SZ Boo	39288.670	22280	0.014	M. Baldwin	0.006
SZ Boo	39311.666	22324	0.006	M. Baldwin	0.003
SZ Boo	39323.686	22347	0.001	M. Baldwin	0.004
SZ Boo	39324.737	22349	0.006	M. Baldwin	0.006
SZ Boo	39598.698	22873	0.010	M. Baldwin	0.003
SZ Boo	39655.674	22982	–0.002	M. Baldwin	0.004
SZ Boo	39678.690	23026	0.010	M. Baldwin	0.006
SZ Boo	40324.891	24262	0.006	M. Baldwin	0.002
SZ Boo	40333.786	24279	0.013	M. Baldwin	0.005
SZ Boo	42531.719	28483	0.012	T. Cragg	0.003
SZ Boo	42567.795	28552	0.013	M. Baldwin	0.005
SZ Boo	42576.688	28569	0.018	M. Baldwin	0.002
SZ Boo	42898.734	29185	0.007	M. Baldwin	0.003
SZ Boo	43629.634	30583	0.005	M. Baldwin	0.006
SZ Boo	43630.692	30585	0.017	M. Baldwin	0.003
SZ Boo	43631.725	30587	0.005	M. Baldwin	0.006
SZ Boo	44375.701	32010	0.008	M. Baldwin	0.003
SZ Boo	44410.723	32077	0.001	G. Hanson	0.005
SZ Boo	44696.713	32624	0.009	M. Baldwin	0.005
SZ Boo	45496.620	34154	0.002	G. Chaple	0.004
SZ Boo	46150.682	35405	0.016	M. Baldwin	0.005
SZ Boo	46173.670	35449	0.000	M. Baldwin	0.003
SZ Boo	46527.618	36126	–0.001	M. Baldwin	0.005
SZ Boo	46550.616	36170	–0.007	M. Baldwin	0.003
SZ Boo	46563.707	36195	0.013	R. Hill	0.003
SZ Boo	46883.667	36807	0.008	M. Baldwin	0.005
SZ Boo	46905.627	36849	0.009	M. Baldwin	0.007
SZ Boo	46906.677	36851	0.014	M. Baldwin	0.007
SZ Boo	47242.830	37494	–0.007	M. Baldwin	0.005
SZ Boo	47260.627	37528	0.015	M. Baldwin	0.006
SZ Boo	47261.664	37530	0.006	M. Baldwin	0.004
SZ Boo	47296.695	37597	0.008	M. Baldwin	0.008
SZ Boo	47331.730	37664	0.014	M. Baldwin	0.005
SZ Boo	47650.639	38274	0.003	M. Baldwin	0.004
SZ Boo	47685.668	38341	0.003	M. Baldwin	0.004
SZ Boo	48006.681	38955	0.005	M. Baldwin	0.004
SZ Boo	48330.835	39575	0.010	M. Baldwin	0.005
SZ Boo	48452.656	39808	0.014	M. Baldwin	0.004
SZ Boo	48753.796	40384	0.010	M. Baldwin	0.003
SZ Boo	49095.721	41038	0.011	M. Baldwin	0.005
SZ Boo	49117.677	41080	0.009	M. Baldwin	0.005
SZ Boo	49208.645	41254	0.006	M. Baldwin	0.003
SZ Boo	49417.777	41654	0.010	M. Baldwin	0.004
SZ Boo	49428.750	41675	0.004	M. Baldwin	0.003
SZ Boo	49430.839	41679	0.002	M. Baldwin	0.003
SZ Boo	49450.710	41717	0.005	M. Baldwin	0.003
SZ Boo	49460.648	41736	0.010	M. Baldwin	0.004
SZ Boo	49483.649	41780	0.007	M. Baldwin	0.004
SZ Boo	49564.692	41935	0.013	M. Baldwin	0.004
SZ Boo	49873.667	42526	0.001	M. Baldwin	0.006
SZ Boo	50184.754	43121	0.010	R. Hill	0.007
SZ Boo	50285.657	43314	0.009	M. Baldwin	0.004
SZ Boo	50548.634	43817	0.008	M. Baldwin	0.004
SZ Boo	50629.666	43972	0.003	G. Chaple	0.008
SZ Boo	50926.638	44540	0.013	G. Samolyk	0.004
SZ Boo	50949.631	44584	0.002	G. Chaple	0.004
SZ Boo	50950.678	44586	0.003	M. Baldwin	0.007
SZ Boo	51040.603	44758	0.003	M. Baldwin	0.004
SZ Boo	51327.632	45307	0.004	G. Chaple	0.006
SZ Boo	51350.630	45351	–0.002	G. Samolyk	0.002
SZ Boo	51396.654	45439	0.014	M. Baldwin	0.002
TV Boo	39290.715	46971	–0.026	M. Baldwin	0.004
TV Boo	39311.687	47038	0.005	M. Baldwin	0.005
TV Boo	39315.723	47051	–0.022	M. Baldwin	0.007
TV Boo	39316.687	47054	0.004	M. Baldwin	0.016
TV Boo	39595.805	47947	0.006	M. Baldwin	0.005
TV Boo	39672.711	48193	0.023	M. Baldwin	0.012
TV Boo	41135.785	52874	0.006	T. Cragg	0.008
TV Boo	41766.532	54892	0.009	M. Baldwin	0.008
TV Boo	42531.692	57340	0.023	T. Cragg	0.005
TV Boo	42571.699	57468	0.023	M. Baldwin	0.007
TV Boo	42873.638	58434	0.029	M. Baldwin	0.005
TV Boo	42898.653	58514	0.040	M. Baldwin	0.006
TV Boo	42903.654	58530	0.040	M. Baldwin	0.009
TV Boo	43244.663	59621	0.046	M. Baldwin	0.013
TV Boo	43639.711	60885	0.019	M. Baldwin	0.012
TV Boo	43981.655	61979	0.023	M. Baldwin	0.006
TV Boo	43982.627	61982	0.058	M. Baldwin	0.008
TV Boo	45455.705	66695	0.043	M. Heifner	0.002
TV Boo	45471.646	66746	0.044	M. Baldwin	0.006
TV Boo	46193.663	69056	0.049	M. Baldwin	0.017
TV Boo	46529.648	70131	0.033	M. Baldwin	0.008
TV Boo	46534.654	70147	0.038	M. Baldwin	0.008
TV Boo	46544.664	70179	0.046	G. Samolyk	0.003
TV Boo	46910.683	71350	0.058	M. Baldwin	0.006
TV Boo	48029.650	74930	0.062	M. Baldwin	0.006
TV Boo	48746.666	77224	0.067	M. Baldwin	0.012
TV Boo	50280.676	82132	0.036	M. Baldwin	0.003
TV Boo	51705.655	86691	0.057	G. Samolyk	0.004
TW Boo	39293.768	23301	0.003	M. Baldwin	0.002
TW Boo	39315.643	23342	0.055	M. Baldwin	0.005
TW Boo	39325.701	23361	0.000	M. Baldwin	0.005
TW Boo	39556.707	23795	–0.001	M. Baldwin	0.005
TW Boo	39664.767	23998	0.008	M. Baldwin	0.005
TW Boo	39671.676	24011	–0.003	M. Baldwin	0.003
TW Boo	39672.744	24013	0.001	M. Baldwin	0.004
TW Boo	40331.697	25251	0.000	M. Baldwin	0.005
TW Boo	40357.769	25300	–0.010	T. Cragg	0.003
TW Boo	41815.684	28039	0.009	T. Cragg	0.002
TW Boo	41865.708	28133	–0.001	T. Cragg	0.007
TW Boo	41882.751	28165	0.010	T. Cragg	0.003
TW Boo	42155.790	28678	–0.007	M. Baldwin	0.004
TW Boo	42476.756	29281	–0.002	M. Baldwin	0.005
TW Boo	42508.696	29341	0.002	M. Baldwin	0.009
TW Boo	42509.753	29343	–0.006	M. Baldwin	0.005
TW Boo	42523.598	29369	0.000	M. Baldwin	0.003
TW Boo	42567.778	29452	0.001	M. Baldwin	0.004
TW Boo	42863.709	30008	–0.012	M. Baldwin	0.005
TW Boo	42871.701	30023	–0.004	M. Baldwin	0.008
TW Boo	42873.825	30027	–0.009	M. Baldwin	0.004
TW Boo	42886.607	30051	–0.001	M. Baldwin	0.005
TW Boo	42887.680	30053	0.007	M. Baldwin	0.006
TW Boo	42895.657	30068	0.000	M. Baldwin	0.006
TW Boo	42897.792	30072	0.006	M. Baldwin	0.008
TW Boo	42903.647	30083	0.006	M. Baldwin	0.005
TW Boo	43217.676	30673	–0.006	M. Baldwin	0.006
TW Boo	43241.628	30718	–0.007	M. Baldwin	0.006
TW Boo	43242.694	30720	–0.005	M. Baldwin	0.004
TW Boo	43340.639	30904	0.002	M. Baldwin	0.003
TW Boo	43373.642	30966	0.004	M. Baldwin	0.003
TW Boo	43612.627	31415	–0.002	M. Baldwin	0.005
TW Boo	43629.655	31447	–0.007	M. Baldwin	0.003
TW Boo	43630.720	31449	–0.006	M. Baldwin	0.006
TW Boo	43631.795	31451	0.004	M. Baldwin	0.004
TW Boo	43670.655	31524	0.008	M. Baldwin	0.006

Table continued on next page

Table 1. Recent times of minima of stars in the AAVSO short period pulsator program, cont.

Star	JD (max) Hel. 2400000 +	Cycle	O–C (day)	Observer	Error (day)
TW Boo	43967.654	32082	–0.001	M. Baldwin	0.006
TW Boo	43983.623	32112	0.000	M. Baldwin	0.003
TW Boo	44314.686	32734	–0.011	M. Baldwin	0.002
TW Boo	44453.622	32995	0.001	M. Baldwin	0.005
TW Boo	44630.873	33328	0.005	G. Hanson	0.004
TW Boo	44686.752	33433	–0.004	G. Hanson	0.004
TW Boo	44701.657	33461	–0.003	M. Baldwin	0.005
TW Boo	44726.668	33508	–0.009	M. Baldwin	0.004
TW Boo	45131.733	34269	–0.004	M. Baldwin	0.006
TW Boo	45459.628	34885	0.011	M. Baldwin	0.009
TW Boo	45460.675	34887	–0.006	M. Baldwin	0.007
TW Boo	45493.675	34949	–0.007	M. Baldwin	0.009
TW Boo	45509.649	34979	–0.002	G. Chaple	0.004
TW Boo	45550.637	35056	0.001	G. Chaple	0.003
TW Boo	46178.702	36236	–0.016	M. Baldwin	0.007
TW Boo	46193.612	36264	–0.010	M. Baldwin	0.005
TW Boo	46194.679	36266	–0.007	M. Baldwin	0.008
TW Boo	46196.811	36270	–0.004	M. Baldwin	0.003
TW Boo	46210.652	36296	–0.002	M. Baldwin	0.008
TW Boo	46523.620	36884	–0.011	M. Baldwin	0.004
TW Boo	46531.597	36899	–0.018	M. Baldwin	0.004
TW Boo	46532.667	36901	–0.013	M. Baldwin	0.006
TW Boo	46556.616	36946	–0.016	M. Baldwin	0.004
TW Boo	46679.591	37177	0.004	M. Baldwin	0.005
TW Boo	46831.809	37463	–0.008	M. Baldwin	0.006
TW Boo	46878.649	37551	–0.008	M. Baldwin	0.005
TW Boo	46881.856	37557	0.005	P. Atwood	0.005
TW Boo	46888.767	37570	–0.003	M. Baldwin	0.006
TW Boo	46894.614	37581	–0.011	M. Baldwin	0.007
TW Boo	46911.645	37613	–0.013	M. Baldwin	0.004
TW Boo	46944.650	37675	–0.009	M. Baldwin	0.005
TW Boo	46945.723	37677	0.000	M. Baldwin	0.007
TW Boo	46970.733	37724	–0.007	R. Hill	0.004
TW Boo	47002.668	37784	–0.009	M. Baldwin	0.004
TW Boo	47083.574	37936	–0.008	M. Baldwin	0.004
TW Boo	47233.671	38218	–0.012	M. Baldwin	0.007
TW Boo	47241.656	38233	–0.011	M. Baldwin	0.006
TW Boo	47242.730	38235	–0.002	M. Baldwin	0.007
TW Boo	47266.678	38280	–0.006	M. Baldwin	0.007
TW Boo	47299.660	38342	–0.025	M. Baldwin	0.004
TW Boo	47325.760	38391	–0.007	M. Baldwin	0.004
TW Boo	47557.814	38827	–0.024	M. Baldwin	0.004
TW Boo	47628.612	38960	–0.018	M. Baldwin	0.004
TW Boo	47670.668	39039	–0.012	M. Baldwin	0.004
TW Boo	47943.721	39552	–0.015	M. Baldwin	0.005
TW Boo	47976.725	39614	–0.012	M. Baldwin	0.005
TW Boo	48067.746	39785	–0.009	M. Baldwin	0.003
TW Boo	48331.749	40281	–0.014	M. Baldwin	0.008
TW Boo	48412.648	40433	–0.020	M. Baldwin	0.005
TW Boo	48413.726	40435	–0.007	M. Baldwin	0.005
TW Boo	48421.712	40450	–0.005	M. Baldwin	0.003
TW Boo	49428.750	42342	–0.028	M. Baldwin	0.005
TW Boo	49929.633	43283	–0.014	M. Baldwin	0.004
TW Boo	50285.728	43952	–0.009	M. Baldwin	0.005
TW Boo	50539.611	44429	–0.021	M. Baldwin	0.007
TW Boo	50564.629	44476	–0.020	M. Baldwin	0.006
TW Boo	50614.660	44570	–0.022	G. Chaple	0.003
TW Boo	50632.752	44604	–0.028	M. Baldwin	0.003
TW Boo	55377.403	53518	–0.059	J. Starzomski	0.008
UU Boo	39293.803	7024	–0.017	M. Baldwin	0.004
UU Boo	39310.720	7061	–0.006	M. Baldwin	0.006
UU Boo	39315.739	7072	–0.013	M. Baldwin	0.003
UU Boo	39348.631	7144	–0.019	M. Baldwin	0.006
UU Boo	39595.829	7685	–0.015	M. Baldwin	0.006
UU Boo	39655.675	7816	–0.026	M. Baldwin	0.004
UU Boo	39671.680	7851	–0.013	M. Baldwin	0.003
UU Boo	39918.877	8392	–0.010	M. Baldwin	0.003
UU Boo	40327.808	9287	–0.023	M. Baldwin	0.003
UU Boo	42571.767	14198	0.000	M. Baldwin	0.004
UU Boo	42572.671	14200	–0.010	M. Baldwin	0.003
UU Boo	42576.791	14209	–0.002	M. Baldwin	0.006
UU Boo	42873.788	14859	–0.004	M. Baldwin	0.004
UU Boo	42874.699	14861	–0.007	M. Baldwin	0.003
UU Boo	42895.736	14907	0.012	M. Baldwin	0.006
UU Boo	42917.659	14955	0.003	M. Baldwin	0.003
UU Boo	43228.819	15636	0.000	M. Baldwin	0.004
UU Boo	43244.813	15671	0.002	M. Baldwin	0.002
UU Boo	43245.730	15673	0.005	M. Baldwin	0.006
UU Boo	43272.688	15732	0.005	M. Baldwin	0.007
UU Boo	43606.692	16463	0.000	M. Baldwin	0.004
UU Boo	43610.811	16472	0.007	M. Baldwin	0.004
UU Boo	43612.638	16476	0.006	M. Baldwin	0.004
UU Boo	43626.803	16507	0.006	M. Baldwin	0.004
UU Boo	43631.837	16518	0.014	M. Baldwin	0.007
UU Boo	43654.673	16568	0.004	M. Baldwin	0.004
UU Boo	43669.760	16601	0.013	M. Baldwin	0.003
UU Boo	43670.672	16603	0.011	M. Baldwin	0.005
UU Boo	44349.660	18089	0.015	M. Baldwin	0.006
UU Boo	44365.642	18124	0.005	M. Baldwin	0.002
UU Boo	44375.711	18146	0.022	M. Baldwin	0.005
UU Boo	44731.640	18925	0.010	M. Baldwin	0.003
UU Boo	45447.647	20492	0.022	G. Chaple	0.003
UU Boo	45511.618	20632	0.024	G. Chaple	0.003
UU Boo	45532.640	20678	0.028	G. Chaple	0.005
UU Boo	46142.636	22013	0.035	M. Baldwin	0.005
UU Boo	46142.646	22013	0.045	G. Samolyk	0.003
UU Boo	46173.704	22081	0.032	M. Baldwin	0.004
UU Boo	46174.620	22083	0.035	M. Baldwin	0.005
UU Boo	46178.732	22092	0.034	M. Baldwin	0.005
UU Boo	46194.718	22127	0.028	M. Baldwin	0.005
UU Boo	46210.712	22162	0.030	M. Baldwin	0.003
UU Boo	46280.619	22315	0.028	M. Baldwin	0.008
UU Boo	46511.824	22821	0.031	G. Samolyk	0.002
UU Boo	46523.701	22847	0.028	M. Baldwin	0.004
UU Boo	46529.649	22860	0.036	M. Baldwin	0.005
UU Boo	46534.676	22871	0.037	M. Baldwin	0.004
UU Boo	46550.666	22906	0.035	M. Baldwin	0.004
UU Boo	46565.747	22939	0.038	R. Hill	0.006
UU Boo	46570.776	22950	0.041	R. Hill	0.002
UU Boo	46850.862	23563	0.034	M. Baldwin	0.003
UU Boo	46861.836	23587	0.042	M. Baldwin	0.008
UU Boo	46888.792	23646	0.040	M. Baldwin	0.005
UU Boo	46905.698	23683	0.040	M. Baldwin	0.004
UU Boo	46906.616	23685	0.044	M. Baldwin	0.004
UU Boo	46910.723	23694	0.039	M. Baldwin	0.001
UU Boo	46911.634	23696	0.036	M. Baldwin	0.003
UU Boo	46916.656	23707	0.032	M. Baldwin	0.003
UU Boo	46942.705	23764	0.036	M. Baldwin	0.004
UU Boo	46968.758	23821	0.045	R. Hill	0.003
UU Boo	46973.779	23832	0.040	M. Baldwin	0.003
UU Boo	46974.692	23834	0.039	M. Baldwin	0.005
UU Boo	47001.654	23893	0.042	M. Baldwin	0.003
UU Boo	47038.661	23974	0.039	M. Baldwin	0.005
UU Boo	47260.736	24460	0.051	M. Baldwin	0.008
UU Boo	47261.642	24462	0.043	M. Baldwin	0.005
UU Boo	47266.675	24473	0.050	M. Baldwin	0.006
UU Boo	47293.641	24532	0.057	M. Baldwin	0.006
UU Boo	47615.766	25237	0.053	R. Hill	0.004
UU Boo	47648.667	25309	0.056	M. Baldwin	0.007
UU Boo	47678.815	25375	0.047	R. Hill	0.002

Table continued on next page

Table 1. Recent times of minima of stars in the AAVSO short period pulsator program, cont.

Star	JD (max) Hel. 2400000 +	Cycle	O–C (day)	Observer	Error (day)	Star	JD (max) Hel. 2400000 +	Cycle	O–C (day)	Observer	Error (day)
UU Boo	47679.741	25377	0.059	R. Hill	0.011	UY Boo	44340.666	3849	–0.097	M. Baldwin	0.005
UU Boo	47685.669	25390	0.048	M. Baldwin	0.004	UY Boo	44342.628	3852	–0.088	M. Baldwin	0.009
UU Boo	47976.731	26027	0.051	M. Baldwin	0.002	UY Boo	44351.735	3866	–0.093	M. Baldwin	0.005
UU Boo	48004.613	26088	0.061	M. Baldwin	0.005	UY Boo	44353.685	3869	–0.095	M. Baldwin	0.006
UU Boo	48330.858	26802	0.065	M. Baldwin	0.005	UY Boo	44368.647	3892	–0.103	M. Baldwin	0.006
UU Boo	48353.703	26852	0.064	M. Baldwin	0.004	UY Boo	44407.704	3952	–0.096	G. Hanson	0.006
UU Boo	48364.664	26876	0.059	M. Baldwin	0.005	UY Boo	44696.677	4396	–0.094	M. Baldwin	0.008
UU Boo	48421.780	27001	0.060	M. Baldwin	0.004	UY Boo	44726.620	4442	–0.089	M. Baldwin	0.005
UU Boo	48454.686	27073	0.067	M. Baldwin	0.004	UY Boo	45464.646	5576	–0.113	M. Baldwin	0.003
UU Boo	48508.594	27191	0.059	M. Baldwin	0.004	UY Boo	46150.696	6630	–0.044	M. Baldwin	0.004
UU Boo	48685.880	27579	0.060	M. Baldwin	0.002	UY Boo	46174.764	6667	–0.057	M. Baldwin	0.005
UU Boo	48746.659	27712	0.068	M. Baldwin	0.003	UY Boo	46176.724	6670	–0.050	M. Baldwin	0.005
UU Boo	48762.650	27747	0.067	G. Samolyk	0.002	UY Boo	46193.637	6696	–0.059	M. Baldwin	0.004
UU Boo	49104.894	28496	0.077	M. Baldwin	0.005	UY Boo	46521.698	7200	–0.019	M. Baldwin	0.006
UU Boo	49117.679	28524	0.069	M. Baldwin	0.004	UY Boo	46523.649	7203	–0.021	M. Baldwin	0.005
UU Boo	49122.714	28535	0.078	M. Baldwin	0.006	UY Boo	46532.749	7217	–0.032	M. Baldwin	0.004
UU Boo	49133.676	28559	0.073	M. Baldwin	0.003	UY Boo	46534.702	7220	–0.032	M. Baldwin	0.004
UU Boo	49158.800	28614	0.067	M. Baldwin	0.002	UY Boo	46560.736	7260	–0.031	R. Hill	0.006
UU Boo	49208.611	28723	0.073	M. Baldwin	0.004	UY Boo	46564.687	7266	0.015	R. Hill	0.005
UU Boo	49213.643	28734	0.079	M. Baldwin	0.004	UY Boo	46601.726	7323	–0.044	R. Hill	0.008
UU Boo	49240.596	28793	0.074	M. Baldwin	0.002	UY Boo	46888.781	7764	–0.008	M. Baldwin	0.009
UU Boo	49483.679	29325	0.075	M. Baldwin	0.004	UY Boo	46894.632	7773	–0.014	M. Baldwin	0.005
UU Boo	49880.770	30194	0.102	R. Hill	0.008	UY Boo	46905.693	7790	–0.017	M. Baldwin	0.005
UU Boo	49901.784	30240	0.098	M. Baldwin	0.007	UY Boo	46935.627	7836	–0.022	M. Baldwin	0.005
UU Boo	49918.679	30277	0.087	M. Baldwin	0.004	UY Boo	46948.648	7856	–0.018	M. Baldwin	0.005
UU Boo	49955.685	30358	0.082	M. Baldwin	0.004	UY Boo	47233.733	8294	0.001	M. Baldwin	0.006
UU Boo	50539.635	31636	0.088	M. Baldwin	0.003	UY Boo	47604.721	8864	0.012	G. Samolyk	0.005
UU Boo	50542.847	31643	0.102	M. Baldwin	0.003	UY Boo	47621.651	8890	0.021	M. Baldwin	0.006
UU Boo	50921.645	32472	0.113	M. Baldwin	0.004	UY Boo	48005.695	9480	0.071	M. Baldwin	0.009
UU Boo	50958.644	32553	0.101	G. Chaple	0.003	UY Boo	48007.644	9483	0.067	M. Baldwin	0.005
UU Boo	50967.795	32573	0.114	R. Berg	0.005	UY Boo	48357.835	10021	0.108	M. Baldwin	0.003
UU Boo	51005.714	32656	0.108	R. Berg	0.004	UY Boo	48413.779	10107	0.081	M. Baldwin	0.005
UU Boo	51021.707	32691	0.109	R. Berg	0.003	UY Boo	48743.785	10614	0.112	M. Baldwin	0.011
UU Boo	51253.827	33199	0.113	M. Baldwin	0.004	UY Boo	48745.735	10617	0.110	M. Baldwin	0.005
UU Boo	51253.827	33199	0.113	R. Berg	0.002	UY Boo	49433.763	11674	0.204	M. Baldwin	0.009
UU Boo	51275.762	33247	0.116	M. Baldwin	0.004	UY Boo	49450.659	11700	0.178	M. Baldwin	0.004
UU Boo	51276.672	33249	0.112	M. Baldwin	0.003	UY Boo	49457.840	11711	0.199	M. Baldwin	0.004
UU Boo	51281.697	33260	0.111	R. Berg	0.005	UY Boo	49474.767	11737	0.204	M. Baldwin	0.006
UU Boo	51318.711	33341	0.115	M. Baldwin	0.005	UY Boo	49787.890	12218	0.276	M. Baldwin	0.006
UU Boo	51329.681	33365	0.119	G. Chaple	0.005	UY Boo	49812.682	12256	0.336	M. Baldwin	0.006
UU Boo	51420.601	33564	0.111	M. Baldwin	0.003	UY Boo	49813.782	12258	0.134	R. Hill	0.007
UU Boo	51629.879	34022	0.120	R. Berg	0.007	UY Boo	49920.693	12422	0.308	M. Baldwin	0.007
UU Boo	51641.752	34048	0.113	R. Hill	0.007	UY Boo	50222.732	12886	0.359	M. Baldwin	0.005
UU Boo	51657.758	34083	0.127	R. Berg	0.005	UY Boo	50518.880	13341	0.376	M. Baldwin	0.006
UU Boo	53445.736	37996	0.175	R. Huziak	0.003	UY Boo	50539.695	13373	0.364	M. Baldwin	0.004
UY Boo	39315.707	–3872	0.052	M. Baldwin	0.005	UY Boo	50542.928	13378	0.343	M. Baldwin	0.006
UY Boo	39330.672	–3849	0.048	M. Baldwin	0.005	UY Boo	50580.684	13436	0.351	M. Baldwin	0.006
UY Boo	42560.714	1114	–0.011	M. Baldwin	0.008	UY Boo	50923.681	13963	0.357	M. Baldwin	0.007
UY Boo	42586.627	1154	–0.132	M. J. Taylor	0.007	UY Boo	50951.644	14006	0.333	M. Baldwin	0.006
UY Boo	42873.709	1595	–0.070	M. Baldwin	0.006	UY Boo	50990.717	14066	0.357	M. Baldwin	0.007
UY Boo	43242.723	2162	–0.079	M. Baldwin	0.003	UY Boo	51007.639	14092	0.357	M. Baldwin	0.005
UY Boo	43244.676	2165	–0.080	M. Baldwin	0.006	UY Boo	51275.802	14504	0.376	M. Baldwin	0.005
UY Boo	43246.627	2168	–0.081	M. Baldwin	0.004	UY Boo	51318.756	14570	0.375	M. Baldwin	0.003
UY Boo	43626.678	2752	–0.118	M. Baldwin	0.004	UY Boo	54574.639	19572	0.773	G. Chaple	0.005
UY Boo	43654.664	2795	–0.118	M. Baldwin	0.005	UY Boo	54615.660	19635	0.792	G. Chaple	0.007
UY Boo	43669.640	2818	–0.112	M. Baldwin	0.009						

Recent Minima of 196 Eclipsing Binary Stars

Gerard Samolyk
P.O. Box 20677, Greenfield, WI 53220; gsamolyk@wi.rr.com

Received September 18, 2017; accepted September 18, 2017

Abstract This paper continues the publication of times of minima for eclipsing binary stars from observations reported to the AAVSO Eclipsing Binary section. Times or minima from observations received from February 2017 through August 2017 are presented.

1. Recent Observations

The accompanying list contains times of minima calculated from recent CCD observations made by participants in the AAVSO's eclipsing binary program. This list will be web-archived and made available through the AAVSO ftp site at ftp://ftp.aavso.org/public/datasets/gsamo-452.txt. This list, along with the eclipsing binary data from earlier AAVSO publications, is also included in the Lichtenknecker database administrated by the Bundesdeutsche Arbeitsgemeinschaft für Veränderliche Sterne e. V. (BAV) at: http://www.bav-astro.de/LkDB/index.php?lang=en. These observations were reduced by the observers or the writer using the method of Kwee and van Woerden (1956). The standard error is included when available. Column F indicates the filter used. A "C" indicates a clear filter.

The linear elements in the *General Catalogue of Variable Stars* (GCVS; Kholopov *et al.* 1985) were used to compute the O–C values for most stars. For a few exceptions where the GCVS elements are missing or are in significant error, light elements from another source are used: CD Cam (Baldwin and Samolyk 2007), AC CMi (Samolyk 2008), CW Cas (Samolyk 1992a), DV Cep (Frank and Lichtenknecker 1987), DF Hya (Samolyk 1992b), DK Hya (Samolyk 1990), EF Ori (Baldwin and Samolyk 2005), GU Ori (Samolyk 1985).

The light elements used for V376 And, IR Cnc, IU Cnc, DX CVn, DY CVn, YY CrB, V728 Her, V878 Her, V1034 Her, V1042 Her, V400 Lyr, V1128 Tau are from (Kreiner 2004).

The light elements used for GW Boo, NO Com, VW LMi, FG Lyn, and V502 Oph are from (Paschke 2014).

The light elements used for CC Lyn are from (Nelson 2014). O–C values listed in this paper can be directly compared with values published in the AAVSO EB monographs.

References

Baldwin, M. E., and Samolyk, G. 2005, *Observed Minima Timings of Eclipsing Binaries No. 10*, AAVSO, Cambridge, MA.
Baldwin, M. E., and Samolyk, G. 2007, *Observed Minima Timings of Eclipsing Binaries No. 12*, AAVSO, Cambridge, MA.
Frank, P., and Lichtenknecker, D. 1987, *BAV Mitt.*, No. 47, 1.
Kreiner, J. M. 2004, "Up-to-date linear elements of eclipsing binaries," *Acta Astron.*, **54**, 207 (http://www.as.up.krakow.pl/ephem/).
Kholopov, P. N., *et al.* 1985, *General Catalogue of Variable Stars*, 4th ed., Moscow.
Kwee, K. K., and van Woerden, H. 1956, *Bull. Astron. Inst. Netherlands*, **12**, 327.
Nelson, R. 2014, Eclipsing Binary O–C Files (https://www.aavso.org/bob-nelsons-o-c-files).
Paschke, A. 2014, "O–C Gateway" (http://var.astro.cz/ocgate/).
Samolyk, G. 1985, *J. Amer. Assoc. Var. Star Obs.*, **14**, 12.
Samolyk, G. 1990, *J. Amer. Assoc. Var. Star Obs.*, **19**, 5.
Samolyk, G. 1992a, *J. Amer. Assoc. Var. Star Obs.*, **21**, 34.
Samolyk, G. 1992b, *J. Amer. Assoc. Var. Star Obs.*, **21**, 111.
Samolyk, G. 2008, *J. Amer. Assoc. Var. Star Obs.*, **36**, 171.

Table 1. Recent times of minima of stars in the AAVSO eclipsing binary program.

Star	JD (min) Hel. 2400000 +	Cycle	O–C (day)	F	Observer	Error (day)
RT And	57963.8546	26747	–0.0121	V	G. Samolyk	0.0001
UU And	57978.8808	10986	0.0929	V	G. Samolyk	0.0002
WZ And	57952.8492	24553	0.0781	V	G. Samolyk	0.0001
AB And	57911.8644	65691	–0.0421	V	G. Samolyk	0.0002
AB And	57959.8225	65835.5	–0.0424	V	G. Samolyk	0.0001
BD And	57959.8655	49681	0.0163	V	G. Samolyk	0.0001
BX And	57974.8469	35151	–0.0951	V	G. Samolyk	0.0001
V376 And	57786.5340	6618.5	0.0135	V	K. Menzies	0.0002
XZ Aql	57936.8037	7495	0.1811	V	G. Samolyk	0.0001
KP Aql	57942.7315	5210.5	–0.0121	V	R. Sabo	0.0005
OO Aql	57912.8085	38082	0.0674	V	G. Samolyk	0.0001
OO Aql	57943.7219	38143	0.0667	V	G. Samolyk	0.0001
OO Aql	57978.6915	38212	0.0679	V	N. Simmons	0.0001
V343 Aql	57949.6506	15996	–0.0360	V	G. Samolyk	0.0003
V346 Aql	57910.8478	14455	–0.0134	V	G. Samolyk	0.0002
V346 Aql	57938.5069	14480	–0.0133	V	T. Arranz	0.0001
V346 Aql	57948.4648	14489	–0.0127	V	T. Arranz	0.0001
V346 Aql	57979.4424	14517	–0.0133	V	T. Arranz	0.0001
V346 Aql	57989.3999	14526	–0.0130	V	T. Arranz	0.0001
SS Ari	57790.6114	46214	–0.3718	V	G. Samolyk	0.0001
SS Ari	57984.8727	46692.5	–0.3785	V	R. Sabo	0.0002
RY Aur	57811.5580	7163	0.0193	V	G. Samolyk	0.0002
WW Aur	57815.7174	9849.5	0.0013	V	G. Samolyk	0.0001
AP Aur	57807.5633	26984	1.6258	V	G. Samolyk	0.0002
AP Aur	57824.6452	27014	1.6283	V	K. Menzies	0.0001
CL Aur	57787.5353	19946	0.1790	V	G. Samolyk	0.0001
CL Aur	57828.5993	19979	0.1790	V	G. Samolyk	0.0002
EM Aur	57803.5804	14716	–1.1098	V	G. Samolyk	0.0002

Table continued on following pages

Table 1. Recent times of minima of stars in the AAVSO eclipsing binary program, cont.

Star	JD (min) Hel. 2400000 +	Cycle	O–C (day)	F	Observer	Error (day)
EP Aur	57784.7104	53257	0.0153	V	K. Menzies	0.0003
EP Aur	57790.6202	53267	0.0151	V	G. Samolyk	0.0001
HP Aur	57832.5433	10596	0.0671	V	K. Menzies	0.0002
SS Boo	57878.5829	4888	7.0998	V	G. Samolyk	0.0002
TU Boo	57797.8204	76264.5	–0.1543	V	R. Sabo	0.0001
TU Boo	57844.6790	76409	–0.1551	V	G. Samolyk	0.0001
TU Boo	57844.8418	76409.5	–0.1544	V	G. Samolyk	0.0001
TU Boo	57886.6747	76538.5	–0.1545	V	N. Simmons	0.0001
TU Boo	57911.6452	76615.5	–0.1541	V	G. Samolyk	0.0001
TY Boo	57815.9054	73579	0.0698	V	G. Samolyk	0.0001
TY Boo	57832.8727	73632.5	0.0697	V	K. Menzies	0.0001
TY Boo	57895.5070	73830	0.0673	V	T. Arranz	0.0001
TY Boo	57897.4110	73836	0.0684	V	T. Arranz	0.0001
TY Boo	57915.4880	73893	0.0680	V	T. Arranz	0.0001
TY Boo	57918.5034	73902.5	0.0705	V	T. Arranz	0.0002
TY Boo	57920.7226	73909.5	0.0697	V	S. Cook	0.0004
TY Boo	57930.7105	73941	0.0674	V	R. Sabo	0.0001
TZ Boo	57526.6652	60215.5	0.0650	V	G. Lubcke	0.0003
TZ Boo	57526.6655	60215.5	0.0653	Ic	G. Lubcke	0.0003
TZ Boo	57526.6662	60215.5	0.0660	B	G. Lubcke	0.0004
TZ Boo	57788.9084	61098	0.0627	V	G. Samolyk	0.0001
TZ Boo	57824.8638	61219	0.0615	V	K. Menzies	0.0001
TZ Boo	57828.7276	61232	0.0622	V	G. Samolyk	0.0003
TZ Boo	57828.8773	61232.5	0.0633	V	G. Samolyk	0.0002
TZ Boo	57832.8878	61246	0.0621	V	K. Menzies	0.0001
TZ Boo	57887.7156	61430.5	0.0636	V	G. Samolyk	0.0002
TZ Boo	57910.4462	61507	0.0613	V	T. Arranz	0.0001
TZ Boo	57911.4892	61510.5	0.0642	V	T. Arranz	0.0001
TZ Boo	57914.7566	61521.5	0.0628	V	K. Menzies	0.0001
TZ Boo	57917.4315	61530.5	0.0633	V	T. Arranz	0.0002
TZ Boo	57925.4562	61557.5	0.0646	V	T. Arranz	0.0001
UW Boo	57807.9331	15331	–0.0012	V	G. Samolyk	0.0001
VW Boo	57788.9352	77750	–0.2629	V	G. Samolyk	0.0001
VW Boo	57866.6404	77977	–0.2655	V	G. Samolyk	0.0001
VW Boo	57882.7296	78024	–0.2656	V	R. Sabo	0.0001
AD Boo	57860.7774	15880	0.0352	V	G. Samolyk	0.0001
AD Boo	57919.7388	15937	0.0357	V	S. Cook	0.0005
GW Boo	57805.9387	9439.5	–0.0040	V	K. Menzies	0.0003
GW Boo	57811.7840	9450.5	–0.0057	V	K. Menzies	0.0002
i Boo	57906.6323	67412	0.1365	V	G. Persha	0.0002
CD Cam	57811.6565	6607	–0.0075	V	G. Samolyk	0.0003
WW Cnc	57841.4128	1700	0.0214	V	T. Arranz	0.0001
WW Cnc	57850.3409	1708	0.0219	V	T. Arranz	0.0001
WW Cnc	57851.4565	1709	0.0216	V	T. Arranz	0.0001
IR Cnc	57824.6700	7418	–0.0101	V	K. Menzies	0.0006
IU Cnc	57846.5540	12680	0.0134	V	K. Menzies	0.0001
BI CVn	57504.8008	34204	–0.2576	V	B. Harris	0.0002
DX CVn	57850.4343	14971	–0.0248	V	C. Beech	0.0001
DY CVn	57850.4758	21754	–0.0020	V	C. Beech	0.0001
R CMa	57786.7284	11882	0.1224	V	G. Samolyk	0.0001
TU CMa	57802.5758	27332	–0.0109	V	G. Samolyk	0.0001
TU CMa	57829.6454	27356	–0.0086	V	S. Cook	0.0004
TZ CMa	57797.6220	16047	–0.2230	V	G. Samolyk	0.0001
XZ CMi	57807.7457	26543	0.0034	V	G. Samolyk	0.0001
YY CMi	57828.6360	27244	0.0163	V	G. Samolyk	0.0001
AC CMi	57811.6545	6726	0.0046	V	K. Menzies	0.0001
AK CMi	57803.6638	25980	–0.0252	V	G. Samolyk	0.0001
RW Cap	57600.7741	4403	–0.6976	V	G. Samolyk	0.0004
RW Cap	57963.7399	4510	–0.7236	V	G. Samolyk	0.0001
TY Cap	57974.6911	9260	0.0940	V	G. Samolyk	0.0001
RZ Cas	57925.8270	12320	0.0777	V	G. Samolyk	0.0001
RZ Cas	57943.7558	12335	0.0778	V	N. Simmons	0.0001
AB Cas	57684.5991	10952	0.1345	V	N. Simmons	0.0001
AB Cas	57964.8104	11157	0.1367	V	G. Samolyk	0.0001
CW Cas	57973.7027	51249.5	–0.1080	V	G. Samolyk	0.0001
CW Cas	57973.8615	51250	–0.1086	V	G. Samolyk	0.0001
IR Cas	57938.8299	22881	0.0133	V	G. Samolyk	0.0001
OR Cas	57936.8538	11019	–0.0313	V	G. Samolyk	0.0004
PV Cas	57973.6340	10138	–0.0338	V	G. Samolyk	0.0002
SU Cep	57936.7064	35069	0.0062	V	G. Samolyk	0.0001
WZ Cep	57916.8596	71569.5	–0.1766	V	G. Samolyk	0.0002
DK Cep	57997.6928	24756	0.0310	V	K. Menzies	0.0001
DV Cep	57906.6860	9590	–0.0053	V	G. Samolyk	0.0001
DV Cep	57978.7283	9652	–0.0055	V	G. Samolyk	0.0001
EG Cep	57844.8943	28002	0.0113	V	G. Samolyk	0.0001
EG Cep	57890.6429	28086	0.0117	V	G. Samolyk	0.0001
EG Cep	57964.7106	28222	0.0108	V	N. Simmons	0.0001
GK Cep	57964.7036	20584	0.1416	V	N. Simmons	0.0002
RW Com	57784.9159	74838	0.0071	V	K. Menzies	0.0003
RW Com	57817.9076	74977	0.0078	V	K. Menzies	0.0001
RW Com	57856.4756	75139.5	0.0070	V	T. Arranz	0.0001
RW Com	57864.4276	75173	0.0080	V	T. Arranz	0.0001
RW Com	57870.7167	75199.5	0.0074	V	S. Cook	0.0004
RW Com	57890.6534	75283.5	0.0070	V	G. Samolyk	0.0001
RW Com	57914.6265	75384.5	0.0082	V	K. Menzies	0.0001
RW Com	57929.6986	75448	0.0088	V	R. Sabo	0.0003
RZ Com	57784.9665	67790.5	0.0530	V	K. Menzies	0.0007
RZ Com	57844.7143	67967	0.0545	V	G. Samolyk	0.0002
RZ Com	57905.6449	68147	0.0540	V	G. Samolyk	0.0001
SS Com	57803.8631	79460	0.9087	V	G. Samolyk	0.0003
SS Com	57880.6493	79646	0.9156	V	G. Samolyk	0.0004
SS Com	57888.4886	79665	0.9119	V	T. Arranz	0.0001
CC Com	57805.8279	82797.5	–0.0274	V	K. Menzies	0.0001
CC Com	57866.6275	83073	–0.0268	V	G. Samolyk	0.0001
CC Com	57909.6607	83268	–0.0275	V	G. Samolyk	0.0001
NO Com	57817.8342	3611	0.0258	V	K. Menzies	0.0004
RW CrB	57815.8630	23491	0.0026	V	G. Samolyk	0.0001
RW CrB	57896.4959	23602	0.0038	V	T. Arranz	0.0001
RW CrB	57904.4863	23613	0.0037	V	T. Arranz	0.0001
RW CrB	57912.4772	23624	0.0041	V	T. Arranz	0.0002
TW CrB	57825.8960	33840	0.0564	V	K. Menzies	0.0001
TW CrB	57881.8371	33935	0.0546	V	G. Samolyk	0.0001
YY CrB	57943.6692	14456	0.0224	V	G. Persha	0.0001
W Crv	57797.9380	46769	0.0197	V	G. Samolyk	0.0001
W Crv	57880.4063	46981.5	0.0208	V	T. Arranz	0.0002
W Crv	57881.3742	46984	0.0185	V	T. Arranz	0.0001
RV Crv	57857.7588	22520.5	–0.1161	V	G. Samolyk	0.0004
Y Cyg	57929.7199	16178.5	0.1305	V	G. Samolyk	0.0001
SW Cyg	57923.7254	3511	–0.3658	V	G. Samolyk	0.0001
WW Cyg	57925.7108	5289	0.1446	V	G. Samolyk	0.0001
ZZ Cyg	57910.8081	20538	–0.0733	V	G. Samolyk	0.0001
AE Cyg	57902.8564	13740	–0.0045	V	G. Samolyk	0.0001
BR Cyg	57916.6797	12290	0.0009	V	G. Samolyk	0.0001
BR Cyg	57952.6588	12317	0.0008	V	G. Samolyk	0.0001
BR Cyg	57952.6599	12317	0.0019	V	G. Persha	0.0002
CG Cyg	57939.7209	29335	0.0776	V	G. Samolyk	0.0001
CG Cyg	57942.8761	29340	0.0771	V	R. Sabo	0.0001
DK Cyg	57911.7943	42304	0.1175	V	G. Samolyk	0.0001
DK Cyg	57976.7511	42442	0.1190	V	R. Sabo	0.0002
KR Cyg	57905.8250	34076	0.0227	V	G. Samolyk	0.0001
MY Cyg	57928.8082	6012.5	0.0126	V	G. Samolyk	0.0001
MY Cyg	57952.8389	6018.5	0.0121	V	G. Samolyk	0.0002
MY Cyg	57958.8343	6020	–0.0002	V	R. Sabo	0.0002
V346 Cyg	57959.6493	8119	0.1927	V	G. Samolyk	0.0002
V387 Cyg	57939.7704	46760	0.0217	V	G. Samolyk	0.0001
V388 Cyg	57909.8319	18575	–0.1214	V	G. Samolyk	0.0001
V401 Cyg	57878.9478	24100	0.0886	V	R. Sabo	0.0001
V401 Cyg	57881.8613	24105	0.0885	V	G. Samolyk	0.0001
V456 Cyg	57931.7234	14610	0.0524	V	G. Samolyk	0.0001
V466 Cyg	57906.8372	20935	0.0079	V	G. Samolyk	0.0001
V548 Cyg	57959.6608	7480	0.0222	V	G. Samolyk	0.0001
V548 Cyg	57997.5680	7501	0.0195	V	K. Menzies	0.0002

Table continued on following pages

Table 1. Recent times of minima of stars in the AAVSO eclipsing binary program, cont.

Star	JD (min) Hel. 2400000 +	Cycle	O–C (day)	F	Observer	Error (day)
V704 Cyg	57931.7764	35031	0.0356	V	G. Samolyk	0.0003
V836 Cyg	57931.5581	20015	0.0226	V	T. Arranz	0.0001
V836 Cyg	57948.5482	20041	0.0240	V	T. Arranz	0.0001
V836 Cyg	57963.5756	20064	0.0230	V	T. Arranz	0.0001
V836 Cyg	57978.6036	20087	0.0224	V	T. Arranz	0.0001
V836 Cyg	57982.5243	20093	0.0226	V	T. Arranz	0.0001
V1034 Cyg	57963.6727	15380	0.0149	V	G. Samolyk	0.0002
TY Del	57949.8456	12585	0.0687	V	G. Samolyk	0.0001
YY Del	57964.8274	18920	0.0110	V	G. Samolyk	0.0001
FZ Del	57992.6936	34050	–0.0244	V	R. Sabo	0.0001
RZ Dra	57807.8936	24743	0.0677	V	G. Samolyk	0.0001
RZ Dra	57902.6439	24915	0.0677	V	G. Samolyk	0.0001
RZ Dra	57939.5522	24982	0.0674	V	T. Arranz	0.0001
RZ Dra	57944.5106	24991	0.0680	V	T. Arranz	0.0001
RZ Dra	57949.4685	25000	0.0680	V	T. Arranz	0.0001
RZ Dra	57951.6716	25004	0.0676	V	N. Simmons	0.0001
RZ Dra	57961.5881	25022	0.0684	V	T. Arranz	0.0001
RZ Dra	57978.6651	25053	0.0683	V	G. Samolyk	0.0001
TW Dra	57861.7453	4890	–0.0315	V	G. Samolyk	0.0001
UZ Dra	57881.6900	5001.5	0.0030	V	G. Samolyk	0.0001
AI Dra	57824.8927	12123	0.0363	V	G. Samolyk	0.0001
YY Eri	57786.5347	50404.5	0.1588	V	G. Samolyk	0.0001
TX Gem	57830.5625	13565	–0.0394	V	K. Menzies	0.0001
AL Gem	57807.7455	22628	0.0912	V	G. Samolyk	0.0001
SZ Her	57881.8227	19579	–0.0287	V	G. Samolyk	0.0001
SZ Her	57919.4540	19625	–0.0299	V	T. Arranz	0.0001
SZ Her	57923.5445	19630	–0.0299	V	T. Arranz	0.0001
SZ Her	57936.6348	19646	–0.0292	V	G. Samolyk	0.0001
SZ Her	57950.5419	19663	–0.0297	V	T. Arranz	0.0001
SZ Her	57959.5408	19674	–0.0299	V	T. Arranz	0.0001
TT Her	57880.8412	19609	0.0455	V	G. Samolyk	0.0001
TU Her	57905.7886	6107	–0.2455	V	G. Samolyk	0.0001
TU Her	57928.4587	6117	–0.2454	V	T. Arranz	0.0001
UX Her	57866.8257	11747	0.1309	V	G. Samolyk	0.0001
UX Her	57925.6838	11785	0.1328	V	G. Samolyk	0.0001
UX Her	57967.5035	11812	0.1336	V	T. Arranz	0.0001
AK Her	57909.6759	37301	0.0234	V	G. Persha	0.0001
CC Her	57922.5291	10527	0.3080	V	T. Arranz	0.0001
CC Her	57929.4656	10531	0.3085	V	T. Arranz	0.0001
CC Her	57962.4134	10550	0.3102	V	T. Arranz	0.0001
CT Her	57817.8854	8562	0.0124	V	K. Menzies	0.0002
CT Her	57921.4934	8620	0.0106	V	T. Arranz	0.0001
LT Her	57910.6330	15825	–0.1512	V	G. Samolyk	0.0005
LT Her	57911.7163	15826	–0.1519	V	N. Simmons	0.0003
LT Her	57923.6396	15837	–0.1531	V	G. Samolyk	0.0002
V728 Her	57910.6738	11480	0.0141	V	G. Samolyk	0.0001
V728 Her	57951.6756	11567	0.0134	V	G. Samolyk	0.0003
V878 Her	57915.6505	10228	–0.0066	V	G. Persha	0.0002
V1034 Her	57929.6331	6659	–0.0023	V	G. Silvis	0.0001
V1042 Her	57931.6756	10626	–0.0051	V	G. Silvis	0.0001
WY Hya	57804.5735	24069	0.0375	V	G. Silvis	0.0001
AV Hya	57811.6982	30931	–0.1150	V	K. Menzies	0.0001
AV Hya	57811.6993	30931	–0.1139	V	G. Samolyk	0.0001
DF Hya	57802.7122	45416.5	0.0036	V	G. Samolyk	0.0002
DF Hya	57863.7110	45601	0.0058	V	R. Sabo	0.0002
DI Hya	57845.6008	43356	–0.0357	V	G. Samolyk	0.0001
DK Hya	57797.7914	28652	0.0015	V	G. Samolyk	0.0002
SW Lac	57906.8628	39385	–0.0775	V	G. Samolyk	0.0001
SW Lac	57938.6128	39484	–0.0789	V	T. Arranz	0.0001
SW Lac	57952.5646	39527.5	–0.0785	V	T. Arranz	0.0001
SW Lac	57955.6114	39537	–0.0785	V	T. Arranz	0.0001
SW Lac	57967.6383	39574.5	–0.0787	V	T. Arranz	0.0001
SW Lac	57981.5906	39618	–0.0777	V	T. Arranz	0.0001
VX Lac	57969.8172	11830	0.0848	V	R. Sabo	0.0001
VX Lac	57997.7542	11856	0.0850	V	R. Sabo	0.0002
AR Lac	57978.7933	8262	–0.0516	V	N. Simmons	0.0001
DG Lac	57997.7004	6113	–0.2289	V	K. Menzies	0.0001
Y Leo	57788.7676	7326	–0.0667	V	G. Samolyk	0.0001
Y Leo	57844.4074	7359	–0.0682	V	T. Arranz	0.0001
Y Leo	57854.5253	7365	–0.0669	V	T. Arranz	0.0001
Y Leo	57876.4439	7378	–0.0677	V	T. Arranz	0.0001
UV Leo	57815.7069	32287	0.0433	V	G. Samolyk	0.0001
UV Leo	57830.7094	32312	0.0437	V	K. Menzies	0.0001
UV Leo	57848.4126	32341.5	0.0444	V	T. Arranz	0.0001
UV Leo	57866.4162	32371.5	0.0454	V	T. Arranz	0.0001
UV Leo	57872.4181	32381.5	0.0465	V	T. Arranz	0.0003
UV Leo	57893.4202	32416.5	0.0456	V	T. Arranz	0.0001
VZ Leo	57803.7467	24442	–0.0518	V	G. Samolyk	0.0003
VZ Leo	57875.6766	24508	–0.0556	V	S. Cook	0.0010
XY Leo	57784.8632	44739	0.1614	V	K. Menzies	0.0001
XY Leo	57845.6634	44953	0.1649	V	G. Samolyk	0.0002
XZ Leo	57842.6207	26279	0.0720	V	K. Menzies	0.0001
AM Leo	57810.4362	41873	0.0127	V	L. Corp	0.0002
AM Leo	57828.3599	41922	0.0123	R	L. Corp	0.0002
AM Leo	57880.6688	42065	0.0122	V	G. Samolyk	0.0003
AP Leo	57858.5885	42574	0.0020	V	G. Silvis	0.0001
AP Leo	57865.4751	42590	0.0029	V	L. Corp	0.0002
T LMi	57911.6428	4144	–0.1286	V	G. Samolyk	0.0002
VW LMi	57856.3860	19592	0.0247	V	L. Corp	0.0003
VW LMi	57860.4434	19600.5	0.0229	V	L. Corp	0.0002
SS Lib	57866.8134	11621	0.1752	V	G. Samolyk	0.0001
SS Lib	57928.6493	11664	0.1771	V	G. Samolyk	0.0001
SS Lib	57951.6585	11680	0.1784	V	G. Samolyk	0.0001
CC Lyn	57788.5516	6244	0.0140	V	G. Persha	0.0006
FG Lyn	57825.5789	4432	–0.0168	V	K. Menzies	0.0004
UZ Lyr	57902.8139	7515	–0.0419	V	G. Samolyk	0.0001
EW Lyr	57938.7290	16133	0.2838	V	G. Samolyk	0.0001
V400 Lyr	57931.7302	21433	–0.0155	G	M. Sadh	0.0003
V400 Lyr	57931.7309	21433	–0.0148	R	M. Sadh	0.0006
V400 Lyr	57931.8557	21433.5	–0.0167	R	M. Sadh	0.0006
V400 Lyr	57931.8591	21433.5	–0.0134	G	M. Sadh	0.0004
RW Mon	57786.7352	12647	–0.0852	V	G. Samolyk	0.0001
RW Mon	57830.5750	12670	–0.0856	V	K. Menzies	0.0001
BB Mon	57803.6724	42476	–0.0046	V	G. Samolyk	0.0001
BO Mon	57815.7355	6430	–0.0216	V	G. Samolyk	0.0001
EP Mon	57827.6151	21722	0.0261	V	G. Samolyk	0.0003
V501 Oph	57902.6834	27885	–0.0085	V	G. Samolyk	0.0001
V501 Oph	57964.6318	27949	–0.0089	V	G. Samolyk	0.0001
V502 Oph	57921.4992	20780	–0.0017	V	L. Corp	0.0002
V508 Oph	57905.6802	37191	–0.0269	V	G. Samolyk	0.0001
V508 Oph	57939.4707	37289	–0.0260	V	L. Corp	0.0001
V839 Oph	57949.6371	42790	0.3145	V	G. Samolyk	0.0002
V1010 Oph	57878.8412	28637	–0.1879	V	G. Samolyk	0.0005
V1010 Oph	57880.8241	28640	–0.1893	V	G. Samolyk	0.0001
V1010 Oph	57943.6588	28735	–0.1900	V	G. Samolyk	0.0001
EF Ori	57788.7031	3358	0.0067	V	G. Samolyk	0.0003
EQ Ori	57786.7027	15090	–0.0404	V	G. Samolyk	0.0002
ER Ori	57807.5755	38217	0.1324	V	G. Samolyk	0.0001
ER Ori	57827.6857	38264.5	0.1311	V	S. Cook	0.0004
FH Ori	57786.5766	14823	–0.4551	V	G. Samolyk	0.0002
FT Ori	57787.5693	5218	0.0207	V	G. Samolyk	0.0001
FT Ori	57831.6763	5232	0.0219	V	S. Cook	0.0002
FZ Ori	57802.5611	34446.5	–0.0356	V	G. Silvis	0.0001
FZ Ori	57811.5599	34469	–0.0365	V	K. Menzies	0.0001
GU Ori	57788.7403	31271.5	–0.0636	V	G. Samolyk	0.0002
U Peg	57951.8129	57207.5	–0.1645	V	G. Samolyk	0.0001
BB Peg	57926.8746	39177	–0.0266	V	R. Sabo	0.0001
BB Peg	57949.8313	39240.5	–0.0253	V	G. Samolyk	0.0002
BX Peg	57951.7154	49056.5	–0.1247	V	G. Samolyk	0.0002
BX Peg	57951.8552	49057	–0.1251	V	G. Samolyk	0.0002
BX Peg	57967.8385	49114	–0.1258	V	R. Sabo	0.0001
DI Peg	57972.8953	17949	0.0076	V	R. Sabo	0.0001

Table continued on following pages

Table 1. Recent times of minima of stars in the AAVSO eclipsing binary program, cont.

Star	*JD (min) Hel. 2400000 +*	*Cycle*	*O–C (day)*	*F*	*Observer*	*Error (day)*
GP Peg	57942.8029	17122	–0.0548	V	G. Samolyk	0.0001
KW Peg	57951.7139	11995.5	0.2121	V	G. Samolyk	0.0003
XZ Per	57817.6087	12426	–0.0743	V	K. Menzies	0.0001
IT Per	57684.7488	18453	–0.0391	V	N. Simmons	0.0002
V432 Per	57997.8297	68809.5	0.0297	V	K. Menzies	0.0001
RV Psc	57973.7965	60637	–0.0631	V	G. Samolyk	0.0002
UZ Pup	57786.7570	16573	–0.0102	V	G. Samolyk	0.0001
AV Pup	57828.6580	47903	0.2247	V	G. Samolyk	0.0001
U Sge	57910.8331	12063	0.0107	V	G. Samolyk	0.0001
V505 Sgr	57943.8541	11398	–0.1066	V	G. Samolyk	0.0001
V1968 Sgr	57925.8552	35695	–0.0190	V	G. Samolyk	0.0003
RS Ser	57949.6892	38499	0.0451	V	G. Samolyk	0.0002
RS Ser	57964.6428	38524	0.0452	V	G. Samolyk	0.0001
AO Ser	57942.6648	27076	–0.0108	V	G. Samolyk	0.0001
CC Ser	57878.8478	39527	1.1007	V	G. Samolyk	0.0004
CC Ser	57906.7139	39581	1.1025	V	G. Samolyk	0.0001
CC Ser	57952.6415	39670	1.1055	V	G. Samolyk	0.0002
Y Sex	57860.5983	38336	–0.0166	V	G. Samolyk	0.0002
WY Tau	57827.6119	29484	0.0652	V	G. Samolyk	0.0003
AC Tau	57788.5766	5947	0.1485	V	G. Samolyk	0.0001
AQ Tau	57787.6786	23137	0.5338	V	K. Menzies	0.0001
EQ Tau	57807.5846	51543.5	–0.0358	V	G. Samolyk	0.0001
V1128 Tau	57778.3388	17284.5	0.0001	R	L. Corp	0.0001
V Tri	57786.5469	56924	–0.0074	V	G. Samolyk	0.0001
TX UMa	57802.7122	4180	0.2290	V	G. Samolyk	0.0001
TY UMa	57817.6835	51573.5	0.3905	V	K. Menzies	0.0001
TY UMa	57878.6671	51745.5	0.3935	V	G. Samolyk	0.0001
UX UMa	57786.9201	103493	–0.0011	V	K. Menzies	0.0001
UX UMa	57842.7749	103777	–0.0009	V	K. Menzies	0.0001
UX UMa	57907.6763	104107	–0.0010	V	G. Samolyk	0.0001
VV UMa	57476.6726	16965	–0.0656	V	G. Lubcke	0.0001
VV UMa	57476.6729	16965	–0.0653	B	G. Lubcke	0.0002
VV UMa	57476.6730	16965	–0.0652	Ic	G. Lubcke	0.0002
VV UMa	57797.6737	17432	–0.0710	V	G. Samolyk	0.0001
VV UMa	57797.6745	17432	–0.0702	B	G. Lubcke	0.0001
VV UMa	57797.6746	17432	–0.0701	Ic	G. Lubcke	0.0001
VV UMa	57797.6746	17432	–0.0701	V	G. Lubcke	0.0001
VV UMa	57798.7053	17433.5	–0.0704	Ic	G. Lubcke	0.0003
VV UMa	57798.7066	17433.5	–0.0691	V	G. Lubcke	0.0006
VV UMa	57798.7075	17433.5	–0.0682	B	G. Lubcke	0.0011
VV UMa	57828.6061	17477	–0.0707	B	G. Lubcke	0.0001
VV UMa	57828.6061	17477	–0.0707	V	G. Lubcke	0.0001
VV UMa	57828.6063	17477	–0.0705	Ic	G. Lubcke	0.0001
VV UMa	57830.6685	17480	–0.0704	V	K. Menzies	0.0001
XZ UMa	57798.6597	9515	–0.1411	V	G. Samolyk	0.0001
AW UMa	57881.6430	30125.5	–0.1139	V	G. Persha	0.0002
RU UMi	57788.7201	30847	–0.0143	V	G. Samolyk	0.0001
VV Vir	57860.8295	59712	–0.0476	V	G. Samolyk	0.0003
AG Vir	57798.9299	19243	–0.0131	V	G. Samolyk	0.0003
AG Vir	57878.6157	19367	–0.0160	V	G. Samolyk	0.0001
AG Vir	57885.6853	19378	–0.0155	V	S. Cook	0.0004
AH Vir	57828.7977	29481	0.2861	V	G. Samolyk	0.0001
AH Vir	57851.4163	29536.5	0.2873	V	L. Corp	0.0001
AH Vir	57930.6789	29731	0.2870	V	S. Cook	0.0004
AK Vir	57886.6516	12827	–0.0392	V	G. Samolyk	0.0001
AW Vir	57811.8766	36128	0.0298	V	G. Samolyk	0.0002
AW Vir	57890.6396	36350.5	0.0285	V	G. Samolyk	0.0001
AW Vir	57931.7047	36466.5	0.0299	V	S. Cook	0.0003
AX Vir	57876.7469	43139	0.0252	V	G. Samolyk	0.0001
AX Vir	57921.7124	43203	0.0290	V	S. Cook	0.0008
AZ Vir	57811.8914	39567.5	–0.0228	V	G. Samolyk	0.0001
Z Vul	57939.7471	6107	–0.0125	V	G. Samolyk	0.0002
Z Vul	57976.5703	6122	–0.0133	V	T. Arranz	0.0001
AW Vul	57929.7880	14439	–0.0289	V	G. Samolyk	0.0001
AW Vul	57938.6601	14450	–0.0278	V	G. Samolyk	0.0001
AX Vul	57929.7615	6458	–0.0362	V	G. Samolyk	0.0001
BE Vul	57925.8473	11478	0.1053	V	G. Samolyk	0.0001
BE Vul	57964.6488	11503	0.1057	V	G. Samolyk	0.0001
BE Vul	57975.5135	11510	0.1061	V	T. Arranz	0.0001
BO Vul	57938.8180	11280	–0.0153	V	G. Samolyk	0.0001
BS Vul	57943.8421	30826	–0.0324	V	G. Samolyk	0.0001
BT Vul	57964.8505	19771	0.0053	V	G. Samolyk	0.0001
BU Vul	57925.8584	42869	0.0145	V	G. Samolyk	0.0001
BU Vul	57973.6536	42953	0.0143	V	G. Samolyk	0.0001

New Variable Stars Discovered by Data Mining Images Taken during Recent Asteroid Photometric Observations. II. Results from July 2015 through December 2016

Riccardo Papini
Wild Boar Remote Observatory (K49), via Potente 52, San Casciano in val di Pesa, Florence, 50026, Italy; riccardo.papini@yahoo.it

Alessandro Marchini
Astronomical Observatory, DSFTA - University of Siena (K54), via Roma 56, Siena, 53100, Italy; alessandro.marchini@unisi.it

Fabio Salvaggio
Wild Boar Remote Observatory (K49), Saronno, Italy Gruppo Astrofili Catanesi, Catania, Italy

Davide Agnetti
Osservatorio Aldo Agnetti di Lomazzo, Como, Italy

Paolo Bacci
GAMP Gruppo Astrofili Montagna Pistoiese (104), San Marcello Pistoiese, Italy

Massimo Banfi
Osservatorio di Nova Milanese (A25), Nova Milanese, Italy Osservatorio delle Prealpi orobiche (A36), Ganda di Aviatico, Italy

Giorgio Bianciardi
Telescopio Remoto UAI, Remote Telescope Unione Astrofili Italiani, Italy

Matteo Collina
Avalon Instruments Merlino, Aprilia, Italy

Lorenzo Franco
Balzaretto Observatory (A81), Rome, Italy

Gianni Galli
GiaGa Observatory (203), Pogliano Milanese, Italy Osservatorio Ca' del Monte (B14), Pavia, Italy

Mauro Ghiri
Alessandro Milani
Avogadro Observatory, Manciano, Italy

Claudio Lopresti
IRAS Istituto Spezzino Ricerche Astronomiche, La Spezia, Italy

Giuseppe Marino
Gruppo Astrofili Catanesi, Catania, Italy

Luca Rizzuti
Associazione Astropollino, Lauria, Italy

Nello Ruocco
Osservatorio Astronomico Nastro Verde (C82), Sorrento, Italy

Ulisse Quadri
Osservatorio Bassano Bresciano (565), Bassano Bresciano, Italy

Received November 3, 2017; revised November 27, 2017; accepted December 1, 2017

Abstract This paper follows the previous publication of new variables discovered at Astronomical Observatory, DSFTA, University of Siena, while observing asteroids in order to determine their rotational periods. Usually, this task requires time series images acquisition on a single field for as long as possible on a few nights not necessarily consecutive. Checking continually this "goldmine" allowed us to discover 57 variable stars not yet listed in catalogues or databases. While most of the new variables are eclipsing binaries, a few belong to the RR Lyrae or delta Scuti class. Since asteroid work is definitely a time-consuming activity, coordinated campaigns of follow-up with other observatories have been fundamental in order to determine the elements of the ephemeris and sometimes the right subclass of variability. Further observations of these new variables are therefore strongly encouraged in order to better characterize these stars, especially pulsating ones whose data combined with those taken during professional surveys seem to suggest the presence of light curve amplitude and period variations.

1. Introduction

In this paper, we present the results of the new variables discovered while taking CCD images for other purposes from July 2015 through December 2016 at the Astronomical Observatory of the University of Siena, inside the facilities of the Department of Physical Sciences, Earth, and Environment (DSFTA 2017). In fact, one of the many activities of the observatory, besides student mentoring in astronomy, is taking CCD images of asteroids for plotting their light curves in order to work out their synodic rotational period, and therefore plenty of images are available for checking for new variable stars (Papini *et al.* 2015). During that period, thanks to the remote control capabilities of the observatory, our group discovered 57 new variables—specifically, 46 eclipsing binaries and 11 short period pulsators—which include the 14 discovered in first half of 2015. In the end, new variable stars have been added to VSX (Variable Star Index) operated by the AAVSO, for sharing them with the larger community of professionals and amateurs (Watson *et al.* 2014).

2. Instrumentation and methods

We refer the reader to our previous paper (Papini *et al.* 2015) for a detailed description of the observation strategy, hardware and software systems, which characterized our observations that did not undergo any relevant change during the second season apart from new observers and therefore telescopes involved. Table 1 lists the main features of the instruments. Actually, all the variables were discovered in the images taken at the Astronomical Observatory of the University of Siena. For roughly half of these, the number of images was large enough for a complete characterization, but for the other half a follow-up involving other observers and telescopes was necessary to let the main scope at Siena keep on following asteroids and other institutional projects. Most of the authors that helped in the follow-up are members of the Variable Star Section of the Unione Astrofili Italiani (SSV-UAI 2017).

3. Results

In Table 2 we summarize the main parameters for the 57 new variables. Each of them can easily be looked for in the AAVSO VSX database through its identifier, as it appears in the first column. In the table, Epoch means time of maximum brightness for pulsating stars and time of primary minimum for eclipsing binaries.

Table 1. Observers and main features of the instruments used.

Observer	*Telescope**	*CCD*
Agnetti	11" SCT f/10	Sbig ST-10
Bacci (104)	23" NEW f/4.3	Apogee U7
Banfi (A25)	10" SCT f/5	Sbig ST-7
Banfi (A36)	20" NEW f/5	Sbig ST-9
Bianciardi	6" NEW f/5	Sbig ST-8XME
Collina	8" SCT f/10	QHYCCD QHY163M
Galli (B14)	9.25" SCT f/6.3	Sbig ST-8XME
Ghiri, Milani	8" RC f/4.6	ATIK One 6.0
Lopresti	7" MNT f/4	Sbig ST-10XME
Marchini (K54)	12" MCT f/5.6	Sbig STL-6303E
Marino	10" NEW f/4.8	Sbig ST-7XME
Rizzuti	8" SCT f/7	Sbig ST-7
Ruocco (C82)	10" SCT f/10	Sbig ST-7
Quadri (565)	12" SCH f/3.1	Starlight Trius SX9

** Telescope types: MCT—Maksutov-Cassegrain, MNT—Maksutov-Newton, NEW—Newton, RC—Ritchey–Chrétien, SCH—Schmidt, SCT—Schmidt-Cassegrain.*

Over 80% of the new variables are eclipsing binaries: 33 of them are EW type, 10 are EA type and 3 are EB type. The other 20% are mainly pulsating stars: 3 of them are HADS, 3 are RRc, 2 are DSCT, one is EC+BY, one is RRab/BL, and one is RRc/BL. Some of them show interesting peculiarities in their light curves, and are presented below.

3.1. GSC 00563-00194

GSC 00563-00194 shows very low amplitude periodic light curve variations. The frequency analysis has revealed a strong peak at about 2.91 cycles/day and a few weaker peaks. With the support of the VSX moderator, Sebastian Otero, we concluded that fast variation was not likely a real pulsation but the result of two red stars, one perhaps a BY Dra, rotating quickly around the common center of mass. The magnitude varies from 13.42 to 13.65 CV. In Figure 1, the light curve is phased with the period of the strongest peak of the power spectrum. Further observing of this star should be encouraged in order to refine the knowledge of this peculiar system.

3.2. GSC 00153-00900

GSC 00153-00900 is an eclipsing binary with a period of 0.330478 day that has a very low amplitude light curve variation between magnitudes 13.49 and 13.62 CV. It shows clearly the O'Connell effect (O'Connell 1951; Liu and Yang 2003) where the two out-of-eclipse maxima are of different brightnesses. No survey data were available for this star. In Figure 2, the light curve is phased with the main period of the binary.

Table 2. Main information and results for the new variables discovered.

Star (VSX identifier)	*R.A. (J2000)* h m s	*Dec. (J2000)* ° ′ ″	*Const.*	*V*	*Period* (days)	*Epoch* (HJD-2450000)	*Type*
UCAC4 458-000015	00 00 43.40	+01 34 07.7	Psc	15.38–15.66	0.292532 ± 0.000002	7641.6336 ± 0.0001	EW
2MASS J00211826+4233308	00 21 18.26	+42 33 30.8	And	16.30–16.71	0.235728 ± 0.000003	7248.5553 ± 0.0001	EW
GSC 01826-00950	04 06 29.72	+29 46 10.7	Tau	13.72–13.98	3.104790 ± 0.000003	7366.3030 ± 0.0002	EA
GSC 01274-01261	04 37 06.22	+19 37 06.1	Tau	13.65–14.08	0.350189 ± 0.000002	7377.5471 ± 0.0002	EW
GSC 01849-01030	05 06 18.62	+24 44 48.4	Tau	14.41–14.87	0.528494 ± 0.000003	7729.4341 ± 0.0002	EW
UCAC4 574-014734	05 13 23.13	+24 47 27.5	Tau	15.27–15.63	0.401251 ± 0.000003	7730.5028 ± 0.0002	EW
CMC15 J051332.5+245225	05 13 32.51	+24 52 25.7	Tau	16.44–17.19	0.263871 ± 0.000003	7723.3653 ± 0.0002	EW
UCAC4 575-015133	05 13 33.05	+24 53 47.3	Tau	15.45–15.57	0.079055 ± 0.000003	7730.3316 ± 0.0002	DSCT
UCAC4 575-015216	05 14 03.89	+24 57 07.4	Tau	15.64–15.85	0.510915 ± 0.000003	7730.4856 ± 0.0002	EW
UCAC4 574-014986	05 14 54.57	+24 36 10.0	Tau	14.35–15.28	0.305952 ± 0.000003	7722.3963 ± 0.0002	EW
UCAC4 574-015078	05 15 40.84	+24 44 16.6	Tau	15.58–15.87	0.469001 ± 0.000003	7730.4662 ± 0.0002	EW
UCAC4 576-015082	05 17 36.38	+25 01 50.4	Tau	15.25–16.05	0.330558 ± 0.000003	7721.6502 ± 0.0002	EW
UCAC4 593-021345	05 42 28.61	+28 24 52.4	Tau	15.13–15.50	1.072244 ± 0.000005	7387.4874 ± 0.0003	EA
UCAC4 593-021583	05 44 07.39	+28 31 40.8	Tau	15.77–16.55	1.275370 ± 0.000004	7384.3341 ± 0.0003	EW
UCAC4 617-029871	05 55 14.35	+33 17 15.4	Aur	16.35–16.73	0.584840 ± 0.000003	7750.5405 ± 0.0002	EW
UCAC4 617-029939	05 55 29.30	+33 20 24.2	Aur	16.18–16.33	0.342309 ± 0.000003	7744.4945 ± 0.0002	EW
CMC15 J055640.5+331906	05 56 40.56	+33 19 07.0	Aur	16.40–16.80	0.487440 ± 0.000003	7751.4689 ± 0.0002	EW
UCAC4 617-030583	05 58 19.23	+33 17 15.5	Aur	15.41–15.83	0.464030 ± 0.000003	7744.5700 ± 0.0002	EW
UCAC4 623-031110	06 09 03.11	+34 31 25.5	Aur	15.13–15.42	0.395718 ± 0.000003	7738.4823 ± 0.0002	EW
GSC 02428-00994	06 10 43.14	+34 38 50.1	Aur	13.20–13.69	0.854036 ± 0.000003	7731.6384 ± 0.0002	EA
UCAC4 625-030777	06 11 13.37	+34 49 15.1	Aur	16.78–17.19	0.534203 ± 0.000003	7740.6175 ± 0.0002	EW
UCAC4 625-030811	06 11 25.00	+34 49 22.0	Aur	15.92–16.25	0.272109 ± 0.000003	7738.4233 ± 0.0002	EW
UCAC4 549-029087	06 32 51.16	+19 40 26.8	Gem	16.12–16.46	0.35234 ± 0.00003	7746.5757 ± 0.0002	EW
GSC 00153-00641	06 57 57.90	+02 44 55.1	Mon	13.88–14.18	0.845821 ± 0.000003	7440.28477 ± 0.00003	EA
UCAC4 464-024612	06 58 33.84	+02 46 10.5	Mon	15.09–15.27	0.300049 ± 0.000003	7424.41937 ± 0.00002	EW
GSC 00153-00900	06 58 37.32	+02 39 53.1	Mon	13.49–13.62	0.330478 ± 0.000004	7424.27473 ± 0.00002	EW
GSC 01357-00941	07 06 09.29	+21 23 08.8	Gem	13.78–14.88	0.606386 ± 0.000005	7858.4307 ± 0.0003	EB
GSC 01357-00131	07 07 28.08	+20 54 40.5	Gem	12.60–12.83	0.372912 ± 0.000003	7752.41947 ± 0.00003	EW
UCAC4 555-037258	07 07 39.59	+20 57 04.2	Gem	15.03–15.25	0.30430 ± 0.00003	7753.3270 ± 0.0002	EW
GSC 01357-00639	07 08 50.00	+21 10 29.2	Gem	14.01–15.01	0.51556 ± 0.00003	7754.5389 ± 0.0002	EB
UCAC4 555-037760	07 10 53.56	+20 52 24.1	Gem	16.18–16.71	0.37237 ± 0.00003	7753.4253 ± 0.0002	EW
GSC 00777-00241	07 32 48.17	+14 31 11.8	Gem	14.09–14.84	0.659291 ± 0.000005	7409.6781 ± 0.0003	EA
GSC 00777-00233	07 33 57.85	+14 34 46.2	Gem	13.44–13.88	0.322852 ± 0.000003	7373.6834 ± 0.0002	RRc
GSC 00913-01147	14 31 19.78	+10 00 42.7	Boo	13.68–13.83	0.303115 ± 0.000003	7489.43435 ± 0.00003	EW
UCAC4 424-061076	14 58 05.48	–05 17 22.1	Lib	14.90–15.60	0.290211 ± 0.000003	7495.45966 ± 0.00002	EW
UCAC4 501-063071	16 03 24.62	+10 05 09.0	Ser	14.93–15.15	0.347757 ± 0.000003	7515.6348 ± 0.0002	EW
UCAC4 374-078489	16 57 05.54	–15 19 29.0	Oph	16.03–16.75	0.858035 ± 0.000003	7545.4693 ± 0.0001	EA
UCAC4 373-080823	16 58 40.03	–15 33 07.7	Oph	16.66–17.40	0.307275 ± 0.000001	7545.5041 ± 0.0001	EW
UCAC4 373-080978	16 59 41.41	–15 32 34.3	Oph	14.45–15.56	0.447718 ± 0.000003	7564.5318 ± 0.0001	RRab/BL
UCAC4 371-080964	17 06 11.75	–15 59 34.3	Oph	15.09–15.78	0.331897 ± 0.000001	7538.552 ± 0.002	EW
UCAC4 373-082585	17 08 29.46	–15 35 43.1	Oph	15.53–16.01	0.077260 ± 0.000003	7536.4818 ± 0.0001	HADS
UCAC4 372-080369	17 09 02.69	–15 44 44.5	Oph	14.24–14.77	0.296369 ± 0.000003	7591.4285 ± 0.0001	RRc
UCAC4 372-080463	17 09 26.20	–15 40 53.9	Oph	15.39–15.85	0.263596 ± 0.000003	7536.4684 ± 0.0001	RRc
UCAC4 373-083099	17 10 29.47	–15 33 08.9	Oph	15.46–15.95	0.072193 ± 0.000003	7539.3864 ± 0.0001	HADS
GSC 05747-01746	20 08 13.41	–12 48 31.6	Cap	13.23–13.49	1.989495 ± 0.000003	7227.4105 ± 0.0004	EA
GSC 04263-01334	22 06 08.81	+60 12 04.1	Cep	12.03–12.34	0.553207 ± 0.000002	7615.6304 ± 0.0001	EB
UCAC4 753-074179	22 07 51.61	+60 29 09.6	Cep	12.71–12.94	0.697644 ± 0.000016	7643.5687 ± 0.0001	EW
2MASS J22080014+6026144	22 08 00.14	+60 26 14.5	Cep	17.40–17.90	0.594572 ± 0.000002	7615.5067 ± 0.0001	EW
GSC 05806-01614	22 09 17.60	–10 08 40.1	Aqr	14.74–14.84	0.041375 ± 0.000003	7654.4345 ± 0.0002	DSCT
UCAC4 751-072394	22 09 21.69	+60 06 48.4	Cep	15.45–15.72	0.439675 ± 0.000002	7615.5778 ± 0.0001	EW
UCAC4 751-072412	22 09 29.80	+60 03 26.4	Cep	14.18–14.54	1.273040 ± 0.000002	7615.5520 ± 0.0001	EA
UCAC4 751-072684	22 10 45.65	+60 04 23.2	Cep	15.50–15.94	4.291477 ± 0.000004	7615.5190 ± 0.0003	EA
2MASS J22111437+6002162	22 11 14.37	+60 02 16.3	Cep	16.41–16.83	0.546590 ± 0.000022	7635.5256 ± 0.0001	EW
UCAC4 700-108862	22 19 05.70	+49 53 26.6	Lac	14.45–14.78	0.70440 ± 0.00003	7233.3997 ± 0.0002	EA
GSC 00563-00194	22 28 19.26	+03 22 02.4	Peg	13.42–13.65	0.343580 ± 0.000005	7603.4517 ± 0.0003	EC+BY
UCAC4 442-129803	23 51 44.10	–01 46 28.0	Psc	15.34–15.89	0.392769 ± 0.000003	7657.5208 ± 0.0002	RRc/BL
GSC 00587-00276	23 55 14.60	+00 03 22.2	Psc	13.80–14.13	0.078703 ± 0.000002	7651.4269 ± 0.0001	HADS

3.3. GSC 00913-01147

GSC 00913-01147 is an eclipsing binary with a period of 0.303115 day that has a very low amplitude light curve variation of only 0.15 magnitude between 13.68 and 13.83 CV. It shows clearly the O'Connell effect. Data from CRTS survey were available for this star. In Figure 3, the light curve is phased with the main period of the binary.

3.4. UCAC4 373-080978

UCAC4 373-080978 is an RRab stars with a period of 0.447718 day and an amplitude of about 1.1 magnitude between 14.45 and 15.56 CV. It shows a slight amplitude light curve variation compared to the old data from the CRTS survey. This behavior is often associated with the Blazhko effect (Blazhko 1907). In Figure 4, the light curve is phased with the main period of the pulsator.

3.5. UCAC4 442-129803

UCAC4 442-129803 is an RRc star with a period of 0.392769 day and an amplitude of 0.55 magnitude between 15.34 and 15.89 CV. It shows clearly a phase light curve variation compared to the old data from CRTS survey. This behavior is often associated with the Blazhko effect. In Figure 5, the light curve is phased with the main period of the pulsator.

4. Conclusions

After having observed asteroids for about one year and half in order to determine their mean light curves and periods, we have collected thousands of images, many of which are centered for the entire night on the same field. Doing variable star search in these fields allowed us to discover 57 new variable stars, specifically, 46 eclipsing binaries and 11 short period pulsators. The details of each of the new variable stars are given in Table 2 in order of increasing Right Ascension. Phase plots for few peculiar stars are shown in Figures 1 through 5.

5. Acknowledgements

The authors firstly want to thank Alessio Batazzi, a student of the course in Physics and Advanced Technologies, who attended some observing sessions at the Astronomical Observatory of the University of Siena during his internship activities and helped us in preparing this paper.

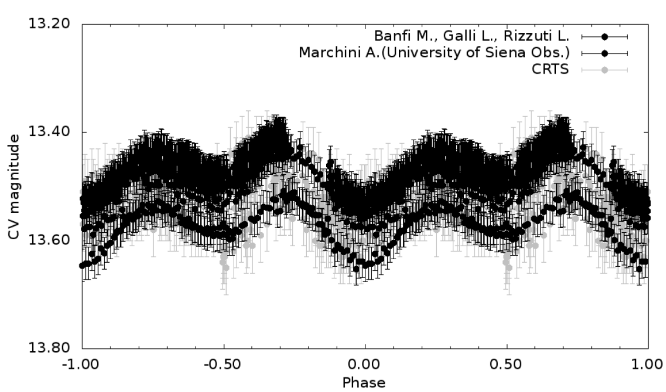

Figure 1. Folded light curve of GSC 00563-00194.

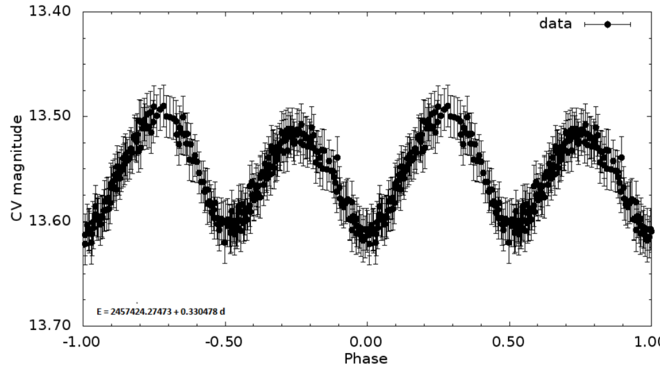

Figure 2. Folded light curve of GSC 00153-00900.

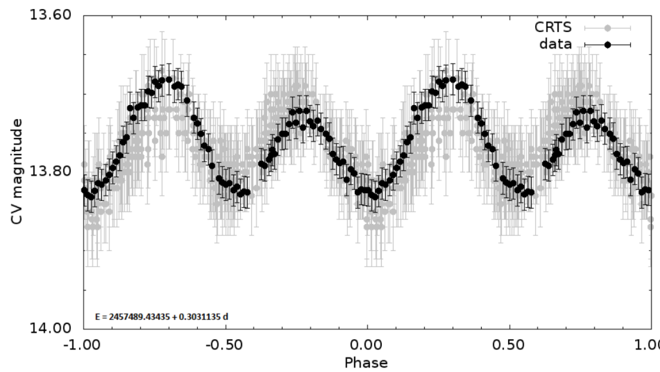

Figure 3. Folded light curve of GSC 00913-01147.

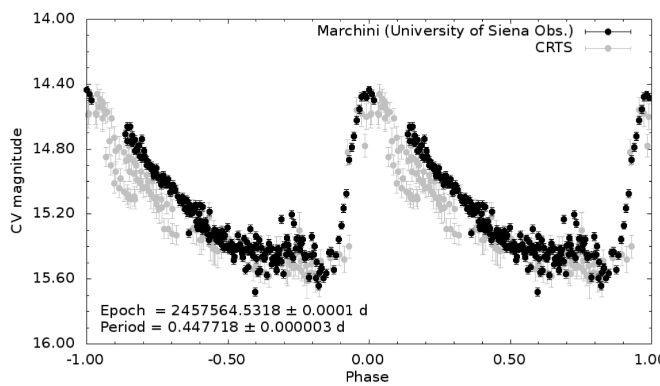

Figure 4. Folded light curve of UCAC4 373-080978.

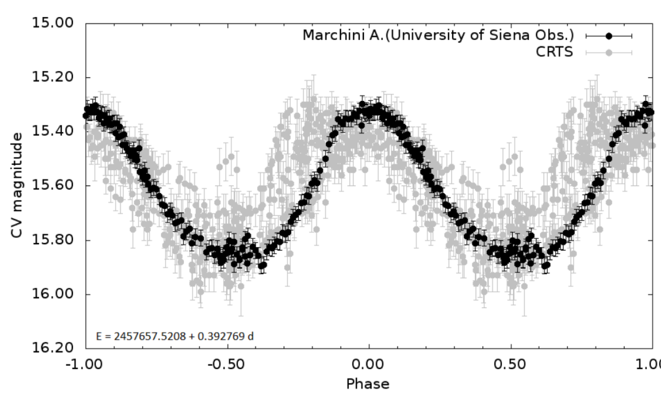

Figure 5. Folded light curve of UCAC4 442-129803.

We gladly thank here Sebastian Otero, too, one of the VSX moderators, who kindly and eagerly helped us during the submission process with most valuable suggestions that were always crucial.

This work has made use of the VizieR catalog access tool, CDS, Strasbourg, France, the ASAS catalog, the CRTS catalog, the NSVS catalog, and of course the International Variable Star Index (VSX) operated by the AAVSO.

This publication makes use of data products from the Two Micron All Sky Survey, which is a joint project of the University of Massachusetts and the Infrared Processing and Analysis Center/California Institute of Technology, funded by the National Aeronautics and Space Administration and the National Science Foundation.

In the end, we acknowledge with thanks the variable star observations from the AAVSO International Database contributed by observers worldwide and used in this research.

References

Blazhko, S. 1907, *Astron. Nachr.*, **175**, 325.

DSFTA. 2017, Department of Physical Sciences, Earth and Environment (http://www.dsfta.unisi.it).

Liu, Q. Y., and Yang, Y. L. 2003, *Chin. J. Astron. Astrophys.*, **3**, 142.

O'Connell, D. J. K. 1951, *Riverview Coll. Obs. Publ.*, **2**, 85.

Papini, R., Franco, L., Marchini, A., and Salvaggio, F. 2015, *J. Amer. Assoc. Var. Star Obs.*, **43**, 207.

SSV-UAI. 2017, Unione Astrofili Italiani – Sezione Stelle Variabili (http://stellevariabili.uai.it).

Watson, C., Henden, A. A., and Price, C. A. 2014, AAVSO International Variable Star Index VSX (Watson+, 2006–2017; http://www.aavso.org/vsx).

Abstracts of Papers Presented at the Joint Meeting of the Society for Astronomical Sciences and the American Association of Variable Star Observers (AAVSO 106th Spring Meeting), Held in Ontario, California, June 16–17, 2017

OV Bootis: Forty Nights of World-Wide Photometry

Joseph Patterson
Enrique de Miguel
Douglas Barret
Stephen Brincat
James Boardman Jr.
Denis Buczynski
Tut Campbell
David Cejudo
Lew Cook
Michael J. Cook
Donald Collins
Walt Cooney
Franky Dubois
Shawn Dvorak
Jules P. Halpern
Anthony J. Kroes
Damien Lemay
Domenico Licchelli
Dylan Mankel
Matt Marshall
Rudolf Novak
Arto Oksanen
George Roberts
Jim Seargeant
Huei Sears
Austin Silcox
Douglas Slauson
Geoff Stone
J. R. Thorstensen
Joe Ulowetz
Tonny Vanmunster
John Wallgren
Matt Wood
Center for Backyard Astrophysics, 25 Claremont Avenue, Apt. 7C, New York, NY 10027; jop@astro.columbia.edu

Abstract Among the ~1000 known cataclysmic variables, only one appears to belong to the "Galactic halo"—the Population II stars. We report round-the-world photometry of this star (OV Boo) during March–April 2017, when it staged its first certified dwarf-nova outburst. The star is remarkable for its short binary period (66 minutes), high proper motion, metal-poor composition, substellar secondary, sharp white-dwarf eclipses, and nonradial pulsations. Something for everybody—and it even had the good manners to erupt in northern springtime, when it transits near local midnight. Move over, SS Cyg and WZ Sge; there's a new celebrity in town!

An Ongoing Program for Monitoring the Moon for Meteoroid Impacts

Brian Cudnik
Seth Saganti
Fazal Ali
Salman Ali
Trevannie Beharie
Brittany Anugwom
Department of Chemistry and Physics, Prairie View A&M University, P.O. Box 519, M.S. 2230, Prairie View, TX 77446; bmcudnik@pvamu.edu

Abstract Lunar meteor impacts are surprisingly frequent phenomena, with well over one hundred observable events occurring each year. Of these a little over half arise from members of annual meteor showers (e.g. Perseids, Leonids, etc.), with the rest being sporadic in origin. Five years ago, I (BC) introduced to the SAS Symposium the idea of observing lunar meteoroid impact phenomena and applying these observations to a space mission (LADEE-Lunar Atmosphere and Dust Environment Explorer) that launched the following year. Now, five years later I revisit and reintroduce the activities of the Association of Lunar and Planetary Observers-Lunar Meteoritic Impact Search (ALPO-LMIS) section and share some of the latest observations that have been received. For over 17 years now, ALPO has hosted the LMIS section, for which I have served as coordinator since its inception. In this paper, I will revisit the main ideas of the earlier paper, share some recent observations of lunar meteors, and provide new initiatives and projects interested persons can participate in.

Taxonomy Discrimination of the Tina Asteroid Family via Photometric Color Indices

Mattia A. Galiazzo
University of Vienna, Department of Astrophysics, Turkenschanzstraße 17, A-1180 Vienna, Austria; mattia.galiazzo@univie.ac.at-mattia.galiazzo@gmail.com

Werner W. Zeilinger
University of Vienna, Department of Astrophysics, Turkenschanzstraße 17, A-1180 Vienna, Austria; werner.zeilinger@univie.ac.at

Giovanni Carraro
Dipartimento di Fisica e Astronomia, Universitá di Padova, Vicolo Osservatorio 3, I-35122, Padova, Italy; giovanni.carraro@unipd.it

Dagmara Oszkiewicz
Astronomical Observatory Institute, Faculty of Physics, Adam Mickiewicz University; Sloneczna 36, 60-286, Poznan, Poland

Abstract This work aims to expand our understanding of the physical characteristics of the Tina asteroid family in the main belt. This small group is unusual, as the only asteroid group currently known to be completely contained in the stable island of one of the principal secular resonances of the main belt, the n6. This family is almost near the center of the main asteroid belt, having its members with a semi-major axis between 2.765 au and 2.807 au. Its largest body is (1222) Tina, 21 km in diameter and an X-type asteroid. We aim to find their taxonomic types by performing correlations with their color indices.

Observations of the Star Cor Caroli at the Apple Valley Workshop 2016

Reed Estrada
Northrop Grumman Corporation; reed.estrada@ngc.com

Sidney Boyd
Victor Valley College; sidneymarieboyd@gmail.com

Chris Estrada
California State University, Los Angeles; pr1est0112@hotmail.com

Cody Evans
Victor Valley College; Cjevens85@gmail.com

Hannah Rhoades
Apple Valley High School; hlr@rhoadesfamily.net

Mark Rhoades
Vanguard Preparatory Parent; rhoadesma@gmail.com

Trevor Rhoades
Vanguard Preparatory School

Abstract Using a 22-inch Newtonian Alt/Az telescope and Celestron Micro Guide eyepiece, students participating in a workshop observed the binary star Cor Caroli (STF 1692; α CVn) and found a position angle of 231.0 degrees as well as an average separation of 18.7" This observation compared favorably with the 2015 Washington Double Star published position. This project was part of Mark Brewer's Apple Valley Double Star Workshop. The results were analyzed using bias and circle error probability calculations.

Exoplanet Observing: from Art to Science

Dennis M. Conti
Chair, AAVSO Exoplanet Section, Annapolis, MD 21403; dennis@astrodennis.com

Jack Gleeson
AAVSO Exoplanet Database Lead, Liverpool, England; me@jackgleeson.co.uk

Abstract This paper will review the now well-established best practices for conducting high precision exoplanet observing with small telescopes. The paper will also review the AAVSO's activities in promoting these best practices among the amateur astronomer community through training material and online courses, as well as through the establishment of an AAVSO Exoplanet Database. This latter development will be an essential element in supporting followup exoplanet observations for upcoming space telescope missions such as TESS and JWST.

Multiwavelength Observations of the Eclipsing Binary NSV 3438 between January 2013 and March 2016

Carter M. Becker
Desert Pass Observatory, Green Valley, AZ; Cbecker310@aol.com

Abstract The eclipsing binary NSV 3438 in Canis Minor consists of two M-type stars having approximate effective temperatures of 3235 K (M4V) and 2898 K (M6V). The period for a cycle during this study was 1.535 days, essentially unchanged from that reported in 1996. A modification of the bisected chord method provides estimates of mid-eclipse Julian Dates with 95% confidence limits for 22 primary and 29 secondary eclipses. The mean depths of primary and secondary eclipses with filter B are 0.69 and 0.62 magnitude, respectively, and 0.65 and 0.61 magnitude, respectively for filter V. APASS standard stars closely associated with NSV 3438 provide a means of determining the magnitude of NSV 3438. In addition, B–V color indexes and effective temperatures of the binary can be assessed at critical stages throughout the eclipse cycle.

New Observations and Analysis of ζ Phoenicis

Coen van Antwerpen
Coki Observatory, 8 Carman Close, Hillbank, SA 5112, Australia; coenva15@gmail.com

Tex Moon
Centauri Observatory, 14 Ada St, Scottsdale, TAS 7260, Australia; texmoon0@gmail.com

Abstract From new and published photometry of the eclipsing binary ζ Phe (HR 338) a period of 1.66977220(3) days was determined and a new epoch of HJD 2432500.021511 selected. Using the 60+ years of photometry, published radial velocities, and new values for the period and epoch, the physical characteristics of the ζ Phe system were modeled using a software package called PHOEBE. Of note, the masses of the B6V and B9V components were determined to be 3.75 and 2.35 $M_{\odot}$, somewhat less than previous determinations. The period of apsidal motion of ζ Phe's eccentric orbit was calculated to be 53.7 ± 0.3 years, indicating that one full cycle has been completed since photoelectric measurements of this star were first undertaken in 1950.

WD1145+017

Mario Motta
AAVSO, 19 Skipper Way, Gloucester, MA 01930; mmotta@massmed.org

Abstract WD1145 is a 17th magnitude white dwarf star 570 light years away in Virgo that was discovered to have a disintegrating planetoid in close orbit by Andrew Vanderburg, a graduate student at Harvard CfA, while data mining the Kepler 2 mission. He contacted me to obtain transit data to elucidate the nature of its rather bizarre transit light curves. I obtained multiple observations of WD1145 over the course of a year, and found a series of complex transit light curves that could only be interpreted as a ring complex or torus in close orbit around WD1145. Combined with data from other amateur astronomers, professional observations, and satellite data, it became clear that WD1145 has a small planetoid in close orbit at the Roche limit and is breaking apart, forming a ring of debris material that is then raining down on the white dwarf. The surface of the star is "polluted" by heavy metals, determined by spectroscopic data. Given that in the intense gravitational field of a white dwarf any heavy metals could not for long last on the surface, this confirms that we are tracking in real time the destruction of a small planet by its host star.

Spectrophotometry of Symbiotic Stars

David Boyd
5 Silver Lane, West Challow, Wantage, OX12 9TX, United Kingdom; davidboyd@orion.me.uk

Abstract Symbiotic stars are fascinating objects—complex binary systems comprising a cool red giant star and a small hot object, often a white dwarf, both embedded in a nebula formed by a wind from the giant star. UV radiation from the hot star ionizes the nebula, producing a range of emission lines. These objects have composite spectra with contributions from both stars plus the nebula and these spectra can change on many timescales. Being moderately bright, they lend themselves well to amateur spectroscopy. This paper describes the symbiotic star phenomenon, shows how spectrophotometry can be used to extract astrophysically useful information about the nature of these systems, and gives results for three symbiotic stars based on the author's observations.

How to Use Astronomical Spectroscopy to Turn the Famous Yellow Sodium Doublet D Bands into a Stellar Speedometer and Thermometer

Joshua Christian
Matthew King
John W. Kenney, III
Chemical Physics Laboratory, Concordia University, 1530 Concordia West, Irvine, CA 92612

Abstract The twin, closely spaced D bands of sodium, which appear in the spectra of many stars, turn out to be easy to identify and, owing to their intensity, easy to use as "speedometer bands" via spectral Doppler shifts for the analysis of differential radial velocities in binary star systems and other systems for which astronomical velocity measurements are needed. Moreover, temperature data can be extracted from an analysis of the widths of the sodium band profiles. In order to demonstrate the effectiveness of these techniques and calculations, terrestrial sources of sodium and a simulated Doppler shift were used. A visible and quantifiable difference in band profile widths was seen corresponding to temperature, encouraging further studies.

Modeling Systematic Differences In Photometry by Different Observers

John C. Martin
University of Illinois Springfield, One University Plaza MS HSB 314, Springfield, IL 62704; Jmart5@uis.edu

Abstract Photometric monitoring campaigns commonly increase their cadence and length of coverage by combining measurements from multiple observers (typically using different telescope/detector systems). However, systematic offsets between the calibration of different contributors can cause problems which may threaten to degrade the quality of an effort when analyzing the results. This is particularly common when the collaboration is put together post-hoc after the campaign but it can also be an unwelcome surprise for even the most carefully planned joint efforts. Here we will explore some of the issues and explore solutions which can be helpful for identifying and mitigating systematic offsets between observers during post-hoc analysis.

How Faint Can You Go?

Arne Henden
AAVSO, 106 Hawkins Pond Road, Center Harbor, NH 03226; arne@aavso.org

Abstract For many scientific projects, knowledge of the faint limit of your exposure can be extremely important. In addition, it can be just plain fun to know how faint your equipment can go under varying circumstances. This paper describes the concept and gives some guidance as to how to increase the scientific value of your reports.

Shoestring Budget Radio Astronomy

John E. Hoot
SSC Observatory, Center For Solar Systems Studies, Las Campanas Remote Observatory, 1303 S. Ola Vista, San Clemente, CA 92672; jhoot@ssccorp.com

Abstract The commercial exploitation of microwave frequencies for cellular, WiFi, Bluetooth, HDTV, and satellite digital media transmission has brought down the cost of the components required to build an effective radio telescope to the point where, for the cost of a good eyepiece, you can construct and operate a radio telescope. This paper sets forth a family of designs for 1421 MHz telescopes. It also proposes a method by which operators of such instruments can aggregate and archive data via the Internet. With 90 or so instruments it will be possible to survey the entire radio sky for transients with a 24 hour cadence.

Using All-Sky Imaging to Improve Telescope Scheduling

Gary M. Cole
Starphysics Observatory, 14280 W. Windriver Lane, Reno, NV 89511; garycole@mac.com

Abstract Automated scheduling makes it possible for a small telescope to observe a large number of targets in a single night. But when used in areas which have less-than-perfect sky conditions such automation can lead to large numbers of observations of clouds and haze. This paper describes the development of a "sky-aware" telescope automation system that integrates the data flow from an SBIG AllSky340c camera with an enhanced dispatch scheduler to make optimum use of the available observing conditions for two highly instrumented backyard telescopes. Using the minute-by-minute time series image stream and a self-maintained reference database, the software maintains a file of sky brightness, transparency, stability, and forecasted visibility at several hundred grid positions. The scheduling software uses this information in real time to exclude targets obscured by clouds and select the best observing task, taking into account the requirements and limits of each instrument.

A Community-Centered Astronomy Research Program

Pat Boyce
Boyce Research Initiatives and Education Foundation, 3540 Carleton Street, San Diego, CA, 92016; pat@boyce-astro.org

Grady Boyce
Boyce Research Initiatives and Education Foundation, 1433 Burroughs Street, Oceanside, CA, 92015; grady@boyce-astro.org

Abstract The Boyce Research Initiatives and Education Foundation (BRIEF) is providing semester-long, hands-on, astronomy research experiences for students of all ages that results in their publishing peer-reviewed papers. The course in astronomy and double star research has evolved from a face-to-face learning experience with two instructors to an online hybrid course that simultaneously supports classroom instruction at a variety of schools in the San Diego area. Currently, there are over 65 students enrolled in three community colleges, seven high schools, and one university as well as individual adult learners. Instructional experience, courseware, and supporting systems were developed and refined through experience gained in classroom settings from 2014 through 2016. Topics of instruction include Kepler's Laws, basic astrometry, properties of light, CCD imaging, use of filters for varying stellar spectral types, and how to perform research, scientific writing, and proposal preparation. Volunteer instructors were trained by taking the course and producing their own research papers. An expanded program was launched in the fall semester of 2016. Twelve papers from seven schools were produced; eight have been accepted for publication by the *Journal of Double Star Observations* (JDSO) and the remainder are in peer review. Three additional papers have been accepted by the JDSO and two more are in process papers. Three college professors and five advanced amateur astronomers are now qualified volunteer instructors. Supporting tools are provided by a BRIEF server and other online services. The server-based tools range from Microsoft Office and planetarium software to top-notch imaging programs and computational software for data reduction for each student team. Observations are performed by robotic telescopes worldwide supported by BRIEF. With this success, student demand has increased significantly. Many of the graduates of the first semester course wanted to expand their astronomy knowledge and experience. To answer this demand, BRIEF is developing additional astronomy research courses with partners in advanced astrometry, photometry, and exoplanets. The program provides a significant opportunity for schools, teachers, and advanced amateur astronomers to introduce high school and college students to astronomy, science, and STEM careers.

Engaging Teenagers in Astronomy Using the Lens of Next Generation Science Standards and Common Core State Standards

Sean Gillette
Vanguard Preparatory School; sean_gillette@avusd.org

Debbie Wolf
Vanguard Preparatory School; debbie_wolf@avusd.org

Jeremiah Harrison
Sandia Academy; jeremiah_harrison@avusd.org

Abstract The Vanguard Double Star Workshop has been developed to teach eighth graders the technique of measuring position angle and separation of double stars. Through this program, the students follow in the footsteps of a professional scientist by researching the topic, performing the experiment, writing a scientific article, publishing a scientific article, and finally presenting the material to peers. An examination of current educational standards grounds this program in educational practice and philosophy.

An Overview of Ten Years of Student Research and JDSO Publications

Rachel Freed
Sonoma State University, 416 4th Street, W. Sonoma, CA 95476; r.freed2010@gmail.com

Michael Fitzgerald
Edith Cowan Institute for Educational Research, 270 Joondalup Drive, Joondalup, WA 6027, Australia; mfitzasp@gmail.com

Russell Genet
California Polytechnic State University, San Luis Obispo, 4995 Santa Margarita Lake Road, Santa Margarita, CA 93453; russmgenet@aol.com

Brendan Davidson
Desert Hills Middle School, 2564 E. 2150 S. Circle, St. George, UT 84790; bjrocket141@gmail.com

Abstract The astronomy research seminar, initially designed and taught by Russell Genet at Cuesta College over the past decade, has resulted in over 100 published student research papers in the Journal of Double Star Observations along with dozens of other papers and conference presentations. While the seminar began at a single community college, it has now spread to include students from dozens of institutions and instructors, reaching students from middle school through graduate school. The seminar has integrated the large community-of-practice of amateur and professional astronomers, educators, students, and hardware and software engineers while providing an important experience for student researchers. In this paper, we provide an overview analysis of 109 publications authored by 320 individual students involved in the astronomy research seminar over the last decade.

Use of the AAVSO's International Variable Star Index (VSX) in an Undergraduate Astronomy Course Capstone Project

Kristine Larsen
Central Connecticut State University, 1615 Stanley Street, New Britain, CT 06050; larsen@ccsu.edu

Abstract The author discusses a capstone project that utilizes the AAVSO's International Variable Star Index (VSX), ASAS light curves and phase plots, and the SIMBAD astronomical data repository in a laboratory-based undergraduate Stellar and Galactic Astronomy course.

Student Scientific Research within Communities-of-Practice

Russell Genet
California Polytechnic State University, San Luis Obispo, CA

James Armstrong
University of Hawaii, Maui, HI

Philip Blanko
Grossmont College, San Diego, CA

Grady Boyce
Pat Boyce
Boyce Research Initiatives and Education Foundation, San Diego, CA

Mark Brewer
California State University, San Bernardino, CA

Robert Buchheim
Society for Astronomical Sciences, Ontario, CA

Jae Calanog
Miramar College, San Diego, CA

Diana Castaneda
University of Hawaii, Honolulu, HI

Rebecca Chamberlin
The Evergreen State College, Olympia, WA

R. Kent Clark
University of Southern Alabama, Mobile, AL

Dwight Collins
Collins Educational Foundation, San Rafael, CA

Dennis Conti
American Association of Variable Star Observers, Annapolis, MD

Sebastien Cormier
Grossmont College, San Diego, CA

Michael Fitzgerald
Edith Cowen University, Perth, Australia

Chris Estrada
California State University, Los Angeles, CA

Reed Estrada
Northrop Aviation, Lancaster, CA

Rachel Freed
California State University, Sonoma, CA

Edward Gomez
Los Cumbres Observatory, Santa Barbara, CA

Paul Hardersen
Planetary Science Institute, Tucson, AZ

Richard Harshaw
Brilliant Sky Observatory, Cave Creek, AZ

Jolyon Johnson
Sammamish High School, Belleview, WA

Stella Kafka
American Association of Variable Star Observers, Cambridge, MA

John Kenney
Concordia University, Irvine, CA

Kakkala Mohanan
Leeward Community College, Pearl City, Oahu, HI

John Ridgely
California Polytechnic State University, San Luis Obispo, CA

David Rowe
PlaneWave Instruments, Rancho Dominguez, CA

Mark Silliman
Waipaha High School, Waipaha, Oahu, HI

Irena Stojimirovic
Mesa College, San Diego, CA

Kalee Tock
Stanford Online High School, Palo Alto, CA

Douglas Walker
Estrella Mountain Community College, Avondale, AZ

Abstract Social learning theory suggests that students who wish to become scientists will benefit by being active researchers early in their educational careers. As coauthors of published research, they identify themselves as scientists. This provides them with the inspiration, motivation, and staying power that many will need to complete the long educational process. This hypothesis was put to the test over the past decade by a one-semester astronomy research seminar where teams of students managed their own research. Well over a hundred published papers coauthored by high school and undergraduate students at a handful of schools substantiated this hypothesis. However, one could argue that this was a special case. Astronomy, after all, is supported by a large professional-amateur community-of-practice. Furthermore, the specific area of research—double star astrometry—was chosen because the observations could be quickly made, the data reduction and analysis was straight forward, and publication of the research was welcomed by the Journal of Double Star Observations. A recently initiated seminar development and expansion program—supported in part by the National Science Foundation—is testing a more general hypothesis that: (1) the seminar can be successfully adopted by many other schools; (2) research within astronomy can be extended from double star astrometry to time series photometry of variable stars, exoplanet transits, and asteroids; and (3) the seminar model can be extended to a science beyond astronomy: environmental science—specifically atmospheric science. If the more general hypothesis is also supported, seminars that similarly feature published high school and undergraduate student team research could have the potential to significantly improve science education by increasing the percentage of students who complete the education required to become professional scientists.

The SPIRIT Telescope Initiative: Six Years On

Paul Luckas
International Centre for Radio Astronomy Research, The University of Western Australia, 35 Stirling Highway, Crawley, Western Australia 6009; paul.luckas@uwa.edu.au

Abstract Now in its sixth year of operation, the SPIRIT initiative remains unique in Australia, as a robust web-enabled robotic telescope initiative funded for education and outreach. With multiple modes of operation catering for a variety of usage scenarios and a fully supported education program, SPIRIT provides free access to contemporary astronomical tools for students and educators in Western Australia and beyond. The technical solution itself provides an excellent model for low cost robotic telescope installations, and the education program has evolved over time to include a broad range of student experiences—from engagement activities to authentic science. This paper details the robotic telescope solution, student interface, and educational philosophy, summarizes achievements and lessons learned, and examines the possibilities for future enhancement including spectroscopy.

Techniques of Photometry and Astrometry with APASS, Gaia, and Pan-STARRs Results

Wayne Green
7131 Oriole Lane, Longmont, CO 80503; dxwayne@gmail.com

Abstract The databases with the APASS DR9, Gaia DR1, and the Pan-STARRs 3π DR1 data releases are publicly available for use. There is a bit of data-mining involved to download and manage these reference stars. This paper discusses the use of these databases to acquire accurate photometric references as well as techniques for improving results. Images are prepared in the usual way: zero, dark, flat-fields, and WCS solutions with Astrometry.net. Images are then processed with Sextractor to produce an ASCII table of identifying photometric features. The database manages photometics catalogs and images converted to ASCII tables. Scripts convert the files into SQL and assimilate them into database tables. Using SQL techniques, each image star is merged with reference data to produce publishable results. The VYSOS has over 13,000 images of the ONC5 field to process with roughly 100 total fields in the campaign. This paper provides the overview for this daunting task.

Exploring the Unknown: Detection of Fast Variability of Starlight

Richard H. Stanton
Jet Propulsion Laboratory (Retired), Big Bear City, CA 92314; rhstanton@gmail.com

Abstract In previous papers the author described a photometer designed for observing high-speed events such as lunar and asteroid occultations, and for searching for new varieties of fast stellar variability. A significant challenge presented by such a system is how one deals with the large quantity of data generated in order to process it efficiently and reveal any hidden information that might be present. This paper surveys some of the techniques used to achieve this goal.

A Wide Band SpectroPolarimeter

John Menke
22500 Old Hundred Rd, Barnesville, MD 20838; john@menkescientific.com

Abstract This is the third paper in a series describing experiments in developing amateur spectropolarimetry instrumentation and observational methods. Spectropolarimetry (SP) can provide insight into the extra-stellar environment, including presence of dust and alignment forces (e.g., magnetic fields). The first two papers (SAS 2014, 2016) described the SP1, a spectropolarimeter based on the medium-resolution spectrometer on our 18-inch, f3.5, Newtonian. The desire to observe fainter stars led to the development of the SP2 reported here that uses a low resolution spectrometer. The SP2 has been used with a C11 f10 telescope, and has allowed observations down to about mag. 8. This paper describes the SP2 and observational results to date.

A Slitless Spectrograph That Provides Reference Marks (revised 2017)

Tom Buchanan
Atlanta Astronomy Club, P.O. Box 187, Hiwasse, AR 72739; tombuchan@hughes.net

Abstract The author designed and built a slitless spectrograph to record reference marks along the spectrum of a point light source. Spectra can be taken of transient, clustered, or moving lights when a spectrograph cannot be accurately aimed at the lights to capture slit spectra. Three beams of undispersed light, directed by mirrors and lenses, provide reference marks. Near each end of the spectrum a reference mark barely varies from the corresponding point on the spectrum when the aim toward the light source varies. Within 2 degrees of perfect aim toward the light source, the variation is less than 7 angstroms. The third reference mark enables this variation to be quantified. The locations and orientations of the optical components are mathematically derived. Additional features of the spectrograph enable the use of a slit and comparison spectrum, and the recording of higher orders by moving the camera and using specific Wratten filters.

Astronomical Instrumentation Systems Quality Management Planning: AISQMP

Jesse Goldbaum
Tierra Astronomical Institute, 23717 Miranda Street, Woodland Hills, CA 91367; jesse@tierra-astro.org

Abstract The capability of small aperture astronomical instrumentation systems (AIS) to make meaningful scientific contributions has never been better. The purpose of AIS quality management planning (AISQMP) is to ensure the quality of these contributions such that they are both valid and reliable. The first step involved with AISQMP is to specify objective quality measures not just for the AIS final product, but also for the instrumentation used in its production. The next step is to set up a process to track these measures and control for any unwanted variation. The final step is continual effort applied to reducing variation and obtaining measured values near optimal theoretical performance. This paper provides an overview of AISQMP while focusing on objective quality measures applied to astronomical imaging systems.

Scintillation Reduction using Conjugate-Plane Imaging

Gary A. Vander Haagen
Stonegate Observatory, 825 Stonegate Road, Ann Arbor, MI 48103; garyvh2@gmail.com

Abstract All observatories are plagued by atmospheric turbulence exhibited as star scintillation or "twinkle" whether a high altitude adaptive optics research or a 30-cm amateur telescope. It is well known that these disturbances are caused by wind and temperature-driven refractive gradients in the atmosphere and limit the ultimate photometric resolution of land-based facilities. One approach identified by Fuchs (1998) for scintillation noise reduction was to create a conjugate image space at the telescope and focus on the dominant conjugate turbulent layer within that space. When focused on the turbulent layer little or no scintillation exists. This technique is described whereby noise reductions of 6 to 11/1 have been experienced with mathematical and optical bench simulations. Discussed is a proof-of-principle conjugate optical train design for an 80-mm, f7 telescope.

Erratum: Visual Times of Maxima for Short Period Pulsating Stars I

Gerard Samolyk
P.O. Box 20677, Greenfield, WI 53220; gsamolyk@wi.rr.com

In the article "Visual Times of Maxima for Short Period Pulsating Stars 1" (*JAAVSO*, 2017, **45**, 116–120), the page numbers in some of the references were given incorrectly. The corrected references are as follows:

Samolyk, G. 2010, *J. Amer. Assoc. Var. Star Obs.,* **38**, 12.
Samolyk, G. 2011, *J. Amer. Assoc. Var. Star Obs.,* **39**, 23.
Samolyk, G. 2012, *J. Amer. Assoc. Var. Star Obs.,* **40**, 923.
Samolyk, G. 2013, *J. Amer. Assoc. Var. Star Obs.,* **41**, 85.
Samolyk, G. 2014, *J. Amer. Assoc. Var. Star Obs.,* **42**, 124.
Samolyk, G. 2015, *J. Amer. Assoc. Var. Star Obs.,* **43**, 74.
Samolyk, G. 2016, *J. Amer. Assoc. Var. Star Obs.,* **44**, 66.

Index to Volume 45

Author

Subject

NOTES